Steel Bridge Design Handbook

CHAPTER 4
Strength Behavior and Design of Steel

February 2022

Smarter.
Stronger.
Steel.

© AISC 2022

by

American Institute of Steel Construction

Printed in the United States of America

Foreword

The Steel Bridge Design Handbook covers a full range of topics and design examples to provide bridge engineers with the information needed to make knowledgeable decisions regarding the selection, design, fabrication, and construction of steel bridges. The Handbook has a long history, dating back to the 1970s in various forms and publications. The more recent editions of the Handbook were developed and maintained by the Federal Highway Administration (FHWA) Office of Bridges and Structures as FHWA Report No. FHWA-IF-12-052 published in November 2012, and FHWA Report No. FHWA-HIF-16-002 published in December 2015. The previous development and maintenance of the Handbook by the FHWA, their consultants, and their technical reviewers is gratefully appreciated and acknowledged.

This current edition of the Handbook is maintained by the National Steel Bridge Alliance (NSBA), a division of the American Institute of Steel Construction (AISC). This Handbook, published in 2021, has been updated and revised to be consistent with the 9th edition of the AASHTO LRFD Bridge Design Specifications which was released in 2020. The updates and revisions to various chapters and design examples have been performed, as noted, by HDR, M.A. Grubb & Associates, Don White, Ph.D., and NSBA. Furthermore, the updates and revisions have been reviewed independently by Francesco Russo, Ph.D., P.E., Brandon Chavel, Ph.D., P.E., and NSBA.

The Handbook consists of 19 chapters and 6 design examples. The chapters and design examples of the Handbook are published separately for ease of use, and available for free download at the NSBA website, www.aisc.org/nsba.

The users of the Steel Bridge Design Handbook are encouraged to submit ideas and suggestions for enhancements that can be implemented in future editions to the NSBA and AISC at solutions@aisc.org.

TECHNICAL REPORT DOCUMENTATION PAGE

1. Title and Subtitle Steel Bridge Design Handbook Chapter 4: Strength Behavior and Design of Steel	2. Report Date February 2022
3. Original Author(s) Don White, Ph.D. (Georgia Institute of Technology)	4. Revision Author(s) Don White, Ph.D. (Georgia Institute of Technology)
5. Sponsoring Agency Name and Address National Steel Bridge Alliance, a division of the American Institute of Steel Construction 130 E. Randolph, Suite 2000 Chicago, IL 60601	6. Revision Performing Organization Name and Address Don White, Ph.D. (Georgia Institute of Technology)

7. Supplementary Notes

The previous edition of this Handbook was published as FHWA-HIF-16-002 and was developed to be current with the 7th edition of the AASHTO LRFD Bridge Design Specifications. This edition of the Handbook was updated to be current with the 9th edition of the AASHTO LRFD Bridge Design Specifications, released in 2020.

8. Abstract

The behavior of steel structures is an intricate and fascinating topic. This chapter is intended to serve as a guide to the AASHTO Load and Resistance Factor Bridge Design (LRFD) Specifications and their representation of the strength behavior and design of steel bridge systems and members. The volume focuses on the structural form and function of bridge systems and members, with emphasis on strength limit states. Where relevant, recent advances in the AISC Specification for Structural Steel Buildings as well as findings from research developments are discussed in addition to explanation of the AASHTO LRFD Specifications. There are numerous areas where a broad understanding of the fundamental behavior of structures is key to the proper interpretation, application, and where necessary, extension of the AASHTO LRFD Specifications. This chapter aims to aid the Engineer in understanding and applying the essential principles of steel system and member strength behavior and design.

9. Keywords Steel Bridge Structural Behavior, Buckling, I-Section Members, Box-Section Members, Tension Members, Compression Members, Flexural Members, Beam-Columns, Unstiffened Plates, Stiffened Plates	10. AISC Publication No. B904-22

Steel Bridge Design Handbook:
Strength Behavior and Design of Steel

Table of Contents

List of Figures

List of Tables

1.0 INTRODUCTION

The behavior of steel bridge structures is an intricate and fascinating topic. This volume is intended to serve as a guide to the AASHTO (2020) Load and Resistance Factor Design (LRFD) Bridge Design Specifications, 9th Edition, and their representation of the behavior of steel bridge systems and members. The volume focuses on the structural form and function of bridge systems and members, with emphasis on strength limit states. Where relevant, recent advances in the AISC (2016) *Specification for Structural Steel Buildings* as well as findings from research developments are discussed in addition to the AASHTO provisions.

Selection of the most cost effective bridge structural systems and members is of course dependent on many factors far beyond the fundamental behavior, that is factors which affect the overall material, fabrication, shipping, construction and maintenance costs for a given bridge. The companion Steel Bridge Design Handbook volumes address these considerations. Also, steel bridge behavior is tied inextricably to the physical loadings or actions that the structure must resist, the corresponding load models implemented by the AASHTO Specifications to represent these actions, and the analysis of the structural systems to predict the overall responses and the individual component requirements. The Steel Bridge Design Handbook volume titled Loads and Load Combinations addresses the AASHTO (2020) load models and the volume titled Structural Analysis discusses methods of analysis. Service and fatigue limit states, redundancy and fracture control, and constructability are addressed in separate volumes. In addition, the design of cross frames and diaphragms and their connections, girder splices, bearings, decks and substructure units are addressed separately.

Many of the words of J.A.L. Wadell (1916), a famous engineer and teacher of the early 20th century, are still relevant to the design of bridge structures today. Principle V in Wadell's Chapter XV on "First Principles of Designing," which he refers to as "the most important (chapter) in the book," reads:

> "There are No Bridge Specifications Yet Written, and there Probably Never Will be Any, which will Enable an Engineer to Make a Complete Design for an Important Bridge without Using His Judgment to Settle Many Points which the Specifications Do Not thoroughly Cover… the science of bridge-designing is such a profound and intricate one that it is absolutely impossible in any specification to cover the entire field and to make rules governing the scientific proportioning of all parts of all structures.

> The author, however, has done his best in Chapter LXXVIII of this treatise to render the last statement incorrect."

Certainly, the AASHTO LRFD Bridge Design Specifications (AASHTO 2020) have also done their best in this regard. Nevertheless, there are numerous areas where a broad understanding of the fundamental behavior of structures is key to the proper interpretation, application, and where necessary, extension of the AASHTO provisions. This volume aims to aid the Engineer in reviewing and understanding the essential principles of steel system and member strength behavior and design, as well as the manner in which these principles are implemented in (AASHTO 2020). This volume is intended as a resource providing the background to the many different system and member strength provisions of the 9th Edition of the AASHTO LRFD Specifications.

2.0 BEHAVIOR AND STRUCTURE TYPES

There are many ways to classify steel highway bridges. Classification of bridge systems in terms of maximum achievable span lengths is possibly the most relevant pertaining to fundamentals of the structural behavior. Steel highway bridges range from minor structures spanning only a few feet over creeks or streams to major technical achievements with spans larger than 4000 feet that define the geographic regions in which they are located. For bridges with spans ranging up to about 400 feet, stringer systems are very common. These types of structures are very important since they constitute the majority of the highway bridges within the nation's transportation system. These types of bridges are discussed first, followed by other systems that are viable at longer span lengths.

2.1 Rolled I-Section Stringer Systems

Steel bridge spans smaller than about 100 feet are often achieved most economically using rolled I-section members. For the shortest spans, the efficiency of the structural system tends to play a minor role in the overall cost and competitiveness relative to other attributes pertaining to simplicity, standardization, and speed of design, fabrication, delivery and construction. The Short Span Steel Bridge Alliance (SSSBA 2021) has developed a free web-based tool that provides preliminary simple-span and modular designs addressing these considerations. For the shortest spans, the main structural members in these types of bridges are typically simple-span rolled I-beams. Both composite and noncomposite deck systems are common in these types of bridges.

Spans longer than 100 feet start to push the technical limits of rolled I-beam stringer systems. Flexibility of the structure, vibration and motion perception tend to become more significant considerations in simple-span I-beam systems as the ratio of the span length, L, to the total structural section depth, D_{total}, exceeds roughly $L/D_{total} = 25$. These limits may be extended by establishing continuity between structural elements (i.e., making the I-beams composite with a concrete deck), use of continuous spans or simple-spans for dead load that are subsequently made continuous for live load (Talbot 2005), making the I-beams integral with the substructure at piers (Wasserman 1997), or use of rigid-frame bridges in which major structural elements of the superstructure and a portion of the substructure are steel I-sections (Heins and Firmage 1979). In addition, other modifications to the structural system are possible such as the use of cover plates within negative moment regions and/or longitudinal post-tensioning (Troitsky 1990, Xanthakos 1994). However, these modifications have only a minor influence on the structure stiffness and dynamic characteristics, and their cost may often outweigh their benefits. Generally, one can achieve the largest overall stiffness for a minimum constant depth by using composite continuous spans with integral piers, and by applying AASHTO (2020) Appendix B6 to allow for minor inelastic redistribution of the interior pier moments. Nevertheless, L/D_{total} values larger than about 35 are exceedingly difficult to achieve in stringer-type systems by any of the above measures. Also, as discussed in the Stringer Bridges: Making the Right Choices volume, where the depths are not limited due to clearance restrictions, etc., often the greatest economy can be achieved by using sections that are deeper than suggested by the above maximum L/D_{total} limits.

2.2 General I-Section Stringer Systems

2.2.1 Overview

Welded plate I-girders become an attractive option at span lengths within the upper range applicable for rolled I-beams. Furthermore, depending on the costs of welded I-section fabrication versus the production costs of rolled I-shapes, welded I-section members can be cost-effective at smaller span lengths. Figure 1 shows a typical composite rolled I-beam or welded I-girder bridge cross section. In this system, the I-sections are spaced such that the deck spans between them. The I-section members are referred to generally as girders in the following discussions.
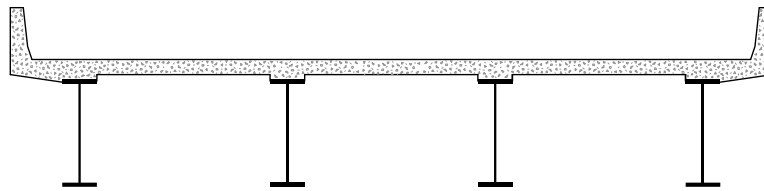
Figure 1. Typical composite rolled I-beam or welded I-girder bridge cross section.

Cast-in-place composite concrete slabs may be designed in straight bridges of these types, without skew or with small skew, using the AASHTO (2020) Article 9.7.2 Empirical Design rules. AASHTO (2020) does not explicitly restrict the use of empirical design to straight bridges with small skew; however, it does require additional reinforcing in the end zones if the skew exceeds 25 degrees. Additional considerations may be prudent in some cases with horizontally curved bridges. The slab empirical design rules account for beneficial arching action in transferring loads to the girders, and are allowed for cast-in-place slabs up to approximately 13.5 feet spacing between the girders, S, or a maximum ratio of the girder spacing to the slab thickness of $S/t_s = 18$, among other requirements.

Precast decks and a number of other deck systems also are capable of spanning a large S with relatively small t_s. Wider girder spacing potentially eliminates one or more extra girder lines and the corresponding cross frames and bearings, and also tends to give a more efficient structural system. This is because the live loads are positioned to produce the maximum response in each girder in the design analysis, but they do not generally produce the maximum effects in all the girders at a given bridge cross section simultaneously. With wider girder spacing, the sum of the girder resistances in a given bridge cross section will tend to be closer to the total required live load capacity for the various positions of the live load. Trade-offs associated with wider girder spacing include increases in deck thickness, and reinforcing and forming costs (which are typically offset by reduced labor costs). Also, future staged redecking considerations may influence how many girders may be removed from the cross section. Cross-frame forces tend to be larger with wider girder spacing, due to larger differential live loads and live load deflections of the girders, as well as larger stiffness of the cross frames relative to the slab. Interestingly, the design efficiency associated with wider spacing in ordinary stringer bridges is no longer impacted by the approximation of slab shear lag effects by effective width rules. This consideration is discussed below.

Prior AASHTO Specification provisions, such as the AASHTO (2004) Article 4.6.2.6.1, restricted the effective width of the slab, b_{eff}, to a maximum of $12t_s + b_f/2$ or ¼ of the effective span length for interior girders, along with a comparable limit for exterior girders, to account for the effect of shear lag in the slab (illustrated in Figure 2). Basically, slab flexural stresses arising from major-axis bending of the girders are developed by shear stresses in the plane of the slab. This can be seen by making a longitudinal cut to isolate a portion of the slab from the rest of a given girder and drawing a free-body diagram. The shear deformations associated with these shear stresses tend to reduce the magnitude of the flexural stresses at the slab locations farther from the girder webs. The prior slab effective width rules limited the slab contribution to the composite section in some situations with wider girder spacing.
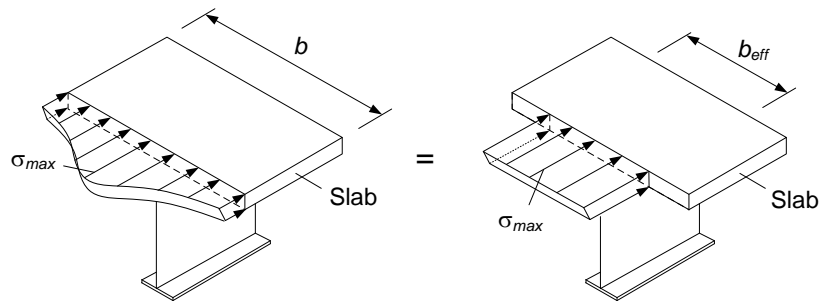
Figure 2. Effect of Shear lag.

The 2008 interims of Article 4.6.2.6.1, and subsequent editions of this article, have replaced the above traditional rules simply with the use of the full tributary width perpendicular to the axis of the member. These provisions are applicable to all concrete deck slabs in composite or monolithic construction, except that separate slab effective width requirements are retained for segmental concrete box and single-cell cast-in-place box beams, orthotropic steel decks, and for noncomposite box section members and transverse floor beams and integral bent caps. In negative moment regions, the corresponding simplified rule is based on the use of the idealized fully cracked section for cross-section-level resistance calculations under both service and strength loading conditions. However, for the structural analysis, AASHTO (2020) Article 6.10.1.5 states that the concrete deck is to be assumed fully effective (uncracked) over the entire bridge length for structural analysis, using specified concrete modular ratios for short- and long-term loadings applied to the composite bridge. The 2008 and post-2008 Article 4.6.2.6.1 provisions are based on extensive studies by Chen et al. (2005) and others. Chen's studies indicated that the use of a slab effective width b_e equal to the full tributary width has a negligible influence on the design calculations relative to the physical bridge response in the above permitted situations. The research by Chen et al. (2005) demonstrated that there is no significant relationship between the slab effective width and the slab thickness within the practical ranges of the deck proportions in ordinary stringer bridge systems, which was implied by the pre-2008 Specifications.

Similar to rolled I-beam bridges, the structural efficiency of welded I-girder bridges can be improved substantially by establishing continuity between the various components or sub-systems. Also, welded I-girder cross-section proportions are typically changed at field splice locations or at the limits of available plate lengths. The use of cross-section transitions at other locations may or may not be cost effective depending on the specifics of the bridge and the economics of welding and inspecting a splice compared to the cost of extending a thicker plate. The Steel Bridge Design

Handbook volume titled Stringer Bridges: Making the Right Choices discusses these considerations in detail. Variable web depth members with haunches over the interior supports may be used in continuous spans, giving section capacities that follow the shape of the elastic moment envelopes more closely. Hall (1992) indicates that haunched composite girders are usually advantageous for spans in excess of 250 feet, when the depth is limited in a portion of the span, or when a decrease in the positive moments reduces critical fatigue stresses. Current rules of thumb place the span limits of I-section stringer systems typically at 350 to 400 feet. Up to these span lengths, AASHTO (2020) Appendix B6 can be used to design the lightest straight I-girder bridges with limited skews using prismatic sections between the field splice locations.

At spans exceeding about 250 feet, the I-girders in a bridge cross section such as the one shown in Figure 1 need to be spaced relatively close together compared to their depths for the deck to span efficiently between the girders while keeping its thickness low to minimize the dead weight. In these cases, it may be attractive to use a girder-substringer system such as in Figure 3. In this type of system, shallower rolled I-section substringers are framed over the top of the cross frames to support the deck between the main girders. Both the main girders and the substringers may be designed compositely. In addition, it is advantageous for the substringers to be continuous over two or more of their supports.
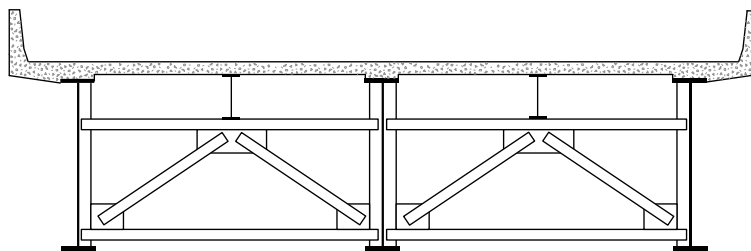
Figure 3. Typical composite I-girder substringer system.

For larger spans, the Engineer may consider using multiple substringers between each of the main girders. This eventually leads to the consideration of two-girder systems with floor beams and stringers, as shown in Figure 4. A two-girder system with cross-girders (Figure 5) is another option (Brown 1992). In this system, the bridge deck spans longitudinally between the cross-girders. As such, the deck must be designed for the combined loading due to the local bending between the cross-girders plus the stresses due to overall composite action with the main girders. Conversely, for the systems shown in Figure 1 through Figure 4, the local bending of the deck is predominantly in the transverse direction; hence, it may be considered separately from the composite action with the main girders. Furthermore, in the system shown in Figure 5, the shear connectors near the intersection of the main- and cross-girders are subjected to significant combined longitudinal and transverse loads. Because of the above complexities, the system in Figure 5 requires greater design effort. However, it may be a viable option in some longer-span applications such as cable-stayed bridges. For these types of structures, design of the deck to span in two-way action between the main girders and the cross-girders also may be an option worth considering. Another significant factor in designs such as those shown in Figure 4 and Figure 5 is that two-girder systems are often identified as being nonredundant, and thus fracture critical. Nevertheless, fractures have occurred in the main members of a number of two-girder bridges in the past without precipitating the collapse of the structure (Fisher et al. 1988, Fisher et al. 1977). Redundancy considerations and

fracture control are discussed in detail in the Steel Bridge Design Handbook volume titled Redundancy.
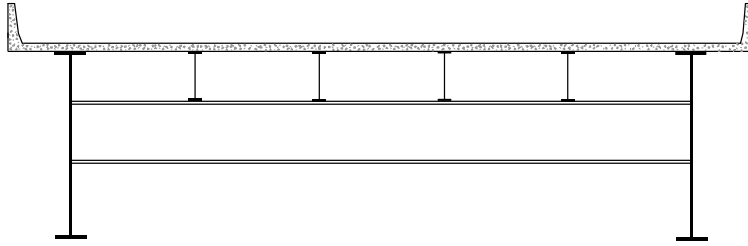
Figure 4. Two-girder system with floor beams and stringers.
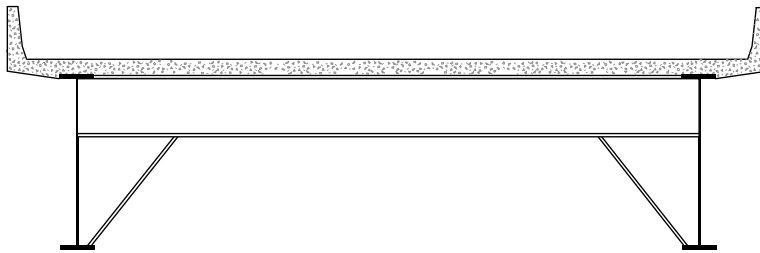
Figure 5. Two-girder system with cross-girders.

I-girder bridges typically become less practical at spans above about 400 feet, although there are multiple recent examples of I-girder spans in excess of 500 feet. Economical main I-girders at these span lengths tend to have relatively narrow flanges compared to their web depths. As such, the girders are less efficient with respect to lateral-torsional buckling. Also, the flange thicknesses start to become inordinately large, particularly for the bottom flanges in composite I-girders, and the contribution of a composite slab becomes a smaller fraction of the overall stiffness and resistance of the main members.

I-girders with span lengths larger than 400 to 500 feet come with some unique challenges that designers should consider, including the use of deeper webs which may require a shop welded or field bolted longitudinal horizontal splice; wider and thicker flanges; larger noncomposite bending moments; multiple stage deck placement sequences; global stability of partially erected sections; and challenges with weight, shipping, and erection of larger field pieces. The use of High Performance Grade 70W Steel (HPS70W) has helped to allow for longer I-girder spans, as it is often used for the flanges of the girder sections in the negative moment regions in a hybrid fashion.

For spans somewhat beyond those of the shortest rolled I-beam systems and typically somewhat less than the largest practical spans for welded I-girders, significant site and highway geometry restrictions often lead to demands for complex bridge geometries. These include horizontally curved alignments, bifurcated structures, splayed girder arrangements, stacked roadways, unequal spans and/or significant support skew. Figure 6 shows one example of a complex framing plan for a highway exit ramp.
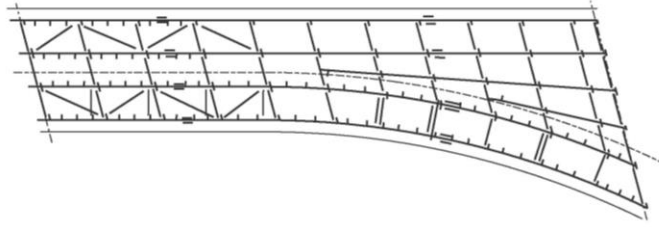
Figure 6. Example complex plan geometry (courtesy of HDR).

2.2.2   Fundamental Behavior of I-Section Stringer Systems

An obvious behavioral characteristic of I-section members, but one that is essential to note, is their efficiency in major-axis bending. For welded I-girders, a single relatively thin web provides for efficient transfer of shear forces while the flanges, located at the top and bottom of the cross section, provide an efficient transfer of bending moments for a given cross-section depth. Straight composite I-girder bridges without skew behave largely as a set of parallel singly symmetric I-girders with a large top flange (i.e., the bridge deck) when the bridge is subjected predominantly to overall major-axis bending. However, individual I-section members are relatively inefficient in weak-axis bending and in torsion. As such, they need to be braced laterally by diaphragms or cross frames, or alternatively in the final constructed configuration, the top flange needs to be embedded in or compositely connected to the slab in positive bending regions, to achieve adequate strength with respect to lateral-torsional buckling.

In horizontally curved and/or skewed bridges, the structure is commonly subjected to significant torsion. Figure 7 shows the resultant of the total dead load, *W*, and the resultant of the corresponding total vertical end reactions, *R*, for a simply supported horizontally curved bridge with radial supports. If the resultant reactions *R* are assumed to act at the middle of the bridge cross section at the end supports, one can observe that additional end torques, *T*, are necessary for equilibrium. These torques increase the vertical reactions on the outside girders (the ones farther away from the center of curvature) and decrease the vertical reactions on the inside girders.
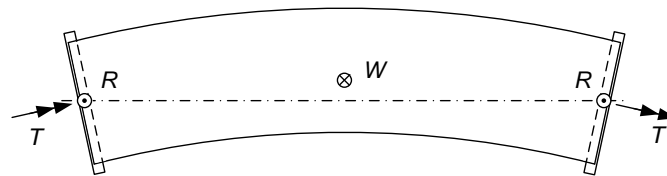
Figure 7. Plan view illustrating the required resultants for the reactions due to dead load at the ends of a simply supported horizontally curved bridge with radial supports.

The internal torsional resistance of horizontally curved I-girder bridges is developed predomi-nantly via the transfer of vertical shear forces between the girders by the cross frames and the slab as shown in Figure 8. These vertical shears increase the downward forces on the outside I-girders and offset the applied vertical loads on the inside I-girders. This increases the major-axis bending moments and end reactions on the outside girders and decreases them on the inside girders. The overall internal torque on the structure at any bridge cross section is developed predominantly by these shears, at the exterior girders, and by the differences between the cross-frame and slab shear

7

forces at each of the girders on the interior girders. These forces, V_1, $V_2 - V_1$, $V_2 - V_3$, and V_3 in the Figure 8 example, are referred to traditionally as the V-loads (NSBA 1996). These V-loads are commonly assumed to increase linearly relative to the mid-width of the bridge cross section in the approximate V-load analysis method (NSBA 1996). The couples generated by the slab and cross-frame shears acting on each of the individual girder free-body diagrams of Figure 8 also resist the tendency of the I-girders to twist about their individual axes relative to the overall torsional rotation of the bridge cross section.
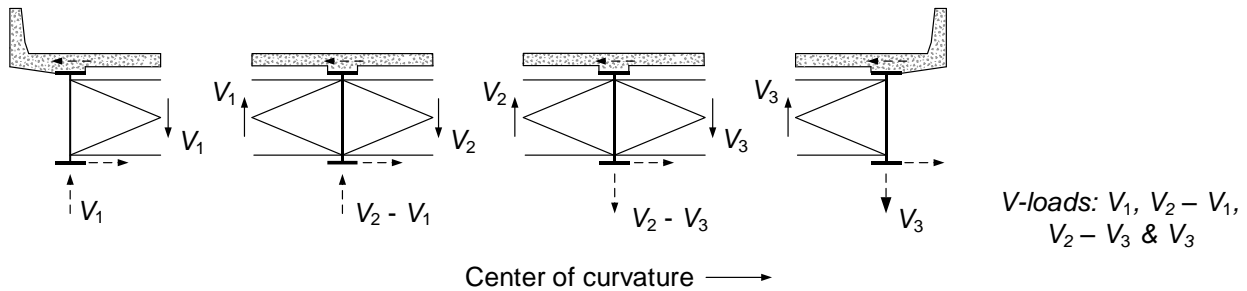
Figure 8. Transfer of vertical shear forces due to torsion by the cross frames and the slab, and the resultant V-loads acting on the girders in a curved bridge.

In continuous-span curved I-girder bridges, the portion of the major-axis bending moments in the outside girders due to the downward V-loads can be negative in shorter adjacent spans, due to the transfer of the associated hogging moments at the interior supports into the adjacent spans. Conversely, upward V-loads on the inside girders can induce additional positive moments in the inside girders of shorter adjacent spans due to the rotational continuity across the interior supports.

Since individual I-girders are relatively flexible and weak in torsion, curved I-girders must be supported by cross frames or diaphragms at relatively close intervals along their lengths to avoid having large torsional stresses and rotations between these brace points. Therefore, the cross frames are essential (primary) components in horizontally curved I-girder bridges. They are essential not only to transfer a large share of the shears due to the torsional action of the bridge between the I-girders, but also they provide torsional support to the individual I-girders.

For cross-frame spacings necessary to ensure adequate stiffness and bending resistance in completed I-girder bridges, the girder torsional responses are dominated generally by nonuniform or warping torsion. Warping torsion is tied to the lateral bending of the I-section flanges in opposite directions (i.e., the cross-bending of the flanges) due to the twisting of the members. Figure 9 illustrates the idealized case of a cantilever I-beam subjected to end torque. The warping torque is developed by the shear forces associated with the flange lateral bending moments developed at the fixed end, where warping is restrained. These forces are labeled as H_ℓ and the flange lateral bending moments are labeled as M_ℓ in the figure. Figure 10 shows a simplified model for calculation of the flange lateral bending stresses on a curved I-girder subjected to uniform major-axis bending moment. Twisting of the member is assumed restrained at the cross-frame locations in this analysis; the focus is on the localized twisting of the member between the cross-frame locations. The horizontal curvature induces a radial loading effect on each of the flanges as shown in the figure. This radial loading effect in turn gives a maximum first-order elastic lateral bending stress of approximately

$$f_\ell = 0.5 \frac{L_b}{b_f} \frac{L_b}{R} f_b \tag{2.2.2-1}$$

in the flanges (White et al. 2001) where L_b is the unsupported length between the cross frames, b_f is the width of the flange under consideration, R is the horizontal radius of curvature of the I-girder, L_b/R is the subtended angle between the cross-frame locations, and f_b is the flange stress due to major-axis bending. In traditional practice, the coefficient 0.5 often is increased to 0.6 in Eq. 1 to compensate for the simplifying assumptions utilized in the derivation. AASHTO (2020) Article C4.6.1.2.4b gives an expression for M_ℓ corresponding to Eq. 1.
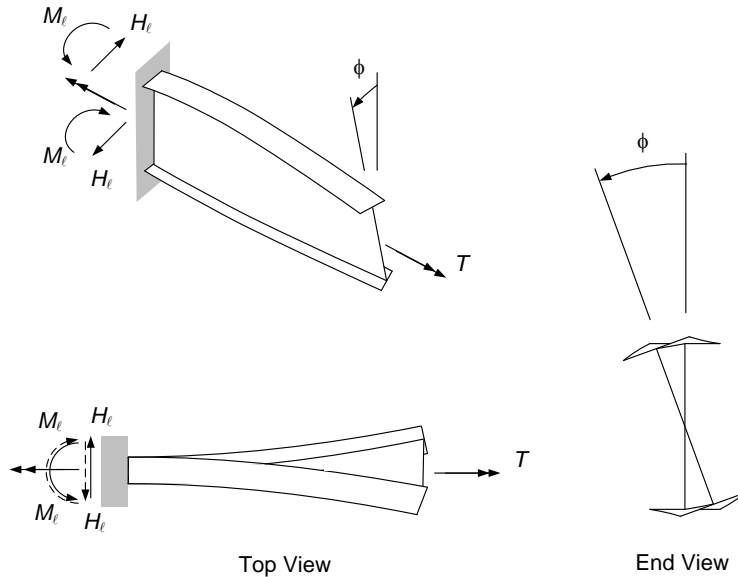
Figure 9. Illustration of twisting and warping deformation of an I-section member.

If one considers a spacing of the cross frames such that the subtended angle between them is equal to the maximum value of $L_b/R = 0.1$ permitted by AASHTO (2020) Article 6.7.4.2 for curved I-girder bridges in the final constructed condition, then one can see that L_b/b_f must be limited to 6.0 in order to restrict f_ℓ to $0.3f_b$. At $L_b/R = 0.05$, the corresponding value of L_b/b_f increases to 12. The value $f_\ell = 0.3f_b$ is suggested as a target for preliminary design in the Commentary to this article.

Torsional loading on fascia girders, due to eccentric concrete deck overhang loads acting on cantilever forming brackets, can be important to consider during construction in straight as well as curved bridges. Also, the use of discontinuous cross frames in straight or curved bridges with significant support skew, while alleviating excessive cross-frame forces in certain situations, can lead to significant torsional loading and flange lateral bending in the I-girders. Furthermore, significant flange-level lateral bending can be induced due to wind loads acting laterally on the bridge, particularly prior to placement of the slab. In this latter case, it is sometimes beneficial to provide flange-level lateral bracing in one or a few unbraced lengths adjacent to the piers and abutments, as shown in Figure 11, to reduce the span of the I-girders in weak-axis lateral bending. AASHTO (2020) Article C6.7.5.2 recommends this practice, and suggests that this type of bracing should be considered in general to help prevent relative horizontal movement of the girders in spans larger than 200 feet. Heins et al. (1982) have showed that there is rarely a need for bottom

flange wind bracing on I-girder bridges in the final constructed condition when full-depth cross frames are used. Shorter span bridges can be designed efficiently and economically without the use of flange-level lateral bracing.

Top flange lateral bending moments (M_ℓ)

$qL_b^2/12$ $qL_b^2/24$ $qL_b^2/12$

M

M

$q = M/Rh$

$=$

M

M

Cross-frame reaction (typ.)

$q = M/Rh$

Equivalent radial load on curved flanges

h = distance between flange centroids
L_b = unbraced length between cross-frames
R = horizontal radius of curvature

Bottom flange lateral bending moments (M_ℓ)

$qL_b^2/12$ $qL_b^2/24$ $qL_b^2/12$
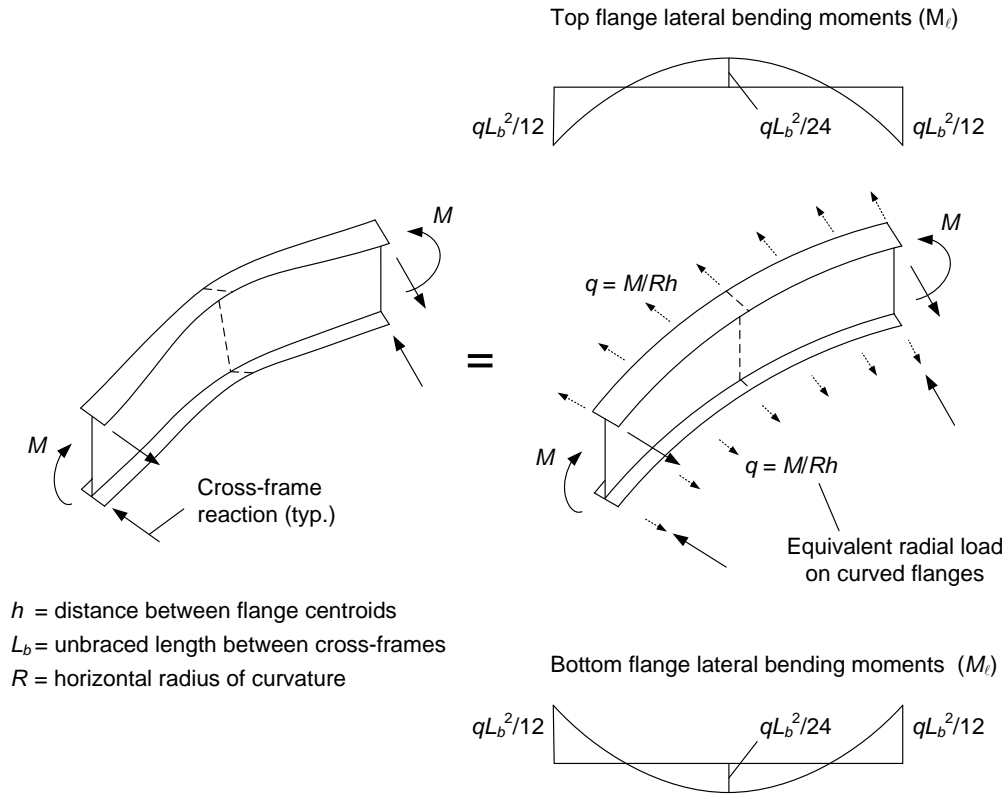
Maximum flange lateral bending stress:

$$f_\ell = \frac{M_\ell}{S_{yf}} = \frac{qL_b^2/12}{A_f b_f/6} = \frac{[M/Rh]L_b^2/12}{A_f b_f/6} = \frac{[(f_b A_f h)/Rh]L_b^2/12}{A_f b_f/6} = 0.5\frac{L_b}{R}\frac{L_b}{b_f}f_b$$

Figure 10. Simplified calculation of flange lateral bending stresses on a curved I-girder subjected to uniform bending moment.
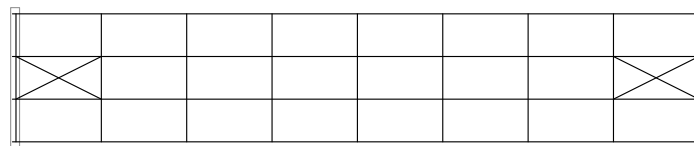
Figure 11. Use of lateral bracing within a few unbraced lengths adjacent to supports to reduce I-girder lateral bending stresses due to wind.

Article C6.7.5.2 recommends that when flange lateral bracing is employed, it should be placed near the top flange of the I-girders. Otherwise, the bracing acts with the deck in the final constructed configuration to form a pseudo box section, in which case it must be designed in general for significant live-load effects. The structural response of the completed bridge system is

10

more efficient when the bracing is placed near the bottom flange, but the lateral bracing and its connections to the I-girders must be designed appropriately for the resulting forces.

Skewed cross frames or diaphragms at bridge support lines tend to deform negligibly in their own plane when the girders experience major-axis bending rotations. Rather, at the support lines, these components tend to rotate about their own skewed axis and/or warp out of their plane due to the major-axis bending girder rotations, as illustrated by the sketch in Figure 12 (NSBA 2016b). This induces a coupled torsional rotation of the girders. When subjected to major-axis bending rotations at the support lines, the girders have to twist to maintain compatibility with the bearing-line cross frames or diaphragms. Furthermore, right (non-skewed) intermediate cross frames in skewed bridges connect to the girders at different points along their spans. As a result, these intermediate cross frames are subject to differential displacements as shown in Figure 13 (Coletti and Yadlosky 2005). Due to the typical large in-plane stiffness of the cross frames relative to the resistance of the girders to vertical displacement at the cross-frame connections, the intermediate cross frames (i.e., the cross frames within the span) tend to rotate about an axis parallel to the longitudinal axis of the girders to follow the girder differential deflections. These cross-frame rotations cause the girders and the overall bridge cross section to twist.

When one end of a cross-frame line is close to the vertical supports while the other end frames into the girders at a significantly larger distance into the span (see Figure 14a), relatively large forces are attracted to the cross-frame members. When the skew angle is larger than 20°, in which case AASHTO (2020) Article 6.7.4.2 requires that the intermediate cross frames must be perpendicular to the girders, the cross-frame member forces may be reduced, at the expense of larger flange lateral bending in the I-girders, by removing the cross frames that frame into the girders closest to the supports or by using staggered cross frames as illustrated in Figure 14b. Another way of reducing the cross-frame member forces near the supports, as well as to eliminate a large number of cross frames, is to use lean-on bracing concepts. The use of lean-on bracing is discussed subsequently in Section 5.2 of this volume.
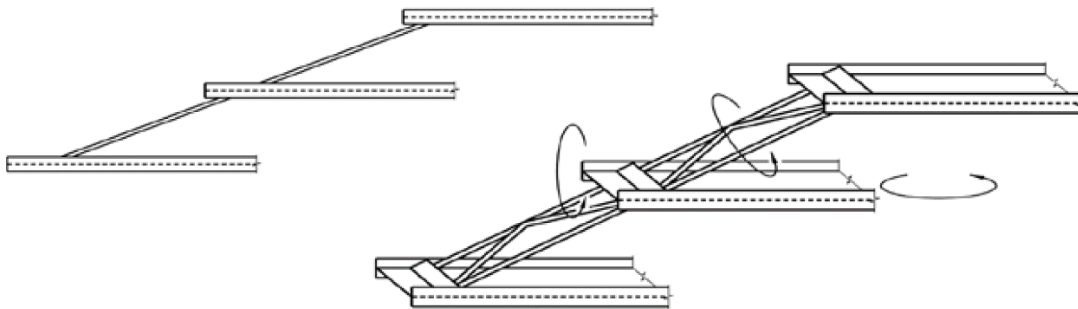
Figure 12. Plan view showing major-axis bending rotations of the girders, corresponding cross-frame rotations along a skewed support line, and the corresponding twist rotation required in the girders, adapted from (NSBA 2016b).
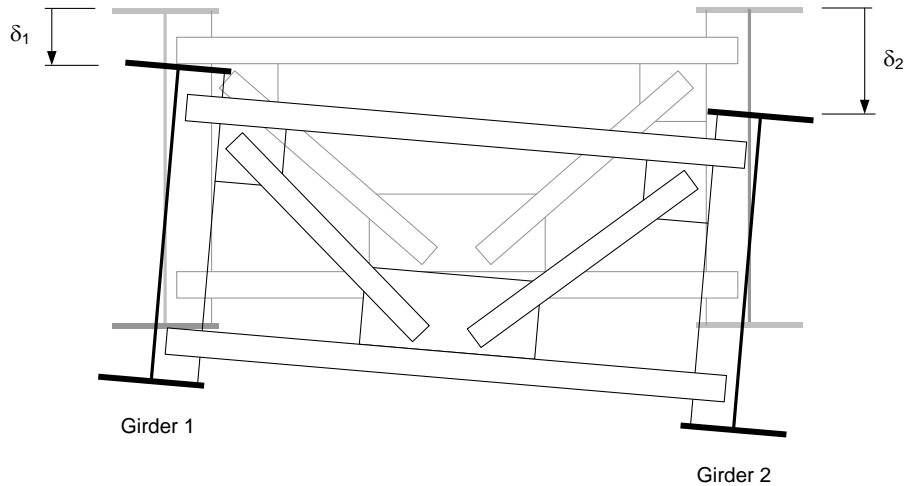
Figure 13 Cross frame, bridge cross section, and girder torsional rotations due to differential girder displacements in skewed bridges (Coletti and Yadlosky 2005).

(a) Continuous cross-frame lines across the bridge

(b) Staggered cross-frames
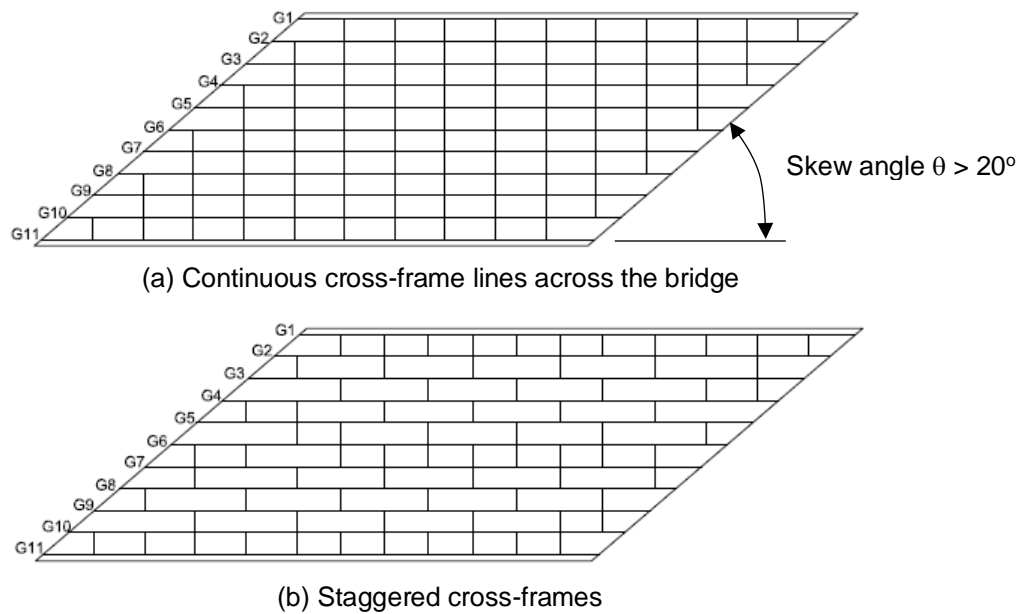
Figure 14. Use of staggered cross frames to reduce the forces attracted to the cross-frame members in skewed I-girder bridges.

AASHTO (2020) Article C6.7.4.2 suggests that, while the girder flange sizes are increased due to the additional flange lateral bending associated with the use of staggered cross frames, this increase often is not significant. Furthermore, the corresponding increased cost is often offset by the reduced cost of providing fewer and smaller diaphragms or cross frames, and smaller diaphragm or cross-frame connections. The bridge in Figure 14a uses 100 cross frames while the equivalent bridge in Figure 14b uses only 75 cross frames to accomplish the same bracing of the girders. In addition, the forces tend to be smaller in the cross frames in the bridge shown in Figure 14b compared to Figure 14a.

In addition, AASHTO (2020) Article C6.7.4.2 indicates that the smallest unbraced lengths, offsets and/or stagger distances should be as large as practicable, but not smaller than $4b_f$, where b_f is the largest girder flange width within the unbraced lengths on either side of the cross frame or diaphragm. In addition, Article C6.7.4.2 recommends that the smallest unbraced length, offsets and/or stagger distances should be larger than $0.4L_b$, where practicable, where L_b is the smallest unbraced length adjacent to the unbraced length, offset or stagger distance under consideration. These practices relax the large transverse stiffness that would otherwise be developed in the short diagonal direction between the obtuse corners of the span in parallel skew bridges. This concept, and other beneficial framing concepts are discussed further in NSBA (2016b).

2.2.3   Integral Piers and Abutments

The use of integral piers allows the Engineer to remove skewed interior support conditions by moving the pier cap up into the superstructure and using a single column pier as shown in Figure 15 or a straddle bent as shown in Figure 16. Continuity of the cap with the pier as shown in Figure 15 maximizes the pier column efficiency by approximately halving the longitudinal moments compared to conventional cantilever columns. Furthermore, integral pier caps help satisfy vertical clearance requirements and improve the design aesthetics. Abu-Hawash et al. (2005) suggest that redundancy requirements at integral steel pier caps can be satisfied by using twin HPS I-girders.

Figure 15. Typical post-tensioned concrete integral bent cap with a single column pier (Wasserman 1997) (courtesy of Tennessee DOT and NSBA).

In addition, jointless bridge decks and integral abutments are used commonly in many U.S. states for steel stringer-type bridges having maximum total lengths from 250 up to 400 feet (Wasserman 1987; Wasserman and Walker 1996). In these bridges, the girders are encased in the abutments at the ends of the structure, thus eliminating joints that potentially leak and damage the girder ends, and are costly to maintain. Thermal movements are accommodated within the foundation, and are assumed unrestrained in the design of the superstructure. Figure 17 shows a typical integral abutment detail for a steel I-girder bridge. Various devices are utilized by different organizations to accommodate the thermal movements without causing damage to the substructure or superstructure. These include: (a) limiting the bridge length, skew and/or horizontal curvature, (b) using select backfill materials and/or uncompacted backfill, (c) spanning the area disturbed by the

foundation movements immediately behind the abutments with the approach slab, thus avoiding settlement of the slab and the associated surcharge loads, (d) limiting the foundations to a single row of vertical piles, (e) specifying the pile type and requiring a minimum pile length, (f) orienting vertical H-piles such that they are subjected to weak-axis bending due to the longitudinal movements, (g) providing a hinge detail within the abutment to limit the moment developed at the tops of the piles, (h) anchoring the approach slab to the superstructure with a detail that allows rotation of the approach slab at the abutment, to accommodate settlement of the approach fill and (i) provision of an expansion joint at the roadway end of the approach pavement (FHWA 1980; Wasserman 1987; Wasserman and Walker 1996; Weakley 2005; Yannotti et al. 2005).

Figure 16. Straddle bents with integral steel pier caps (Abu-Hawash et al. 2005) (courtesy of Iowa DOT, HDR Engineering, and NSBA).
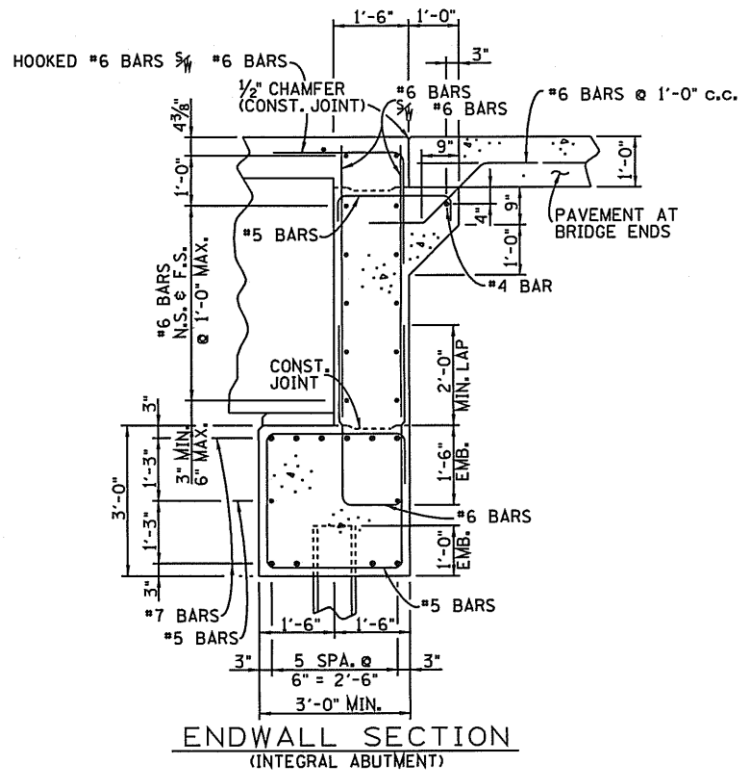
Figure 17. Typical integral abutment detail (courtesy of Tennessee DOT).

In cases involving longer bridges, larger skew angles, abutments resting on rock, massive cantilever abutments, etc., where the foundation is less likely to accommodate the required movements, semi-integral abutments are a second option to eliminate deck joints. In this case, the girders typically are integral with the backwall, but the required movements are accommodated by separating the backwall from the abutment stem, as shown in Figure 18. In semi-integral abutments, the girders are seated on expansion bearings.
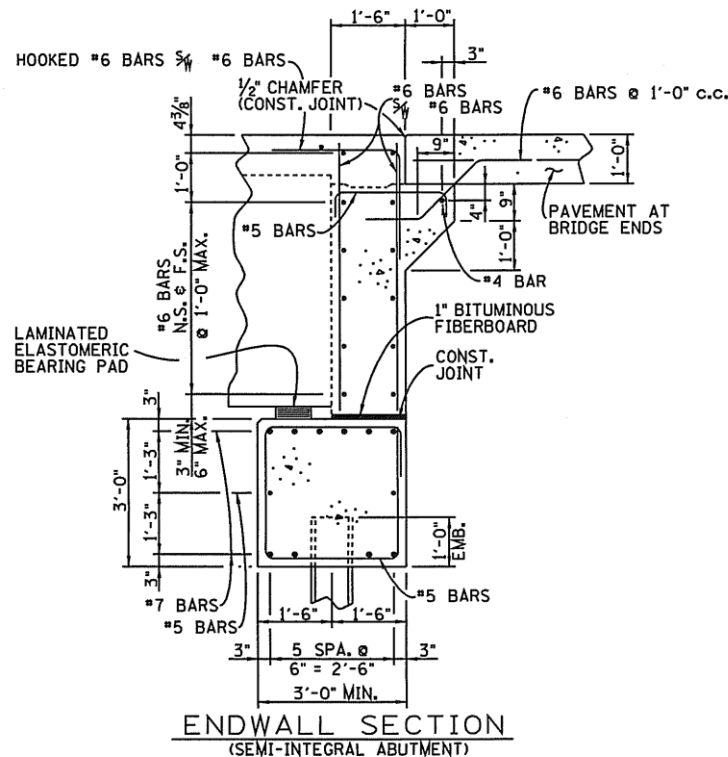
Figure 18. Typical semi-integral abutment detail (courtesy of Tennessee DOT).

2.2.4 Temperature Movements

In bridges where expansion joints are required, orientation of the bearings toward a fixed point allows the bridge to expand freely in both the longitudinal and transverse directions. In curved bridges, this is accomplished by orienting the bearings to permit expansion along a chord that runs from the fixed point to the bearing element under consideration, as shown in Figure 19 (NSBA 2004). This bearing arrangement does not eliminate thermal stresses due to a temperature differential through the depth of the superstructure. AASHTO (2020) Article 3.12.3 provides requirements for consideration of these thermal effects, but the commentary to this section indicates that these effects may be neglected at the discretion of the bridge owner for cases such as multi-beam bridges, where experience has indicated successful performance without their consideration. It should be noted that the orientation of the bearings that minimizes the horizontal forces from the substructure due to thermal expansion of the bridge generally differs from the orientation that minimizes the horizontal forces from the substructure under gravity loads.

Poellot (1997) describes one variation of the above approach used by the Pennsylvania DOT. In this approach, an interior support in a continuous-span unit is fixed in the tangential (longitudinal) direction but is freed to move radially. The end bearings are fixed in the radial direction and are freed to move tangentially. Other interior bearings are designed as "floating," or free to move in all directions. Both the above chord method and the Pennsylvania method are essentially statically determinate and therefore do not develop any forces due to uniform temperature change. The Pennsylvania method eliminates potential misalignments of the roadway at the abutments by allowing radial movements at the interior supports rather than at the end bearings.

EXP.   EXP.   FIXED   EXP.

Chord lines & direction of movement

Guide bars and slotted holes for expansion bearings shall be oriented parallel to the direction of movement
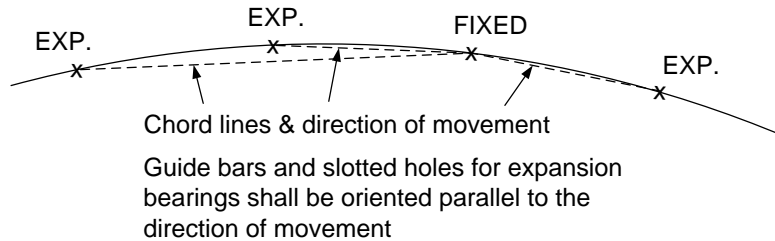
Figure 19. Bearing orientation to accommodate thermal movement on a horizontally curved alignment (NSBA 2004).

2.3   Box-Section Stringer Systems

For bridges subjected to significant torsion, box-girders provide a more efficient usage of material. Because of their significant torsional stiffness, box girders are also better suited for cantilevering during construction and generally exhibit smaller deflections during erection handling. Curved I-girders typically must be connected with cross frames to ensure their stability, but they are more easily deformed to fit up with the other deflected portions of the partially completed structure during erection.

Box girders resist torsion predominantly by uniform (St. Venant) torsional shear stresses that act circumferentially around their closed cross-section periphery as shown in Figure 20. For practical bridge box cross sections, the warping constant is essentially zero and therefore the warping stresses associated with the thin-walled beam theory response are small. Nevertheless, distortion of the cross-sectional shape in box girders leads to important plate bending and longitudinal (warping) stresses (see Figure 20). The magnitude of these stresses must be limited by providing intermediate internal cross frames to maintain the cross-sectional profile of the box.

Box girders are also an efficient option in bridges requiring shallow cross-section depths. Their flanges can be made much wider than in I-girders of comparable depth, thus avoiding the need for inordinately thick flanges with shallow-depth I-girders. Although AASHTO (2020) Article 2.5.2.6.3 does not suggest optional L/D limits for steel box-girder bridges, it does suggest a maximum limit of $L/D = 40$ for continuous-span adjacent box beams in prestressed concrete. This limit also appears to be a reasonable maximum for continuous-span steel boxes. However, box girder web depths usually should not be less than 5 feet to facilitate fabrication and inspection (Hall 1997; Kase 1997). Also, Article 2.5.2.6.3 suggests that girder depths generally should be larger in curved bridges to help control relative girder vertical deflections. Due to these requirements, steel box girders are used as stringers mostly for spans larger than 125 to 150 feet.

Box girders are somewhat less efficient than I-girders in shorter spans having relatively small torsion and/or liberal depth requirements, essentially because they have two webs. Furthermore, support skew in box girder bridges results in high localized stresses that are difficult to analyze and are difficult to design for. Due to this complication, Poellot (1997) states, "I-girders often provide the best solution for skewed bridges." Article C6.11.1 of AASHTO (2020) states, "Transverse bending stresses [i.e., the plate bending stresses illustrated in Figure 20] are of particular concern in boxes that may be subjected to large torques; e.g., single box sections, sharply curved boxes, and boxes resting on skewed supports."
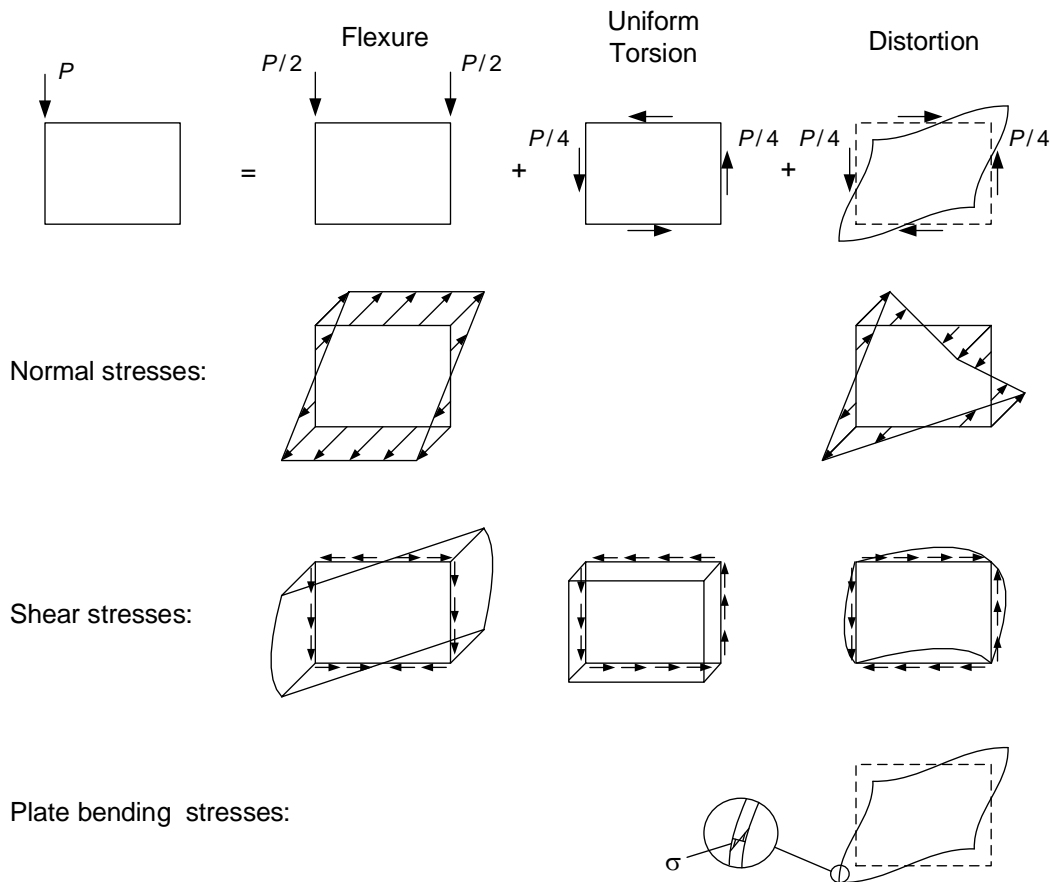
Figure 20. Stresses in a single box girder subjected to an eccentric load.

The torsional equilibrium of box-girder bridges is less dependent on the interaction between the girders, i.e., the transfer of the cross-frame shears associated with the V-loads shown in Figure 8. The significantly higher torsional stiffness of individual box girders allows them to develop substantial St. Venant torques that resist the overall torsion on the structure. This reduces the differences in the girder major-axis bending moments across the bridge width caused by the overall torsion and the V-loads in I-girder bridges. In fact, bridges supporting a roadway with single or dual traffic lanes often can be supported by a single box, assuming that redundancy (fracture critical) member considerations are addressed. Box girders are very efficient in resisting the torsion in curved bridges without the need for interaction between girders through a system of external diaphragms and cross frames. As a result, intermediate external cross frames often can and should be avoided. However, the Engineer should check for differential displacements between girders

17

during construction. For example, in some cases, external cross frames may be beneficial in limiting the differential displacements during partial width slab pours. If a pair of bearings is provided to develop a torsional reaction under each box at the supports, external diaphragms also may be eliminated at these locations unless they are needed to support an expansion joint at end supports. AASHTO (2020) Article 6.7.4.3 requires external cross frames or diaphragms at end supports to accommodate expansion joints and presumably to ensure robust girder end conditions. It is important to note that girder torsional rotations at the support lines produce rotations within the spans that add with the torsional rotations due to the girder deformations.

Tub-girders (Figure 21) are the most common type of steel box cross section in US bridge practice. The use of closed-box sections, i.e., sections with a wide steel plate for both the bottom and top flanges, is rare due to costs associated with safety requirements for working inside of these types of members. AASHTO (2020) Article 6.7.5.3 requires that tub girders must be constructed with a full-length top lateral bracing system with one exception – straight tub girders in which the stability of the top flanges between the diaphragms and the overall global stability of the bridge are investigated using the Engineer's assumed construction sequence. Prior to the composite concrete deck becoming effective, girder lengths that do not have a top lateral bracing system are open sections with a shear center located below the bottom flange (see Figure 22). As such, they exhibit significant torsional warping stresses and deformations, and their overall lateral-torsional buckling resistance is substantially reduced.
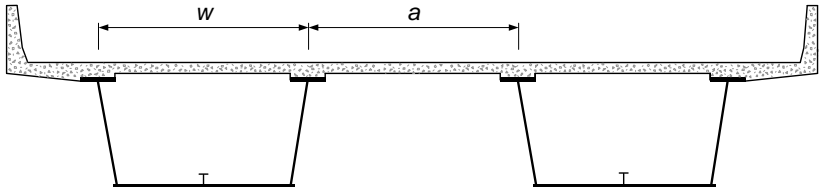
Figure 21. Representative tub-girder bridge cross section.
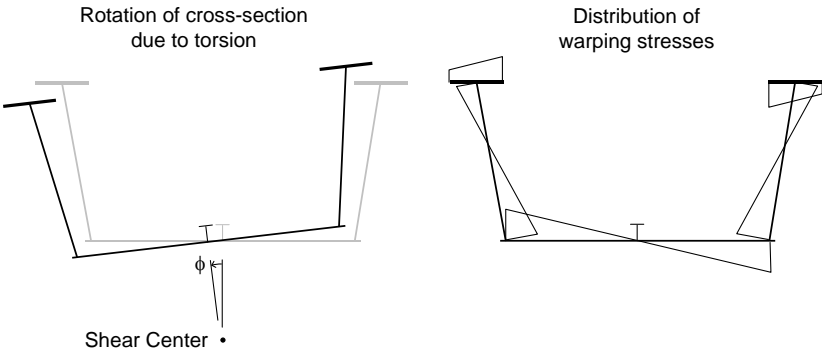
Figure 22 Shear center location and predominant torsional deformations for a tub girder section that does not have a top-flange bracing system.

The top lateral bracing system in tub-girder bridges participates with the girder top flanges in resisting major-axis bending. Fan and Helwig (1999) provide equations for estimating the corresponding bracing member forces due to overall girder flexure. The forces in the lateral bracing system tend to be sensitive to the deck casting sequence. As such, if these members are optimized based on an assumed casting sequence, it is imperative that the casting sequence be shown on the contract plans. AASHTO (2020) Article C6.7.5.3 indicates that field tests have shown that the additional forces attracted to the top lateral bracing system are negligible after composite action of the deck is achieved.

The participation of the top lateral bracing system in resisting the overall flexure also can induce significant lateral bending stresses in tub-girder top flanges during construction. Alternating Warren type single-diagonal lateral bracing systems tend to produce the largest flange lateral bending stresses. In curved bridges, the bracing member forces and top flange lateral bending stresses can be mitigated by the use of a Pratt type configuration for the top lateral bracing (see AASHTO (2020) Article C6.7.5.3). The bracing members are oriented based on the sign of the torque, such that the forces induced in these members due to torsion offset their compressive or tensile forces caused by overall flexure.

Prior to the deck being made composite, lateral bending also occurs in discretely-braced top flanges of tub sections with inclined webs, due to distributed lateral loads transmitted from the webs. These loads come from changes in the web flexural and St. Venant torsional shears per unit length along the members. In terms of elementary beam theory, this is similar to $p = dV/dx$, where p is the transverse distributed load per unit length, V is the internal shear force and x is the position along the member length. Other sources of significant top flange lateral bending are the same as for I-section members. During construction, prior to the slab being made composite, flange lateral bending stresses due to horizontal curvature as well as due to eccentric concrete deck overhang loads acting on cantilever forming brackets are of particular importance. Design Examples 4 (Three-span Continuous Straight Tub Girder Bridge) and 5 (Three-span Continuous Tub-Girder Bridge) of this Handbook discuss the various stresses that need to be considered.

Steel box girders with a normal density concrete deck are efficient up to about 500 to 700 foot span lengths. Beyond these lengths, the dead weight of the structure becomes more and more significant, and the use of an orthotropic steel deck is common. Also, other structural systems discussed below are competitive at these longer span lengths. The two longest steel box girder spans in the world are 980 and 1230 feet respectively in the Costa-e-Silva Bridge in Rio de Janeiro, Brazil (Figure 23 and Figure 24) and the Sfalassà Viaduct in Calabria, Italy (Figure 25). The Costa-e-Silva Bridge has three continuous spans of 660, 980 and 660 feet. Both of the end spans are cantilevered an additional 100 feet into the adjacent spans. The Sfalassà Viaduct achieves its record span by the use of slanted leg supports, reducing the girder bending moments by arch action.

Figure 23. Costa-e-Silva Bridge in Rio de Janeiro, Brazil, second-longest box-girder span, 980 ft (courtesy of www.structurae.de).

(a) Side elevation units: ft
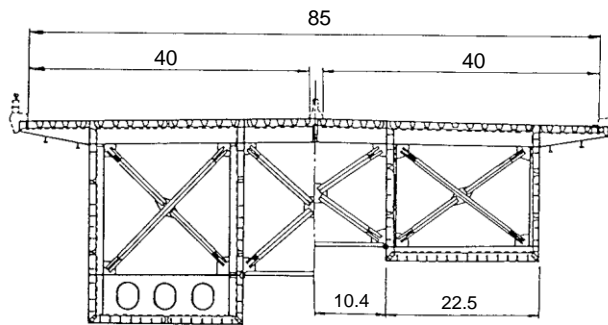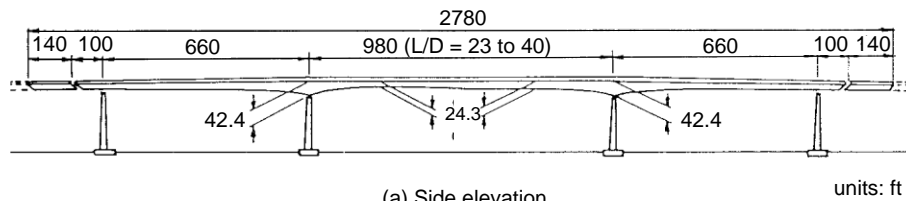
(b) Cross-section

Figure 24. Costa-e-Silva Bridge side elevation and cross section (adapted from Ito et al. (1992) and Wolchuk (1997)).

Figure 25. Sfalassà Viaduct in Calabria, Italy, longest box-girder span, 1230 ft (courtesy of www.structurae.de).

2.4 Truss Bridges

In all of the above bridge types, the structure tends to conform to the roadway and supports it from underneath. Through-girder bridges have been constructed in the past, but these systems are relatively inefficient since the deck cannot be used compositely. Furthermore, all of the above structures support their loads largely by stringer bending actions. In addition, the stringers have solid webs that frame between their flange elements.

As the largest spans discussed in the above sections are approached, the Engineer must consider alternative arrangements that involve "open" webs, greater overall depth, and components that are primarily loaded in tension or compression. The use of high-strength elements becomes particularly beneficial for these systems, due to their larger depth, longer spans, higher dead-to-live load ratios and smaller live-to-dead load stresses. Furthermore, the roadway may be located above, within and or below the structural system, and the roadway geometry tends to be relatively simple compared to complex plans such as that shown previously in Figure 6. Truss and arch bridges are viable for intermediate spans beyond the above limits, while cable-stayed and suspension bridges are necessary for the longest spans. Any of these systems may be used of course for smaller span lengths, where stringer systems are viable, for various aesthetic and/or functional reasons (e.g., maximizing clearance below the roadway). Also, it is common that various combinations of the different structural systems may be used in moderate to longer-span structural systems, e.g., use of bottom flange bracing on an I-girder bridge to accomplish pseudo-box action, use of trussed arches, or use of I-girders, box-girders or trusses as deck systems and stiffening elements in cable-stayed and suspension bridges. Truss bridges are addressed briefly in this section, followed by arch and cable-supported systems in the next two sections.

Truss bridges achieve their efficiency for spanning longer distances via their light weight due to triangulation and the primary action of their members in axial tension and compression. Modern highway truss bridges are predominantly either continuous or cantilever structures. Cantilever bridges have intermediate hinges between the supports in their main span and a central portion of the main span that is suspended between these points. Typical configurations of truss bridges

include deck trusses, half-though trusses and through trusses, based on the location of the roadway with respect to the depth of the structure. The Ikitsuki Ohashi Bridge in Nagasaki, Japan (Figure 26) holds the record span length for a continuous truss bridge (1300 feet) while the Quebec Bridge in Quebec, Canada (Figure 27) has the longest cantilever span at 1800 feet.

Figure 26. Ikitsuki Ohashi Bridge, Nagasaki, Japan, longest-span continuous truss bridge, 1300 ft main span (www.sight-seeing.japan.com).

Figure 27. Quebec Bridge in Quebec, Canada, longest span cantilever truss bridge, 1800 ft main span (courtesy of www.structurae.de).

Truss bridges behave essentially as closed box structures when there are four planes capable of resisting shear and the end portals participate significantly in transferring lateral loads to the bearings. Their chord and web members are typically H, channel, or box-sections. AASHTO (2020) Article 6.14.2.2 requires the members to be symmetrical about the central plane of the truss. The top chord in a half-through truss is typically unsupported in the lateral direction at the panel points, and therefore must be considered as a column with elastic lateral supports at these locations. In deck trusses, the slab provides the dual function of supporting the live loads as well as bracing the top chords of the truss. A concrete deck can be made to act compositely with a deck truss, thus achieving additional structural efficiency.

Trusses are an ideal system to take advantage of advances in high-performance steels (HPS): high strength, high toughness, and improved weldability.

The reader is referred to Kulicki and Reiner (2011) and to Kulicki (2000) for detailed discussions of various attributes of the design of truss bridges.

2.5 Arch Bridges

Arches are one of the most beautiful and expressive structural forms. The arch form reduces the bending moments in the superstructure and resists loads largely by axial compression in the arch ribs, which are the distinctive primary elements of the structure. This compression must be balanced either by large horizontal thrusts at the foundation spring lines or by a tension tie between the ends of the arch. Arches that rely on their foundations to provide these horizontal thrusts are typically referred to as true arches, whereas arches in which the thrusts are developed through tie members are referred to as tied arches. In addition, arch bridges may be classified as deck, through or half-though. True arches are typically deck type, whereas tied arches are often through type. However, both true and tied arches may be constructed with the deck at an intermediate elevation between the spring line and the crown, resulting in a half-through arch. This would occur for example if the foundation needs to be located above the high-water elevation, or if variable foundation conditions require location of the abutments at a specific elevation relative to the height of the deck.

The arch rib itself may be either a truss or a girder. Accordingly, arch bridges are referred to as truss-ribbed or solid-ribbed. Another classification pertains to the articulation of the arch: fixed, two-hinged, or three-hinged. A fixed arch is designed based on complete rotational fixity at its supports. If the span is continuous but free to rotate at is ends, the structure is a two-hinged arch. Tied arches are practically always two-hinged. In some cases, e.g., during construction, a hinge is located at the crown in addition to the end supports. For instance, the top chord in a trussed arch rib may be closed at the crown to complete the erection of the structure. If the axis of the bottom chord follows the load-thrust line for the three-hinged condition, there is zero stress in the top chord and web system. The top chord and the web are stressed only under loads applied after the closure. Therefore, they can be made relatively light and the bottom chord of the rib becomes the main load-carrying member (Wright and Bunner 2011). Solid rib arches are often designed using boxes, to improve their lateral stability. These members may be fabricated with a constant or a variable depth.

In some cases, concrete-filled high-strength steel box sections can be particularly advantageous as arch ribs. The light high-strength steel box section facilitates the construction of the rib, and serves to reduce the overall rib weight, while the concrete infill enhances its compressive strength as well as the completed system stiffness. However, there are unique constructibility challenges with implementing this strategy that need to be considered by the designer.

In a tied arch, the tension tie is typically a plate or box girder. If the tie is relatively stiff in bending compared to the arch rib, it will carry a substantial portion of the live loads. Conversely, if the arch rib is stiff in bending relative to the tie, it will support a larger share of the live loads. Since the contribution of each of these elements to the live load resistance depends on their relative stiffness,

it is possible to optimize their sizes based on aesthetics and/or cost. A shallow flexible tie girder requires a deep stiff arch rib, whereas a shallow flexible arch rib requires a deep stiff tie girder.

Tie girders are fracture critical members. Their redundancy can be improved by bolting their plate components together such that a fracture in one plate will be less likely to precipitate the fracture of the entire member. Tied arches typically experience significant variations in length of the tie under different load conditions. As such, it is common to provide deck joints at intermediate positions along the bridge length. Petzold (2005) discusses a design in which the deck joints are eliminated while the deck is structurally separated from the arch itself. The design by Cassity et al. (2003) utilizes a jointless composite concrete deck with the tie girders to resist residually applied dead loads and live loads.

Most through or half-through arch bridges are constructed with two arch ribs that are each located within a vertical plane. However, the arch ribs are sometimes inclined inwards toward each other to improve their lateral stability. This can also lead to some economy in the design of the bracing system between the arches. A few bridges have been constructed with only one rib and with roadways cantilevered on each side of the rib. In this case, both the arch rib and the deck system must have considerable torsional and lateral rigidity.

Wire rope, bridge strand, prestressing strand/tendons, or rolled sections are used typically for the hangers in tied arch bridges. Bending in the tie girders and the arch rib is reduced generally by shorter spacing of the hangers. Inclined hangers have been used in some tied arch bridges. These types of hangers participate in transferring vertical shear forces and tend to reduce the bending moments in the arch ribs and tie girders. Tied arch bridges with inclined hangers that cross each other at least twice are referred to as network arch bridges

Both the in-plane and out-of-plane stability of arch ribs are essential considerations. AASHTO (2020) provides limited guidance with respect to the stability design of these components. Article 4.5.3.2.2c of AASHTO (2020) gives in-plane effective length factors for use in beam-column moment amplification equations for three-hinge, two-hinged and fixed arches. It is inferred that these effective length factors also may be utilized with the AASHTO column strength equations in determining the axial resistance of prismatic solid-rib arches. AASHTO Article 4.5.3.2.3 also requires that refined methods of analysis for arches, if used, shall include second-order effects. (AASHTO (2020) generally defines refined methods of analysis as methods that consider the entire superstructure as an integral unit such that the combined system and component deflections and actions are provided by the analysis.) The above approximate AASHTO equations do not account for any vertical restraint from the tie girders. Where such restraint exists, refined analysis methods will give larger buckling loads and smaller moment amplification.

For checking stability in the lateral direction (i.e., the direction normal to the plane of the arch rib), the effective length may be taken as the distance between the rib bracing points when a lateral bracing system of adequate stiffness is provided. Special consideration of arch-end portal areas is generally necessary. Refined analysis tools provide one way of assessing the adequacy of the lateral bracing system and the end portals.

Slant-legged rigid-frame bridges such as the one shown in Figure 28 are essentially a deck-type arch form. In this type of bridge, the main I-girders in the center span function both to support the

floor system, which spans between the rigid frames, as well as to resist the overall loads by arch action and axial compression. The slanted legs in these bridge types typically have variable depth webs. The Sfalassà Viaduct shown in Figure 25 is a slant-legged rigid-frame design.

The LuPu Bridge in Shanghai, China (Figure 29 and Figure 30), built in 2003, has the second longest span worldwide for a steel arch bridge (1800 feet). This structure is a two-hinged half-through arch with a steel box girder rib and an orthotropic deck on floor beams and longitudinal box girders. This span was eclipsed by the Chaotianmen Bridge in Chongqing, China in 2009. The Chaotianmen Bridge has a span of 1810 ft, and is a trussed through arch design.

Figure 28. Slant-legged rigid-frame bridge (courtesy of HDR).

Figure 29. LuPu Bridge in Shanghai, China, longest span steel arch, 1800 ft (courtesy of www.structurae.de).

Figure 30. LuPu Bridge deck system (courtesy of www.structurae.de).

The New River Gorge Bridge in West Virginia (Figure 31) is the longest span steel arch bridge in the United States (1700 feet). This structure is a two-hinged deck-type arch with a trussed rib.

The reader is referred to Wright and Bunner (2011), Petzold (2005) and Xanthakos (1994) for detailed discussions of various attributes of the design of arch bridges. Heins and Firmage (1979) discuss the design of slant-legged rigid-frame highway bridges.

Figure 31. New River Gorge Bridge in West Virginia, longest span steel arch in the United States, 1700 ft (courtesy of HDR).

2.6 Cable-Supported Bridges

2.6.1 General

The lightness and overall structural efficiency of cable-supported structures are readily apparent even to non-engineers. The two major classes of cable-supported bridges are suspension and cable-stayed. The fundamental difference between these bridge types is the manner in which the deck system is supported by the cables. In suspension bridges, the deck system is supported at relatively short intervals by vertical suspenders, which in turn, are supported by the main cables (see Figure 32a). Furthermore, the main cables are relatively flexible since they are form-active; that is, their geometry is influenced significantly by the magnitude and distribution of the loadings. Conversely, in cable-stayed bridges, the deck system is supported directly from the towers by relatively straight cables (Figure 32b). This results in a stiff elastic support of the deck by the cable system compared to typical suspension bridges. The suspension bridge tends to be more efficient in supporting dead load, via the load transfer to the towers in pure tension by the funicular action of the main cables. As such, this system type is required for the longest bridge spans, where the dead load stresses become more and more dominant. Conversely, cable-stayed systems are generally more efficient in supporting live loads, which are less uniform.

The Akashi Kaikyo Bridge on the Kobe-Naruto Route in Japan currently has the longest suspension span at 6530 feet (Figure 33), whereas, the world's longest cable-stayed span is the Russky Island Bridge in Vladivostok, Russia at 3620 ft (Figure 34).

The Russky Island Bridge, which opened in 2012, connects Russky Island with the city of Vladivostok, Russia. It crosses the Eastern Bosphorus Strait, linking the mainland with the island. The bridge has 11 spans, two at 197 ft, two at 276 ft, six at 236 ft, and one 3620 ft central span. The deck system is composed of steel inclined-wall box sections with a cast-in-place reinforced concrete slab. The bridge's pylons are 1060 ft in height.
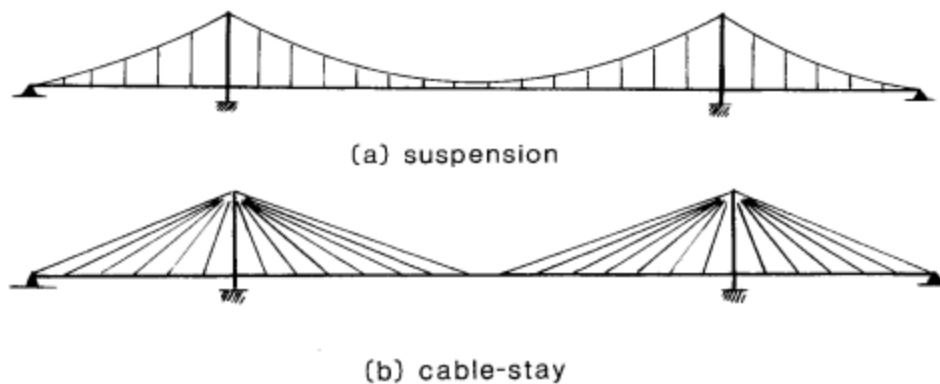
Figure 32. Cable suspended bridge systems, (a) suspension and (b) cable-stayed (reprinted with permission from Podolny and Scalzi).

Figure 33. Akashi Kaikyo Bridge, longest suspension span (6530 ft) (courtesy of www.structurae.de).

Figure 34. Russky Island Bridge, longest cable-stayed span in the world (3260 ft) (courtesy of Road Traffic Technology).

The Cooper River Bridge between Mount Pleasant and Charleston, South Carolina, has the longest cable-stayed span in the United States at 1550 feet (Figure 35). This three-span bridge has steel I-girder edge beams composite with a precast deck system.

Longer spans have been contemplated for both of the above system types; however, for larger span lengths, an increasing fraction of the allowable cable stresses is taken up by dead load. Also, the efficiency of the stays in cable-stayed bridges is reduced more and more by the sag under their self-weight as the length of the stays is increased. The Akashi Kaikyo Bridge utilizes cables with a tensile strength of 260 ksi. Higher strength and/or lighter cables will be needed to achieve significantly longer spans in the future.

(a) Aerial view

(c) Installation of edge girder showing cable anchorage and studs for development of composite concrete deck

(b) Elevation view of pylons and cable stays

(d) Placement of a precast concrete deck panel

Figure 35. Cooper River Bridge, longest cable-stayed span in the USA (1550 ft) (courtesy South Carolina DOT).

2.6.2 Suspension Bridges

Most suspension bridges utilize stiffening box girders or trusses at the deck level to ensure aerodynamic stability of the structure as well as to limit the local live load deformations in the deck system and to distribute these loads among the vertical suspenders. The bridge towers transfer a large vertical compression from the main cables to the foundation, and act as lateral supports for the cables and the deck system. The main cables are tied externally to massive anchorages at the ends of the structure in most suspension bridges. However, for moderate spans, the ends of the main cables can be attached to the stiffening system, in which case the structure is self-anchored. If net uplift occurs at the end supports, a tie-down system is necessary.

Suspension bridges usually have three spans. When the side spans are relatively short or are not required, a single suspended span may be used. In this case, the portions of the main cables from the towers to the anchorages are essentially straight and are referred to as straight backstays. Two- or four-span suspension bridges are rare because generally it is difficult to resist the longitudinal forces at the tops of the towers resulting from live loads; due to the bending of the towers, these types of structures are highly flexible.

The center and side spans of suspension bridges are usually simply supported. The stiffening girder or truss is sometimes made continuous to reduce the difference in slopes occurring between the adjacent spans. However, this results in relatively large bending stresses at the towers. I-girders are not typically used as stiffening elements, except for short spans, because of the better aerodynamic characteristics of boxes and trusses. Typical span-to-depth ratios for stiffening girders or trusses range from about 1/60 to 1/70 of the main span (Podolny and Goodyear 2011).

Most suspension bridges utilize vertical suspender cables. However, inclined suspender cables have been used in some cases. Inclined cables are capable of transferring vertical loads by truss action between the main cables and the stiffening truss or girder.

Typical suspension bridge towers are portal frames. The towers must have a minimum width in the direction of the spans sufficient to provide stability, but the width also must be sufficient at their top to support the cable saddles. Most suspension bridges have their cables fixed at the top of the towers. The towers in longer span bridges generally have fixed bases, but rockers can be used at the base for short spans. Because of the tower relative slenderness, the bending stresses in the towers due to longitudinal deflections at the tower tops are relatively small.

The main cables in modern long-span suspension bridges usually consist of high-strength parallel wire strands. However, helical-strand type cables are used in many small to moderate-length suspension bridges. The strength and modulus of elasticity of these types of cables are reduced by a factor of about one-eighth due to the helical placement of the strands.

Suspension bridges generally require the use of large-deflection theory, or geometric nonlinear analysis, for the calculation of load effects. Use of linear elastic theory results in an overestimation of the system stresses and deflections.

2.6.3 Cable-Stayed Bridges

The deck system in cable-stayed bridges acts as a continuous girder over the interior piers, but with additional intermediate elastic, but relatively stiff, supports at the anchoring points of the stay cables. Typical depths of the deck system range from 1/60 to 1/80 of the span (Podolny and Goodyear 2011). The cables induce compressive forces within the deck system. Generally, the deck is designed to participate with the girders in supporting these forces. The overall structure is usually a closed or self-anchored system.

The designer has a wide range of attributes at his or her disposal that influence the behavior of cable-stayed bridge structural systems. These include the number and arrangement of the spans, the number and orientation of the cable-stay planes, the layout and number of stays, the type of cable, the type of deck system, and the construction of the towers.

Although three-span arrangements such as those shown in Figure 32b and Figure 35a are the most efficient, two-span layouts such as in Figure 36 are also feasible for cable-stayed bridges. It is usually desirable to anchor the stays within the side spans of the bridge. However, if the side-span is relatively short, some or all of the stay cables may be tied to an independent anchorage in the ground. Three-span bridges with a center span length of about 55 % of the total length and two equal side anchor spans are common (see Figure 32b). The cables tied to the end supports or to ground anchorages within the anchor spans attract larger forces than the cables attached to the deck system in these spans.
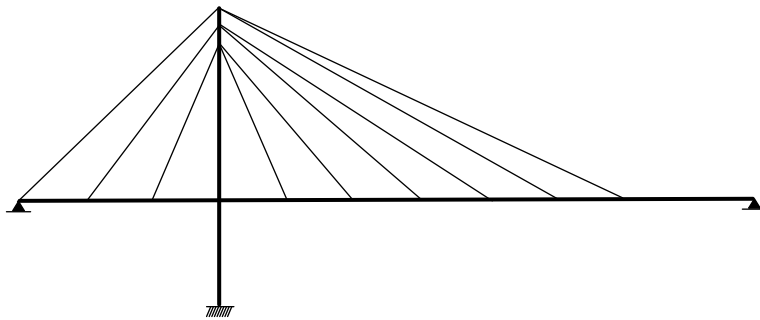
Figure 36. Representative two-span cable-stayed bridge system.

Cable-stayed bridges with more than three spans tend to induce large bending in the towers under live load. The efficiency of these structures can be improved by tying the tower tops together with horizontal cables (Figure 37a), tying the tower tops to the girder and tower intersection points at the adjacent towers (Figure 37b), adding additional tie-down piers at the span centers (Figure 37c) or adding crossing cables at the midspans (Figure 37d) (Tang 2000).
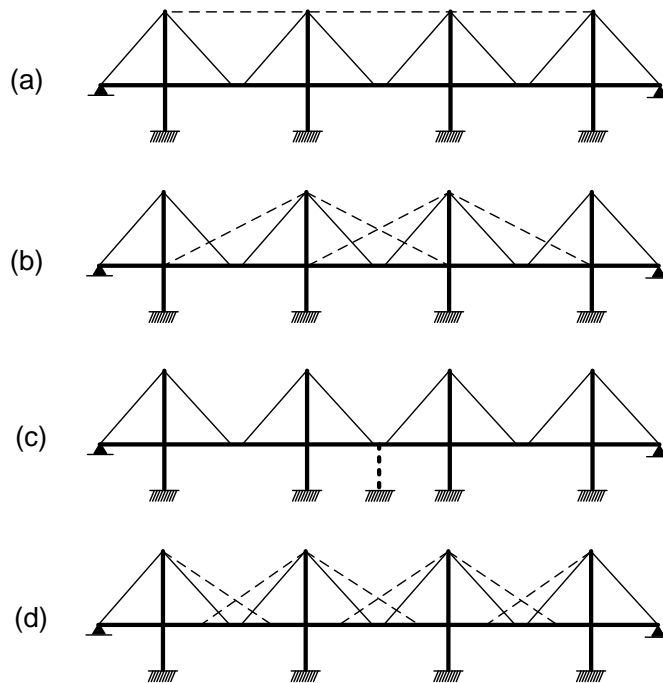
Figure 37. Methods to avoid large tower bending moments in cable-stayed bridge systems with more than three spans (Tang 2000).

The use of one plane of cable stays (Figure 38) is aesthetically pleasing and halves the number of required shafts in the towers. However, this requires the use of a torsionally stiff deck system. Conversely, the use of two planes of stays at the edges of the superstructure permits the use of torsionally flexible I-girders (see Figure 35), although the use of box girders can be advantageous with two-plane systems in certain bridges. The two-plane system can be oriented vertically or twin inclined planes can be connected from the edge of the deck to either an A or inverted Y tower. Inclined stays increase the torsional stiffness of the overall structural system.

(a) Overall view   (b) Deck svstem

Figure 38. Duisberg-Neuenkamp Bridge, Duisberg, Germany, 3-span cable-stayed bridge utilizing a single plane of stay cables (1150 ft main span) (courtesy of www.structurae.de).

The two extreme layouts of cable stays are the radial pattern, in which every stay passes over the top of the tower(s) (Figure 32b) and the harp pattern, in which all the stays are parallel and are

spaced roughly equally over the height of the towers (Figure 39a). Structurally, the radial pattern is the most efficient, since it avoids placing primary bending moments on the towers and gives the largest angle between the stays and the deck. Also, this pattern allows one heavy backstay cable to support the full unbalanced component of force from the other cables. However, this arrangement complicates the detailing at the top of the tower. The harp pattern induces significant bending in the tower unless every backstay cable is anchored to the ground or above a pier. It is less efficient structurally, but it is easier to detail. The semi-harp pattern is often a satisfactory compromise between these two extremes, allowing fixing of individual cables at the towers while reducing the amount of tower bending relative to that caused by the use of the harp pattern. A typical practice requires that cable-stayed bridges must be designed such that the stay cables are individually replaceable under reduced traffic loading. This requirement tends to steer the designer away from systems with only a few stay cables. Also, in most contemporary designs, all the stays are fixed to the towers.

(a) harp pattern
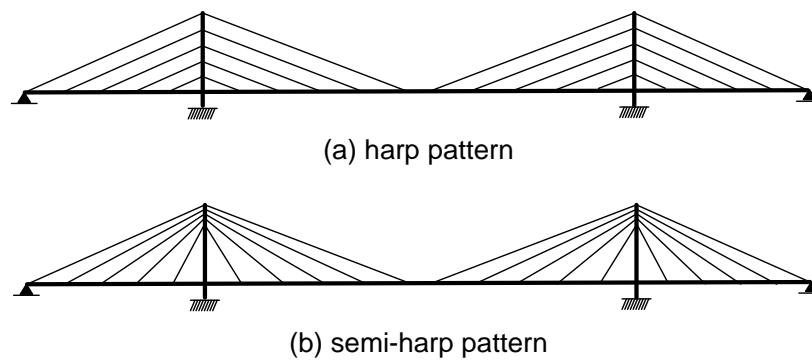
(b) semi-harp pattern

Figure 39. Alternative stay layouts, (a) harp pattern and (b) semi-harp pattern.

Either spiral or parallel wire strand may be used for the stays in cable-stayed bridges. Spiral strand is easier to handle during construction, but has a reduced elastic modulus that depends on the lay length of the spiral. Stays composed of prestressing steels are the most prevalent in recent cable-stayed bridge construction. The pitch of the twisted wires in common seven-wire prestressing strand is relatively long, and therefore the stiffness of the strand is close to that of straight-wire strand and the breaking strength is somewhat larger. The number of strands assembled into the stay cables varies depending on the design force. One of the key considerations in the development of the end sockets or anchorages for cable stays is the fatigue resistance. A number of systems are available that accommodate parallel prestressing strands.

Cable-stayed bridges are highly redundant structures. One important concept of cable-stayed bridge design is the freedom to assign a desired value of force to every unknown in the indeterminate structure. Therefore, the bending moments and forces under the dead load condition can be determined solely based on static equilibrium. There are an infinite number of combinations of dead load conditions for a given cable-stayed bridge. The Engineer can select the one that gives the most advantageous distribution of stresses throughout the structure when the other loads are combined with the dead load.

The construction process must reproduce the selected dead load condition. In a noncomposite bridge, the construction stage analysis, which checks the stresses and deflections in the structure

at every stage of the construction, starts from the selected final condition and works backwards to determine the no-load geometry of all the structural components. However, in composite structures, creep and shrinkage effects also must be accounted for in a forward calculation starting from the beginning of the construction.

For moderate-span cable-stayed bridges, composite concrete decks are common. Though rarely used, orthotropic steel decks may be employed in longer spans, where the dead weight is at a more serious premium. The underlying girders are usually I-sections or box-sections; box sections are essential when torsional stiffness is required. The compression stress in the deck system tends to increase proportionally with the span length. For longer spans, the cross section of the deck system may be increased in size near the towers, where the compression is largest, to offset the axial compression effects.

High-performance steel is ideal for design of the longitudinal girders in cable-stayed bridges. The global moments attracted to the longitudinal girders can be reduced by making the girders smaller and more flexible via the use of higher yield strengths, while influencing the overall stiffness of the structure little.

The towers in cable-stayed bridges may be steel or concrete. For moderate span lengths, steel towers may be advantageous since they can be erected more easily in a limited number of pieces. In addition, their smaller mass can be advantageous for seismic design. The behavior of the bridge differs depending on whether the towers are fixed or pinned at their base. Base fixity increases the moments in the towers significantly, but increases the overall rigidity of the structure. Steel towers generally must be designed for overall and local stability. The tower members typically have a variable cross-section depth, width and plate thickness over their height and are subjected to combined axial compression and biaxial bending moment. In addition, they are supported elastically by the cables and in some cases by the deck system. Therefore, it is most appropriate to design these members using a refined stability analysis.

Tang (1976) considers the elastic buckling of the flexible deck system in cable-stayed bridges. He shows that the buckling load is influenced more by the axial stiffness of the cables than the flexural stiffness of the deck system. Even if the stiffness of the deck system is neglected, the buckling load is typically much larger than the actual loads on the bridge. Model tests (Walther et al. 1999) on cable-stayed bridges with slender concrete decks and closely spaced cables have confirmed that the deck system usually is not critical with respect to buckling.

In contrast to suspension bridge structural systems, the second-order effects on the internal forces and system deflections tend to be significant only in longer-span cable-stayed bridges. Nevertheless, similar to the behavior of arches, the internal stresses in cable-stayed bridges are generally increased due to the second-order effects. This is opposite from the behavior of suspension bridges. The geometric nonlinearity of cable-stayed bridges is small enough such that a first-order analysis is sufficient in many cases. When second-order effects are expected to be more significant, they may be accounted for by first conducting a linear analysis using the nominal geometry to determine the deflections, using these deflections to revise the geometry, and finally conducting a second linear analysis using the revised geometry. The cable stiffnesses are a nonlinear function of the cable tension, due to the sagging of the cables under their self-weight.

AASHTO (2020) gives the following equation for the effective instantaneous elastic modulus of stay cables

$$E_{MOD} = E \Big/ \Big\{ 1 + EAW^2 \cos^5 \alpha / 12H^3 \Big\}$$ (2.6.3-1) (AASHTO 4.6.3.7-1)[1]

where

E = modulus of elasticity of the cable
A = cross-sectional area of the cable
W = cable total weight
α = angle between the chord of the cable and the horizontal
H = horizontal component of the cable force

The reader is referred to Podolny and Goodyear (2011), Walther et al. (1999), ASCE (1992), Troitsky (1988) and Podolny and Scalzi (1986) for detailed discussions pertaining to the behavior and design of cable-supported bridges.

3.0 ELASTIC SYSTEM ANALYSIS, INELASTIC COMPONENT RESISTANCES

The load and resistance factor design approach implemented in AASHTO (2020) uses the general form

$$\Sigma \, \eta_i \, \gamma_i \, Q_i \leq \phi R_n$$ (3-1) (AASHTO 3.4.1-1)

for assessment of the adequacy of the structure. The left-hand side of this equation represents a given design load effect, calculated by analysis. The right-hand side represents the design resistance corresponding to a given limit state. When used to define strength limit states, the left- and right-hand sides of Eq. 1 can be referred to as the required and the available design strengths respectively. A selected component is adequate for a given limit state if the required strength determined by structural analysis is less than or equal to its available design strength. The design load effect or required strength is determined as the largest value from various sums (or combinations) of appropriate nominal load effects, Q_i, multiplied by the load factors η_i and γ_i. The terms γ_i are scale factors that account for the variability and uncertainty associated with each of the nominal loads for a given load combination. The various load combinations account generally for a maximum lifetime event for a certain loading taken with appropriate arbitrary point in time values of other loadings. On the right-hand side of Eq. 1, the ϕ terms are resistance factors, which account for the variability, uncertainty and consequences of failure associated with different limit states. The parameters η_i increase or decrease the nominal loads based on broad considerations of the ductility, redundancy and operational importance of the structure.

---

[1] Note that in Eq. 2.6.3-1, and throughout this volume, the AASHTO equation number is denoted by "AASHTO" and is provided for any equations defined explicitly in the AASHTO (2020) Specifications. That is, for example, Eq. 2.6.3-1 is AASHTO Eq. 4.6.3.7-1. In addition, note that throughout this volume, the section number of the volume is not included in the citation of the equation, when the citation is located in the same section as the equation being referenced. That is, Eq. 2.6.3-1 would be referred to simply as Eq. 1 in Section 2.6.3 of this volume.

With the exception of inelastic redistribution of pier section moments in specific types of continuous-span stringer bridges, and inelastic analysis for extreme event limit states (i.e., earthquake, ice loads, collision by vessels or vehicles and certain hydraulic events), AASHTO (2020) specifies the use of elastic structural analysis for calculation of the design load effects. Conversely, the nominal resistances, R_n, in Eq. 1 are based in general on inelastic behavior of the structural components. For composite stringers, the concrete section is assumed fully effective in positive and negative bending for calculation of the internal forces and moments (in the structural analysis), but it is assumed to be fully cracked in negative bending for calculation of the resistances at strength limit states. These apparent inconsistencies are explicitly addressed at several locations within the AASHTO (2020) Commentary, i.e., see Articles C1.3.1, C4.1, C4.5.2.2, and C6.10.6.2.2, and C6.10.6.2.3. Simply put, the Engineer is allowed to neglect the influence of all material nonlinearity on the distribution of forces and moments within the structure up to the limit of resistance of the most critical component. Neglected effects include residual stresses in the steel, concrete cracking, and various stress contributions that are considered incidental. Numerous physical tests indicate that this approximation is acceptable. It is assumed that the resistance of the complete structure is reached when the left and right-hand sides of Eq. 1 are equal for the most critically loaded component. As explained in Article C1.3.2.4 of AASHTO (2020), multi-stringer bridges usually have substantial additional reserve capacity beyond this resistance level. This is because the live load cannot be positioned to maximize the force effects on all parts of the bridge cross section simultaneously. However, this reserve capacity is not necessary to justify the above elastic analysis assumptions.

There are three situations in steel design where AASHTO (2020) implements specific restrictions to ensure the validity of the above elastic analysis-design approach:

1. For continuous-span girders that are composite in positive bending, AASHTO Article 6.10.7.1 limits the moment capacity to

   $$M_n = 1.3R_hM_y \qquad \text{(3-2) (AASHTO 6.10.7.1.2-3)}$$

   where M_y is the yield moment of the composite section, calculated as defined in AASHTO Section D6.2.2, and R_h is the hybrid factor, unless specific Appendix B6 requirements are satisfied that ensure ductility of the adjacent pier sections. Equation 2 is intended to limit the yielding in positive moment regions of continuous-span girders, where the shape factor M_p/M_y (i.e., the ratio of the composite section plastic moment to its yield moment) can be larger than 1.5, when the inelastic rotation capability of the pier sections is somewhat limited or undefined. The calculation of M_y detailed in Article D6.2.2 accounts for the separate influence of noncomposite and composite loadings on the cross-section elastic stresses.

   In many cases, compact-flange pier sections in straight I-girder bridges satisfy the Appendix B6 requirements without any special modification. However, the support skew must be less than 10 degrees and the ratio of the lateral unbraced length to the compression flange width, L_b/b_{fc}, at the pier sections must be approximately 10 or less (in addition to other requirements) for the use of Appendix B. All continuous-span box girders are required to satisfy Eq. 2 or more restrictive limits. Equation 2 guards against significant partial yielding of the cross section over a relatively large length within the positive

moment region, where the moment diagrams and envelopes are relatively flat. This helps restrict inelastic redistribution of positive moments to pier sections that may have limited ability to sustain these additional uncalculated moments. Also, the Engineer should note that the analysis assumption that the slab concrete is fully effective in tension and compression tends to give a slightly conservative estimate of the true pier section moments, assuming that the cross sections remain predominantly elastic in the positive moment regions.

2. For curved I-girder bridges, all the composite sections in positive bending are required to be considered as "noncompact" sections (see Sections 6.3.3.1 and 6.3.4 of this volume for the definition of a noncompact composite I-section). Furthermore, the use of AASHTO (2020) Appendix A6 is not permitted for curved I-girder sections in negative bending with compact or noncompact webs. Both of these restrictions limit the calculated girder flexural resistance in negative bending to a maximum potential value of

$$M_n = R_b R_h M_{yc} \qquad (3\text{-}3)$$

in the absence of any flange lateral bending, where R_b is the web load-shedding strength reduction factor, equal to 1.0 for noncompact and compact webs and M_{yc} is the nominal yield moment capacity with respect to the compression flange. These restrictions are due to the limited data on the influence of partial cross-section yielding on the distribution of forces and moments within curved I-girder bridges.

Jung and White (2010) provide extensive results from a full-scale curved composite I-girder bridge test as well as parametric extensions of these test results using refined inelastic finite element analysis. All cases considered indicate that the influence of partial yielding on the internal forces and moments is small in curved I-girder bridges up to the limit of resistance of the most critical bridge component based on the plastic moment M_p, with a reduction due to flange lateral bending effects. However, the majority of these studies focus solely on simple-span bridges. Further studies are needed to address the influence of partial cross-section yielding on continuous-span curved I-girder bridges. The benefits of designing positive moment sections using the plastic moment resistance M_p or Eq. 2 can be significant, although AASHTO Article 6.10.7.1.2 specifies a reduction relative to M_p based on ductility considerations (see Section 6.3.3 of this volume). No studies have been conducted to date (2021) that address the potential use of Eq. 2 or another plastic moment-based resistance formula for curved composite box girders in positive bending.

The Engineer should note that the resistance equations for curved I- and box-girders are based generally on some partial cross-section yielding at the calculated limit of the resistance. However, Eq. 2 and other M_p-based resistance equations rely on the development of a larger extent of yielding.

3. The maximum compression stress in the concrete deck is limited to $0.6f'_c$ under all strength loading conditions for noncompact composite I-sections and box-sections in positive bending. This limit is required to ensure linear behavior of the concrete. Furthermore, Article C6.10.1.1.1a of AASHTO (2020) recommends against the use of shored composite construction, which is one of the situations where this limit can potentially be exceeded.

Unshored construction is considered generally more economical. Furthermore, as indicated in AASHTO Article C6.10.1.1.1a, there is limited data on the influence of concrete creep on the response of shored composite I-girders subjected to large dead load.

In addition to the above restrictions, the structural analysis is required generally to consider the separate noncomposite elastic stresses generated in the structure due to self-weight and other loadings before composite action is achieved, as well as the short and long-term elastic stresses generated in the composite structure. Moments from these three different loading conditions may not be added for the purpose of calculating stresses, and stresses from construction processes that include changes in the stiffness of the structure must be determined by considering these changes in the structure. Long-term loading effects are considered by use of a modular ratio of $3n$, where $n = E_s/E_c$ is the modular ratio of the composite section for short term loading. Finally, Article 6.10.1.7 of AASHTO (2020) implements specific slab reinforcing steel requirements for regions subjected to negative flexure. These requirements are intended to control concrete cracking, i.e., to ensure distributed cracking with small crack widths. This helps ensure the validity of the assumption of taking the concrete as fully effective in tension for calculation of the elastic internal forces and moments.

It should be noted that when the I-girders qualify for design using Appendix A6 within the negative bending region, i.e., when:

- The girder webs are classified as compact or noncompact for negative bending,
- F_{yc} and F_{yt} are less than or equal to 70 ksi,
- The I_{yc}/I_{yt} is greater than or equal to 0.3, and
- The bridge is straight with the skew of the support lines less than or equal to 20 degrees,

the corresponding girder major-axis bending resistance can be larger than the yield moments M_{yc} and M_{yt}. As explained in AASHTO (2020) Article A6.1.1, for composite sections with web slenderness values that approach the compact-web limit, the effects of loadings being applied to the different steel noncomposite, and short-term and long-term composite sections are nullified by the yielding within the section associated with the development of the flexural resistance. Therefore, the AASHTO (2020) Specifications define the maximum potential flexural resistance, referred to as M_{max}, as the plastic moment, which is independent of the effects of the different loadings. However, the different types of loading are taken to have an influence on the yield moments, M_{yc} and M_{yt}, and the elastic depth of web in compression, D_c, for the strength calculations.

Similar statements can be made about composite I-sections in positive flexure, defined as sections where according to Article 6.10.6.2.2:

- F_{yc} and F_{yt} are less than or equal to 70 ksi,
- The web has a $D/t_w \leq 150$ and further satisfies a limit on $2D_{cp}/t_w$ (where D_{cp} is the fully-plastic depth of the web in compression) less than a specified compactness limit,
- The bridge is straight,

the girders may be designed for moments significantly larger than the first yield moment. In these cases, the moment capacity is also independent of the apportionment of the applied moment to the noncomposite, short-term composite and long-term composite sections.

AASHTO (2020) Article C4.5.3.1 states that small-deflection theory, or a geometrically linear or first-order analysis, is usually adequate for stringer-type bridges. The terms first-order analysis, geometrically linear analysis, and small-deflection theory all indicate that equilibrium of the structure is considered on the undeflected geometry. Article C4.5.3.1 also indicates that bridges that resist loads by a couple whose tensile and compressive forces remain essentially in fixed positions relative to each other while the bridge deflects, such as trusses and tied arches, tend to be insensitive to deformations. However, the internal forces and bending moments can be influenced significantly by second-order effects in structures with members or components subjected to significant axial compression relative to their corresponding elastic buckling resistance. Also, the internal forces in form-active structures, such as suspension bridges, are influenced significantly by these effects.

In some stringer-type bridges, construction deflections and stresses (prior to the completion of the full structure) may be influenced significantly by second-order effects. For example, the torsional deformations during construction of some curved and/or skewed I-girder bridges are sensitive to these effects (Jung and White 2010; Chang and White 2010). The influence of second-order effects on the flange lateral bending stresses can be significant in straight or curved fascia I-girders subjected to eccentric concrete deck overhang loads acting on cantilever forming brackets. In these cases, an approximate second-order analysis consisting of applying amplification factors to the internal stresses obtained from first-order methods is essential at a minimum. Section 6.3.7.2 of this volume outlines AASHTO (2020) recommendations for such an analysis. As the second-order effects become larger, the use of a refined second-order analysis is prudent. Section 5 of this volume addresses the estimation of a global elastic buckling load capacity in narrow I-girder bridge units composed of two or three girders, and discusses AASHTO (2020) recommendations to avoid situations with significant second-order amplification in these cases.

The term second-order analysis indicates that equilibrium is evaluated on the deflected geometry of the structure. The second-order effects are the changes in the deflections, internal forces and internal moments, relative to those estimated from first-order analysis, due to considering equilibrium on the deflected geometry. First-order analysis is sufficient generally for calculation of live load effects on all stringer-type bridges in their final constructed configuration.

The component resistance equations in AASHTO (2020), and the strength limit states checks represented by Eq. 1, are based on the assumption that the second-order elastic internal stresses on the initially perfect structure (i.e., with no consideration of initial geometric imperfections), are calculated with sufficient accuracy in cases where these effects are important. That is, initial geometric imperfections within fabrication and erection tolerances do not need to be considered in the analysis. These effects are considered in addition to the effects of initial residual stresses within the component resistance equations. Various other incidental contributions to the internal stresses are neglected generally at the discretion of the engineer. These include flange lateral bending stresses in straight non-skewed I-girder bridges, stresses due to restraint of thermal expansion, longitudinal warping stresses in boxes under strength loading conditions, and St. Venant torsional shear stresses in I-section members.

Many of the provisions in AASHTO (2020) Chapter 4 address the appropriate assumptions and limits for the use of approximate analysis methods. The approximate analysis of stringer-type bridges using line-girder models receives substantial attention in this chapter. AASHTO Article 4.1 states:

"The primary objective in the use of more sophisticated methods of analysis is to obtain a better understanding of the structural behavior. Such improved understanding may often, but not always, lead to the potential for saving material…. With rapidly improving computing technology, the more refined and complex methods of analysis are expected to become commonplace. Hence, this section addresses the assumptions and limitations of such methods. It is important that the user understand the method employed and its associated limitations."

One of the limitations of general second-order elastic analysis methods is that superposition of the effects from separate loading types is not valid. With these methods, the structure strictly must be analyzed for each load combination and load placement. However, various simplifications and approximations allow for limited superposition of certain results. For example, for a curved I-girder bridge that is sensitive to second-order effects in its noncomposite condition but insensitive to these effects after the structure is made composite, second-order analysis can be employed to determine the dead load and construction stresses. The results from a first-order geometrically linear analysis then can be subsequently added to these stresses for evaluation of the composite structure (Jung and White 2010; Chang and White 2010). This allows for the use of influence surfaces in the calculation of live load effects. For suspension bridges, Podolny and Goodyear (2011) discuss commonly employed approximate linearized solutions that allow the development and use of influence lines.

4.0 CONSIDERATION OF THE FIT CONDITION IN I-GIRDER BRIDGES

Article 6.7.2 of AASHTO (2020) requires that the "fit condition" to which the cross frames or diaphragms are to be detailed should be stated within the contract documents for the following I-girder bridge types:

- Straight bridges where one or more support lines are skewed more than 20 degrees from normal;
- Horizontally curved bridges where one or more support lines are skewed more than 20 degrees from normal and with L/R in all spans less than or equal to 0.03, where L is the span length bearing-to-bearing along the centerline of the bridge and R is the radius of the curve at the centerline of the bridge;
- Horizontally curved bridges with or without skewed supports and with a maximum L/R greater than 0.03.

The fit condition refers to the deflected girder geometry associated with a specific load condition in which the cross frames or diaphragms are detailed to connect to the girders. The detailer assumes that the girders are nominally plumb at the specified load condition in making this geometry-based calculation. One of three different fit conditions are typically employed in I-girder bridge construction:

- No-Load Fit (NLF): The cross frames are detailed to fit to the girders in their fabricated, plumb, fully-cambered position under zero dead load;
- Steel Dead Load Fit (SDLF): The cross frames are detailed to fit to the girders in their ideally plumb as-deflected positions under the bridge steel dead load at the completion of the steel erection;
- Total Dead Load Fit (TDLF): The cross frames are detailed to fit to the girders in their ideally plumb as-deflected positions under the bridge total dead load.

The fit condition generally should be selected to accomplish the following objectives, in the order of priority:

1. Facilitate the construction of the bridge;

2. Offset large girder dead load twist rotations and corresponding lateral movements at the deck joints and barrier rails, which occur predominantly at sharply skewed abutment lines;

3. Reduce the dead load forces in the cross frames or diaphragms, and the flange lateral bending stresses in the girders, in straight skewed bridges; and

4. Select the load condition in which the girders will be approximately plumb.

Article 6.7.2 states that TDLF should not be specified for curved I-girder bridges with or without skew when L/R is greater than 0.03. This article states that such bridges may be detailed for SDLF or NLF unless the maximum L/R is greater than or equal to 0.2, in which case the bridge should be detailed for NLF or the additive locked-in force effects associated with the SDLF detailing should be considered. Article C6.7.2 provides summary guidance for selecting the fit condition, and points to various references. The NSBA (2016a) white paper provides an overview of the key considerations and NSBA (2016b) publication provides more detailed guidance. White et al. (2012 and 2015), Grubb et al. (2015), and AASHTO/NSBA (2019) provide additional in-depth discussions.

The most relevant aspect of the fit condition pertaining to strength design is its influence on the internal forces and stresses in the structure. SDLF and TDLF introduce a lack-of-fit between the cross frames and the girders within the no-load geometry of the structure. That is, the cross-frame geometry does not fit to the girder geometry in the idealized case when none of the components are subjected to any dead load stresses (i.e., when the components are all unstressed). In straight skewed bridges, the effects of this lack-of-fit tend to reduce the girder flange lateral bending stresses and the internal forces in the cross frames in the targeted dead load condition.

The simplest case to understand conceptually is a straight skewed I-girder bridge detailed for SDLF. If the cross frames are detailed to fit to the girders in the steel dead load condition, and if the girder deflection calculations are based on a line girder analysis considering all the steel dead load in the final erected condition, the cross-frame forces are essentially zero in this dead load condition, and the girder flange lateral bending stresses are also essentially zero in this dead load condition. The lack-of-fit between the cross frames and the girders before they are subjected to any steel dead load twists the girders in the direction opposite from that which they deform under the steel dead load. Under the full steel dead load, the lack-of-fit in the no-load geometry offsets

the effect of the steel dead loads acting on the structure with regard to the cross-frame forces and the girder flange lateral bending stresses. Or stated another way, if the girders could be placed independently of one another, without the cross frames or diaphragms being engaged (i.e., suppose they are simply "pin" connected to the girders on each of their ends), and the girders were allowed to deflect under their self-weight and the weight of the cross frames, they would deflect according to the line girder analysis idealization. Under this scenario, the cross frame or diaphragm connections to the girders then could be completed theoretically without introducing any additional forces in the structure, which is already subjected to the full steel dead load.

The various aspects of the problem become more complex if one considers the calculation of the girder steel dead load deflections from a 2D grid or a 3D finite element analysis in which the gravity load is simply "turned on."

In the basic case of a radially curved I-girder bridge, the lack-of-fit stresses due to SDLF or TDLF detailing of the cross frames tend to be additive with other dead load stresses in the girders and the cross frames. That is, the lack-of-fit cross-frame forces required to twist the I-girders in the direction opposite to their twist under the targeted dead load condition is additive with the corresponding dead load cross-frame forces in a basic radially curved I-girder bridge. This is opposite to the lack-of-fit effects in a straight skewed I-girder bridge, where the lack-of-fit forces offset the forces from the corresponding dead load effects.

Article C6.7.2 provides a number of recommendations for estimating different locked-in force effects, assuming the typical practice in which the structural analysis of the bridge does not directly include these effects, i.e., assuming that the structural analysis is conducted based on NLF.

When determined to be beneficial and/or necessary by the engineer, it is possible to directly calculate the internal locked-in forces associated with SDLF or TDLF detailing within either an accurate 2D grid or a 3D finite element analysis. These effects can be handled in a manner similar to the calculation of the effects of temperature change. The calculations involve the consideration of the initial lack-of-fit offsets between the cross-frame connection work points and the corresponding work points on the girders in the undeformed no-load geometry of the structure. These lack-of-fit offsets are then used to calculate initial strains in the cross-frame members, or initial fixed-end forces in a beam element representation of the cross frames (similar to the initial strains or initial fixed-end forces due to the effects of temperature change). These initial strains or fixed-end forces induce nodal loads in the structural analysis model that account for the lack-of-fit effects. The structural analysis model is analyzed for these nodal loads, producing deformations/deflections and corresponding internal forces/stresses in the model. The response of the structure to these nodal loads is then added to the above "initial effects" in the undeformed configuration of the structure to determine the corresponding total internal forces and stresses that are "locked-in" to the structure due to the SDLF or TDLF detailing (NSBA 2016b; White et al. 2015). At the current time (2021), most software providers have not seamlessly integrated these types of SDLF or TDLF calculations into their refined structural analysis calculations. Ultimately, such integration would result in the best accounting for these effects.

For straight skewed I-girder bridges designed by line girder analysis and detailed for SDLF, the solution is relatively easy. The cross-frame forces and girder flange lateral bending stresses may be taken equal to zero in the steel dead load condition. White et al. (2020) provide guidance for

estimating the cross-frame forces and girder flange lateral bending stresses under other loading conditions in the context of the line-girder analysis and design of straight I-girder bridges with small to moderate skew.

5.0 OVERALL SYSTEM BUCKLING VERSUS INDIVIDUAL MEMBER BUCKLING

5.1 Key Concepts

One essential question with regard to constructability is the following – what type of analysis and/or design checks are sufficient to assess the overall stability of a bridge structural system during construction. For instance, what constitutes a sufficient check of the overall stability of a straight tub girder that does not have a full-length top lateral bracing system? At issue is the fact that in most cases, the overall stability of stringer-type bridges is implicit and the engineer need only check the member buckling resistances for the unbraced lengths between the cross-frame or diaphragm locations. However, checking of the top flanges of a single tub girder in this fashion does not provide an adequate assessment of the overall stability of the structure. For this type of system, a direct global assessment of the buckling load of the full structure is necessary. Yura and Widianto (2005) discuss a number of approximate and refined solutions for assessment of the overall buckling of tub girders that do not have a full-length top-flange bracing system. In addition, an expanded set of related recommendations have been published for I-girders by Yura et al. (2008). Yura and Widianto demonstrate that the overall elastic buckling of individual tub-girders with no top-flange bracing is represented accurately, for the case of uniform bending ($C_b = 1$), by the analytical solution for a singly symmetric thin-walled open-section member. This solution may be written concisely as

$$M_{cr} = \frac{\pi^2 E I_y}{L^2} \left\{ \frac{\beta_x}{2} + \sqrt{\left(\frac{\beta_x}{2}\right)^2 + \frac{C_w}{I_y}\left[1 + 0.039\frac{J}{C_w}L^2\right]} \right\} \tag{5-1}$$

(White and Jung 2003b), where β_x and C_w are respectively the coefficient of monosymmetry and the warping constant for the cross section. These constants are determined from thin-walled open-section beam theory, e.g., see Galambos (1968) and Heins (1975). The properties I_y and J are the moment of inertia of the tub section about the axis orthogonal to the axis of bending and the St. Venant torsional constant, and L is the overall span length. Yura and Widianto (2005) also show that modified forms of Eq. 1, which account for the influence of pre-buckling displacements on M_{cr}, have little practical significance because of necessary stress and deflection limits. In addition, they point out that the alternate modified forms are not appropriate for cambered girders. Since the camber offsets the dead load deflection, the girder may actually be close to having a straight longitudinal axis at incipient buckling; that is, the beneficial "inverted arch" type pre-buckling geometry is not actually what is present at incipient buckling of the girder.

The Engineer should note that Eq. 1 applies only to tub girders that do not have top-flange bracing. Tub girders designed with a full-length top lateral bracing system satisfying the AASHTO (2020) Article 6.7.5.3 requirements do not need to be checked for overall lateral-torsional buckling. In addition, it should be noted that this equation applies to both straight and curved tub-girders. Similar to the fact that the in-plane *elastic* flexural buckling of a beam-column is relatively

insensitive to the applied bending moments (McGuire 1968), the overall elastic buckling load of bridge girders generally is insensitive to horizontal curvature.

Yura and Widianto (2005) and Yura et al. (2008) also show that two and three I-girder systems can be susceptible to overall lateral-torsional buckling in some cases. That is, their equations show that in certain cases, the stability of two or three I-girder assemblies connected together by cross frames may be governed by overall global buckling rather than by buckling of the individual I-girders between the cross-frame locations. The elastic critical moment of a simply supported doubly symmetric twin I-girder system with the cross section shown in Figure 40 is obtained for the case of uniform bending simply by substituting $I_y = 2I_{yo}$, $J = 2J_o$ and $C_w = 2I_{yo}(h/2)^2 + 2I_{xo}(w_g/2)^2$ into the classical elastic LTB equation from Timoshenko and Gere (1961),

$$M_{cr} = \frac{\pi}{L}\sqrt{EI_yGJ + \left(\frac{\pi E}{L}\right)^2 I_yC_w} \tag{5-2}$$

where

J_o = St. Venant torsional constant of one of the individual I-girders
I_{yo} = weak-axis moment of inertia of one of the individual I-girders
I_{xo} = strong-axis moment of inertia of one of the individual I-girders
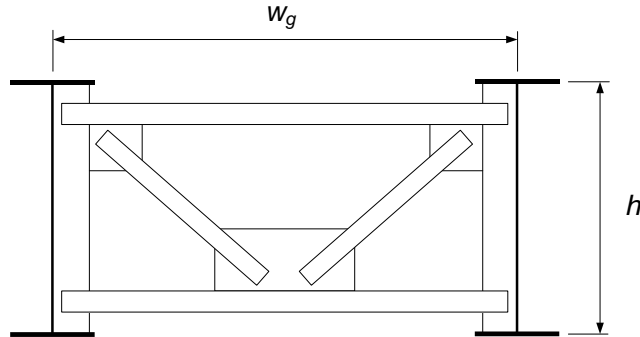
Figure 40. Twin I-girder subassembly composed of doubly symmetric I-girders.

The above expression for C_w is obtained from thin-walled open-section beam theory for the twin I-girder cross section. The above substitutions result in the following estimate for the total global elastic buckling moment of the girder system:

$$M_{gs} = \frac{2\pi}{L}\sqrt{EI_{yo}GJ_o + \left(\frac{\pi E}{2L}\right)^2 I_{yo}^2 h^2 + \left(\frac{\pi E}{2L}\right)^2 I_{yo}I_{xo}w_g^2} \tag{5-3}$$

By retaining only the term involving I_{xo} from Eq. 3, Yura and Widianto (2005) and Yura et al. (2008) obtain the following simplified expression, which is typically only a few percent conservative as long as w_g is larger than h:

$$M_{gs} = \frac{\pi^2 w_g E}{L^2} \sqrt{I_{yo} I_{xo}} \qquad (5\text{-}4)$$

In some two-girder cases, M_{cr} from Eq. 4 is smaller than the sum of the elastic buckling capacities of the two girders based on the unbraced lengths between the cross frames. That is, the lateral-torsional buckling strength of two I-girders, connected together by cross frames, is governed by overall global buckling of the assembly, not by the buckling of the members between the brace points.

Yura et al. (2008) generalize Eq. 3 to address twin singly symmetric I-girder systems subjected to nonuniform major-axis bending moment by:

1. Multiplying the overall expression by a moment gradient, C_b, factor,

2. Substituting $2I_{yc}$ for I_{yo} in the first and second terms of Eq. 3, where I_{yc} is the moment of inertia of the compression flange about the vertical y-y axis, and

3. Substituting I_{eff} for I_{yo} in the third term of Eq. 3

where

$$I_{eff} = I_{yc} + \left(\frac{t}{c}\right) I_{yt} \qquad (5\text{-}5)$$

t and c are the distances from the centroidal axis to the centroid of the tension and compression flanges, and I_{yt} is the moment of inertia of the tension flange about the vertical y-y axis. (Note that I_{eff} reduces to $2I_{yc} \cong I_{yo}$ for doubly symmetric I-girders.)

This gives

$$M_{gs} = \frac{2C_b \pi E}{L} \sqrt{\frac{I_{yc} J_o}{1.3} + \frac{\pi^2 I_{yc}^2 h^2}{L^2} + \frac{\pi^2 I_{eff} I_{xo} w_g^2}{4L^2}} \qquad (5\text{-}6)$$

which for $h > w_g$ can be written with little loss of accuracy as

$$M_{gs} = C_b \frac{\pi^2 w_g E}{L^2} \sqrt{I_{eff} I_{xo}} \qquad (5\text{-}7)$$

Equation 7 appears as Eq. 6.10.3.4.2-1 in the AASHTO (2020) Specifications. Yura et al. (2008) show accurate predictions by the above equations for simply supported prismatic twin-girder systems, including the use of ordinary beam C_b factors of 1.12 for uniformly distributed loading and 1.35 for cases where the moment diagram is based on a mid-span concentrated load. Subsequent extensions conducted in the preparation of AASHTO Article 6.10.3.4.2-1 have led to the recommendations that C_b should be taken as 1.1 for simply supported units and partially-erected continuous-span units, and 2.0 for fully-erected continuous-span units.

AASHTO Article 6.10.3.4.2 employs the simplified Eq. 7 also for three I-girder systems, where w_g is taken as the total width between the outside girders. It can be observed that the middle girder does not deflect vertically upon twisting of a three-girder system, assuming the cross section of the unit is symmetric about the middle girder; therefore, the simplified Eq. 7 does not recognize any contribution from the middle girder to the global system buckling for a three-girder system. If Eq. 6 is employed, Yura et al. (2008) explain that I_{yc} should be replaced by $1.5I_{yc}$, J_o should be replaced with $1.5J_o$, and w_g should be taken as the total width between the exterior girders.

In addition, AASHTO Article 6.10.3.4.2 generalizes the application of Eq. 7 for cases involving continuous spans, nonprismatic girder geometry within the spans, and/or where the girder cross sections vary across the width of the unit by recommending the calculation of a length-weighted average of the moments of inertia within the positive moment sections of the girders for the calculation of I_{xo}, I_{yo}, I_{yc} and I_{yt}. These AASHTO provisions recommend the use of Eq. 6 when the girder spacing is less than the girder depth, referencing Yura et al. (2008) for the presentation of the equation. It is recommended that a length-weighted average also be utilized for J_o when this equation is employed. Furthermore, Yura et al. (2008) recommend the use of $0.9M_{gs}$ when Eq. 6 is used with top-flange loaded cases, to account for the destabilizing nature of the tipping effects of loads that are applied to the top flange.

AASHTO Article 6.10.3.4.2 requires that Eq. 7 (or Eq. 6 as applicable) be employed to check the global stability of straight I-girder bridge units with three or fewer girders, interconnected by cross frames or diaphragms, in their noncomposite condition during the deck placement operation, unless:

- The unit is braced by other structural units and/or by external bracing within the span; or
- The unit contains flange-level lateral bracing, or lateral bracing from a hardened deck within the span.

Specifically, the sum of the largest total factored girder moments during the deck placement within the span under consideration should not exceed 70 percent of the global buckling moment, M_{gs}, from Eq. 7 (or 6 as applicable), with consideration of the additional 10 % capacity reduction associated with top flange loading, if applicable. If this check is violated Article 6.10.3.4.2 recommends that one of the following actions should be taken:

- Consider the addition of flange-level lateral bracing adjacent to the supports of the span, as discussed in AASHTO Article 6.7.5.2 and in Section 2.2.2 of this volume;
- Revise the design for the unit to increase the system stiffness; or
- Evaluate the amplified second-order displacements of the span during the deck placement to verify they are within acceptable tolerances permitted by the Owner.

The primary concern addressed by the Article 6.10.3.4.2 provisions is the amplification of lateral and torsional displacements in narrow bridge units in their noncomposite condition during the deck placement. Large global torsional rotations associated with differential vertical displacements between the girders and/or large lateral deflections from a first-order analysis are indicative of the potential for significant second-order global amplification. Situations with unevenly applied deck weight causing torsion can be particularly problematic when a narrow bridge unit is approaching its global elastic buckling load as a system. Article 6.10.3.4.2 indicates that the $0.7M_{gs}$ limit

restricts the maximum second-order amplification of the lateral and torsional displacements to approximately 2.0. Depending on the affinity of the displacements under the applied loads with the system buckling mode of the narrow bridge unit, the amplification theoretically can be larger.

Article C6.10.3.4.2 states that narrow horizontally curved I-girder bridge units in their noncomposite condition during the deck placement may be subject to significant second-order amplification and should be analyzed using a global second-order load-deflection analysis to evaluate their behavior. Flange-level lateral bracing adjacent to the supports, or bracing of the unit against other structural units by external bracing within the span, should be employed to limit these effects.

The above are useful base equations that are helpful for gaging when overall system buckling may govern relative to the common design assumption of buckling of the girders between the brace points. For realistic practical cases involving deep, closely-spaced, narrow-flange I-section members, the Engineer should consider running a refined buckling analysis to check the lateral-torsional buckling capacity of girder assemblies during construction. If the governing elastic buckling load is sufficiently large relative to the applied loads, then neither local nor global stability is an issue. Section 5.3 of this volume outlines the specifics of this type of global stability check.

5.2 Lean-On Bracing Systems

It is possible to achieve substantial economy in the design of cross frames in straight I-girder bridges by utilizing lean-on bracing concepts (Helwig et al. 2005; Herman et al. 2005; Farris 2018). Using these concepts, multiple I-girders can be braced by a single cross frame, given that they are tied to the cross frame by top and bottom struts as shown in Figure 41. This approach can be particularly useful to eliminate cross frames that may otherwise attract large forces, and to reduce the I-girder flange lateral bending stresses, in skewed I-girder bridges. Such a case is illustrated in Figure 42, which illustrates the cross frame placement in a two-span TxDOT proof-of-concept bridge as presented by Helwig et al. (2005) and Herman et al. (2005). In this design, the individual I-girders tend to respond in a fashion closer to that of a non-skewed bridge. The top and bottom struts across the width of the bridge work with the bays containing cross-frame diagonals to provide the lateral stability to all of the girders. However, the bays containing only top and bottom struts and no diagonals rack due to differential girder vertical displacements (i.e., the top and bottom struts rotate relative to the girder cross sections in the plane of the cross frames), thus reducing the twisting of the girders and avoiding the development of large cross-frame forces.

Cross-Frame   Lean-on bracing provided
                     by top and bottom struts
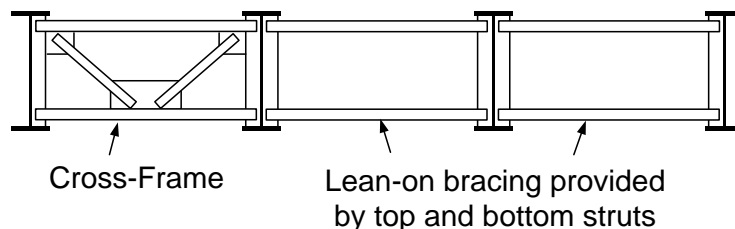
Figure 41. A bridge cross section showing multiple I-girders braced by a single cross frame.

Equations 4 and 7 are not valid for bridges that utilize lean-on bracing concepts. The cross-frame sizes and their locations must be designed to provide overall lateral and lateral-torsional stability

of the structural system at all stages of the erection process. Helwig et al. (2005) and Herman et al. (2005) provide equations for estimating the bracing stiffness and force requirements due to stability effects. Refined analysis tools can be valuable for checking the overall stability of this type of bridge during various stages of construction.

In the design shown in Figure 42, cross frames are placed across the entire width of the bridge at the supports. Also, a pair of cross frames is provided at the mid-width of the bridge near the middle of each span. Furthermore, at least one intermediate (in-span) cross frame is located between each of the girders, several additional cross frames are located near the field splice locations, and a few additional cross frames are provided to limit the differential deflection between adjacent girders during the slab casting. The reader is referred to Helwig et al. (2005) or Herman et al. (2005) for discussion of the detailed considerations. The total number of intermediate cross frames is reduced from 128 to 35 after accounting for all of these factors. The authors suggest that a larger number of cross frames should be used in broader implementation of the lean-on bracing concepts, with an important goal being flexibility for the erector to select various sequences of erection. For instance, they suggest that cross frames should be located between each of the girders near field splice locations.
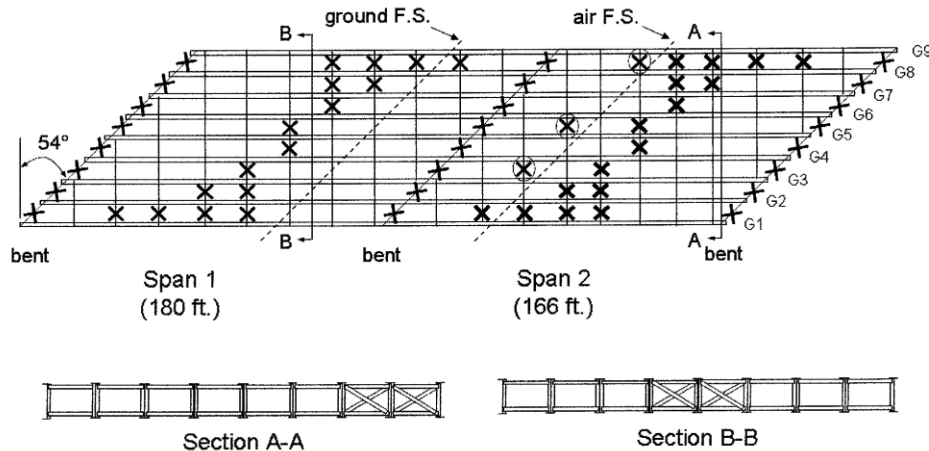
Figure 42. Plan view of a proof-of-concept skewed I-girder bridge utilizing lean-on bracing to alleviate large cross-frame forces and to reduce the number of required cross frames. (Herman et al. 2005) (reprinted with permission from Texas DOT). The x marks indicate the location of cross frames.

5.3 General Consideration of System Stability Effects in Design

In all of the above cases, if the *system* elastic buckling resistance is smaller than the elastic lateral-torsional buckling resistance of the I-girders between the cross-frame brace points, then strictly speaking, the Engineer generally should evaluate whether the corresponding maximum compression flange elastic buckling stress is larger than the nominal stress magnitude, F_{yr}, at which yielding occurs due to residual stress and geometric imperfection effects. When the elastic critical stress $F_e = M_e/S_{xc}$ is larger than F_{yr}, inelastic system buckling should be considered using the generalized equations discussed subsequently in Section 6.3.6 of this volume. These situations will rarely occur in practical stringer bridges. The structure in its final constructed configuration will typically be such that its member strengths are not governed by an overall global buckling mode,

and for the structure at critical intermediate stages during construction, the stresses should generally be small enough such that the structure is not close to the onset of any nominal yielding.

In cases where the girder flanges are subjected to significant lateral bending in addition to the major-axis bending stresses, f_b, the Engineer should consider the second-order elastic amplification of the flange lateral bending stresses due to the overall system stability effects when f_b/F_e is larger than about 0.1 to 0.2. For most bridges where this consideration may be important, it is expected that it will be important only during construction.

For large arch and cable-supported bridges, detailed three-dimensional finite element analyses of the overall structure including geometric and material nonlinearity, residual stresses and geometric imperfections may be desirable for assessment of the overall response at strength load levels. This type of analysis may be conducted with a number of the most sophisticated commercially available software packages. Detailed elastic finite element analysis of these types of structures is commonly employed for evaluation of component stresses at a minimum (Ito et al. 1992). However, it must always be recognized that good design of bridges is not achieved simply by running sophisticated computer programs. Computer software should be considered as only one of many essential design tools. Also, the Engineer should always keep in mind the famous words of Professor Hardy Cross (1952),

"…strength is essential and otherwise unimportant.

Various sources aid the engineer in determining strength. No one of them is more important than another. Analyses, tests, experience and such intuitive common sense as may be personally developed about structural stability; these are all helpful, but they can also be dangerously misleading. Evidence from the four sources rarely agrees completely. Great engineers are those who can weigh this evidence and arrive at a reasonable answer through judgment as to its dependability….

The important point here is that some types of planning, designing and experimenting can be put on an assembly line and some types can be put on an assembly line of skilled brains only, but much of the most important work cannot be done by using fixed rules, standardized formulas or rigid methods.

In general the objectives are flexibility of design and simplicity of construction….

…Men must learn to think more clearly in space and be less restricted to two-dimensional design. They must pay more attention to movements and vibrations. They need much more information on the properties of materials. Probably they need to reappraise seriously the importance of durability…"

6.0 MEMBER BEHAVIOR AND DESIGN STRENGTH

6.1 Tension Members

6.1.1 Rolled or Built-Up Tension Members

The strength of rolled section tension members, or tension members built up from rolled sections and/or steel plates, is governed by the most critical of the following limit states:

- Overall tension yielding of the member along its length,

- Tension fracture of the member across a net section (referred to by AISC (2016) as tension rupture),

- Block shear rupture along a shear failure path or paths combined with a perpendicular tension failure path at an end connection,

- Failure of the connecting bolts or welds in one of a number of modes, or

- Failure of the connecting elements, e.g., gusset plates, connection plates or splice plates.

The last three of these are considered as connection limit states by AASHTO (2020) and hence are not within the scope of this volume. They are addressed in Article 6.13 of the AASHTO Specification. However, the first two limit states are considered as member limit states and are addressed in AASHTO Article 6.8. The tension yielding resistance is given by the equation

$$\phi_y \, P_{ny} = 0.95 \, F_y \, A_g \qquad \qquad \text{(6.1.1-1) (AASHTO 6.8.2.1-1)}[2]$$

where

$\quad\quad F_y \quad = \quad$ specified minimum yield strength and

$\quad\quad A_g \quad = \quad$ gross cross-sectional area of the member,

while the tension fracture resistance is expressed as

$$\phi_u \, P_{nu} = 0.80 \, F_u \, A_n \, R_p \, U \qquad \qquad \text{(6.1.1-2) (AASHTO 6.8.2.1-2)}$$

where

$\quad\quad F_u \quad = \quad$ ultimate tensile strength

$\quad\quad A_n \quad = \quad$ member net area

---

[2] Note, equation numbers that are not preceded by the term "AASHTO", e.g., Eq. 6.1.1-1 herein, correspond to Section 6 of this volume. The AASHTO (2020) equation numbers, where applicable, are denoted by the term "AASHTO." For example Eq. 6.1.1-1 herein corresponds to the equation number 6.8.2.1-1 in AASHTO (2020). Furthermore, this equation is simply referred to as Eq. 1 in Section 6.1.1 of this volume.

R_p = reduction factor for holes, taken equal to 0.90 for bolt holes punched full size and 1.0 for bolt holes drilled full size or subpunched and reamed to size

U = shear lag factor

Although steel members loaded in axial tension can generally resist a force greater than the product of their gross area and the specified minimum yield stress, substantial elongation due to yielding throughout the gross area along the member length could precipitate the failure of the structural system of which the member is a part. Therefore, overall yielding of the gross area is considered as a strength limit state.

On the other hand, depending on the mechanical properties of the steel (the most important of which is the tensile-to-yield ratio F_u/F_y), the ratio of the net area to the gross area A_n/A_g and the end connection geometry (captured by the parameter U), a member can fail by tension fracture at one of its end connections before full yielding of its gross area. However, the larger tensile strains at the end connections are highly localized. Therefore, yielding at the end connections does not constitute a limit state of practical significance.

If fastener holes are located at some position along the member length, the net section at these holes also must be checked in general for tension fracture on the net section through the holes. However, AASHTO (2020) Article 6.8.1 indicates appropriately that holes larger than typical fastener holes shall be deducted from the gross area rather than from the net area. This includes access holes and perforations in built-up members. In other words, these locations are designed for general yielding over their net area.

The net area for the tension fracture check can be expressed generally as:

$$A_n = A_g - \text{area lost due to holes} \qquad (6.1.1-3)$$

Therefore, for fully welded connections without any plug or slot welds, $A_n = A_g$. In cases with plug or slot welds, the width of the original hole for the weld is handled in the same fashion as a fastener hole. For hole arrangements without any stagger, Eq. 3 becomes:

$$A_n = A_g - \Sigma\, d_e\, t \qquad (6.1.1-4)$$

where

d_e = effective width deducted for a given hole, equal to the nominal diameter or width of the hole perpendicular to the tension direction.

t = thickness of the plate at the hole.

Although AISC (2016) adds an additional 1/16 in to the nominal diameter in its calculation of d_e, to account in general for potential damage due to the fabrication of the hole, AASHTO (2020) Article 6.8 does not. In the AASHTO provisions, the influence of damage around the hole is included, for bolt holes punched full size, by the using $R_p = 0.9$. No area in addition to that obtained from the nominal dimensions is deducted for bolt holes drilled full size or subpunched and reamed to size.

The summation in Eq. 4 is over all of the holes located across a potential transverse fracture path through all of the components of the member cross section. For staggered hole arrangements, the net area is given by:

$$A_n = A_g - \Sigma \, d_e \, t + \Sigma \, (s^2/4g) \, t \qquad\qquad (6.1.1\text{-}5)$$

where

s = longitudinal center-to-center spacing (pitch) between two consecutive holes

g = transverse center-to-center spacing (gage) between the hole gage lines

t = plate thickness along a given diagonal.

The second summation is over each diagonal in a potential zigzag fracture path through a chain of holes across all the cross-section components.

For angles, channels, boxes, etc. where the diagonal in the fracture path goes around a corner from one to another plate, the gage, g, is taken as the transverse distance between the adjacent holes along the mid-thickness of the plates. That is, the gage can be determined by imagining that the plates are unfolded into a single flat plate at the mid-thickness of the plates. The critical chain of holes is taken as the one that gives the smallest net area. The corresponding fracture path can be either a straight or a zigzag transverse line.

The above approach is based on the assumption that the full tensile force acts at every potential straight or zigzag transverse fracture path through a set of holes. AASHTO (2020) Article C6.8.3 indicates that a slightly less conservative calculation is obtained by subtracting the force removed by each bolt ahead of the fracture path being considered, i.e., closer to the mid-length of the member, from the full tensile force. The full force is assumed to be transferred equally by each bolt in the connection in making this calculation. In this case, a pseudo net area that can be used to determine the full member tension fracture resistance may be calculated as

$$A_n = \left[A_g - \Sigma \, d_e t + \Sigma \left(s^2 / 4g \right) \right] \frac{n_{total}}{n_r} \qquad\qquad (6.1.1\text{-}6)$$

where

n_{total} = total number of bolts in the connection

n_r = remaining number of bolts after deducting the number ahead of the fracture path

McGuire (1968) provides extensive discussion of the "$s^2/4g$" rule for estimating the effect of zigzag paths on the tension fracture resistance. Although other approaches exist that have a stronger theoretical basis, the corresponding equations are more complex and do not give any significant improvement in accuracy.
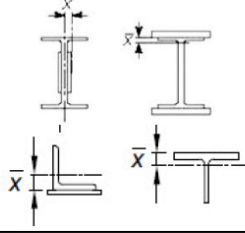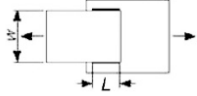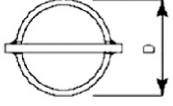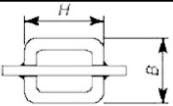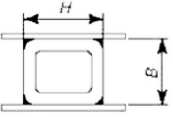
As noted in the definitions just after Eq. 2, *U* accounts for the shear lag effects associated with the end connection geometry. If a line of fastener holes is placed across the cross section of a member at some location within the member length, but no bolts or welds that transmit tension force to the member are located in these holes, $U = 1$. Also, if the tension force is transmitted directly to every component plate of a member cross section by bolts or welds, $U = 1$. However, if some of the components are unconnected at the member ends, the critical net section may not be fully effective. Table 1 gives the recommended values and equations for *U* in AASHTO (2020). These are the same as, and are based on, the values specified in AISC (2016). In addition, AASHTO Article 6.8.2.2 states that for members composed of more than one plate element, the calculated value of *U* should not be taken less than the ratio of the gross area of the connected element(s) to the member gross area. The commentary to this article states that this provision does not apply to closed sections, such as HSS, nor to plates. These recommendations parallel the guidelines in AISC (2016). The reason for the exclusion clause is that the proper calculation of *U* for closed sections and plates is addressed directly in the table.

The above AASHTO and AISC shear lag factor rules are based on the research by Munse and Chesson (1963), Easterling and Gonzales (1993), Cheng and Kulak (2000), and Fortney and Thornton (2012). The AISC (2016) Commentary provides a relatively extensive discussion of these rules.

It should be noted that AASHTO (2020) Article C6.8.2.2 and the commentary to Section D3.3 of AISC (2016) indicate that the moments due to the eccentricities of the connection of single angle or light structural tee members loaded eccentrically in axial tension may be ignored in the design of the member and the connections; the effect of the connection eccentricity is addressed via the shear lag reduction factor, *U*. Figure C-D3.3 of the AISC (2016) Commentary, and the corresponding Commentary discussion, provides a detailed explanation of how the eccentric moment is significantly relieved.

AASHTO (2020) Articles 6.8.4 and 6.9.3 specify limits on the member slenderness ratio *L/r* to ensure adequate performance, where *L* is the member unsupported length and *r* is the minimum radius of gyration of the cross section. For primary members subjected to stress reversals, *L/r* is limited to 120, for primary members subjected to tension only, *L/r* is limited to 200, for secondary members subjected to stress reversal, *L/r* is limited to 140, and for secondary members subjected to tension only, *L/r* is limited to 240. To provide context, AASHTO (2020) Article 6.2 defines a primary member as a steel member or component that transmits gravity loads through a necessary as-designed load path (these types of members are commonly subjected to more stringent fabrication and testing requirements, which is discussed in detail in AASHTO Article 6.6.2.1). For tension members with perforated plates or tie plates with or without lacing, a number of other requirements (dimensional, etc.) are specified in AASHTO (2020) Article 6.8.5 or are provided in the commentary to this section by reference to AISC (2016) and AASHTO (2002).

Table 1. AASHTO (2020) values and equations for the shear lag factor U.

Case	Description of Element		Shear Lag Factor, U	Example
1	All tension members where the tension load is transmitted directly to each of cross-sectional elements by fasteners or welds (except as in Cases 4, 5, and 6).		$U = 1.0$	—
2	All tension members, except plates and HSS, where the tension load is transmitted to some but not all of the cross-sectional elements by fasteners or longitudinal welds. (Alternatively, for W, M, S, and HP shapes, Case 7 may be used. For angles, Case 8 may be used.)		$U = 1 - \dfrac{\overline{x}}{L}$	
3	All tension members where the tension load is transmitted by transverse welds to some but not all of the cross-sectional elements.		$U = 1.0$ and A_n = area of the directly connected elements	—
4	Plates, angles, channels with welds at heels, tees, and W-shapes with connected elements, where the tension load is transmitted by longitudinal welds only. See Case 2 for definition of $\overline{x}$. L shall not be less than 4 times the weld size.		$U = \dfrac{3L^2}{3L^2 + w^2}\left(1 - \dfrac{\overline{x}}{L}\right)$	
5	Round HSS with a single concentric gusset plate through slots in the HSS.		$L \geq 1.3D \ldots U = 1.0$ $D \leq L < 1.3D \ldots U = 1 - \dfrac{\overline{x}}{L}$ $\overline{x} = \dfrac{D}{\pi}$	
6	Rectangular HSS	with a single concentric gusset plate	$L \geq H \ldots U = 1 - \dfrac{\overline{x}}{L}$ $\overline{x} = \dfrac{B^2 + 2BH}{4(B + H)}$	
		with 2 side gusset plates	$L \geq H \ldots U = 1 - \dfrac{\overline{x}}{L}$ $\overline{x} = \dfrac{B^2}{4(B + H)}$	
7	W, M, S, or HP shapes or tees cut from these shapes (If U is calculated per Case 2, the larger value is permitted to be used.)	with flange connected with 3 or more fasteners per line in direction of loading	$b_f \geq \dfrac{2}{3}d \ldots U = 0.90$ $b_f < \dfrac{2}{3}d \ldots U = 0.85$	—
		with web connected with 4 or more fasteners per line in direction of loading	$U = 0.70$	—
8	Single and double angles (If U is calculated per Case 2, the larger value is permitted to be used.)	with 4 or more fasteners per line in direction of loading	$U = 0.80$	—
		with 3 fasteners per line in direction of loading (with fewer than 3 fasteners per line in direction of loading, use Case 2)	$U = 0.60$	—

where L = length of connection (in.); w = plate width (in.); $\overline{x}$ = connection eccentricity (in.); B = overall width of rectangular HSS member, measured normal to the plane of the connection (in.); D = outside diameter of round HSS (in.); H = overall height of rectangular HSS member, measured in the plane of the connection (in.); d = full nominal depth of the section, for tees, depth of the section from which the tee was cut (in.); b_f = flange width (in.)

6.1.2 Eyebars and Pin-Connected Plates

AASHTO (2020) Article 6.8.6 specifies that the factored resistance of eyebars is given by Eq. 6.1.1-1 based on the area of the body, $w\,t$, and provides dimensional requirements to ensure that tension fracture will not occur. Figure 43 shows these and several additional dimensional requirements. Two requirements are listed from AISC (2016) that are believed to be intended, given the origins of the rules (McGuire 1968). AISC (2016) states that the adherence to these limits assures that the controlling limit state will be tensile yielding of the body; thus, additional limit state checks are unnecessary. The requirements in Figure 43 are based largely on judgment and traditional rules of practice that have evolved over many years. McGuire (1968) points out that the behavior of eyebars and pin-connected plates differs somewhat from that of bolted or riveted tension members and provides an extensive review of the traditional requirements and their relationship to theory and experimental studies. The in-plane bending deformations and localized strains tend to be larger around the large pin hole compared to typical local deformations in bolted or riveted connections.

AASHTO Article 6.8.7 requires that pin-connected plates shall be designed using Eqs. 6.1.1-1 and 6.1.1-2 with $U = 1.0$. Pin-connected plates are defined as members in which "pin-plates" may be attached to a main plate by bolts or welds to increase the thickness near the pin (see Figure 44).

AASHTO Article 6.8.7.2 requires that the pin plates, if used, should be arranged to minimize the load eccentricity, and that they must be attached to the main plate by sufficient welds or bolts to transmit the pin bearing forces from the pin-plates to the main plate. The combination of the main and pin plates must be checked for net section fracture at the pin hole. Also, the main plate and pin plates must be checked for fracture across their individual net sections at the attachments of the pin plates to the main plate, considering the force transfer between the plates. The main plate must be checked for yielding on its gross area based on Eq. 6.1.1-1 (AASHTO Eq. 6.8.2.1-1). Furthermore, AASHTO (2020) specifies a bearing resistance on the projected area at the pin, $A_b = t_m\,d_p$ or $t_p\,d_p$, of

$$\phi_b P_n = 1.0\,A_b\,F_y \qquad\qquad\qquad (6.1.2\text{-}1)\ (\text{AASHTO } 6.8.7.2\text{-}1)$$

for each of the plates, where F_y is the specified minimum yield strength of the plate. Figure 44 summarizes additional requirements for a specific pin-connected plate with two equal size pin plates bolted on each side of the main plate, a width of the pin plates equal to the width of the main plate, w, and an end distance from the pin to the end of the pin plates equal to that of the main member, a. These requirements, combined with the above tension yielding, tension fracture and plate bearing checks, are intended to ensure acceptable behavior of the assembly.

One additional requirement is shown in Figure 44 that is not specified explicitly in AASHTO (2020) or AISC (2016). It would appear that the dimension from the edge of the pin-hole to the edge of the pin-plates parallel to the direction of the load should be essentially the same on each side of the pin to ensure good performance (hence the dimension labeled "$\approx a$"). Also, the connection of the pin plates to the main plates should be distributed over the pin plates such that the localized effects of the pin are diminished at the critical net section for the tension fracture check of the main plate.

AASHTO (2020) states that pin-connected plates should be avoided wherever possible. AISC (2016) indicates that pin-connected plates are not recommended when there is sufficient variation in live loading to cause wearing of the pins in the holes. McGuire (1968) points out that pin-connected plates and eyebars were common in the nineteenth century, when they were more economical and faster to erect than hand-riveted construction, and when Engineers were often concerned with minimizing secondary stresses. Also, he indicates that given current knowledge about secondary stresses, and when they are or are not important, there is less concern in modern design about their minimization in all structures. Consequently, trusses having all or most joints pinned have largely disappeared.
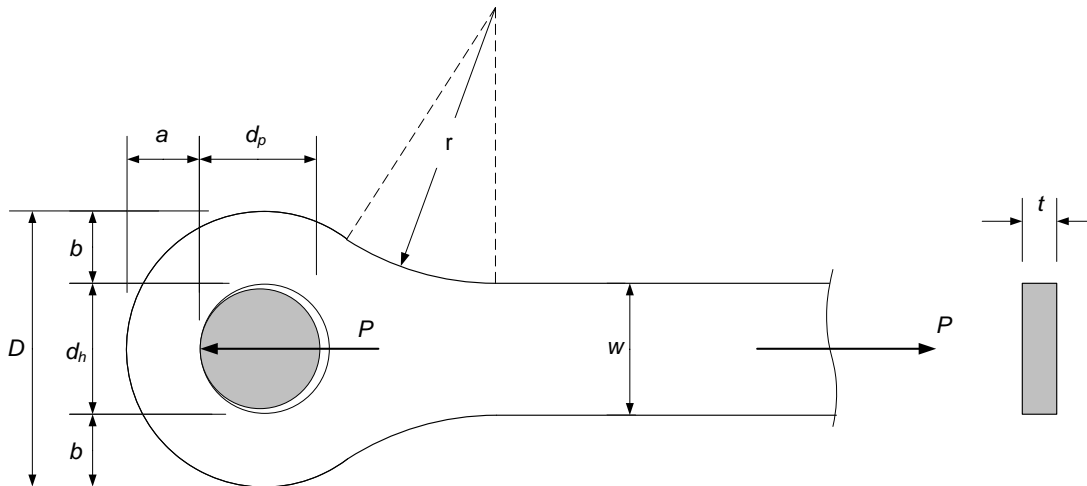
(1) Thickness (*t*) shall be uniform, with no hole reinforcement

(2) 0.5 in $\leq t \leq$ 2 in

(3) $r \geq D$

(4) $D \geq 1.35\ w$

(5) $a \geq 0.75\ w$

(6) $w \leq 8\ t$

(7) $d_h - d_p \leq$ 1/32 in

(8) $d_h \leq 5t$ for steels with $F_y >$ 70 ksi

(9) $a = b$ (AISC 2016)

(10) $d_p \geq 0.875\ w$ (AISC 2016)

(11) Eyebars of a set shall be sym. about central plane of member & as parallel as practical

(12) Eyebars shall be restrained against lateral movement on the pins and lateral distortion

(13) Adjacent bars in the same panel shall be separated by at least 0.5 in; Ring shaped spacers shall be provided to fill gaps between adjacent eyebars on a pin

(14) Intersecting diagonal bars that are not sufficiently spaced to clear each other at all times shall be clamped together at the intersection

Figure 43. Dimensional requirements for eyebars specified to ensure good member performance and development of the full yield capacity of the eyebar.
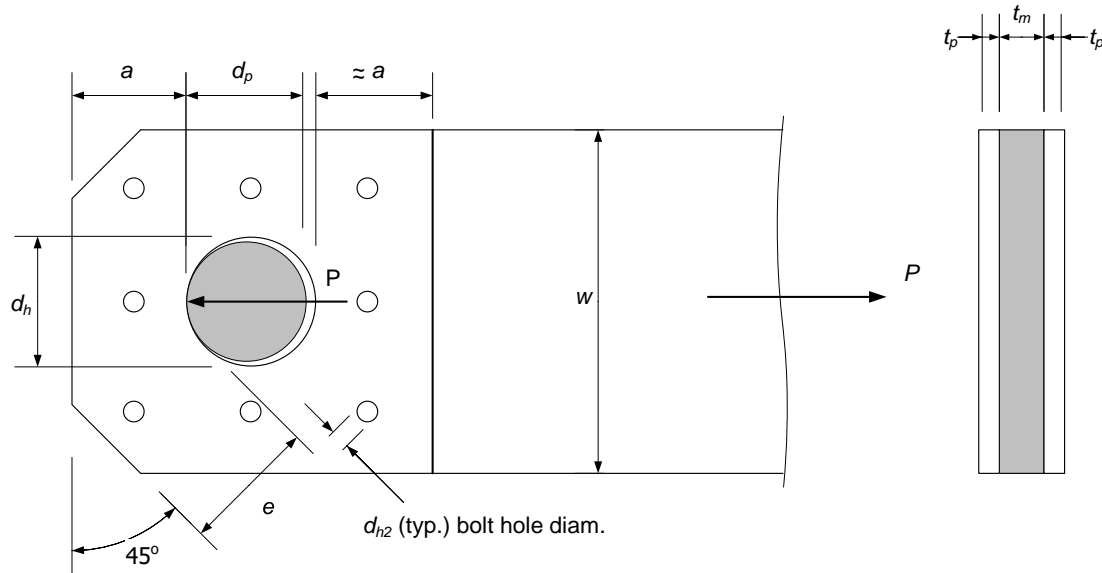
(1) Thickness (*t*) need not be uniform, i.e., the main plate may be reinforced by pin plates in the vicinity of the pin hole

(2) The pin plates, if used, shall be arranged to minimize the load eccentricity

(3) The pin plates, if used, shall be attached to the main plate by sufficient welds or bolts to transmit the bearing forces from the pin plates to the main plate

(4) Transverse net area requirement, to ensure against tensile fracture at a transverse section through the centerline of the pin hole:

$$\left\{ \left[w - \left(d_h + \frac{1}{16} \right) - 2 \left(d_{h2} + \frac{1}{16} \right) \right] \left(t_m + 2 t_p \right) \right\} \geq 1.4 \left(\frac{P_u}{0.8 F_{u,main}} \right)$$

(5) Longitudinal net area requirement, to ensure against tearing of the pin out of the end of the pin connected member:

$$\left\{ \left[a - \left(d_{h2} + \frac{1}{16} \right) \right] \left(t_m + 2 t_p \right) \right\} \geq \frac{P_u}{0.8 F_{u,main}}$$

(6) The pin hole shall be centered on the longitudinal axis of the main plate

(7) $d_h - d_p < 1/32$ in

(8) $d_h \leq 5 \, (2 t_p + t_m)$ for steels with $F_y > 70$ ksi

(9) $2 t_p + t_m \geq 0.12 \, [w/2 - (d_h + 1/16)/2 - (d_{h2} + 1/16)]$

(10) $w \leq 8 \, t_m$

(11) Pin-connected plates shall be restrained against lateral movement on the pins and lateral distortion

(12) Corners may be cut at 45° if e ≥ a (assuming one bolt hole along *e*, and one bolt hole along *a* in this example) (AISC 2016)

Figure 44. Requirements in addition to the checks of tension yielding, tension fracture and plate bearing, for a specific pin-connected plate with two equal size pin plates (dimensions *w*, *a* and *e* of pin plates = *w*, *a* and *e* of main plate) bolted on each side of the main plate.

6.1.3   Strands

AASHTO (2020) references three types of strand commonly used in bridge construction:

- Uncoated low-relaxation seven-wire strand for prestressed concrete (also used for stay cables and for prestressing of steel members), ASTM A416,

- Zinc-coated parallel and helical wire structural strand, ASTM A586, and

- Zinc-coated steel structural wire rope, ASTM A603.

The latter two strand types are referred to generally as bridge strand. Bridge strand is not used for major cable-stayed bridges or for prestressing steel, generally due to its lower stiffness. However, structural strand and structural wire rope are used for hangers in arch and suspension bridges.

In helical steel wire structural strand, the wires are laid helically about a center wire to produce a symmetrical section. Structural wire rope involves a group of strands placed helically around a core composed of either a strand or another rope. Both of these bridge strand types are usually prestretched by the manufacturer to remove the permanent "constructional stretch" caused by lengthening of the strand lay due to adjustment of the wires into a denser cross section under load. The prestretching is achieved by subjecting the strand to a load up to 55 % of the breaking strength for a sufficient length of time to permit the adjustment of the wires to that load. As a result, under working loads, the elongation of the strand is effectively elastic and can be calculated using the elastic moduli given in Table 2. These moduli are reduced relative to that of the base material due to the helical geometry of the wires and the zinc coating. The wires tend to straighten when subjected to tension. Also, the strength is reduced due to the helical geometry. The breaking strengths of Grade 1 structural strand and wire rope with Class A zinc coating are approximately 190 to 200 ksi based on the gross metallic area. The breaking strength of Grade 2 structural strand with Class A zinc coating is approximately $F_u = 220$ to 230 ksi based on the gross metallic area of the strand.

Table 2. Effective minimum elastic moduli of prestretched structural strand and structural rope (ASTM 2018; ASTM 2019).

Type	Nominal Diameter (in)	Minimum Modulus (ksi) Class A Coating[*]
Strand	½ to 2 $^9/_{16}$	24,000
	2 $^5/_8$ and larger	23,000
Rope	$^3/_8$ to 4	20,000

[*] For Class B or Class C weight of zinc-coated outer wires, reduce minimum modulus by 1000 ksi

Seven-wire prestressing strand has a straight core wire surrounded by a single layer of six helically-placed outer wires with a uniform pitch of not less than 12 and not more than 16 times the nominal diameter of the strand. This pitch is longer than that of bridge strand such that the elastic stiffness is essentially the same as that of the base material. AASHTO (2020) Article 5.4.4.2 specifies $E = 28,500$ ksi for seven-wire strand. ASTM 416 covers two types of seven-wire strand: low-relaxation and stress-relieved (normal relaxation). ASTM 416 states that low-relaxation strand shall be regarded as the standard type, and that stress-relieved (normal-relaxation) strand will not

be furnished unless specifically ordered, or by arrangement between the purchaser and supplier. Low-relaxation strand is produced by a combined process of low-temperature heat treatment and high tension. Seven-wire strand is produced with nominal breaking or ultimate strengths F_u of both 250 ksi and 270 ksi on the nominal area of the strand (smaller than the area based on the nominal diameter). The minimum yield strength F_y of low relaxation strand is 90 % of F_u, measured at 1% extension under load. Both seven-wire and bridge strand exhibit a gradual (non-sharp) yield response.

AASHTO (2020) does not specify a procedure for design of bridge strands or cables composed of seven-wire strand. In past practice, bridge strands were checked against working loads using a factor of safety of 3 to 4 with respect to their breaking strength (Podolny and Scalzi 1986). Cables composed of seven-wire strand were commonly checked against working loads using a factor of safety of 2 with respect to their minimum yield strength (Podolny and Scalzi 1986). Chapter 5 of AASHTO (2020) addresses the use of prestressing in concrete structures, but does not specifically address the use of prestressing steel for composite or noncomposite steel construction. The design calculations for prestressed steel structures may be based largely on the same fundamental principles of equilibrium and strain compatibility utilized within the AASHTO concrete provisions, combined with the steel design provisions of Chapter 6 for consideration of the stability of the structural steel elements. However, prestress losses due to elastic shortening and long-term shrinkage and creep of the concrete are in general different in structural steel applications. The reader is referred to Troitsky (1990) for detailed discussion of the design of prestressed steel bridges.

6.2 Compression Members

6.2.1 Base Column Strength Equations

AASHTO (2020) and AISC (2016) both effectively use the following single column-curve equations to characterize the nominal axial resistance of all types of steel and composite steel-concrete members to concentrically-applied axial compression:

$$P_n = \left[0.658^{\left(\frac{P_o}{P_e} \right)} \right] P_o \quad \text{for } \frac{P_o}{P_e} \leq 2.25 \tag{6.2.1-1a}$$

(AASHTO 6.9.4.1-1 & 6.9.5.1-1, AISC E3-1 & E3-2, E7-1 & I2-2)[3]

and

$$P_n = 0.877\, P_e \quad \text{for } \frac{P_o}{P_e} > 2.25 \tag{6.2.1-1b}$$

(AASHTO 6.9.4.1.1-2 & 6.9.5.1-2, AISC E3-1 & E3-3, E7-1 & I2-3)

where P_e is the elastic or effective elastic member buckling load, which can be calculated by the famous expression

---

[3] Throughout this volume, the number for equations specified within the AISC (2016) *Specification* is preceded by the term "AISC" followed by the equation number.

$$P_e = \frac{\pi^2 EI}{(KL)^2} \qquad\qquad\qquad (6.2.1\text{-}2a)$$

or

$$\frac{\pi^2 E}{(KL/r)^2} A_g = F_e\, A_g \qquad\qquad (6.2.1\text{-}2b)\ (\text{AASHTO } 6.9.4.1.2\text{-}1,\ \text{AISC E3-4})$$

for flexural buckling about either the major or minor principal axis of the cross section, and P_o is the effective cross-section or stub-column yield strength. That is, P_o is the strength in the limit of zero length ($KL = 0$). For a homogeneous prismatic steel member in which none of the cross-section plates are classified as slender, P_o is the full yield capacity given by

$$P_o = P_y = F_y\, A_g \qquad\qquad\qquad (6.2.1\text{-}3)$$

Equations 1, 2, and 3 are expressed in various specific forms in the AASHTO and AISC Specifications. The format shown here allows for a unified discussion of all the different column strength calculations. For column buckling, the square root of P_o/P_e,

$$\sqrt{\frac{P_o}{P_e}} = \left(\frac{KL}{r}\right)\frac{1}{\pi}\sqrt{\frac{F_y}{E}} \qquad\qquad (6.2.1\text{-}4)$$

for flexural buckling, is commonly employed within the structural stability literature as the member normalized slenderness. The other terms in Equations 1 through 4 are defined as follows:

A_g = gross area of the cross section,

E = steel elastic modulus, taken equal to 29,000 ksi,

F_y = column minimum specified yield strength,

I = moment of inertia of the cross section about the principal axis normal to the plane of buckling,

r = radius of gyration about the principal axis normal to the plane of bucking = $\sqrt{I/A_g}$,

K = effective length factor in the plane of buckling.

Equations 1 and 2 represent the nominal inelastic and elastic column buckling resistances respectively, as illustrated in Figure 45 in terms of both KL/r and $\sqrt{P_o/P_e}$. Although these equations are often considered solely in terms of the column effective slenderness ratio KL/r, the above general form of these equations is utilized in AASHTO (2020) and in AISC (2016) to define the resistance of all types of steel and composite steel concrete columns, including cases where P_e corresponds to limit states other than flexural buckling. Furthermore, this form is applied in White et al. (2021a) to quantify the resistance of columns having general tapered and/or stepped cross sections subjected to uniform or nonuniform axial compression. Equations 1 and 2 account in a broad fashion for the influence of residual stresses and geometric imperfections (out-of-straightness and out-of-plumbness) on the column resistance. They provide a close fit to SSRC

column curve 2P, which is based on a mean initial out-of-straightness of 1/1470 of the equivalent simply supported column length *KL* (Ziemian 2010) (see Figure 45).

Generally, there are significant differences in the mean column resistances depending on the column type. This is evidenced by the differences between SSRC curves 1P, 2P and 3P in Figure 45. Table 3 summarizes the recommended usage of these multiple column curves for a range of steel column cross sections. One can observe that the normalized column resistances are larger on average for lightweight sections, larger yield strengths and buckling about the major-axis of bending for I-shapes. They tend to be smaller for heavy sections, low yield strengths, and buckling about the minor-axis of bending for I-shapes. Column curve 3P applies only to heavy W-shapes with $F_y < 50$ ksi and welded H-shapes built-up from universal mill plate with $F_y < 50$ ksi for major-axis buckling and $F_y < 60$ ksi for minor-axis buckling. Welded built-up shapes are no longer manufactured from universal mill plates; furthermore, the minimum yield strength is usually 50 ksi or larger in new construction. Therefore, the resistances of all practical columns in new construction are best fit by column curves 1P and 2P, with 2P being the appropriate curve for most of the column types. AASHTO (2020) applies a resistance factor of $\phi_c = 0.95$ to Eqs. 6.2.1-1 for all types of steel-only members and $\phi_c = 0.90$ for composite steel-concrete members. This is consistent with the use of the single column curve Eqs. 6.2.1-1 and the use of a smaller ϕ_c factor for composite steel-concrete columns in AISC (2016). The AISC *Specification* has employed a larger ϕ_c factor of 0.90 versus its previous value of 0.85 for steel columns since AISC (2005) in recognition of the fact that column curve 3P is no longer applicable for new steel construction.
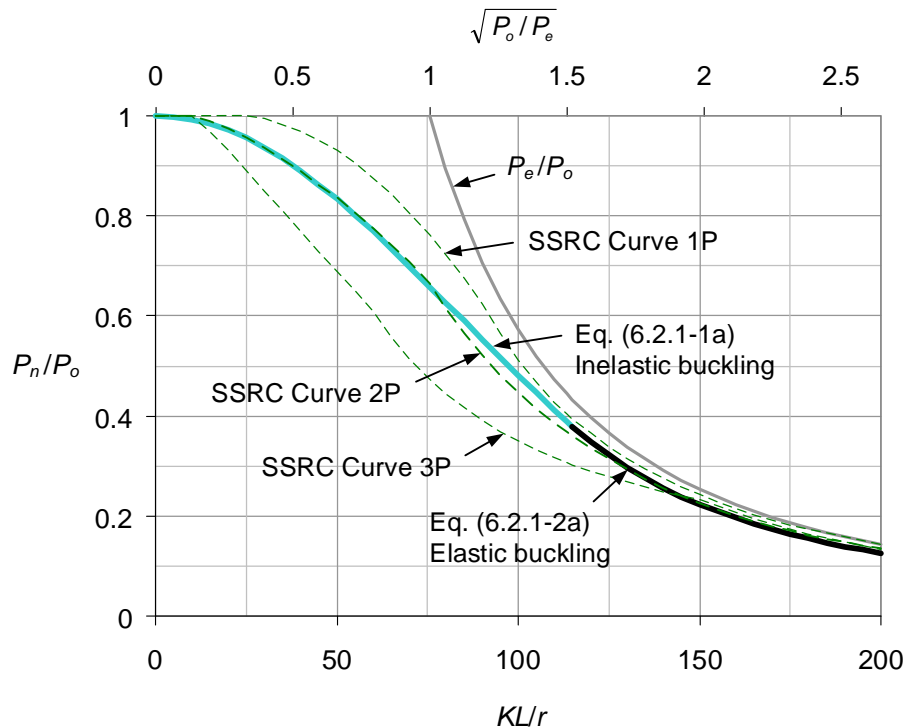
Figure 45. AASHTO (2020) and AISC (2016) column strength curve in terms of both *KL/r* and $\sqrt{P_o/P_e}$ versus the SSRC multiple column curves 1P, 2P and 3P (Ziemian 2010) and the theoretical elastic buckling strength, steel columns with $F_y = 50$ ksi.

Table 3. Recommended SSRC column curves for various types of steel cross sections, adapted from (Ziemian 2010).
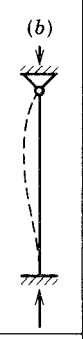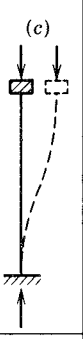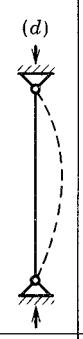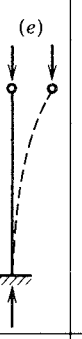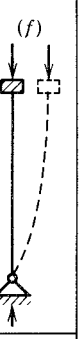
Cross-section type		Axis of Bending	Specified Minimum Yield Strength F_y (ksi)				
			≤ 36	37 to 49	50 to 59	60 to 89	≥ 90
Hot-rolled W-shapes	Light and medium Weight sections	Major	2	2	1	1	1
		Minor	2	2	2	1	1
	Heavy sections (flange thickness > 2 in)	Major	3	2	2	2	2
		Minor	3	3	2	2	2
Welded Built-up H-shapes	Flame-cut plates	Major	2	2	2	1	1
		Minor	2	2	2	2	1
	Universal mill plates	Major	3	3	2	2	2
		Minor	3	3	3	2	2
Welded Box Shapes	Flame-cut and Universal mill plates	Major	2	2	2	1	1
		Minor	2	2	2	1	1
Square and Rect. Tubes	Cold-formed	Major	N/A	2	2	2	2
		Minor	N/A	2	2	2	2
	Hot-formed and cold-formed heat-treated	Major	1	1	1	1	1
		Minor	1	1	1	1	1
Circular Tubes	Cold-formed	N/A	2	2	2	2	2
	Hot-formed	N/A	1	1	1	1	1

6.2.2 Flexural Buckling and Column Effective Length

The effective length factor K accounts for the influence of the column end conditions on the flexural buckling resistance, including interactions with other members in the structure. Table 4, from AISC (2016), summarizes the theoretical K values for cases in which the rotational and/or translational restraints at the ends of a column are either full (i.e., effectively rigid compared to the column stiffness) or nonexistent. Recommended design values are also provided. These values are simple modifications of the ideal values, taking into account the fact that the physical end translations and rotations can never be perfectly fixed or perfectly unrestrained.

In numerous other cases, K values are often specified based on established practice. For instance, Ziemian (2010) recommends the use of $K = 0.85$ for in-plane buckling of web members in bridge trusses. This is because the position of live load that produces the maximum force in a given web member typically causes less than the maximum force in the adjacent members. Therefore, the adjacent members are able to provide some rotational restraint. In lieu of analysis, AASHTO (2020) Article 4.6.2.5 allows a more liberal value of $K = 0.75$ for any truss or frame member that has bolted or welded end connections and is braced against lateral translation at its ends, with the exception of single angle members where $K = 1.0$ is suggested (Section 6.2.3.5 discusses equivalent KL/r values for design of single angles).

Table 4. Approximate values of effective length factor *K* for cases where the rotational and/or translational end restraints are either nominally fixed or nonexistent (reprinted with permission from AISC (2016)).

	(a)	(b)	(c)	(d)	(e)	(f)
Buckled shape of column is shown by dashed line						
Theoretical *K* value	0.5	0.7	1.0	1.0	2.0	2.0
Recommended *K* value when ideal conditions are approximated	0.65	0.80	1.2	1.0	2.10	2.0

End condition code	
⊤	Rotation fixed, Translation fixed
⊽	Rotation free, Translation fixed
⊡	Rotation fixed, Translation free
○	Rotation free, Translation free

In many situations where rotational restraint exists at the ends of a single bridge column or at the ends of the columns in a bridge frame, e.g. pier columns integral with bridge girders, the traditional sidesway inhibited or sidesway uninhibited alignment charts (AASHTO 2020; AISC 2016; Kavanagh 1962) provide acceptable solutions for *K*. However, it is essential to recognize that the alignment charts are based on idealized assumptions that in certain cases are invalid. The commentary to Appendix 7 of AISC (2016) discusses these assumptions in detail and provides a number of modifications to the alignment chart procedures that extend their range of applicability. AASHTO (2020) Article C4.6.2.5 gives closed form equations that provide a close fit to the base sidesway inhibited and sidesway uninhibited alignment charts. The AISC (2016) modifications also must be applied in general in the use of these equations.

As noted previously in Section 2.5 of this volume, AASHTO (2020) Article 4.5.3.2.2c provides suggested effective length factors for in-plane buckling of arches. These values range from 0.70 for a fixed arch with a small rise-to-span ratio to 1.16 for two- or three-hinged arches with a large rise-to-span ratio. These values are applied to *one-half* of the total arc length of the arch rib. For checking stability in the out-of-plane direction, the effective length *KL* may be taken as the distance between the rib bracing points when a lateral bracing system of adequate stiffness is provided. However, special consideration of arch-end portals is generally necessary. Refined eigenvalue buckling analysis is the simplest way to check the out-of-plane stability of these assemblies. The reader is referred to the discussion in Section 6.2.6 of this volume for the handling of nonuniform compression and/or nonuniform cross-section properties along the length of an arch.

In trusses, frames and arches where a refined analysis is employed to assess the stability, it is simpler and more convenient to work directly with the member elastic buckling load, P_e, than

back-calculate an equivalent pinned-ended length *KL*. In this case, P_e in Eqs. 6.2.1-1 is simply the axial load in a given member at incipient elastic buckling of the structure or subassembly considered in the buckling analysis. The use of P_e in Eqs. 6.2.1-1 is also essential for the application of these equations in determining the torsional and torsional-flexural buckling resistances of certain types of members (see Section 6.2.3 below). All of the above *K* factor considerations pertain solely to flexural buckling. In several of the following sections, *KL* is taken as an "equivalent length" accounting for attributes other than just the flexural response.

6.2.3 Column Torsional and Torsional-Flexural Buckling

AASHTO (2020) Article C6.9.4.1.3 and AISC (2016) Section E4 give the applicable resistance equations for members susceptible to torsional or torsional-flexural buckling. These include some singly symmetric members such as double angles and tees, and built-up members such as columns with cruciform cross sections and/or with relatively thin cross-section plate elements. As noted in the previous section, all the AISC (2016) and AASHTO (2020) column resistance calculations use Eqs. 6.2.1-1; however, the calculation of P_e differs based on column buckling mode.

6.2.3.1 Torsional buckling of doubly symmetric cross-section members

Doubly symmetric cross section members that are relatively weak in torsion, e.g., cruciform columns or columns that are braced but are not sufficiently restrained against twisting at a number of their brace points, can fail by a buckling mode involving a pure twisting about the axis of the member (see Figure 46). In these cases, the elastic torsional buckling load may be expressed as

$$P_e = P_{ez} = \left[\frac{\pi^2 E C_w}{\left(KL_z\right)^2} + GJ\right]\frac{A_g}{I_x + I_y}$$ (6.2.3-1) (AASHTO 6.9.4.1.3-1, AISC E4-2)

where

C_w = warping constant for the cross section, equal to zero for a cruciform section,

KL_z = effective length for torsional buckling,

G = steel shear modulus, taken as 11,200 ksi,

J = St. Venant torsional constant for the cross section, and

I_x and I_y = moments of inertia about the major and minor principal axes of bending respectively.
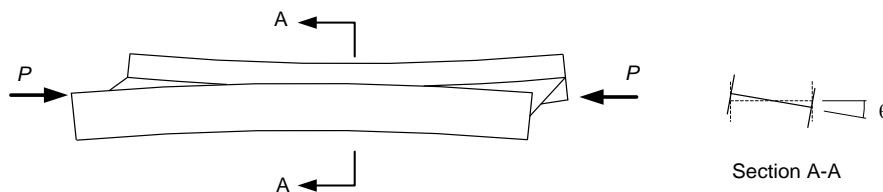
Figure 46. Torsional buckling of an I-section member.

The effective length for torsional buckling, KL_z, is usually taken as the distance between locations where the member is restrained against twisting. For the case of a cantilever column fully restrained against twisting and warping at one end and with the other end free, $KL_z = 2L$. For a member where twisting and warping are fully restrained at each of its ends, $KL_z = 0.5L$. (Note that the notation "KL_z" is a simplification of the different symbols used for these terms in AASHTO (2020); in this volume, the subscripts x, y, or z are placed at the end of the general effective length symbol, KL, to indicate the effective lengths for flexural buckling about the major (x) or minor (y) principal axes of the section, or torsional buckling about the longitudinal z axis of the member. AISC (2016) simplifies further by adopting the notation L_{cx}, L_{cy}, and L_{cz} for these different effective lengths)

Doubly symmetric compression members can fail either by flexural buckling about one of the cross-section principal axes, or by torsional buckling. However, torsional buckling rarely governs except for members such as cruciforms. Torsional buckling never needs to be considered for doubly symmetric I-section members that satisfy the AASHTO Article 6.10.2 proportion limits, unless KL_z is significantly larger than the weak-axis flexural buckling effective length, KL_y. Generally, P_{nz}/P_{ny} (the ratio of the nominal column strengths using Eq. 1 with KL_y rather than Eq. 3 for calculation of P_e) is smaller for smaller D/b_f, larger b_f/t_f, larger D/t_w and larger P_o/A_g. Based on $D/b_f = 1$, $b_f/t_f = 24$, $D/t_w = 192$ (corresponding to $t_f/t_w = 8$) and $P_o/A_g = 100$ ksi as a worst-case set of cross-section parameters, the smallest value of P_{nz}/P_{ny} is still only 0.974 at $KL_y/r_y = 37$, assuming $KL_z = KL_y$. That is, torsional buckling leads to a maximum reduction of only 2.6 percent for all practical doubly symmetric I-shapes. The consideration of end-restraint effects (if they are accounted for at all) in the calculation of the column buckling loads is not anywhere near this precise. Also, P_{nz}/P_{ny} increases rapidly with increases in D/b_f.

6.2.3.2 Flexural or torsional-flexural buckling of singly symmetric cross-section members

Compression members with singly symmetric cross sections, where the y-axis is taken as the axis of symmetry, either can fail by flexural buckling about the x-axis or by torsion combined with flexure about the y-axis. The elastic torsional-flexural buckling load for these types of members is given by the expression

$$P_e = P_{eTF} = \left(\frac{P_{ey} + P_{ez}}{2H} \right) \left[1 - \sqrt{1 - \frac{4 P_{ey} P_{ez} H}{\left(P_{ey} + P_{ez} \right)^2}} \right] \tag{6.2.3-2}$$

(AASHTO 6.9.4.1.3-2, AISC E4-5)

where

$$P_{ey} = \frac{\pi^2 E I_y}{(KL_y)^2} = \frac{\pi^2 E}{(KL_y / r_y)^2} A_g \qquad \text{(6.2.3-3) (AASHTO 6.9.4.1.3-4, AISC E4-8)}$$

$$P_{ez} = \left[\frac{\pi^2 E C_w}{(KL_z)^2} + GJ \right] \frac{1}{\left(y_o^2 + \dfrac{I_x + I_y}{A_g} \right)} = \left[\frac{\pi^2 E C_w}{(KL_z)^2} + GJ \right] \frac{1}{\bar{r}_o^2} \qquad (6.2.3\text{-}4)$$

<div align="right">(AASHTO 6.9.4.1.3-5, AISC E4-9)</div>

$$H = 1 - \frac{y_o^2}{\bar{r}_o^2} \qquad (6.2.3\text{-}5) \text{ (AASHTO 6.9.4.1.3-3, AISC E4-10)}$$

KL_y = effective length for flexural buckling about the y-axis (the axis of symmetry of the cross section),

C_w = cross-section warping constant, equal to zero for cross sections where the component plates are all joined at a single common point, e.g., tee sections,

y_o = distance along the y-axis between the shear center and the cross section centroid,

$\bar{r}_o$ = polar radius of gyration about the shear center

$$\bar{r}_o^2 = y_o^2 + \frac{I_x + I_y}{A_g} \qquad (6.2.3\text{-}6) \text{ (AASHTO 6.9.4.1.3-6, AISC E4-11)}$$

The governing column strength, P_n, is obtained by substituting the smaller value of P_{eTF} (which is always smaller than P_{ey}) or P_{ex} (flexural buckling about the x-axis) into Eqs. 6.2.1-1.

As noted above, P_{eTF} is generally smaller than P_{ey}. However, the flanges of singly symmetric I-sections often have equal widths (only the flange thicknesses differ). Therefore, for these types of member, y_o tends to be relatively small and the influence of the smaller P_{eTF} on P_n is always less than 4 % as long as

$KL_z \le KL_y$ and $0.67 \le t_{f1}/t_{f2} \le 1.5$

where t_{f1} and t_{f2} are the flange thicknesses. For I-section members with equal-width flanges, the largest reduction in P_n due to the smaller P_{eTF} occurs for $D/t_w = 150$, $b_f/t_f = 24$ and $D/b_f = 6$, (the maximum limits in AASHTO (2020) Articles 6.10.2.1.1 and 6.10.2.2), $P_o/A_g = 100$ ksi, $KL_y/r_y = 114$ and $KL_z = KL_y$ (smaller D/t_w gives a larger reduction for this case, but causes $t_f/t_w \le 1$). Therefore, if the above limit is satisfied, torsional-flexural buckling never needs to be considered for practical I-section members with equal-width flanges and $KL_z \le KL_y$.

Interestingly, the reductions in the torsional-flexural buckling resistance for I-section members with unequal width flanges are significant in many practical cases even when there are rather small differences in the flange widths. This is because the lateral moment of inertia of the flanges varies with b_f^3, and hence only minor changes in the relative flange widths result in a significant shift in the cross-section shear center relative to the centroid. The shift in the cross-section shear center is similar to the shift in the centroid due to changes in the flange thickness; however, the shift in the shear center is significantly different than the shift in the centroid due to changes in the flange

width. Therefore, there does not appear to be any simple way to exclude the need to consider torsional-flexural buckling for I-section members with unequal flange widths.

6.2.3.3 Torsional-flexural buckling of general unsymmetric cross-section members

Lastly, for members with no cross-section axis of symmetry, the failure mode under axial compression always involves torsion combined with flexure about both the x and y axes. In this case, P_e is the smallest root of the following cubic equation

$$\left(P_e - P_{ex}\right)\left(P_e - P_{ey}\right)\left(P_e - P_{ez}\right) - P_e^2\left(P_e - P_{ey}\right)\left(\frac{x_o}{\bar{r}_o}\right)^2 - P_e^2\left(P_e - P_{ex}\right)\left(\frac{y_o}{\bar{r}_o}\right)^2 = 0 \qquad (6.2.3\text{-}9)$$

(AASHTO 6.9.4.1.3-7, AISC E4-6)

where

$$P_{ex} = \frac{\pi^2 E I_x}{\left(KL_x\right)^2} = \frac{\pi^2 E}{\left(KL_x / r_x\right)^2} A_g \qquad (6.2.3\text{-}10)\ (\text{AASHTO 6.9.4.1.3-8, AISC E4-7})$$

P_{ey} is as defined in Eq. 3,

$$P_{ez} = \left[\frac{\pi^2 E C_w}{\left(K_z L\right)^2} + GJ\right]\frac{1}{\bar{r}_o^2} \qquad (6.2.3\text{-}11)\ (\text{AASHTO 6.9.4.1.3-5, AISC E4-9})$$

$$\bar{r}_o^2 = x_o^2 + y_o^2 + \frac{I_x + I_y}{A_g} \qquad (6.2.3\text{-}12)\ (\text{AASHTO 6.9.4.1.3-9, AISC E4-11})$$

and

$x_o, y_o = x$ and y coordinates of the shear center with respect to the cross-section centroid.

As noted previously, once the elastic buckling load, P_e, is calculated, it is substituted into Eqs. 6.2.1-1 to determine the nominal elastic or inelastic column buckling resistance.

6.2.3.4 Special handling of single angle compression members in AASHTO (2020) and AISC (2016)

Single angle compression members are used extensively as cross-frame and lateral-bracing members in steel bridge construction. The AISC (2016) and AASHTO (2020) Specifications provide highly simplified provisions for design of specific types of single angle web members subjected to axial compression. These provisions define an equivalent slenderness (KL/r) for use with Eqs. 6.2.1-1 and 6.2.1-2 applicable when:

1. The end connections are to a the same leg,

2. The member is loaded through the same leg at each of its ends,

3. The end connections are welded or use a minimum of two bolts,

4. The member is not subjected to any intermediate transverse loads, and

5. If used as web members in trusses, all adjacent web members are attached to the same side of the gusset plate or chord.

For these types of single-angle members, the equivalent *KL/r* accounts for the effects of the end eccentricities and restraints, and the member may be proportioned using Eqs. 6.2.1-1 and 6.2.1-2 as if it were a concentrically compressed strut subjected solely to flexural buckling. The equivalent *KL/r* expressions presume significant end rotational restraint about the *Y*-axis shown in Figure 47, where the *Y*-axis is the geometric axis perpendicular to the connected leg and to the gusset or the plate component of another member to which the angle is connected. This leads to the angle member tending to buckle primarily about the *X*-axis. As such, *r* is taken as the r_X for the angle for bending *about an axis parallel to the connected leg*. It is *not* taken as the minimum $r = r_z$ about the angle minor principal axis. In addition, it should be noted that a capital *X* is used here because, for an unequal leg angle, the *X* axis can be either the *x* or *y* axis of the angle shown in property tables, depending on which of the legs is the connected one.
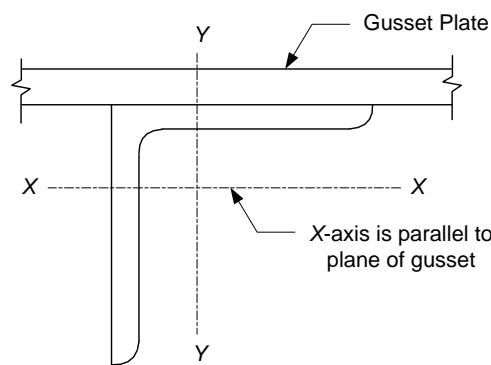
Figure 47. Single-angle cross section and definition of geometric axes utilized by the AISC (2016) and AASHTO (2020) equivalent *KL/r* expressions.

AISC (2016) provides two sets of equations for the equivalent *KL/r*, one based on the assumption of significant rotational restraint about the *X* and *Y* axes in Figure 47 and the other based on tests having close to the knife-edge end conditions shown in Figure 48 (with less than rigid *Y*-axis restraint and considering some minor *X*-axis restraint). The more optimistic equations, which assume substantial *X*- and *Y*-axis end restraint, are essentially equivalent to the ASCE 10-97 (ASCE 2000) equations for equal-leg angles in latticed transmission towers. These equations are classified by AISC (2016) as being applicable for "web members of box or space trusses." The less optimistic equations are classified by AISC (2016) as being applicable for "web members of planar trusses." Based on the data presented by Lutz (2006), these equations are considered applicable for all types of single angles commonly employed in bridge cross frames and lateral bracing systems. These equations are as follows.
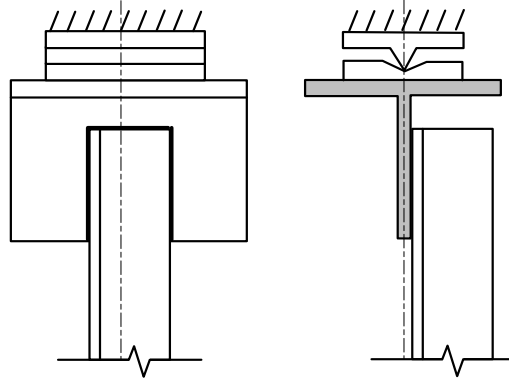
Figure 48. Test end conditions associated with the recommended equivalent *KL/r* equations for single angle struts.

For equal-leg angles, and unequal-leg angles connected through the longer leg,

$$\frac{KL}{r} = 72 + 0.75\frac{L}{r_X} \quad \text{when } 0 \le \frac{L}{r_X} \le 80 \qquad \text{(6.2.3-15a) (AASHTO 6.9.4.4-1, AISC E5-1)}$$

and

$$\frac{KL}{r} = 32 + 1.25\frac{L}{r_X} \quad \text{when } \frac{L}{r_X} > 80 \qquad \text{(6.2.3-15b) (AASHTO 6.9.4.4-2, AISC E5-2)}$$

where *L* is the length of the member between the end-connection work points. It is intended that the design should not be used in any case where the maximum value of *KL/r* in Eq. 15b is greater than 200.

For unequal-leg angles with the ratio of the leg widths less than 1.7, connected through the shorter leg,

$$\frac{KL}{r} = 72 + 0.75\frac{L}{r_X} + 4\left[\left(\frac{b_\ell}{b_s}\right)^2 - 1\right] \ge 0.95\frac{L}{r_z} \quad \text{when } 0 \le \frac{L}{r_X} \le 80 \qquad \text{(6.2.3-16a)}$$

$$\text{(AASHTO 6.9.4.4-3, AISC E5-1)}$$

and

$$\frac{KL}{r} = 32 + 1.25\frac{L}{r_X} + 4\left[\left(\frac{b_\ell}{b_s}\right)^2 - 1\right] \ge 0.95\frac{L}{r_z} \quad \text{when } \frac{L}{r_X} > 80 \qquad \text{(6.2.3-16b)}$$

$$\text{(AASHTO 6.9.4.4-4, AISC E5-2)}$$

where b_ℓ and b_s are the widths of the longer and shorter legs respectively, r_z is the minimum radius of gyration of the angle, and as in Eq. 15b, it is intended that the design should not be used if the equivalent *KL/r* is greater than 200 in Eq. 16b.

It is important to emphasize in the above that r_X is the radius of gyration about the angle geometric axis parallel to the connected leg. For an unequal-leg angle connected through the longer leg, r_X is actually the smaller r value about the angle's geometric axes, typically listed as r_y in section property tables. Equations 16 account for the fact that the strength is enhanced by using the longer leg as the outstanding leg, but also recognize that this tends to force the actual buckling axis to be closer to the z-axis of the angle (Lutz 2006). The limit of $b_\ell/b_s \leq 1.7$ is based on the limits of the available experimental tests.

Lutz (2006) obtains a mean professional bias factor for the above equations of $P_n/P_{max} = 0.998$ with a coefficient of variation of 0.109 relative to single-angle tests approximating the knife-edge end conditions shown in Figure 48. In addition, Lutz (2006) shows a representative equal-leg angle example in which the above equations give results close to those obtained using the more generally applicable approach of treating the single-angle as a beam-column under specific conditions. The more general procedure requires the use of Eq. 9, the calculation of moments based on assumed end eccentricities, the calculation of single-angle moment capacities, and beam-column interaction checks. The two approaches are roughly equivalent when:

1. The end eccentricity e_X (normal to the X-axis) is taken as $\bar{Y} + t/2$, where $\bar{Y}$ is the distance from the outside face of the angle leg to the geometric centroidal axis perpendicular to the plane of the gusset or connection plate and t is the thickness of the connection plate,

2. The end eccentricity e_Y is taken as the value necessary to theoretically achieve uniform stress along the connected leg,

3. The effective length for buckling about the X-axis (parallel to the connected leg and the connection plate) is calculated using $K_X = 1.0$, and

4. The effective length for buckling about the Y-axis is calculated using $K_Y = 0.65$ (Lutz (1992) gives a procedure for calculating this effective length factor).

Lutz (2006) also compares the AISC/AASHTO equations to other equivalent KL/r procedures in Eurocode 3 (CEN 2005) and in the British Standard BS5950 (BSI 1990). The Eurocode 3 procedure gives results that are very close to the AISC space truss equations for $L/r_X > 60$, but is more optimistic than the AISC space-truss provisions for smaller L/r_X values. The BS5950 equations predict larger capacities than the AISC space-truss provisions for $L/r_X < 120$ in Lutz's equal-leg angle example, and predict essentially the same capacities for larger L/r_X. The above Eqs. 15 fall below the European and British predictions for all ranges of L/r_X. Eq. 15a gives a result that is 21 and 44 percent below these predictions at $L/r_X = 40$.

One of Lutz's (2006) examples is a single angle strut with legs that qualify as slender elements. For this case, Lutz uses an equivalent yield strength QF_y, where $Q < 1$ is the AISC (2010) form factor accounting for local buckling effects. ASCE 10-97 (ASCE 2000) applies a similar reduction for these types of angles. The procedures in AISC (2016) and AASHTO (2020) for members with slender elements now employ the unified effective width approach as discussed in Section 6.2.4. The unified effective width approach is generally accepted as providing improved generality, accuracy and simplicity relative to the more traditional Q factor approaches.

The fifth restriction on the equivalent *KL*/*r* equations, listed at the beginning of this section, is based largely on the test results presented by Woolcock and Kitipornchai (1986). These investigators found that single angle web members in trusses have a smaller theoretical capacity when they are connected alternately on opposite sides as opposed to connecting the members all on the same side of the stem of T-section truss chords. This is apparently due to the shear transfer within a Warren-type truss system with the diagonals alternating in tension and compression, and the corresponding additive eccentricity effects of compression in one web diagonal with tension in the other adjacent web diagonal.

With the exception of "X" bracing in cross frames or lateral bracing systems, single-angle members typically are all connected on the same side at their end connections (NSBA 2006). Nevertheless, it is common in some bridge applications to have both diagonals in compression at a joint in a Warren truss. This can occur for example when a Warren truss is used for the top lateral bracing system in a box girder. In this case, the compression in the two adjacent diagonals would cause an additive detrimental eccentric loading effect if both members are connected on the same side. That is, depending on the specific loads being transferred at the bracing connections, connecting the angles on the same side could be detrimental or beneficial.

Upon looking at the fifth restriction more broadly, considering the potential restraints from typical single-angle connection details in steel bridge cross frames and lateral-bracing systems, it is recommended that the approximate knife-edge boundary conditions about the *X*-axis, upon which Eqs. 15 and 16 are based, are an acceptable approximation for calculation of the single-angle capacities for any configuration of cross frames or flange-level lateral bracing in steel bridge applications. The approximate knife-edge boundary conditions are judged typically to be more detrimental to the angle member strengths than the physical end conditions for these members.

The special case of "X" bracing systems merits some further discussion. In cases where one diagonal is in tension, and if this member has an axial force of not less than 20 % of the force in the compression member, ASCE 10-97 (ASCE 2000) indicates that the cross-over point may be considered as a braced point for out-of-plane buckling. It would appear that a similar approach might be applied with Eqs. 15 and 16. However, this approach needs validation. If only a single bolt is used to connect the angles at the cross-over point, the restraint about the *Y*-axis assumed in Eqs. 15 and 16 may not be present at this point.

Equations 15 and 16 may be applied conservatively in X-bracing systems by using the full length of the diagonal between the end connection work points for *L*. This is a prudent design approach, since it streamlines the design calculations.

El-Tayem and Goel (1986) have studied the X-bracing problem where the compression and tension member are equally loaded and the connections are welded. Their research has involved both theoretical and experimental investigations. They indicate that the compression diagonal of X-bracing systems made of equal-leg single-angle members may be checked neglecting the effect of end eccentricity, using a *KL* in Eq. 6.2.1-2 equal to 85 % of the half-length of the compression diagonal and using the radius of gyration $r = r_z$ taken about the minor principal axis of the angle cross section.

6.2.4 Axial Compressive Resistance of Members Containing Slender Longitudinally Unstiffened Elements Under Uniform Axial Compression

This section discusses the axial compressive resistance of members containing slender longitudinally unstiffened elements under uniform axial compression, that is, cross-section elements that do not contain longitudinal stiffeners. The axial compressive resistance of more general members utilizing plates containing longitudinal stiffeners is discussed subsequently in Section 7 of this volume.

6.2.4.1 Plate local buckling under uniform axial compression

Plate local buckling involves the out-of-plane bending of the plate elements with the line junctures between the elements remaining straight. The elastic critical stress for local buckling has been investigated extensively and is summarized by Bleich (1952), Timoshenko and Gere (1961), Bulson (1970) and Allen and Bulson (1980). The elastic critical stress for local buckling of a plate element in compression may be written as

$$F_{e\ell} = \frac{\pi^2 E k_c}{12\left(1-\nu^2\right)\left(b/t\right)^2} \tag{6.2.4-1}$$

where

$\quad k_c \quad = \quad$ plate local buckling coefficient

$\quad \nu \quad = \quad$ Poisson's ratio for steel (commonly taken as 0.3)

$\quad b/t \quad = \quad$ relevant width-to-thickness ratio.

Salmon and Johnson (1996) summarize the theoretical minimum k_c values for elastic plate buckling under uniform compression as shown in Figure 49. For example, a plate with simply supported edge conditions on all four sides (Case C) has a minimum k_c of 4.0. The aspect ratio of the plate, a/b, influences the half-wavelength of the local buckles and hence influences the elastic local buckling strength. The minimum values of k_c are realized when an integer number of half-wavelengths of length b fit within the total length of the plate, a, that is when $a/b = 1, 2, 3, \ldots$ etc. Plates with one longitudinal edge free, and with the other edges simply supported, always buckle at a half-wavelength equal to the length of the plate, a. As a/b becomes larger, k_c approaches the minimum value of 0.425. However, for $a/b = 2.0$, $k_c = 0.675$. Plate local buckling design rules are usually based on minimum theoretical k_c values for different hypothetical edge conditions. Various idealized cases are illustrated in Figure 49.
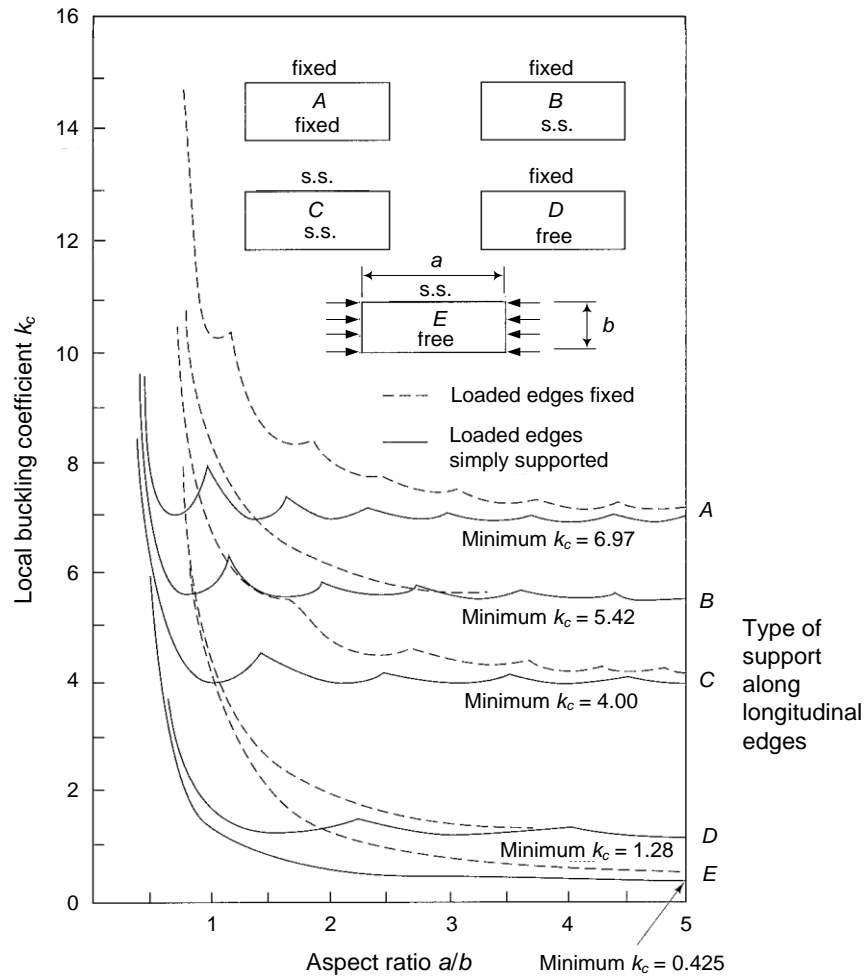
Figure 49. Theoretical k_c values for elastic plate buckling (adapted from Salmon and Johnson (1996)).

For a given member cross section subjected to uniform axial compression, the different plates generally have different k_c values if they are analyzed in isolation, ignoring the compatibility of deformations between the plates at their common edges. For example, for an I-section member, the b/t of each of the flanges would be taken as $b_f/2t_f$ and k_c could be taken as 0.425, whereas the b/t of the web would be taken as h/t_w and k_c could be taken as 4.0. A local buckling analysis of the entire cross section would show that the flange and web elements all buckle simultaneously at a stress larger than either of the stresses for the isolated elements. This is due to the changes required to make the half-wavelengths compatible.

Common practice in AISC (2016) and in AASHTO (2020) is to consider each of the plate elements within the cross section in isolation, but using various implicit semi-rational k_c values based on collective judgement over many years.

73

6.2.4.2　Postbuckling strength of longitudinally unstiffened plate elements in compression

A key attribute of the stability behavior of plates is that local buckling does not correspond to the maximum compressive resistance. Plates subjected to uniform compressive displacements (shortening) between rigid frictionless platens will bend out-of-plane after buckling as shown in Figure 50, and will redistribute their longitudinal membrane stresses from uniform compression to those shown in the figure. This occurs regardless of whether the plates are supported on both longitudinal edges or on only one longitudinal edge. The plates continue to support increased loads, although with a reduction in their effective axial stiffness. Furthermore, the line of action of the resultant compressive force will move toward the supported edge in the plate that is supported only on one longitudinal edge.

The analysis of the postbuckling action and the subsequent load capacity of a plate generally requires a sophisticated geometric nonlinear load-deflection solution. Von Karman et al. (1932) suggested a simple approximation for the ultimate strength of plates in which both longitudinal edges are supported transversely:

- They proposed that the actual stress distribution be replaced by two effective widths of $b_e/2$ < $b/2$ on each side of the plate, each subjected to a uniform stress, f, equal to the actual maximum stress at the edge of the plate (see Figure 51), and where the effective width b_e is determined such that $f\, b_e\, t$ is equal to the total load supported by the plate.

- They also suggested that the above two strips be considered as a rectangular plate of total width b_e, and that the maximum load capacity of the plate corresponds to when the elastic critical stress of that plate becomes equal to the yield strength of the material, F_y.

Therefore, according to von Karman et al. (1932) and based on Eq. 1, the ultimate load capacity of a plate may be derived from

$$F_y = \frac{\pi^2 E k_c}{12\left(1-\nu^2\right)\left(b_e / t\right)^2} \tag{6.2.4-2}$$

Dividing Eq. 1 by Eq. 2, one obtains

$$\frac{b_e}{b} = \sqrt{\frac{F_{e\ell}}{F_y}} \tag{6.2.4-3}$$

at the ultimate strength condition.

(a) Plate transversely supported on both longituidnal edges

(b) Plate transversely supported on one longituidnal edge
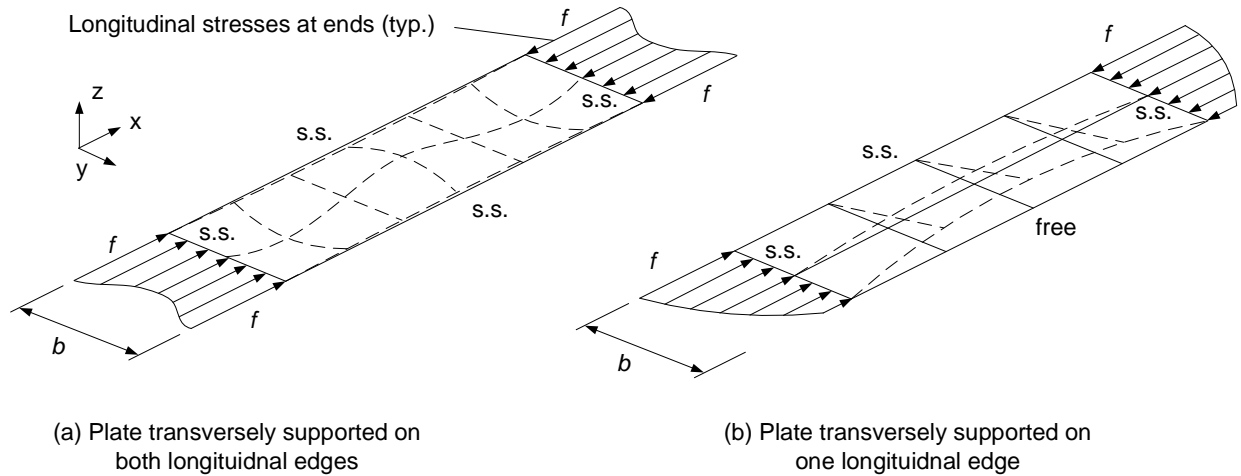
Figure 50. Postbuckled plate deformations and longitudinal stresses at ends.

(a) Plate transversely supported on both longituidnal edges

(b) Plate transversely supported on one longituidnal edge
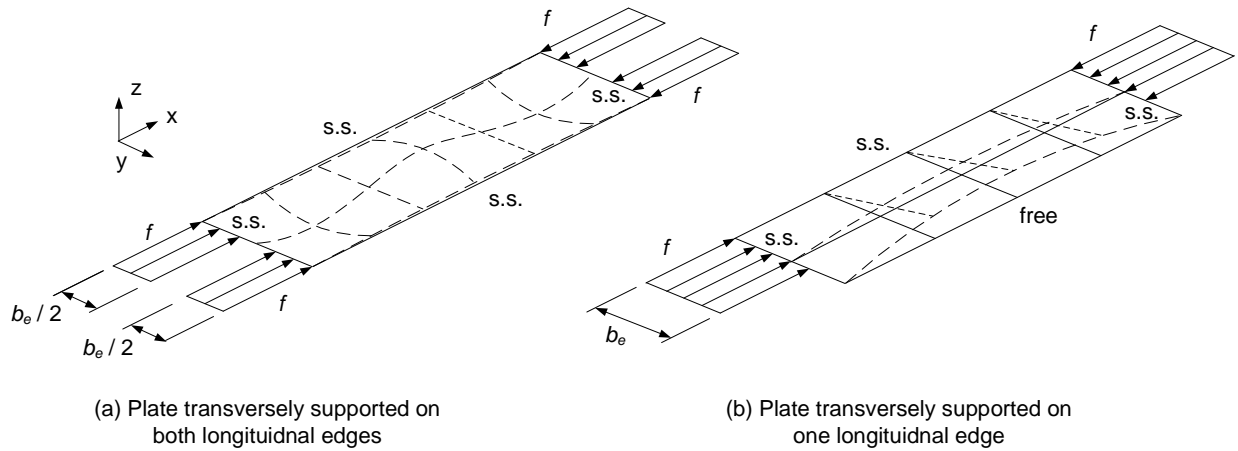
Figure 51. Effective stress distributions on postbuckled plates.

Although von Karman et al. only suggested the above effective width formula for plate elements with two transversely supported longitudinal edges, this idealization works satisfactorily for the effective width of a plate having only one transversely supported longitudinal edge as well. An important caveat, however, is that Eq. 3 does not provide a sufficient description of the strength of plates having geometric imperfections and residual stresses. Considering these attributes, Winter (1968) proposed and verified experimentally the following formula for plates in which both longitudinal edges are transversely supported:

$$\frac{b_e}{b} = \sqrt{\frac{F_{e\ell}}{F_y}} \left(1 - 0.22 \sqrt{\frac{F_{e\ell}}{F_y}} \right) \qquad\qquad (6.2.4\text{-}4a)$$

Although another more optimistic equation was originally proposed for plates transversely supported only on one longitudinal edge, the data from Kalyanaraman et al. (1977) indicated that Eq. 4a provides a more accurate estimate for stockier plates. Consequently, the AISI *Specifications* for cold-formed steel design adopted Eq. 4a for all types of plates subjected to uniform longitudinal compression. This of course has the advantage of simplicity, since one equation can be employed for all types of plates.

The AISC (2016) and AASHTO (2020) Specifications replace the coefficient 0.22 in Eq. 4a by the variable c_1, to accommodate additional manipulations of this equation discussed subsequently:

$$\frac{b_e}{b} = \sqrt{\frac{F_{e\ell}}{F_y}}\left(1 - c_1\sqrt{\frac{F_{e\ell}}{F_y}}\right) \tag{6.2.4-4b}$$

It is of interest to determine the value of b/t below which a given plate is fully effective at the yield strength of the material, F_y, that is, the value of b/t below which that plate is able to support the full longitudinal yield load $F_y\, b\, t$ with $b_e = b$. This value of b/t is referred to as the nonslender plate limit, λ_r. Upon setting b_e/b in Eq. 4b to 1.0, one can solve for the value

$$c_2 = \sqrt{\frac{F_{e\ell-r}}{F_y}} \tag{6.2.4-5}$$

above which the plate is nonslender, i.e., effective at developing the material yield strength over the full plate cross-sectional area. Substituting Eq. 5 for $\sqrt{F_{e\ell}/F_y}$ in Eq. 4b, one obtains

$$1 = c_2\left(1 - c_1 c_2\right) \tag{6.2.4-6}$$

Upon solving this quadratic equation for c_2, one obtains

$$c_2 = \frac{1 - \sqrt{1 - 4c_1}}{2c_1} \tag{6.2.4-7} \text{ (AISC E7-4)}$$

as the appropriate solution.

Given Eq. 5 as well as the above definition of λ_r, the elastic buckling stress corresponding to the nonslender plate limit may be written as

$$F_{e\ell-r} = c_2^2 F_y = \frac{\pi^2 E k_c}{12\left(1 - \nu^2\right)\lambda_r^2} = F_{e\ell}\left(\frac{\lambda}{\lambda_r}\right)^2 \tag{6.2.4-8}$$

where λ is a compact notation for the b/t of the plate. The second and fourth expressions of this equation may be solved for $F_{e\ell}$ to obtain the following alternative general expression for the local elastic buckling stress of the plate:

$$F_{e\ell} = \left(c_2 \frac{\lambda_r}{\lambda} \right)^2 F_y \qquad\qquad (6.2.4\text{-}9) \text{ (AISC E7-5)}$$

By equating the second and third expressions in Eq. 8 and solving for λ_r, one can obtain the following general expression for λ_r in terms of c_2 and k_c:

$$\lambda_r = 0.951 \frac{\sqrt{k_c}}{c_2} \sqrt{\frac{E}{F_y}} = \Gamma_r \sqrt{\frac{E}{F_y}} \qquad\qquad (6.2.4\text{-}10\text{a})$$

That is, the coefficient on the nonslender plate limit equation may be expressed generally as

$$\Gamma_r = 0.951 \frac{\sqrt{k_c}}{c_2} \qquad\qquad (6.2.4\text{-}10\text{b})$$

Therefore, given Eqs. 7 and 10b, the specified value of c_1, and the coefficient employed within different expressions for the nonslender plate limit λ_r, i.e., Γ_r, one can back-calculate the plate local buckling coefficient employed implicitly within the AASHTO and AISC plate strength equations. The corresponding equation is

$$k_c = 1.11 \left(c_2 \Gamma_r \right)^2 \qquad\qquad (6.2.4\text{-}10\text{c})$$

It should be noted that Winter also found empirically that Eq. 4a holds well for all levels of stress above that at which the longitudinal stresses start to redistribute and the plate becomes less than fully effective. Therefore, expanding this observation more generally, Eq. 4b may be written as

$$\frac{b_e}{b} = \sqrt{\frac{F_{e\ell}}{f}} \left(1 - c_1 \sqrt{\frac{F_{e\ell}}{f}} \right) \qquad\qquad (6.2.4\text{-}11)$$

applicable for $\lambda > \lambda_r \sqrt{F_y / f}$ where f is a general maximum edge stress on the plate.

As noted above, AASHTO (2020) and AISC (2016) specify coefficients other than $c_1 = 0.22$ for certain types of plate elements. Specifically:

- AISC (2016) Table E7.1 specifies $c_1 = 0.20$ for walls of square and rectangular HSS, whereas AASHTO (2020) Table 6.9.4.2.2b-1 specifies $c_1 = 0.20$ for:

    1. Flanges and webs of nonwelded built-up box sections,

    2. Walls of square and rectangular hot-formed HSS, and

    3. Nonperforated flange cover plates.

- AISC (2016) Table E7.1 specifies $c_1 = 0.18$ for all "stiffened elements" (i.e., plate elements supported transversely on both of their longitudinal edges) other than walls of square and rectangular HSS, whereas AASHTO (2020) Table 6.9.4.2.2b-1 specifies $c_1 = 0.18$ for:

    1. Webs of rolled I- and channel sections,

    2. Webs of nonwelded built-up I- and channel sections,

    3. Webs of welded and nonwelded built-up I-sections containing two or more longitudinal stiffeners, and

    4. Flanges and webs of nonwelded built-up box sections containing two or or more longitudinal stiffeners.

These modifications provide slightly more optimistic characterizations of the plate postbuckling strengths compared to the characterization using $c_1 = 0.22$. The AASHTO rules are considered to be somewhat more appropriate given that there would appear to be no justification for using the smaller $c_1 = 0.18$ on webs of general built-up I-sections containing flanges with a relatively large b/t. In addition, the AASHTO provisions specify $c_1 = 0.22$ for cold-formed HSS sections, which is consistent with the AISI (2016) rules. The AASHTO (2020) c_1 value for plates with two or more longitudinal stiffeners provides some recognition of the additional net lateral restraint from adjacent panels (within the plane of the plate) at the multiple longitudinal stiffener locations in these plates.

AASHTO (2020) specifies one additional form of the plate local buckling strength equations applicable for all other plates supported along both longitudinal edges. This is in recognition of research ranging back to the early work by Dowling and others and reflected in BS 5400-3:2000 (BSI 2000), which indicates that for members composed of general welded plate assemblies, the plate ultimate resistances are smaller than indicated by Winter's classical effective width equation. Johansson and Velijkovic (2009), Schillo (2017) ad Schillo and Taras (2018) have found Winter's effective width equation to be optimistic for unstiffened plates in welded box-section members.

The corresponding equations are applicable to boxes with longitudinally unstiffened plates, and to longitudinally stiffened plates having only one longitudinal stiffener, where one does not have substantial "edge constraint" (i.e., restraint of lateral deflections of the longitudinal plate edges within the plane of the plate). White et al. (2019a) discuss comparisons with the experimental data. The BS5400 curve is described by multiple equations covering different ranges of slenderness. As such, this curve is rather onerous to apply in design. A close approximation to the BS5400 equation is obtained simply by shifting Winter's Eq. 4a vertically by 0.075. When this is done, the effective width Eq. 11 becomes

$$\frac{b_e}{b} = \sqrt{\frac{F_{e\ell}}{f}}\left(1 - c_1\sqrt{\frac{F_{e\ell}}{f}}\right) - c_3 \qquad \text{(6.2.4-12) (AASHTO 6.9.4.2.2b-2 \& Table 6.9.4.2.2b-1)}$$

where c_1 and c_3 are taken equal to 0.22 and 0.075 respectively.

By recognizing that c_2 is the value of $\sqrt{F_{e\ell}/F_y}$, for $f = F_y$, at which $b_e/b = 1.0$ (referred to previously as $c_2 = \sqrt{F_{e\ell-r}/F_y}$) (Eq. 5), then one can solve for c_2 corresponding to Eq. 12 by writing

$$1 = c_2\left(1 - c_1 c_2 - c_3\right)$$

and solving this quadratic equation for c_2:

$$c_2 = \frac{1 - \sqrt{1 - 4c_1\left(1 + c_3\right)}}{2c_1} \qquad\qquad \text{(6.2.4-13) (AASHTO 6.9.4.2.2b-3)}$$

Given the value of c_2 from Eq. 13, Eqs. 10b and 10c still provide the relationship between c_2, Γ_r and k_c.

Table 5 summarizes all the plate local buckling and plate effective width parameters based on the above relationships, as well as the parameters for perforated cover plates. This table is associated with AASHTO (2020) Tables 6.9.4.2.1-1 and 6.9.4.2.2b-1 as follows:

- Cases 1a through 1d in Table 5 correspond to the first entry in AASHTO Table 6.9.4.2.2b-1, and they correspond to the first four entries in AASHTO Table 6.9.4.2.1-1 (they are labeled as elements supported along one longitudinal edge in that table).

- Cases 2 through 6 in Table 5 correspond to the second through the sixth entries in AASHTO Table 6.9.4.2.2b-1, and they correspond to the next five entries in AASHTO Table 6.9.4.2.1-1 (they are labeled as elements supported long two longitudinal edges in that table).

AASHTO Table 6.9.4.2.1-1 gives specific definitions of the plate width b for the different cases.

With the exception of Case 1c, the k_c values are implicit (i.e., not explicitly stated) in the AASHTO Specifications. These k_c values may be calculated given the specified c_1, c_2, c_3 and Γ_r values in AASHTO (2020) using the above relationships.

The explicit equation for k_c in Case 1c is based on the studies by Johnson (1985). The specific AASHTO-AISC equation for k_c in this case, shown in the last column of Table 5, is a simplification of Johnson's recommendations first introduced in AISC (1989). The value of $k_c = 0.77 \cong 0.76$ (i.e., the value specified as the upper limit of the value from the k_c equation in Case 1c) is based on traditional AISC practice.

It is informative to compare the k_c values in Table 5 versus the theoretical minimum k_c values for elastic plate buckling shown in Figure 49. One can observe that the limit of $k_c = 0.35$ in Case 1c corresponds to built-up I-sections with a web-to-thickness ratio, D/t_w, greater than or equal to 131. This value is smaller than the theoretical k_c of 0.425 for s.s. (simply supported) - free longitudinal edge conditions (case E of Figure 49), indicating that the flanges are idealized as being destabilized by the local buckling of the web for these geometries. The Case 1c flange k_c value of 0.76, which is intermediate between the theoretical s.s.-free and fixed-free values of 0.425 and 1.28, corresponds to $D/t_w \leq 28$.

Table 5. AASHTO (2020) Plate local buckling and effective width parameters.

Case	c_1	c_2	$1/c_2$	c_3	Γ_r	k_c
(1a) Stems of rolled tees	0.22	1.49	0.671	0.0	0.75	1.4
(1b) Flanges of rolled I, tee, and channel sections; plates projecting from rolled I-sections; Outstanding legs of double angles in continuous contact	0.22	1.49	0.671	0.0	0.56	0.77
(1c) Flanges of welded and nonwelded built-up I-sections; Plates or angle legs projecting from welded or nonwelded built-up I-sections	0.22	1.49	0.671	0.0	$0.64\sqrt{k_c}$	$4/\sqrt{D/t_w}$ $0.35 \le k_c \le 0.76$
(1d) Outstanding legs of single angles; Outstanding legs of double angles with separators; Flange extensions of box sections; Plates or angle legs projecting from welded and nonwelded built-up I- or box-sections; and all other plates supported along one longitudinal edge	0.22	1.49	0.671	0.0	0.45	0.50
(2) Perforated cover plates	0.22	1.49	0.671	0.0	1.86	8.5
(3) Webs of rolled I- and channel sections; webs of nonwelded built-up I- and channel sections; webs of welded and nonwelded built-up I-sections containing two or more longitudinal stiffeners; and flanges and webs of welded and nonwelded built-up box sections containing two or more longitudinal stiffeners	0.18	1.31	0.763	0.0	1.49	4.2
(4) Flanges and webs of nonwelded built-up box sections; Walls of square and rectangular hot-formed HSS, and nonperforated flange cover plates	0.20	1.38	0.725	0.0	1.40	4.1
(5) Walls of square and rectangular cold-formed HSS	0.22	1.49	0.671	0.0	1.28	4.0
(6) All other plates supported along two longitudinal edges	0.22	1.74	0.575	0.075	1.09	4.0

In addition, one can observe that the k_c of 1.4 for the stems of tee-sections (Case 1a) is slightly larger than the value for the theoretical fixed-free Case D in Figure 49, the k_c value of 0.50 for Case 1d is slightly larger than the minimum value of 0.425 (generally assuming the existence of some edge restraint), the k_c value for perforated cover plates (Case 2) is slightly larger than the value for the theoretical fixed-fixed Case A in Figure 49, and all the other k_c values are equal to 4.0 or are only slightly larger than 4.0 (accounting for some minor edge restraint). It should be noted that the larger k_c values for stems of tee-sections and for angle legs is offset to some extent by the use of the full depth of tees and the full width of the outstanding leg of angles as the b dimension, and the larger k_c value for perforated cover plates is effectively based on judgment in applying the rectangular plate equations to this special case.

Figure 52 shows the various plate local buckling strength curves considered in this section, plotted in a normalized fashion as the average longitudinal compressive design stress divided by the maximum edge stress, F_n/f, which is equal to the ratio of the plate effective width to the actual width, b_e/b. The normalized theoretical elastic buckling stress, $F_{e\ell}/f$, is also shown in the plot. Figure 52 plots these strengths versus the normalized plate slenderness, $\sqrt{f/F_{e\ell}}$. As noted previously, the von Karman strength curve corresponds to the theoretical ultimate strength of a perfectly flat plate with zero initial stresses.
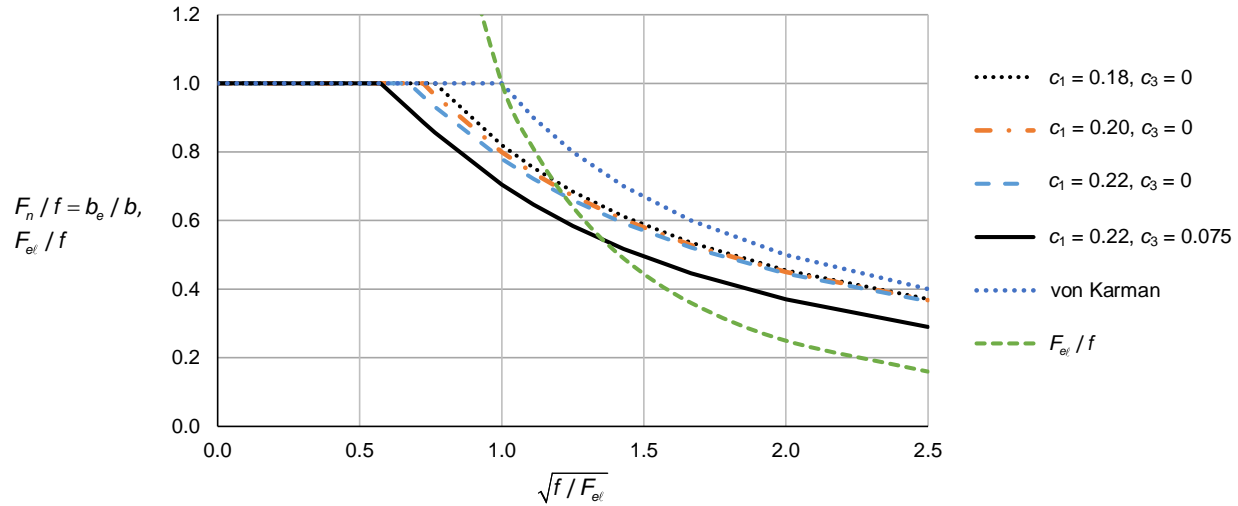
Figure 52. Normalized AASHTO (2020), von Karman et al. (1932) and theoretical elastic buckling plate strengths versus $\sqrt{f/F_{e\ell}}$.

The AASHTO (2020) plate strengths are larger than the theoretical plate elastic buckling resistance when $\sqrt{f/F_{e\ell}} > 1.17$ for Case 3 of Table 5 ($c_1 = 0.18$ and $c_3 = 0$), when $\sqrt{f/F_{e\ell}} > 1.19$ for Case 4 of Table 5 ($c_1 = 0.20$ and $c_3 = 0$), when $\sqrt{f/F_{e\ell}} > 1.22$ for Cases 1a through 1d and Case 5 of Table 5 ($c_1 = 0.22$ and $c_3 = 0$) and when $\sqrt{f/F_{e\ell}} > 1.36$ for Case 6 of Table 5. The corresponding values of $\sqrt{f/F_{e\ell}}$ at which the plates are fully effective are labeled as $1/c_2$ in Table 5.

Figure 53 plots the normalized average compressive design stress, $F_n/f = b_e/b$, and the normalized theoretical elastic buckling stress, $F_{e\ell}/f$, versus b/t, corresponding to $f = 50$ ksi, for several types of plate elements transversely supported only on one longitudinal edge:

- Case 1c with $k_c = 0.35$, which corresponds to built-up I-sections with relatively thin webs ($D/t_w \geq 131$);

- Case 1c with $k_c = 0.76$, which matches with Case 1b within roundoff in the calculation of k_c, corresponding to built-up I-sections with stocky webs ($D/t_w \leq 28$) and to rolled I-sections among the other stated element types in Table 5; and

- Case 1d, which uses an intermediate value for $k_c = 0.50$ and an intermediate value for $\Gamma_r = 0.45$, which applies to outstanding legs of single angles among the other stated element types in Table 5.

One can observe that for the most conservative case, Case 1c with $k_c = 0.35$, the b/t (taken as $b_f/2t_f$ in the AASHTO (2020) provisions) must be smaller than 9.1 for the flange to be fully effective at $f = 50$ ksi. Conversely, for the most aggressive case, Case 1c with $k_c = 0.76$, the b/t must be less than 13.5 for the flange to be fully effective. It should also be noted that all the design strength

curves cross the corresponding implicit elastic buckling strength curve at $F_n/f = F_{el}/f = 0.68$, which for $f = 50$ ksi corresponds to $F_n = F_{e\ell} = 34$ ksi.

Figure 54 plots the normalized average compressive design stress, $F_n/f = b_e/b$, and the normalized theoretical elastic buckling stress, $F_{e\ell}/f$, versus b/t, corresponding to $f = 50$ ksi, for several types of plate elements transversely supported on both longitudinal edges:

- Case 3, $k_c = 4.2$, which corresponds to webs of rolled I- and Channel sections, webs of nonwelded built-up I- and Channel sections, webs of welded and nonwelded built-up I-sections containing two or more longitudinal stiffeners, and flanges and webs of welded and nonwelded built-up box sections containing two or more longitudinal stiffeners;

- Case 4, $k_c = 4.1$, which corresponds to flanges and webs of nonwelded built-up Box sections and walls of square and rectangular hot-formed HSS;

- Case 5, $k_c = 4.0$, which corresponds to walls of square and rectangular cold-formed HSS; and

- Case 6, $k_c = 4.0$, which corresponds to all other plates supported along two longitudinal edges.

As noted previously, Case 3 (with $c_1 = 0.18$) is employed for plates with two or more longitudinal stiffeners to provide some recognition of the additional net lateral restraint from adjacent panels at the multiple longitudinal stiffener locations in these plates. Case 6 applies to the more common case of plates supported along two longitudinal edges but not containing any longitudinal stiffening. It can be observed that the increases in the strengths for Cases 3 and 4 relative to Case 5 are relatively minor. Nevertheless, at the nonslender plate limit for Case 3, the corresponding normalized strengths F_n/f are 0.97 and 0.93 for Cases 4 and 5, respectively. The design strength curves cross the corresponding implicit elastic buckling strength curve at $F_n/f = F_{el}/f = 0.72$ for Case 3, 0.70 for Case 4, 0.68 for Case 5 and 0.55 for Case 6, which for $f = 50$ ksi correspond to $F_n = F_{e\ell} = 36$ ksi, 35 ksi, 34 ksi, and 27.5 ksi respectively.

One other important slenderness limit addressed in AASHTO (2020) Article 6.9.4.2 and AISC (2016) Table B4.1a is the limit for the axial strength of circular tubes not to be influenced by local buckling. This limit is

$$\frac{D}{t} \leq 0.11 \frac{E}{F_y} \qquad \text{(6.2.4-14) (AASHTO Table 6.9.4.2.1-1, AISC Table 4.1a)}$$

where D is the outside diameter of the tube and t is the tube thickness. This limit was first used in the AISC (1978) Allowable Stress Design Specification. Analytical buckling solutions significantly overestimate the physical local buckling resistance of longitudinally compressed cylinders due to imperfections in the shape and eccentricities of the load. Therefore, Eq. 14 is based on test evidence from Sherman (1976), providing a D/t limit below which local buckling can be taken to not occur for an applied axial stress up to F_y.
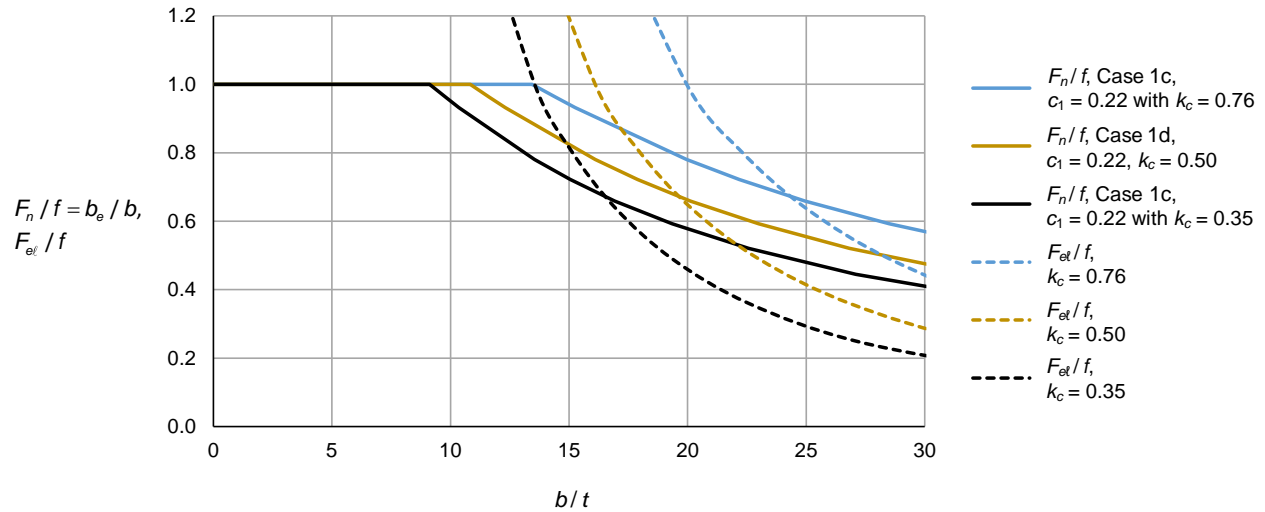
Figure 53. Normalized AASHTO (2020) average compressive design stress and theoretical elastic buckling stress versus *b/t* for plate elements transversely supported only along one longitudinal edge, *f* = 50 ksi.
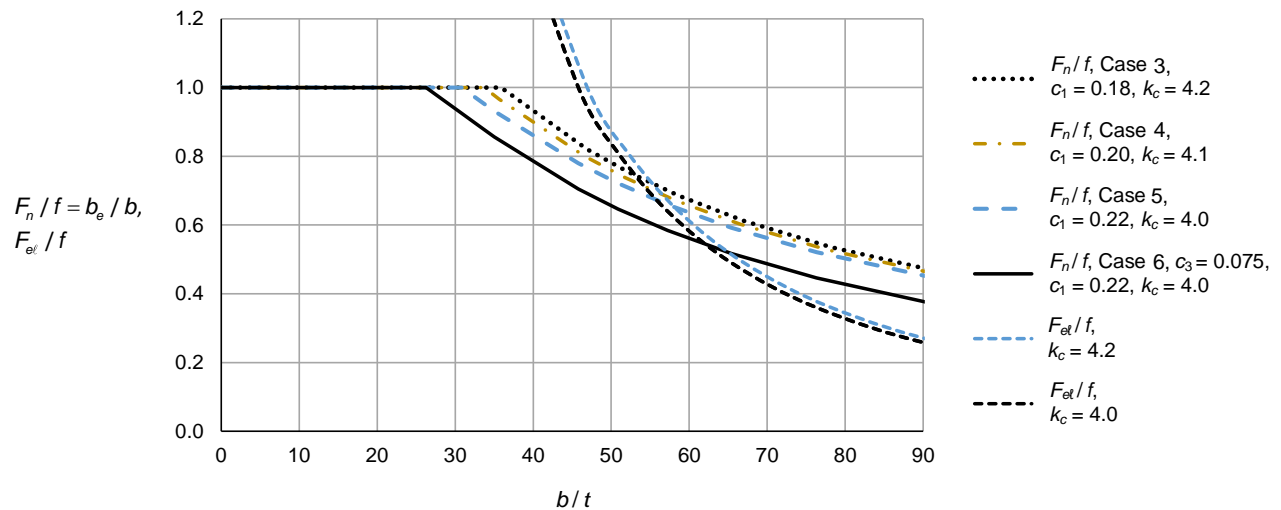
Figure 54. Normalized AASHTO (2020) average compressive design stress and theoretical elastic buckling stress versus *b/t* for plate elements transversely supported along both longitudinal edges, *f* = 50 ksi.

6.2.4.3   Member axial compressive resistance – Unified effective width method

For members containing any slender longitudinally unstiffened cross-section elements, i.e., cross-section elements exceeding the limits defined by Eq. 10a or Eq. 5, local buckling may adversely influence the overall buckling resistance of the member under uniform axial compression. For such members, AASHTO (2020) and AISC (2016) now employ a generalized form of the unified effective width method originally proposed by Peköz (1987). Previous AASHTO and AISC specifications have used a dual philosophy for longitudinally unstiffened plates, commonly

referred to as the Q factor method, in which slender elements supported only on one longitudinal edge were assumed to reach their limit of resistance when they attained their theoretical local buckling stress, while slender elements supported on both longitudinal edges utilized an effective width concept, quantifying their postbuckling resistance. The unified effective width approaches implemented in AASHTO (2020) and AISC (2016) utilize effective width to quantify the influence of potential plate local buckling (and postbuckling) actions on member strengths for all types of plates. This simplifies the resulting calculations and tends to provide a more accurate characterization of the ultimate strength considering the plate postbuckling behavior.

The unified effective width method hinges on the calculation of the effective widths of slender plates using $f = F_{cr}$, where

$$F_{cr} = \frac{P_{cr}}{A_g} \qquad \text{(6.2.4-15) (AASHTO 6.9.4.2.2a-2)}$$

and P_{cr} is the column strength obtained from Eqs. 6.2.1-1, based on the member gross cross-section properties. AISC (2016) uses Eq. 11 whereas AASHTO (2020) uses Eq. 12 for the calculation of the plate effective widths, based on taking $f = F_{cr}$. The constants c_1, c_2 and Γ_r are similar in both standards, with the exception of the use of $c_3 = 0.075$ for Case 6 in Table 5, which recognizes the smaller strengths observed for longitudinally unstiffened plates in welded plate assemblies as discussed in the previous section.

The original developments pertaining to the unified effective width method focused on the calculation of member effective cross-section properties, particularly the effective moment of inertia based on plate effective widths, I_e, in the calculation of the column buckling stress. This type of procedure required iteration, since the effective widths are a function of the applied stresses. However, in the context of column flexural buckling, it was observed that the variation in the effective radius of gyration, $r_{eff} = \sqrt{I_e / A_e}$, relative to the radius of gyration based on the gross cross-section properties was relatively minor. Similar observations were made with regard to other modes of failure under uniform axial compression. Therefore, it was found that the axial compressive strength of members containing slender elements could be calculated accordingly, and non-iteratively, by using the gross cross-section properties to determine the column strength in terms of the axial stress, F_{cr}, and by applying this stress to the effective area of the member cross section, A_e:

$$P_n = F_{cr} A_e \qquad \text{(6.2.4-16) (AASHTO 6.9.4.2.2a-1, AISC E7-1)}$$

One can observe that for members with larger overall slenderness, $\sqrt{P_o / P_e}$ (Eq. 6.2.1-4), the plate effective widths tend to be larger relative to the values associated with $f = F_y$, due to the smaller values of F_{cr}. In fact, it should be emphasized that the classification of a plate as slender under uniform axial compression indicates that the plate is not able to develop the yield capacity on its gross area due to the influence of local buckling. A slender plate element is still fully effective at $f = F_{cr}$ if $\lambda \leq \lambda_r \sqrt{F_y / f}$.

The reader is referred to Ziemian (2010) for a more detailed discussion of the development and basis of the unified effective width method. The original development of the unified effective width method showed that accurate predictions were obtained for general singly symmetric and unsymmetric members, with the exception of single-angle sections, when the moment of the axial loads is taken about the centroidal axis of the effective section determined considering axial compression alone. AISI (2016) relaxes the requirement that the bending moment should be defined with respect to the centroidal axis of the effective section. The increased eccentricity due to local buckling can have a measurable impact on the resistance of an ideally pin-ended member; however, this effect tends to become minor in continuous members or members with ends restrained, where the rotations due to these eccentricities are restrained. AASHTO (2020) and AISC (2016) also neglect these effects.

Many beam-type ASTM A6 rolled wide-flange sections (i.e., sections with $d/b_f \geq 1.7$) have slender webs under uniform axial compression. Also, the stems of a large number of WT sections and one or both legs of many of the rolled angles are slender by the above definitions, i.e., $b/t > \lambda_r$ from Eq. 10a. Welded I- and box-girders practically always have webs that are slender under uniform axial compression. The Engineer should note that, with the exception of the provisions for filled composite-section members in AISC (2016), cross-section components are classified either as slender or non-slender under uniform axial compression in AASHTO (2020) and AISC (2016). There are no compactness requirements for uniform axial compression. Compactness requirements apply only to member flexural resistances, where the flange and web elements need to withstand larger inelastic strains for local buckling not to influence the nominal strength. AISC (2016) clarifies this consideration by splitting its Table B4.1 into two separate tables, Table B4.1a corresponding to uniform axial compression and Table B4.1b corresponding to flexure. The separate approach to classification of filled composite-section members in AISC (2016) is addressed subsequently in Section 6.2.7 of this volume.

6.2.4.4 Axial capacity of hybrid slender-web girders

For girders subjected predominantly to flexural loading, the most economical use of high-performance steels often involves one or two high-performance steel (HPS) flanges combined with a lower strength web. As noted above, the webs of girders designed predominantly for flexure are practically always classified as slender elements under uniform axial compression. Although the use of homogeneous sections is most appropriate for members that resist substantial axial compression, hybrid slender-web girders are still acceptable when the axial loads are small. In these cases, the axial capacity $\phi_c P_n$ may be calculated by taking F_y as the smallest specified yield strength of all the cross-section elements for the calculation of F_{cr}. This is a conservative approximation of the complex behavior associated with the post-buckled state of the cross-section component plates as well as shifts in the effective centroid and shear center of the cross section due to varying extents of yielding in the different component plates as the member strength limit is approached. White et al. (2019a) suggest one potential refinement on this calculation for cases where the cross section is doubly symmetric and the web yield strength is between 0.7 and 1.0 times the minimum flange yield strength.

6.2.4.5 Local buckling criteria for solid-web arch ribs

Prior to the 9th Edition (AASHTO 2020), Article 6.14.4 of the AASHTO LRFD Specifications specified a number of special web and flange width-to-thickness limits written in terms of factored stresses due to the applied loads. These limits were based on the work by Nettleton (1977) and employed a number of simplifying assumptions that can be violated in various practical situations. In addition, the equations were typically configured for the calculation of design strengths in ways that made them highly conservative with respect to the plate local buckling and postbuckling resistances discussed in the previous sections. White et al. (2019a) provide a detailed discussion of the attributes of the prior AASHTO Article 6.14.4 equations.

The AASHTO (2020) Article 6.14.4 provisions are completely rewritten to take advantage of the advancements discussed in Sections 6.2.4.2 and 6.2.4.3 as well as improvements in the calculation of noncomposite box-section member flexural resistances discussed in Section 6.5.3 of this volume. Equations and guidance are provided to account for strength reductions due to the influence of arch rib vertical curvature on plate and lateral-torsional buckling resistances. In addition, not-to-exceed b/t limits are provided for arch rib flanges and webs to avoid significant impacts of vertical curvature on the structural resistances.

6.2.5 Built-up Members Composed of Two or More Shapes

AASHTO (2020) Article 6.9.4.3 addresses the design of built-up columns composed of two or more shapes. These member types include closely-spaced back-to-back angles attached by intermittent bolted or welded filler plates or boxed channels (Figure 55a) as well as large compression members with flange components that are spaced widely apart. In the latter case, the flange components may be connected together by perforated cover plates, lacing with flat bars, angles, channels or other shapes, or batten plates as shown in Figure 55b.

The strength behavior of these types of members differs from the previously discussed cases due to the influence of shearing deformations or displacements between the connected shapes. These deformations or displacements reduce the member buckling capacity and induce stresses in the elements that connect the shapes together.

Box columns with perforated cover plates designed to Specification rules do not require any strength reduction or other special considerations for shear effects. In new bridge construction, perforated cover plates are likely to be used rather than laced or battened columns. Conversely, the member buckling resistance can be reduced significantly for laced or battened members, with the largest reductions occurring for battened columns.

AASHTO Article 6.9.4.3.2 gives an equation for the shear force due to column stability effects, which perforated cover plates must be designed for in addition to the shear force from factored loads. Article 6.8.5.2 provides additional dimensional requirements for perforated plates that ensure adequate member performance.

In built-up members other than box columns with perforated cover plates, the shear deformations or displacements between the connected shapes can have a significant influence on the member axial capacity. In all cases, the end connections must be sufficient to essentially prevent the relative longitudinal slip displacement between the connected shapes at the member ends, if the built-up

member is to be effective as a single structural member. This connection is the dominant contributor to making the connected shapes act together. However, the compressive strength is also influenced to some extent by the shear restraint provided by intermediate connectors along the member length.

Figure 55 Types of built-up columns, (a) columns with closely-spaced components and (b) columns with widely-spaced components.

AASHTO (2020) and AISC (2016) both provide equations for a modified slenderness ratio that accounts for the effect of shearing deformations in the connectors between closely-spaced shapes. Article 6.9.4.3.1 of AASHTO (2020) gives the following equation for members with intermediate connectors that are welded or fully-tensioned bolted:

$$\left(\frac{KL}{r}\right)_m = \sqrt{\left(\frac{KL}{r}\right)_o^2 + 0.82\left(\frac{\alpha^2}{1+\alpha^2}\right)\left(\frac{a}{r_{ib}}\right)^2} \qquad \text{(6.2.5-1) (AASHTO 6.9.4.3.1-1)}$$

where

$\left(\dfrac{KL}{r}\right)_o$ = slenderness ratio of the built-up member acting as a unit (with shear deformation neglected) in the buckling direction being considered,

$\left(\dfrac{KL}{r}\right)_m$ = modified slenderness ratio accounting for shear deformation effects,

a = distance between connectors,

r_{ib} = radius of gyration of an individual component relative to its centroidal axis parallel to the axis of buckling,

α = separation ratio = $h/2r_{ib}$, and

H = distance between the centroids of the individual components perpendicular to the axis of buckling.

This equation is the same as Eq. E6-2 in the AISC (2005) Specification. Given the above modified slenderness ratio $(KL/r)_m$, the normalized slenderness $\sqrt{P_o / P_e}$ is calculated from Eq. 6.2.1-4 and then substituted into Eqs. 6.2.1-1 to determine the nominal column capacity. The buckling capacity about the y-axis of the two channel sections shown in Figure 55a, attached either toe-to-toe or back-to-back at the spacing a, is determined in this fashion. The strength of this type of column is governed either by flexural buckling about the y-axis, including the reduction in strength due to the shear displacement between the shapes via Eq. 1, or by flexural buckling about the x-axis, which is calculated in the manner described in the previous sections and does not include any reduction for shearing deformation effects. In the case of back-to-back double angles such as in Figure 55a, $(KL/r)_m$ is used in place of $(KL/r)_y$ in determining P_{ey}. This modified P_{ey} is then utilized in the torsional-flexural buckling equations as discussed in Section 6.2.3 and 6.2.4 of this volume as applicable. The column strength is governed by the smaller value of the resistance due to flexural buckling about the x-axis or torsional-flexural buckling involving twisting combined with bending about the y-axis.

AISC (2010) and AISC (2016) have adopted a simpler alternative to Eq. 1 that gives somewhat better predictions relative to test results for fully-tensioned bolted built-up members with closely-spaced individual components, i.e., members such as double-angles or double-channels. The corresponding AISC equation is based on the research by Sato and Uang (2007).

AASHTO (2020) Article C6.9.4.3.1 gives a separate equation considered to be applicable for riveted connectors on existing bridges. This equation is adopted from an AISC (2016) equation for snug-tight bolted members, and was developed empirically based on the test results from Zandonini (1985). The ends of the member must be connected rigidly, such as attained by welding, fully-tensioned bolting or the use of end tie plates, for this equation to be valid.

In both of the above cases, the connectors must be adequate to resist the shear forces that develop in the buckled member. AISC (2016) and AASHTO (2020) do not provide guidelines for this check. An AASHTO (2020) Article 6.9.4.3.2 equation for the additional required member transverse shear force in perforated cover plates may be applied for these cases. In addition, AISC (2016) indicates in a user note that it is acceptable to design a bolted end connection of a built-up compression member for the full compressive load with the bolts in bearing and the bolt design based on the shear strength. The user note indicates that the bolts must be pretensioned, however.

The implication is that connections designed in this way are sufficient to prevent slip between the components at the member ends. It is emphasized that the prevention of slip at the member ends is necessary for the structural effectiveness of the built-up member and for the validity of the corresponding AASHTO (2020) and AISC (2016) resistance expressions.

Lastly, an essential requirement for built-up members composed of two or more shapes is that the minimum a/r_i of each component shape between the connectors, lacing or batten plates must be less than or equal to 3/4 the governing L/r of the built-up member as a whole, where r_i is the least radius of gyration of a component part. Duan et al. (2002) studied the influence of larger a values theoretically, and concluded that a wider spacing makes the built-up member susceptible to further reductions in the axial capacity due to interaction between the buckling of the component members within the length a between the intermediate elements and the buckling of the entire member over its full length L.

Neither AASHTO (2020) nor AISC (2016) address the influence of the strain energy developed in lacing or batten plates on the column capacity. Equation 1 is a refinement and generalization of an equation that Bleich (1952) derived for battened columns, neglecting the energy due to local bending of the batten plates and assuming zero shearing deformation of the end tie plates. Aslani and Goel (1991) summarize the theoretical development of this equation and show that it gives accurate to slightly conservative predictions of experimental results for double-angle braces. However, their derivation is general, and they suggest that it is also applicable to built-up columns with widely-spaced components.

Ziemian (2010) outlines other solutions for determining the elastic buckling load, P_e, in laced or battened columns, which include the contribution from the lacing or battens to the strain energy. It references Johnston (1976) for further details and illustrative example designs. Once the load P_e is determined, it may be substituted into Eqs. 6.2.1-1 to determine the nominal design compressive strength P_n. There is little benefit to be gained by using formulations other than Eq. 1 for battened members. However, the alternate formulations from Ziemian (2010) tend to give larger capacities than Eq. 1 for laced columns.

Duan et al. (2000) recommend reduction factor equations for determining an equivalent moment of inertia and an equivalent torsional constant accounting for the behavior of lacing bars or batten plates in built-up members. Their reduction factors are direct functions of the strength properties of the lacing or batten plates and their connections considering their shear flow transfer capacities, rather than the elastic properties of these components. Their reduction factor for calculation of the equivalent moment of inertia modifies the contributions from the separate sections of the full cross section determined using the parallel axis theorem. Their reduction factor for the torsional constant modifies the equivalent thin-walled plate areas associated with the elastic shear racking of a lacing panel or a batten plate panel.

6.2.6 Axial Compressive Resistance of Members having Tapered and/or Stepped Sections and/or Subjected to Nonuniform Axial Force Along their Length

AISC Design Guide 25 (White et al. 2021a) details a procedure for calculation of the compressive resistance of general prismatic or nonprismatic steel members subjected to constant or nonconstant

internal axial force along their length. For these types of members, it is informative to write the axial capacity ratio associated with Eqs. 6.2.1-1, $P_u/\phi_c P_n$, in the following concise form:

$$\frac{P_u}{\phi_c P_n} = \frac{1}{\phi_c} \frac{1}{\left(A_e / A_g\right)} \rho_o \left(0.658^{\frac{-1}{\rho_o \gamma_e}}\right) \quad \text{for } \rho_o \gamma_e \geq \left(\frac{1}{2.25} = 0.444\right) \tag{6.2.6-1a}$$

$$\frac{P_u}{\phi_c P_n} = \frac{1}{\phi_c} \frac{1}{0.877} \frac{1}{\left(A_e / A_g\right)} \frac{1}{\gamma_e} \quad \text{for } \rho_o \gamma_e < \left(\frac{1}{2.25} = 0.444\right) \tag{6.2.6-1b}$$

where P_u is the axial load at a given cross section due to the factored loadings, $\phi_c P_n$ is the corresponding design resistance,

$$\gamma_e = \frac{P_e}{P_u} = \frac{F_e}{f_a} \tag{6.2.6-2}$$

is the ratio of the axial load at theoretical incipient elastic buckling, P_e, to the factored axial load at a given cross section, P_u, and

$$\rho_o = \frac{P_u}{P_y} = \frac{f_a}{F_y} \tag{6.2.6-3}$$

is the ratio of the factored axial load P_u to the stub-column yield load $P_o = P_y$.

It is emphasized that in addition to the terms γ_e and ρ_o representing load ratios, γ_e is also the ratio of the average axial stress at incipient elastic buckling, $F_e = P_e/A_g$, to the average factored axial stress, $f_a = P_u/A_g$, and ρ_o is also the ratio of the average required cross-section axial stress $f_a = P_u/A_g$ to the cross-section yield stress, F_y.

The use of the term γ_e in the evaluation of the member axial compressive resistance provides a number of advantages. This term is the same value throughout an entire member length, whereas the load at elastic buckling, P_e, and/or the stress at elastic buckling, F_e, generally vary along the member length (due to applied loads along the member length, or applied loads as well as the variations in the cross-section area along the member length, respectively). In addition, γ_e facilitates the use of rigorous computational methods to evaluate the buckling resistance of general nonuniformly loaded nonprismatic members since, given a reference factored design loading, γ_e is the eigenvalue obtained from the buckling analysis. White et al. (2021a) discuss various procedures for estimating γ_e as well as refined methods for the calculation of γ_e in general members and frames. Conceptually, given a distribution or diagram of P_u along the member length, the elastic buckling load level is obtained simply by scaling up all the applied loads on the structure, and thus scaling the internal values of P_u and the corresponding elastic stresses, until elastic buckling of the member or structure occurs.

The other two important parameters in Eqs. 1, A_e/A_g and ρ_o, are cross section based. For a nonprismatic member subjected to a variation in the internal axial force along its length, these parameters vary from cross-section to cross-section along the member length.

Generally speaking, the governing axial capacity ratio, $P_u/\phi_c P_n$, is taken as the largest value obtained from Eqs. 1 evaluated at multiple locations along a member's length. As such, if one performs a detailed parametric evaluation of Eqs. 1, it can be shown that:

- If the strength is governed by elastic buckling throughout a member's length, i.e., if Eq. 1b applies for all the cross sections along the member length, the governing axial capacity ratio occurs generally at the cross section that has the smallest A_e/A_g.

- If the strength is governed by inelastic buckling throughout a member's length, i.e., if Eq. 1a applies for all the cross sections along the member length, and if all the cross-section elements are nonslender under uniform axial compression such that $A_e/A_g = 1.0$ everywhere, the largest axial compressive strength ratio occurs generally at the cross section that has the largest ρ_o.

- When the strength is governed by inelastic buckling at some or all of the member cross sections, and if any of the cross sections have slender elements under uniform axial compression, the largest axial capacity ratio can occur theoretically at any location. However, the maximum $P_u/\phi_c P_n$ from the locations that have the largest $\rho_o/\left(A_e/A_g\right) = P_u/P_{ye}$ and/or the smallest A_e/A_g will be very close to or equal to the governing (largest) axial capacity ratio (one should note that P_u/P_{ye} here is the ratio of the factored axial compression to the yield load of the effective cross-sectional area).

Typically, it is not straightforward to determine the cross section with the largest P_u/P_{ye} or the smallest A_e/A_g by inspection. Given the above attributes, Design Guide 25 recommends that it is sufficient to sample at the following locations for the calculation of $P_u/\phi_c P_n$:

- At the member ends, or at the ends of the unbraced length under consideration;

- At the smaller cross section and/or the cross section with a plate having the smaller yield strength, where there is cross-section plate transition;

- At the more highly stressed cross section at any steps in the axial load;

- At the transition points between different linear tapers, in unbraced lengths having multiple linear tapers (if the axial force is constant within the unbraced length, only the "pinch point" having the minimum web depth need be checked); and

- For an I-section member with slender flanges, at the location where $D/t_w = 131$ (this is the web width-to-thickness ratio at which there is no further decrease in the flange local buckling coefficient k_c as the web slenderness increases, considering Case 1c of Table 5).

Once the critical cross section is identified, the corresponding axial compressive strength check can be conceptualized as being performed on an equivalent uniformly-loaded prismatic member that has the same overall γ_e as well as the same A_e/A_g and f_a/F_y as the critical cross section. This concept is illustrated in Figure 56.
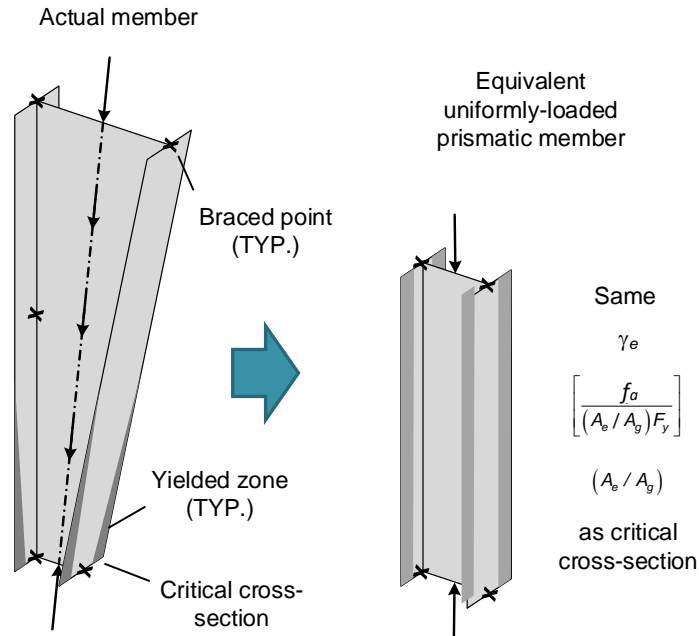
Figure 56. Equivalent uniformly-loaded prismatic member concept.

Based on the above concepts, Design Guide 25 recommends the following basic approach for calculating the axial capacity ratio, $P_u/\phi P_n$:

1. Determine the elastic buckling load ratios for the applicable column buckling modes, γ_{ex}, γ_{ez}, γ_{ez}, γ_{eTF}, etc. for each of the unbraced lengths L_x, L_y and L_z as applicable, where the additional subscripts on the γ_e values indicate the type of buckling mode.

2. Focus on the various potentially critical cross sections. Each of these cross sections is contained within a particular set of unbraced lengths L_x, L_y and L_z. For a given potentially critical cross section, the governing γ_e is the minimum value obtained from the buckling modes associated with the corresponding lengths L_x, L_y and L_z.

3. At each of the potentially critical cross sections, calculate $F_e = \gamma_e f_a$ (or $P_e = \gamma_e P_u$) and determine the corresponding F_{cr} from Eqs. 6.2.1-1 and 6.2.4-15.

4. Given the value of F_{cr} at each of the potentially critical cross sections, calculate the effective widths for all the cross-section elements from Eq. 6.2.4-12 (within the context of AASHTO (2020)), substituting F_{cr} for f;

5. Calculate the axial compressive resistance from Eq. 6.2.4-16 at each of the potentially critical cross sections and determine the axial capacity ratio by dividing the factored axial force at these cross sections, P_u, by the design resistance, $\phi_c P_n$.

It should be noted that when the elastic buckling load ratios are determined computationally, the calculations utilize a single minimum elastic buckling load ratio, γ_e, equal to the smallest eigenvalue obtained from that buckling analysis of the member, subassembly or structural system being evaluated.

6.2.7 Composite Columns

6.2.7.1 Overview

AASHTO (2020) Article 6.9.5.1 specifies the AISC (1999) LRFD Specification approach as the base AASHTO method to quantify the axial compressive resistance of composite columns. These rules address the axial compressive resistance of encased section members as well as closed circular and rectangular concrete-filled section members. In addition, the AASHTO (2020) Specifications provide a separate Article 6.9.6 detailing alternative calculation procedures recognizing the enhanced strength characteristics of circular concrete-filled steel tubes with a sufficiently small tube diameter to thickness ratio, D/t. The Article 6.9.6 provisions are similar to AISC (2016) rules for "compact" circular concrete-filled steel tubes, but with some important differences.

Section 6.2.7.2 below explains the background to the AISC (1999) provisions. This is followed by a summary of the AISC (2016) approach and then a summary of the AASHTO (2020) Article 6.9.6 rules in Sections 6.2.7.3 and 6.2.7.4. Section 6.2.7.5 addresses the separate case of the axial compressive resistance of a steel girder composite with a concrete bridge deck.

6.2.7.2 AASHTO (2020) Article 6.9.5.1 - AISC (1999) approach

The AASHTO (2020) Article 6.9.5.1 - AISC (1999) approach was developed based on the work of SSRC Task Group 20 (SSRC 1979). It uses the steel column strength curve given by Eqs. 6.2.1-1 through 6.2.1-4 with the area of the steel section, $A_g = A_s$, and a modified yield strength, F_{my}, modulus of elasticity, E_m, and radius of gyration, r_m, to account for the effect of the concrete and longitudinal reinforcing bars. The terms F_{my} and E_m are denoted by F_e and E_e, respectively, and the modified radius of gyration is written as r_s in the AASHTO Specifications; the AISC terminology F_{my}, E_m and r_m is adopted in the equations presented below to avoid conflicts with other uses of the subscript e, and to emphasize that r_m is a modified radius of gyration). The modified terms are as follows:

$$F_{my} = F_y + C_1 F_{yr} \frac{A_r}{A_s} + C_2 f_c' \frac{A_c}{A_s} \qquad \text{(6.2.7-1) (AASHTO 6.9.5.1-4, AISC 1999 I2-1)}$$

$$E_m = E\left(1 + \frac{C_3}{n} \frac{A_c}{A_s}\right) \qquad \text{(6.2.7-2) (AASHTO 6.9.5.1-5, AISC 1999 I2-2)}$$

$$r_m = \max\left(r_s, 0.3H_c\right) \qquad \text{(6.2.7-3)}$$

where

    A_c =   area of the concrete,

A_r = area of the continuous longitudinal reinforcing steel bars,

A_s = area of the encased steel section or the steel tube,

E = modulus of elasticity of the steel (29,000 ksi)

F_y = specified minimum yield strength of the steel section or tube,

F_{yr} = specified minimum yield strength of the longitudinal reinforcing steel,

f_c' = specified minimum 28-day compressive strength of the concrete,

n = modular ratio of the concrete as specified in Article 6.10.1.1.1b of AASHTO (2020)

r_s = radius of gyration of the steel section or tube in the direction of buckling, and

H_c = overall width of the composite section in the plane of bending

The coefficients C_1 and C_2 account for the contributions of the reinforcing steel and concrete to the stub-column strength P_o, whereas the coefficient C_3 accounts for the contribution of the concrete to the stiffness of the overall section. In the context of Eqs. 6.2.1-1, the AASHTO (2020) Article 6.9.5.1 - AISC (1999) approach specifically uses

$$P_o = F_{my} A_s \qquad (6.2.7\text{-}4)$$

and

$$P_e = \frac{\pi^2 E_m}{\left(KL/r_m\right)^2} A_s \qquad (6.2.7\text{-}5)$$

For encased sections, AASHTO (2020) and AISC (1999) use

$$C_1 = 0.7, C_2 = 0.6 \text{ and } C_3 = 0.2 \qquad (6.2.7\text{-}6)$$

whereas for filled sections,

$$C_1 = 1.0, C_2 = 0.85 \text{ and } C_3 = 0.4 \qquad (6.2.7\text{-}7)$$

If present in a filled section, the reinforcing steel is always supported sufficiently such that it can develop its full capacity (therefore, $C_1 = 1.0$). However, for encased sections, a reduced C_1 value is employed to account for the potential spalling of the concrete, leaving the steel bars exposed. The coefficient C_2 assumes that the concrete will at least reach a stress of $0.85\, f_c'$ because of the confinement available in filled sections. However, for encased sections, the ACI (1977) reduction to 70 % of the capacity for components relying on unconfined concrete is applied, i.e., $C_2 = 0.7(0.85) \cong 0.6$. For the stiffness coefficient C_3, SSRC (1979) adopted the ACI (1977) recommendations. For confined concrete, ACI (1977) recommended using only 40 % of the initial stiffness of the concrete, whereas for unconfined concrete, only 20 % was used (hence $C_3 = 0.2$ for encased sections and 0.4 for filled sections).

For the modified radius of gyration, r_m, SSRC (1979) noted that in members where the steel section provides the majority of the flexural resistance, the radius of gyration of the steel section, r_s, is appropriate, while if the concrete portion of the section provides the majority of the flexural resistance, the radius of gyration of the concrete section is appropriate. Therefore, the larger of these two values was selected, with $0.3H_c$ being the radius of gyration of a square concrete cross section (i.e., a square column is implicitly assumed in this development).

The AASHTO (2020) Article 6.9.5.1 - AISC (1999) provisions are applicable only for members in which the area of the steel section, A_s, is greater than 4 % of the total composite section. For smaller A_s, the member must be designed as a reinforced concrete column. There is typically a significant discontinuity in the strength predicted by handling the member as a composite steel column versus a reinforced concrete column at this limit. Furthermore, the values for F_{yr} and F_y used in calculating the resistance are restricted to 60 ksi. This is because the concrete stiffness reduces significantly at strains near 0.2 percent, and thus the concrete is considered potentially ineffective in stabilizing the steel for larger yield strengths. Concrete strengths $f_c' \leq 8$ ksi are required for normal weight concrete, since there was limited test data for larger strengths at the time of the original developments. Concrete strengths $f_c' \geq 3$ ksi are required to ensure good quality concrete. In addition, a number of requirements are specified for the longitudinal reinforcing bars, lateral ties and concrete cover in encased sections to ensure good performance of the concrete section.

The AISC (1999) provisions address both rectangular and circular filled sections, specifically filled HSS and pipes. The primary focus of the AASHTO (2020) Specifications pertaining to filled sections is on circular concrete-filled steel tubes. For rectangular filled sections, the AASHTO provisions restrict the cross-section b/t values to $1.40\sqrt{E/F_y}$ or $1.28\sqrt{E/F_y}$ by reference to Article 6.9.4.2.1. This is somewhat more restrictive than the value of $1.7\sqrt{E/F_y}$ specified originally in AISC (1999). For circular filled sections, D/t is limited to $0.11E/F_y$, by reference to Article 6.9.4.2.1, which is comparable to the value of $2.8\sqrt{E/F_y}$ specified in AISC (1999). These limits ensure that the steel section yields before the concrete crushes or significant local buckling occurs.

6.2.7.3   AISC (2016) approach

AISC (2016) provides substantially updated procedures relative to the AASHTO (2020) Article 6.9.5.1 - AISC (1999) approach for calculating the resistance of encased and filled composite columns. These procedures provide larger, more accurate resistances, and reduce differences between the AISC and ACI design provisions. In the AISC (2016) provisions, P_o is calculated as

$$P_o = F_y A_s + F_{ysr} A_{sr} + 0.85 f_c' A_c \qquad \text{(6.2.7-8) (AISC I2-4)}$$

for encased sections, and as

$$P_o = F_y A_s + C_2 f_c' \left(A_c + A_{sr} \frac{E}{E_c} \right) \qquad \text{(6.2.7-9) (AISC I2-9b)}$$

for *compact* filled sections, where $C_2 = 0.85$ and 0.95 for rectangular and circular sections respectively. The variable definitions in Eqs. 8 and 9 are the same as those in Section 6.2.7.2 except for the following in AISC (2016):

A_{sr} = area of the continuous longitudinal reinforcing steel bars, and

F_{ysr} = specified minimum yield strength of the longitudinal reinforcing steel.

These equations recognize the full development of the continuous reinforcing bars for encased columns, and they account for the confinement effects on the concrete strength and the compatibility of the concrete and reinforcing steel strains in circular filled sections. Furthermore, the equivalent member elastic buckling load is calculated directly as

$$P_e = \frac{\pi^2 EI_{eff}}{(KL)^2} \tag{6.2.7-10) (AISC I2-5)}$$

where

$$EI_{eff} = EI_s + EI_{sr} + C_c E_c I_c \tag{6.2.7-11) (AISC I2-6 \& I2-12)}$$

I_s = moment of inertia of the steel section about the axis of buckling,

I_{sr} = moment of inertia of the reinforcing bars about the axis of buckling,

I_c = moment of inertia of the concrete section about the axis of buckling,

$$C_c = 0.25 + 3\left(\frac{A_s + A_{sr}}{A_g}\right) \leq 0.7 \text{ for encased sections,} \tag{6.2.7-12) (AISC I2-7)}$$

$$= 0.45 + 3\left(\frac{A_s + A_{sr}}{A_g}\right) \leq 0.9 \text{ for filled sections.} \tag{6.2.7-13) (AISC I2-13)}$$

and

A_g = gross area of the composite member.

In addition, the AISC (2016) provisions address the reduced column axial resistance for more slender HSS or box sections of uniform thickness or more slender circular hollow sections. AISC (2016) Section I1 provides its own set of tables for classification of these member types as compact, noncompact or slender. For rectangular HSS and box sections of uniform thickness, the compactness limit, which must be satisfied to use the above filled-section equations, is

$$b/t \leq \left[\lambda_p = 2.26\sqrt{\frac{E}{F_y}}\right] \tag{6.2.7-14a}$$

and for filled circular sections (specifically, the AISC provisions address only round HSS), the corresponding compactness limit is

$$D/t \leq \left[\lambda_p = 0.15 \frac{E}{F_y} \right]$$

(6.2.7-14b)

Although the same terminology is used, the implications of the AISC (2016) classification of filled composite sections are fundamentally different than other AISC (2016) and AASHTO (2020) classifications of the steel elements as compact, noncompact and slender in other cross-section types. In quantifying the axial resistance of filled composite section members in AISC (2016) Section I2.2:

- "Compact" indicates that the section is able to develop a maximum "plateau" resistance of the concrete and reinforcing steel, including the influence of confinement from the steel section,

- "Noncompact" indicates that the steel section has sufficient thickness such that it can fully yield in the longitudinal direction, but it cannot adequately confine the concrete infill after it reaches $0.70f_c'$, at which point the concrete starts undergoing significant inelastic deformations and volumetric dilation (pushing against the wall of the steel section).

- "Slender" indicates that the steel section can neither develop full yielding on its area in the longitudinal direction, nor confine the concrete after it reaches $0.70f_c'$.

Furthermore, AISC (2016) Section I3.4 quantifies the flexural resistance of filled composite section members as follows:

- "Compact" indicates that the section can develop its full plastic moment capacity, M_p, in flexure,

- "Noncompact" indicates that the section can develop a moment capacity greater than the nominal first-yield moment of the section, M_{yt}, when the tension flange reaches first yielding, or greater than the moment corresponding to a maximum concrete compressive stress of $0.70f_c'$, but local buckling or inadequate confinement of the concrete in compression precludes the development of M_p, and

- "Slender" means that the flexural resistance of the member is limited to the smaller value of the first yield moment when the tension flange reaches first yielding and the moment corresponding to elastic response of the concrete and a maximum compressive stress of $0.70f_c'$.

These definitions should be contrasted with the following definitions employed elsewhere in the AISC (2016) and AASHTO (2020) Specifications:

- A cross section in which all of the compression elements are "compact" is capable of developing *moments* equal to the fully-plastic flexural resistance M_p,

- With the exception of the AASHTO (2020) provisions for composite sections in positive flexure, a cross section containing "noncompact" compression elements is capable of

developing *moments* larger than the nominal first yield flexural resistance in compression including residual stress effects, i.e., $M_{yr} = F_{yr}S_{xc}$, and

- With the exception of the AASHTO (2020) provisions for composite sections in positive flexure, a cross section with "slender" compression elements has its strength generally limited by local buckling of compression elements prior to reaching M_{yr}.

- In the AASHTO (2020) provisions for composite sections in positive flexure, a "noncompact section" is one in which the maximum potential flexural resistance is limited to a compression flange stress of $R_bR_hF_{yc}$, corresponding to nominal yielding of the steel compression flange, neglecting residual stress effects but including the influence of load shedding from a slender and/or hybrid web, or a tension flange stress of R_hF_{yt}. For these sections, the reasons for limiting the maximum resistance to the above values include yield strength of the steel larger than 70 ksi, web slenderness, and/or limiting potential inelastic redistribution in curved bridge structural systems (see Sections 6.3.3 and 6.3.4 of this volume).

- In the AASHTO (2020) provisions for composite sections in positive flexure, a "compact section" is one in which the maximum potential flexural resistance is the full plastic moment of the composite section (see Section 6.3.3).

The AISC (2016) provisions for composite columns are applicable for A_s/A_c as small as 1 %. Furthermore, the specified minimum yield strength of the structural steel and the reinforcing steel are limited to 75 and 80 ksi respectively. The provisions are extended to concrete strengths up to $f_c' = 10$ ksi for normal weight concrete. Also, the required area for the transverse ties in encased sections is increased slightly relative to AISC (1999), from 0.007 to approximately 0.009 to 0.010 in²/in of tie spacing No. 3 bars spaced at a maximum of 12 in. or No. 4 bars spaced at a maximum of 16 in.), and the minimum reinforcement ratio for continuous longitudinal bars in these sections is relaxed slightly from 0.007 to 0.004.

The above equations for encased sections are based on studies of doubly symmetric composite columns. The commentary to Section I2 of AISC (2016) provides guidelines for the limited use of these equations with columns having nonsymmetric cross sections.

AISC (2016) specifies detailed rules for load transfer to the composite cross section in encased and filled sections that are enhancements on prior AISC provisions.

6.2.7.4   Alternative AASHTO (2020) method for circular concrete-filled steel tubes

AASHTO (2020) Article 6.9.6.3 provides alternative calculations for the axial compressive resistance of circular concrete-filled steel tubes. Article 6.9.6.1 defines the focus of these provisions as circular concrete-filled tubes with or without internal reinforcement. The commentary to this article indicates that the intended applications of these rules are for piles, drilled shafts, piers and columns subjected to significant compression. Article C6.9.6.1 also states specifically that the provisions of Article 6.9.5 are intended for applications where full composite action is not deemed necessary, and references Robinson et al. (2012) and Lehman and Roeder

(2012) as providing evidence to this effect. The intent of the Article 6.9.6 provisions is full composite action.

AASHTO Article C6.9.6.2 points out that large diameter tubes are required for most components in bridge applications. Article 6.9.6.2 limits the application of the Article 6.9.6.3 equations to circular concrete-filled steel tubes satisfying Eq. 14b. Furthermore, this article specifies spiral welded tubes formed from coil steel, straight-seam welded tubes formed from flat plates, or seamless pipes. These provisions also recommend that for steel tubes with straight seam welds and with diameters larger than 24 in., consideration should be given to the use of a low-shrinkage admixture, or to providing a shear transfer mechanism such as shear rings. In addition, the minimum 28-day compressive strength of the concrete is required to be the greater of 3.0 ksi and $0.075F_y$, where F_y is the specified minimum yield strength of the tube.

The Article 6.9.6.3 equations are the same as the AISC (2016) equations for *compact* filled circular sections with the exception that the following equation is specified in place of Eq. 13:

$$C_c = 0.15 + \frac{P}{P_o} + \left(\frac{A_{st} + A_{sb}}{A_{st} + A_{sb} + A_c} \right) \leq 0.9 \qquad \text{(6.2.7-15) (AASHTO 6.9.6.3.2-7)}$$

where all of the variables are as defined previously, except

A_{st} = area of the encased steel section or the steel tube,

A_r = total cross-sectional area of the internal reinforcement bars, and

P = Unfactored axial dead load.

Clearly, it would be beneficial for a consistent set of names to be adopted for several of the variables within the above AASHTO and AISC provisions.

Roeder et al. (2010) show that this expression provides an improved mean value of the composite section rigidity with a smaller standard deviation than the other models.

It should be noted that AASHTO (2020) employs a resistance factor of $\phi_c = 0.90$ for the axial compressive resistance of all types of composite columns, both in the Article 6.9.6.3 calculations for composite concrete-filled steel tubes and in the calculations of Article 6.9.5.1 for general composite members.

6.2.7.5   Axial compressive resistance of composite bridge girders

In some situations, steel bridge girders designed compositely with a concrete deck are subjected to combined flexure and axial compression. This occurs for instance in a cable-stayed bridge with a composite I- or box-girder deck system. Axial compression can also occur due to restraint of thermal expansion in stringer bridges, although these effects typically are rendered negligible by the movements permitted at integral abutments or deck joints. AASHTO (2020) Articles C6.10.6. 1 and C6.11.6.2.1 allow the Engineer to neglect a concentrically-applied axial force P_u in all types of I- and box-girder members whenever $P_u/\phi_c P_n$ is less than 0.05. However, for $P_u/\phi_c P_n$ > 0.05, I- and box-girders must be checked in general as beam-columns. Any moments generated

about the effective centroidal axis, due to eccentric application of axial loads, must be considered. An appropriate calculation of this effective axis is suggested below. Bending moments due to transverse loads and eccentricity of the applied axial loads are addressed separately in the flexural resistance calculations (see Sections 6.3.3 through 6.3.7 and 6.4.6 through 6.4.12 of this volume).

In the above cases where the axial loading must be considered, the Engineer needs to calculate $\phi_c P_n$ for the composite girder. AISC (2016) provides substantial guidelines regarding the calculation of the resistance of flexural members subjected to combined axial load in the Commentary to its Section I7. However, this discussion is primarily directed at the calculation of the strength of collector components in building floor systems. Section I6 of the AISC (2016) Commentary discusses important considerations pertaining to the load path associated the transfer of the load to composite members, and the need to design the shear connection between the concrete and steel to transfer the longitudinal shear necessary to maintain force equilibrium within the composite section. The commentary of AISC (2005) provides the following broad guidance for the calculation of the axial compressive resistance of composite I-section members:

 "Adequate means to transmit axial loading to and from the steel section should be provided. Where shear connectors are used, the top flanges may be considered braced for compressive loading at the shear connector locations…. For load combinations resulting in compressive loading of the lower flange, length effects between brace points should be considered. Inflection points should not be considered as braced points for torsional [lateral] buckling of the unbraced flange."

The most relevant discussion to the calculation of the axial compressive resistance of composite girders within the AISC (2016) commentary pertains to the design of collector beams in building floor systems, and is as follows:

"The available strength of collector beams can be determined according to the noncomposite provisions of Chapter D and E. For compressive loading, collector beams are generally considered as braced for buckling between braced points about their strong axis, and fully braced by the composite diaphragm for buckling about the weak axis. The limit state of constrained-axis torsional buckling about the top flange as discussed in the Commentary Section E4 may also apply… Combined axial force and flexure can be assessed using the interaction equations provided in Chapter H. As a reasonable simplification for design purposes, it is acceptable to use the noncomposite axial strength and the composite flexural strength in combination for determining interaction."

Specifically, the axial compressive resistance of a composite I-girder may be governed either by flexural buckling about the major-axis of bending, or by constrained-axis torsional buckling of the steel I-section about an enforced axis of rotation located at the depth of the shear connectors. The first of these limit states is expected to rarely control. It is suggested that it can be checked conservatively by using Eq. 11 for EI_{eff}, with C_c taken equal to the value of 0.2 implied in the AASHTO (2020) - AISC (1999) composite column provisions, then using Eq. 10 to calculate P_e. Since the composite cross section is singly symmetric, the Engineer will need to determine its effective centroidal axis for calculation of the separate contributions to the effective moment of inertia, I_{eff}. It is suggested that the full steel cross section may be used for this calculation, consistent with the handling of slender-element cross sections discussed in Section 6.2.4 of this

volume, and that a modular ratio of $n/0.2$ should be used for the concrete deck. The contribution of the longitudinal reinforcing steel in Eq. 11 usually will be small compared to the other terms, and thus it is suggested that this term should be neglected. Some judgment must be used in selecting the effective width of the deck concrete for use in Eqs. 4 and 11. Chen et al. (2005) suggest a lower bound effective width of 90 % of the full width for regions away from the towers and 70 % of the full width in regions close to the towers in cable-stayed bridges with two edge girders, two pylons, a semi-harp cable configuration with two planes of cables, a relatively thin concrete slab, cable spacing at approximately 10 % of the back span length, and floor beam spacing approximately one-third of the cable spacing.

The load corresponding to the elastic constrained-axis torsional buckling of the steel I-girder about an enforced axis of rotation at the shear connection to a composite deck is given by

$$P_{eCAT} = \left[\frac{\pi^2 E \left(C_w + I_y a_s^2 \right)}{L_b^2} + GJ \right] \frac{1}{r_x^2 + r_y^2 + a_c^2} \tag{6.2.7-16}$$

where C_w is the warping constant of the steel section, a_s and a_c are the distances from the shear center and centroid of the steel cross section to the fixed axis of rotation respectively, and L_b is the length between the locations where the cross section is prevented from twisting (Timoshenko and Gere 1961; Bleich 1952; White et al. 2021a). Figure 57 shows the typical case where the bottom flange is larger and $a_s > a_c$. Equation 16 gives a substantially larger buckling load than obtained based on the flexural buckling of the unrestrained steel I-section member about its minor principal axis.
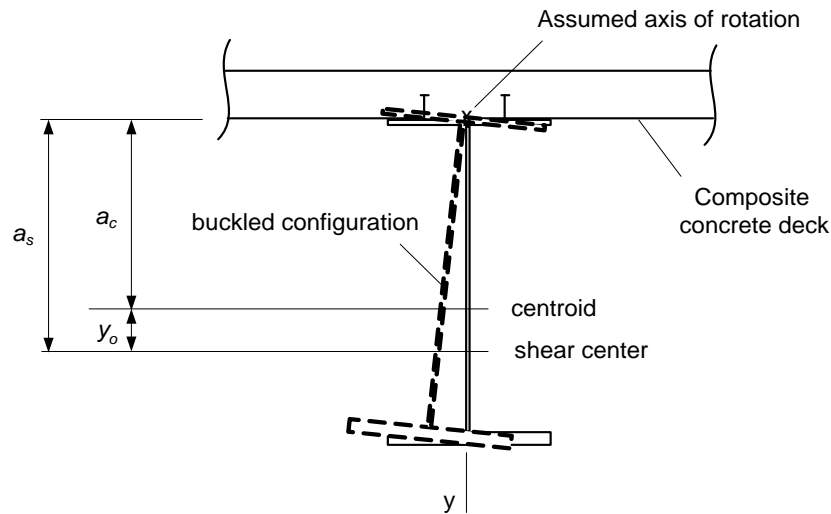
Figure 57. Cross-section displacements and relevant cross-section dimensions for constrained-axis torsional buckling about an enforced axis of rotation at the shear connection to a composite deck.

Equation 16 neglects the torsional restraint potentially provided by the deck to the steel I-section member. The effect of this restraint is reduced substantially in many cases due to web distortion. Torsional restraint of the steel I-section is assumed only at the cross-frame locations, i.e., L_b is the

spacing between the cross frames. Equation 16 also neglects the axial force contribution from the deck at the incipient elastic torsional buckling of the steel section.

Given the above calculations of P_e and P_{eCAT}, it is desired to calculate P_n from Eqs. 6.2.1-1. As such, the Engineer is faced with a decision about the appropriate calculation of P_o. It is recommended that P_o may be calculated as

$$P_o = F_y A_e + F_{yr} A_r + 0.85 f'_c A_c \qquad (6.2.7\text{-}17a)$$

where A_e is determined as discussed in Section 6.2.4 of this volume, using $f = F_y$ in calculating the effective width of the web. Since the top flange is connected compositely to the deck, it should be considered as a nonslender element. For hybrid composite I-girders, the $F_y A_e$ term in Eq. 17a should be determined using the smallest F_y of all the component plate elements, as discussed previously in Section 6.2.4.

Procedures similar to the above can be used to obtain P_e and P_o for a composite box girder. However, torsional buckling is not a consideration for these members. Therefore, P_e may be calculated based solely on flexural buckling about a horizontal axis through the effective centroid. This elastic buckling load usually will be quite large, and therefore P_n will be approximately equal to P_o.

Equation 16 also can be used to calculate the compressive resistance of noncomposite I-girders when the top flange is embedded in the concrete deck. These types of members would be checked for flexural buckling about their major axis of bending using the corresponding KL/r to determine P_e, and using Eq. 16 to calculate $P_e = P_{eCAT}$ corresponding to constrained-axis torsional buckling about an enforced axis of rotation at the top flange.

6.3 I-Section Flexural Members

6.3.1 Introduction

The AASHTO (2020) Article 6.10 and Appendices A6 through D6 provisions for I-section flexure are central to the behavior and design of many of the bridge structural systems discussed in Section 2 of this volume. Because of the large number of I-beam and I-girder stringer bridges used in highway construction, these provisions have possibly the greatest overall impact of all the AASHTO (2020) Specifications with respect to steel bridge construction. Furthermore, a number of the AASHTO (2020) Article 6.11 rules for box-girder design utilize or parallel specific I-section member provisions.

The calculation of the nominal flexural resistance of the various types of I-section members can be explained conceptually with just a few figures. However, numerous parameters must be considered for the wide range of I-section members utilized in design practice. Section 6.3.2 of this volume initiates the discussion of I-section flexural members by outlining basic proportioning limits defined in AASHTO (2020) Article 6.10.2. Sections 6.3.3 and 6.3.4 of this volume then provide an overview of the AASHTO (2020) Article 6.10.7 provisions for composite members in positive major-axis bending. Most of the details for design of I-section members fall under the category of composite members in negative bending and noncomposite members. Section 6.3.5

outlines the key concepts and the basics of the calculations for the various design parameters pertaining to major-axis bending of these member types. All of the discussions of Sections 6.3.3 through 6.3.5 focus on prismatic member unbraced lengths. Section 6.3.6 explains how the prismatic member rules are generalized to handle variable web depth I-section members and/or I-section members with cross-section transitions along their lengths. Section 6.3.7 then addresses the handling of combined major-axis bending, torsion and minor-axis bending of I-girders in AASHTO (2020). Finally, Section 6.3.8 discusses the shear strength of I-section members, Section 6.3.9 addresses the strength of shear connectors for composite construction, and Section 6.3.10 discusses various "secondary" limit states such as web crippling and web yielding due to concentrated transverse loads.

6.3.2 Proportioning Limits

AASHTO (2020) Article 6.10.2 provides basic rules targeted at ensuring the economical and practical proportioning of I-section members in preliminary design. Also, these rules provide practical bounds upon which the flexural resistance provisions are based. AASHTO Article 6.10.2.1.1 requires that webs without longitudinal stiffeners shall satisfy the following depth-to-thickness limitation

$$D/t_w \leq 150 \qquad \text{(6.3.2-1) (AASHTO 6.10.2.1.1-1)}$$

This limit helps ensure ease of handling, permits simplification of resistance calculations for composite members (discussed subsequently in Section 6.3.3 of this volume), and helps ensure adequate performance with respect to web distortion induced fatigue for members that do not have web longitudinal stiffeners. For longitudinally stiffened I-section members (i.e., members with longitudinally stiffened webs), Article 6.10.2.1.2 requires

$$D/t_w \leq 300 \qquad \text{(6.3.2-2) (AASHTO 6.10.2.1.2-1)}$$

Equation 2 is simply a practical upper bound on the slenderness of webs with longitudinal stiffeners. I-girders with larger D/t_w values are more susceptible to secondary limit states such as web crippling under concentrated transverse loads. Both of the above limits are expressed in terms of the total web depth to thickness, for ease of use in preliminary design. It should be noted that AASHTO Article 6.10.11.1.1 requires web transverse stiffener spacing at $d_o \leq 2.0D$ for members with longitudinally stiffened webs.

AASHTO Article 6.10.2.2 specifies limits on the flange dimensions. The half-width to thickness ratio is limited for both compression and tension flanges to

$$b_f / 2t_f \leq 12 \qquad \text{(6.3.2-3) (AASHTO 6.10.2.2-1)}$$

This limit is targeted predominantly at ensuring that the flanges of I-girders will not distort excessively when they are welded to the web. However, it also allows for some simplification of the flange local buckling resistance equations in AASHTO (2020) as discussed subsequently in Section 6.3.5.1. AASHTO Article 6.10.2.2 also specifies

$$b_f \geq D / 6 \qquad \text{(6.3.2-4) (AASHTO 6.10.2.2-2)}$$

$$t_f \geq 1.1\, t_w \qquad\qquad\qquad\qquad \text{(6.3.2-5) (AASHTO 6.10.2.2-3)}$$

and

$$0.1 \leq I_{yc}/I_{yt} \leq 10 \qquad\qquad\qquad\qquad \text{(6.3.2-6) (AASHTO 6.10.2.2-4)}$$

where I_{yc} and I_{yt} are the moments of inertia about the plane of the web for the compression and tension flanges respectively. Few I-section member tests have been conducted with depths D larger than $6b_f$. Furthermore, a number of the available tests for deep narrow-flange members that violate Eq. 4 indicate significant degradation in the resistances relative to the prediction equations in AASHTO (2020) and AISC (2016) as well as in previous Specifications (White and Jung 2008; White and Kim 2008; White and Barker 2008; White et al. 2008). Also, I-sections with narrow flange widths violating Eq. 4 generally require bracing at close intervals to avoid significant reductions in their flexural resistance due to lateral-torsional buckling. However, I-girders with D/b_f approaching 6 can indeed be practical for long spans in which the girders are relatively deep compared to the spacing of the cross frames along the bridge length, L_b, in which case L_b/b_f can be relatively small at $D/b_f = 6$. Equation 5 requires that the flange thicknesses must be slightly larger than the web thicknesses in bridge I-section members. There is evidence of acceptable performance of I-section members with $t_f = t_w$; however, the requirement for the additional flange thickness in Eq. 5 helps ensure member robustness and does not appear to impose any practical or economic limitations on I-girder bridge construction. The combination of Eqs. 4 and 5 restricts the ratio of web-to-flange area for either flange, $A_w/A_f = Dt_w/b_f t_f$, to a maximum value of 5.4. Lastly, Eq. 6 ensures efficient relative flange proportions and prevents the use of extreme singly symmetric I-sections that may be difficult to handle during construction and for which the I-section member flexural resistance equations are generally not valid.

AASHTO Article C6.10.2.2 recommends one additional limit on the top flange width of unspliced individual girder field sections, pertaining to constructability. This limit deserves mention in the context of general I-section proportioning limits. This article recommends

$$b_{tfs} \geq L_{fs}/85 \qquad\qquad\qquad\qquad \text{(6.3.2-7) (AASHTO C6.10.2.2-1)}$$

where L_{fs} is the length of an unspliced individual girder field section and b_{tfs} is the smallest top-flange width within the unspliced field section. This limit helps alleviate potential problems due to out-of-plane deformation of the girder compression flange during fabrication, shipping and erection. This equation assumes that the girder top flange is typically smaller than the girder bottom flange. Article C6.10.2.2 states that this equation is provided only as a guideline for sizing of the flanges in design and is not considered as an absolute requirement. The article also states that it is not intended that the Engineer anticipate how individual field sections may eventually be assembled or spliced together and/or stabilized or supported for shipping and erection at the design stage, and that the stability of the girders for shipping and erection, either as individual shipping pieces or after being spliced together to form larger pieces, should be considered the responsibility of the Contractor. Nevertheless, satisfying this limit may help to alleviate subsequent difficulties during handling, shipping and erection of the girders.

6.3.3 Compact Composite Sections in Positive Flexure

6.3.3.1 Section classification

AASHTO (2020) Article 6.10.6.2.2 defines composite sections in positive bending as compact sections when:

- The specified minimum yield strengths of all the flanges do not exceed 70 ksi
- $D/t_w \leq 150$

$$2D_{cp} / t_w \leq 3.76\sqrt{E / F_{yc}} \qquad \text{(6.3.3-1) (AASHTO 6.10.6.2.2-1, AISC Section I3.2a)}$$

and

- The bridge is straight (no horizontal curvature or kinked (chorded) continuous geometry).

The term composite compact section in positive bending means that the fully-plastic cross-section models shown in Figure 58 may be used as the basis for the member resistance calculations. The first of the above limits is specified to avoid potential crushing of the deck concrete prior to reaching the calculated flexural resistance. For $F_y = 70$ ksi, the yield strain of the steel $\varepsilon_y = F_y/E = 0.0024$ is slightly beyond the level of strain corresponding to the peak compressive stress for typical deck concrete. For $F_y = 100$ ksi, the yield strain of the steel is 0.0034, which is somewhat beyond the nominal concrete crushing strain. The second limit is the Eq. 6.3.2-1 restriction on the web width-to-thickness ratio beyond which longitudinal stiffeners are required. Since members with longitudinally stiffened webs tend to be deeper and are typically used in longer spans with corresponding larger dead load stresses, they often have large elastic $2D_c/t_w$ values. These large web slenderness values may result in significant web bend buckling prior to development of flexural yielding, even if the third limit, discussed below, is satisfied at the theoretical plastic limit state. Furthermore, because of the relative size of the steel section to the concrete deck typical of these types of sections, and due to the thinness of the web, the plastic moment capacity M_p often is not significantly larger than the yield moment M_y (or the yield moment modified for hybrid web effects, R_hM_y). The third limit is the basic AASHTO (2020) - AISC (2016) compact-web limit corresponding to the plastic depth of web in compression, D_{cp} (see Figure 58). The derivation of this limit originates from the consideration of doubly symmetric noncomposite I-section member; it has been commonly applied to composite I-section members in the AISC and AASHTO Specifications as a conservative simplification relative to more elaborate compact-web limits such as discussed in Appendix 6 of AASHTO (2020) and in Section 6.3.5.2.1 of this volume. Webs more slender than the limit given by Eq. 1 are interpreted to be unable to develop the large inelastic strains necessary for the cross section to achieve the plastic moment M_p. The fourth limit has been discussed previously in Section 3 of this volume. The above four limits are simple restrictions intended to limit the use of the plastic cross-section model of Figure 58 to designs where it is supported by test data. Future research may lead to some relaxation of a number of these limits.
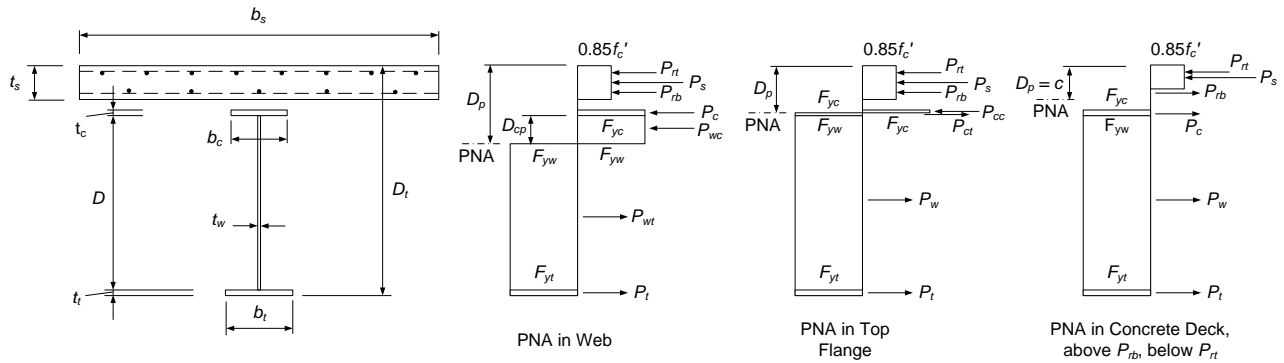
Figure 58. Illustrative plastic cross-section models for composite I-sections in positive bending (cases for plastic neutral axis (PNA) in concrete deck below P_{rb}, concrete deck at P_{rb}, concrete deck at P_{rt} and concrete deck above P_{rt} are not shown).

6.3.3.2   Flexural resistance

The base flexural resistance model shown in Figure 58 is the same as the Whitney rectangular stress block model used in reinforced concrete design except that the concrete rectangular stress block is always taken as the full depth in compression above the plastic neutral axis (PNA) rather than a fraction of this depth. This simplification generally results in a negligible or only a slight increase of the calculated plastic moment. The effective width of the concrete slab is assumed to be stressed in compression at $0.85f_c'$, and all the reinforcing and structural steel elements are assumed to be stressed at their yield strengths F_y. AASHTO (2020) Article D6.1 gives equations for the PNA location and the corresponding M_p for all potential PNA positions in the slab or in the steel I-section. These equations are based simply on equilibrium, considering the fully-plastic stress distributions and assuming zero axial force. The concrete within the haunch over the girder flanges is neglected in the AASHTO (2020) equations for purposes of simplicity. However, the nominal height of the haunch is included. The reader is referred to Article D6.1 for the detailed equations.

AASHTO (2020) Article 6.10.7.1.2 does not necessarily use the full plastic moment M_p as the nominal flexural resistance for compact composite sections in positive bending. This Article specifies

$$M_n = M_p \qquad\qquad \text{(6.3.3-2) (AASHTO 6.10.7.1.2-1)}$$

when $D_p < 0.1D_t$, where D_p is the depth of the plastic neutral axis below the top of the deck (see Figure 58) and D_t is the total depth of the composite section. However, when $D_p/D_t > 0.1$, it specifies

$$M_n = M_p (1.07 - 0.7\, D_p/D_t) \qquad\qquad \text{(6.3.3-3) (AASHTO 6.10.7.1.2-2)}$$

The AASHTO (2020) resistance factor for flexure is $\phi_f = 1.0$ for all types of composite and noncomposite members.

Equation 3 enforces a higher margin of safety for members with larger D_p/D_t, as first recommended by Wittry (1993). The increase in the margin of safety, relative to the theoretical resistance

107

determined from a strain-compatibility analysis at crushing of the deck concrete, varies linearly from 1.0 at $D_p/D_t = 0.1$ to approximately 1.3 at $D_p/D_t = 0.42$. Strain-compatibility analyses of a wide range of practical composite sections indicate only a slight decrease in the cross-section moment below $M = M_p$ when the top of the slab reaches the theoretical crushing strain of 0.003 (Wittry 1993; White 2002). However, composite members with large D_p/D_t tend to have significantly smaller plastic curvature prior to crushing of the deck concrete and thus less ductility. Also, AASHTO (2020) specifies

$$D_p/D_t \leq 0.42 \qquad \text{(6.3.3-4) (AASHTO 6.10.7.3-1)}$$

to ensure significant yielding of the bottom flange (and therefore, significant inelastic bending curvature) prior to reaching the nominal crushing strain at the top of the deck. This limit is consistent with the former maximum reinforcement limit for concrete design given in the AASHTO (2004) Article 5.7.3.3.

In addition to the above equations, AASHTO (2020) Article 6.10.7.1.2 limits the nominal flexural resistance to that given by Eq. 3-2 of this volume in continuous-span beams where the adjacent pier sections are not detailed to accommodate significant inelastic moment redistribution. The reader is referred to Section 3 for discussion of this limit.

AASHTO (2020) generally requires that the separate effects of noncomposite, short-term composite and long-term composite loadings shall be considered in calculating the nominal flexural resistance. However, for compact composite sections in positive bending, the effect of these different types of loadings on the flexural stresses and on partial yielding of the cross section need not be considered. Since these cross-section types are able to sustain inelastic curvatures sufficient to develop their nominal full plastic moment, the effect of the different loadings is negligible with respect to the section maximum strength. AASHTO (2020) Article 6.10.1.5 still requires an analysis of the structure separately for the noncomposite, short-term composite and long-term composite loadings. The relative proportion of the three types of loadings typically will have some effect on the distribution of the moments and forces in the structure.

6.3.3.3 Handling of creep and shrinkage effects

Stresses in the concrete deck due to permanent loads acting on the composite structure cause the concrete to creep. The effect of creep is to relieve the stresses in the concrete and increase the stresses in the steel. AASHTO (2020) Article 6.10.1.1.1a addresses the influence of creep on the steel stresses in a reasonable but approximate fashion by using three times the modular ratio, $3n = 3E_s/E_c$, when transforming the elastic concrete section to an equivalent steel section for analysis of the effects of permanent loads on the steel in composite bridges. Oehlers and Bradford (1999) discuss the accuracy of this type of approximation. AASHTO (2020) Article 6.10.1.1.1d requires the conservative use of the short-term modular ratio $n = E_s/E_c$ for calculation of longitudinal flexural stresses in the concrete due to all permanent and transient loads. This is important primarily for determining where sufficient longitudinal reinforcement should be provided in the concrete deck to control cracking (e.g., see AASHTO Articles 6.10.3.2.4 and 6.10.1.7).

Concrete deck shrinkage also has an effect on the detailed structural behavior. During the first several months after construction, the slab is expected to shrink measurably. In simple-span structures, this induces tensile stresses in the deck, compressive stresses in the top flanges of the steel I-sections and tensile stresses in the bottom flanges of the steel I-sections. Tests have indicated that the unit shrinkage of the slab in composite beams (i.e., the shrinkage strain adjusted for long-term relaxation effects) may be taken equal to 0.0002 (Viest et al. 1958). The corresponding stresses may be computed adequately by assuming that the shrinkage does not cause cracking. The steel stresses in straight simple spans may be approximated by considering the composite cross-section member as an eccentrically loaded column with a load of $0.0002E_cnA_c$ applied at the centroid of the deck and using $n = E_s/E_c$ (Viest et al. 1958).

The shrinkage stresses in the concrete deck for simple spans, and in the positive moment regions of continuous spans, are counteracted by the composite dead and live load stresses. Furthermore, compact composite I-section members in positive bending develop maximum strengths that involve significant yielding and inelastic redistribution of the cross-section stresses. The steel section in noncompact composite members in positive bending (addressed in the next section) tends to be larger relative to the concrete slab, and hence the influence of the loading $0.0002E_cnA_c$ is smaller. Also, any strength beyond first yielding of the steel section is neglected in noncompact composite I-section members. Therefore, AASHTO (2020) neglects the additional incidental compression in the top of the steel I-sections in positive bending regions in all cases with one exception discussed below. In the negative moment regions of continuous beams, the deck concrete is neglected in all cases in determining the member flexural resistance. Also, due to minor slip at the shear connectors between the slab and the steel girders and minor cracking in the slab, the shrinkage forces are not likely to be fully effective. Hence, AASHTO (2020), with one exception, considers that the shrinkage stresses are not an important factor with respect to strength for all types of composite sections in negative bending.

The exception to the above simplifications is addressed in AASHTO (2020) Article 3.4.1 for composite girders where the slab is longitudinally post-tensioned. In this case, the AASHTO provisions indicate that the effect of shrinkage and long-term creep around the shear connectors should be evaluated to ensure that the composite girder is able to maintain the prestressing over the life of the bridge. This article also states that the contribution of long-term deformations in closure pours between precast deck panels that have been aged to reduce the shrinkage and creep may need evaluation. AASHTO (2020) Article C6.10.1.1.1a also indicates that for shored construction where close tolerances on the final girder cambers are important, the above handling of creep effects may not be appropriate. Refined analysis of shrinkage effects also may be important in other types of structures requiring close tolerances on girder cambers, e.g., in spans supporting elevated tracks for maglev trains (Frank 2005). Article C4.6.6 of AASHTO (2020) points out that general creep and shrinkage effects may be analyzed in the same fashion as strains due to temperature gradient through the bridge cross section.

6.3.4 Noncompact Composite Sections in Positive Flexure

AASHTO (2020) classifies composite sections in positive bending as noncompact sections when any of the limits listed in Section 6.3.3 of this volume are violated. The flexural resistance of these section types is defined by limiting the elastically computed compression and tension flange stresses to

$$F_{nc} = R_b R_h F_{yc} \qquad\qquad (6.3.4\text{-}1)\ (\text{AASHTO } 6.10.7.2.2\text{-}1)$$

and

$$F_{nt} = R_h F_{yt} \qquad\qquad (6.3.4\text{-}2)\ (\text{AASHTO } 6.10.7.2.2\text{-}2)$$

respectively, where R_b is the web load-shedding strength reduction factor specified in AASHTO Article 6.10.1.10.2 and R_h is the hybrid web strength reduction factor specified in AASHTO Article 6.10.1.10.1. These factors are discussed further in Sections 6.3.5.2.2 and 6.3.5.2.3 of this volume. AASHTO (2020) specifies the resistance of these types of sections in terms of the elastically computed flange stresses, rather than the stress-resultant moments, for the following reasons:

1. The AASHTO (2020) provisions take the cautious approach of limiting the extent of flexural yielding in the positive moment regions of composite curved I-girder bridges. The rationale behind this approach is discussed previously in Section 3.0 of this volume.

2. Bridge cross sections such as those shown in Figure 3 through Figure 5 are more likely in longer-span structures where it may be desirable to violate the second and/or third stated limits in Section 6.3.3 in particular. In these types of bridges, the appropriate slab effective width for use with the main girders and/or with the secondary stringers potentially can be determined more rationally using a refined analysis that models the plate action of the concrete deck. The stress format for the cross-section resistances allows the Engineer to focus directly on the steel section stresses determined from this type of analysis. Conversely, the use of a moment format for the cross-section resistances requires further processing, including assumptions about the effective width of the deck that acts compositely with each of the steel members. Furthermore, because of the relative size of the steel section to the concrete deck typical for these types of sections, M_p often is not substantially larger than $R_h M_y$.

3. As discussed in Section 6.3.3.1 of this volume, the yield strain of the steel for $F_y = 70$ ksi is slightly beyond the level of strain corresponding to the peak compressive stress for typical deck concrete. This has potential implications on the concrete deck behavior at strength if a top flange yield stress greater than or equal to 70 ksi is utilized in the design (it should be noted that these negative implications do not occur if the steel top flange stresses and strains do not approach these limits). Nevertheless, I-girders with flange yield strengths greater than or equal to 70 ksi will tend to have relatively large bending curvature under service and strength loading conditions. Therefore, Engineers may prefer to employ a first-yield based limit for the strength design of these types of sections.

4. Once one adopts a design philosophy based essentially on first yield in flexure, the separate effects of noncomposite, short-term composite and long-term composite loadings become explicit considerations in the strength assessment. The moments due to the above separate loading effects cannot be added together to determine the overall effect. In this case, the most rational way to address the separate loading effects is to consider the elastic cross-section stresses directly.

For compact composite sections in positive bending, the flexural resistances tend to be larger than the yield moment capacity of the cross section. As a result, if the resistances are expressed in terms of elastically computed flange stresses, they can be larger than the corresponding flange yield stress. Furthermore, as noted at the end of Section 6.3.3, the elastic stresses are generally redistributed by inelastic deformations as the strength limit is approached in compact section members. Therefore, for compact section members, the resistances are expressed more naturally in terms of the total moment.

The elastically computed flange stresses used for checking of noncompact composite I-sections in positive bending are based generally on the assumption that the concrete stress-strain behavior is nominally linear. AASHTO (2020) Article 6.7.2.1 requires that the longitudinal compressive stresses in the concrete deck should be limited to $0.6f_c'$ under the factored load conditions, to ensure linear behavior of the concrete. The commentary to this article points out that this condition is unlikely to govern except in cases involving shored construction, or unshored construction where the noncomposite steel dead load stresses are low, combined with geometries causing the neutral axis of the short- and long-term composite section to be significantly below the bottom of the concrete deck.

6.3.5 Composite Sections in Negative Flexure and Noncomposite Sections

6.3.5.1 Key concepts

In AASHTO (2020), the flexural resistance of all types of composite I-section members in negative flexure, and of all types of noncomposite I-section members, is governed by the most critical of the three following limit states:

- Lateral-torsional buckling (LTB),
- Compression flange local buckling (FLB), and
- Tension flange yielding (TFY).

All of the AASHTO (2020) LTB and FLB resistance equations are based consistently on the logic of identifying the two anchor points shown in Figure 59 for the case of uniform major-axis bending. Anchor point 1 is located at the effective unbraced length $KL_b = L_p$ for LTB or flange slenderness $b_{fc}/2t_{fc} = \lambda_{pf}$ for FLB corresponding to development of the maximum potential flexural resistance, or "plateau" resistance, labeled as F_{max} or M_{max} in the figure. Anchor point 2 is located at the effective length L_r or flange slenderness λ_{rf} at which the elastic LTB or FLB resistances are equal to R_bF_{yr} in terms of stress or $R_bF_{yr}S_{xc}$ in terms of moment. The term F_{yr} is the nominal compression flange stress at the onset of significant yielding including residual stress effects, and R_b is the web load-shedding strength reduction factor (equal to 1.0 for sections with compact or noncompact webs). In most cases, F_{yr} is taken equal to $0.7F_{yc}$. The inelastic FLB and LTB resistances are expressed simply and accurately by linear interpolation between the above two anchor points. For $KL_b > L_r$ or $b_{fc}/2t_{fc} > \lambda_{rf}$, the LTB and FLB resistances are governed by the theoretical elastic buckling strength curves. The format shown in Figure 59, and all the underlying base equations, are with minor exceptions the same as in the AISC (2016) provisions for noncomposite I-section members.
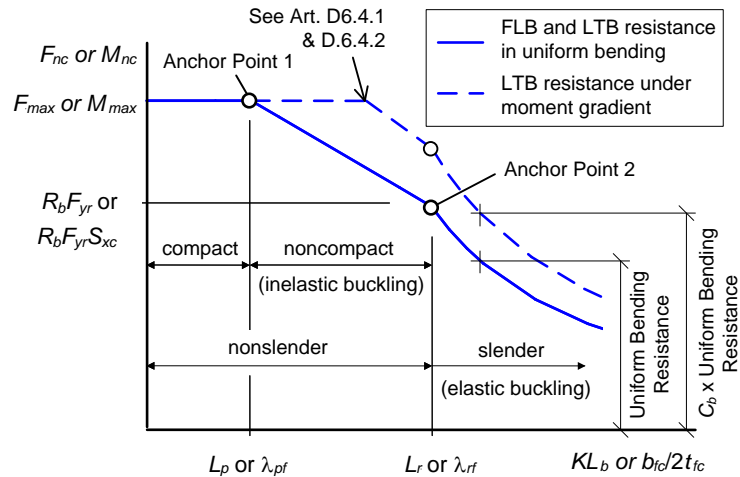
Figure 59. Basic form of flange local buckling (FLB) and lateral-torsional buckling (LTB) strength curves for composite I-section members in negative bending and noncomposite I-section members (reprinted with permission from AASHTO (2020)).

For unbraced lengths subjected to moment gradient, the calculated LTB resistance is modified by the factor C_b as illustrated by the dashed line in Figure 59. In these cases, the uniform bending elastic and inelastic LTB strengths are simply scaled by C_b, with the exception that the resistance is capped by F_{max} or M_{max}. The FLB resistance for moment gradient cases is the same as that for uniform major-axis bending, neglecting the relatively minor influence of moment gradient on the FLB strengths.

AASHTO (2020) Article C6.10.8.2.3 indicates that for rehabilitation design or in extraordinary circumstances, the Engineer may consider modifying L_b in Figure 59 by an elastic effective length factor (K) for lateral-torsional buckling. However, in most design situations, common practice is to take L_b as the actual unsupported length between the brace points corresponding to the compression flange-level bracing and/or the diaphragm or cross-frame locations (i.e., $K = 1$). Article C6.10.8.2.3 recommends a simple hand method from Ziemian (2010) and Nethercot and Trahair (1976) for determining LTB effective length factors K in cases where the additional calculation effort is merited. The application of this procedure to prismatic I-section members is explained in Section 6.3.5.13 of this volume, after discussion of the more fundamental parameters illustrated in Figure 59.

The TFY flexural resistance addresses the general yielding of the tension flange as the name implies. However, depending on the slenderness of the web, the TFY resistance can be larger than just the moment corresponding to nominal first yielding of the tension flange. This aspect is addressed in more detail in Section 6.3.5.3.

The governing flexural resistance is generally taken as the smaller of the values calculated independently for each of the above idealized flexural limit states.

Depending on which of the three regions that the unbraced length L_b falls in, delineated by Anchor Points 1 and 2 in Figure 59, the unbraced length is referred to as compact, noncompact or slender under flexure. Compact unbraced lengths are able to develop the maximum flexural resistance,

112

F_{max} or M_{max}, in uniform bending, assuming that the FLB or TFY resistances are not smaller. The *uniform bending* resistance for noncompact unbraced lengths is reduced relative to F_{max} or M_{max} due to inelastic LTB. Lastly, for slender unbraced lengths *in uniform bending*, the LTB resistance is defined by the corresponding theoretical elastic LTB equations. However, it is important to note that the LTB resistance of unbraced lengths subjected to a moment gradient (i.e., nonuniform bending along the length) can be increased significantly due to the moment gradient effects. As such, F_{max} or M_{max} can be achieved at much larger unbraced lengths than the compact limit L_p. Thus, it is unwise in general to select unbraced lengths or a spacing of the cross frames to enforce $L_b \leq L_p$.

Similar to the above LTB discussions, cross sections with compact compression flanges are able to develop F_{max} or M_{max}, cross sections with noncompact compression flanges have their flexural resistance limited by inelastic FLB, and cross sections with slender flanges have their flexural resistance governed by theoretical elastic FLB, assuming that the LTB or TFY resistances are not smaller. Actually, AASHTO (2020) does not explicitly provide any elastic FLB equations. This is because the proportioning limit $b_f/2t_f \leq 12$ in Article 6.10.2.2 (Eq. 6.3.2-3) precludes elastic FLB for all steel I-section members with $F_{yc} \leq 90$ ksi. AASHTO (2020) simply uses its inelastic FLB expressions into the elastic FLB range for the minor extent that $b_f/2t_f$ can potentially exceed λ_{rf} for $F_{yc} > 90$ ksi. This is justified given the approximations invoked in determining the flange local buckling resistance. Recent studies have shown that the F_{yr} limit for FLB can actually be increased slightly to $0.75F_{yc}$ and the inelastic FLB curve can be extended into the elastic FLB range, providing an improved characterization of FLB resistances in flexure recognizing some benefits from the local postbuckling strength of compression flanges (Latif and White 2021).

Furthermore, as discussed in the following, the webs in I-section members are defined as either compact, noncompact or slender under flexure. The maximum potential resistance M_{max} is equal to the plastic moment capacity M_p for members with a compact web. However, the most economical welded composite I-girders in negative bending, and welded noncomposite I-girders in positive or negative bending, rarely have compact webs. In fact, it is not uncommon for welded I-section webs to be slender under flexural compression. The M_{max} of slender web members is generally smaller than the compression flange yield moment M_{yc} due to web bend buckling and shedding of load to the compression flange. The detailed influences of the web slenderness on M_{max} are discussed in Section 6.3.5.2 of this volume.

All of the above definitions or classifications focus on separate member characteristics, i.e., the unbraced length or LTB slenderness, the compression flange slenderness and the web slenderness. This is slightly different from the classification of composite I-section members in positive flexure, where the entire cross section is defined as either compact or noncompact. It is also somewhat different from prior AASHTO Specifications, which focused on the classification of entire cross sections. The AASHTO (2020) emphasis on these separate member characteristics is consistent with the approaches in AISC (2016).

The main LTB and FLB provisions in AASHTO (2020) Article 6.10.8.2 specify the flexural resistances in terms of elastically computed compression flange stresses. Also, the equations in this article are targeted specifically at the capacity of slender-web I-section members. The Engineer is allowed to use these equations conservatively for all I-section member types as a simplification. This simplification recognizes the fact that, with the exception of rolled I-section

members, bridge I-sections predominantly have slender or nearly slender webs. However, Appendix A6 of AASHTO (2020) specifies comparable and more liberal equations for composite I-section members in negative bending and noncomposite I-section members that have noncompact or compact webs. The Appendix A6 equations are a direct extension of the equations in AASHTO Article 6.10.8.2, and with minor exceptions, are fundamentally the same as the equations for design of noncompact- and compact-web noncomposite I-section members in AISC (2016). AASHTO (2020) Articles C6.10.6.2.3 and C6.10.8.1.1 point out that the Engineer should give strong consideration to utilizing the provisions of Appendix A6 for I-sections with compact or nearly compact webs in straight bridges. In addition, the AASHTO (2020) equations in Article 6.10.8.2 are with minor exceptions fundamentally the same as the AISC (2016) flexural resistance equations for slender-web I-section members. White (2008) details the minor differences between the AASHTO and AISC provisions. Several of the most significant of these differences are outlined in the following Sections.

The AASHTO Appendix A6 equations are expressed in terms of the section bending moment. The rationale for use of the flange stress format in AASHTO Article 6.10.8.2 and the moment format in AASHTO Appendix A6 is essentially the same as that discussed in Section 6.3.4 of this volume for noncompact and compact composite I-sections in positive bending.

The coordinates of the anchor points shown in Figure 59 are (L_p, M_{max}) and $(L_r, R_bF_{yr}S_{xc})$ for LTB and (λ_{pf}, M_{max}) and $(\lambda_{rf}, R_bF_{yr}S_{xc})$ for FLB in terms of the bending moment. The specific terms associated with these anchor points are discussed in detail in the following Sections. Also, since the noncompact bracing limit, L_r, and the noncompact compression flange slenderness limit, λ_{rf}, are associated with the theoretical elastic buckling equations, the base elastic buckling formulas are also presented. The following discussions are targeted at providing an overall conceptual understanding of the AASHTO (2020) flexural resistance calculations. AASHTO (2020) Appendix C6 provides detailed flowcharts that capture the complete application of the flexural design provisions for I-section members. The Engineer is encouraged to consult these flowcharts for an efficient organization of the corresponding calculations. White (2008) gives similar flowcharts that emphasize the unified nature of the AASHTO (2020) Article 6.10.8 and Appendix A6 equations.

6.3.5.2   Maximum potential flexural resistance, M_{max} or F_{max}

6.3.5.2.1 Compact- and noncompact-web sections

As noted in the above, M_{max} is equal to the cross-section plastic moment capacity, M_p, for members with compact webs. However, for members with noncompact or slender webs, the ordinate of Anchor Point 1, M_{max} or F_{max}, varies as a function of the web slenderness $2D_c/t_w$. For noncompact-web members, M_{max} decreases linearly as a function of $2D_c/t_w$ between the compact- and noncompact-web limits λ_{pw} and λ_{rw}, as shown in Figure 60. The noncompact-web limit is given by the equation

$$\lambda_{rw} = c_{rw}\sqrt{\frac{E}{F_{yc}}}$$

(6.3.5-1a) (AASHTO 6.10.6.2.3-3, A6.2.1-3 & A6.2.2-3)

where

$$4.6 \leq c_{rw} = 3.1 + \frac{5.0}{a_{wc}} \leq 5.7 \qquad (6.3.5\text{-}1b)$$

and

$$a_{wc} = \frac{2D_c t_w}{b_{fc} t_{fc}} \qquad (6.3.5\text{-}1c) \text{ (AASHTO 6.10.6.2.3-4, A6.2.1-4, 6.10.1.10.2-8)}$$

(if the compression flange has cover plates, these may be added to $b_{fc} t_{fc}$, giving a total equivalent compression flange area). The λ_{rw} limit is the value of $2D_c/t_w$ at which an I-section member that does not have web longitudinal stiffening is able to develop $M_{max} = R_h M_{yc}$, or a nominal compression flange yield stress $F_{max} = R_h F_{yc}$, just prior to the onset of local web buckling in flexural compression. This type of web local buckling is referred to generally as web bend buckling. The theoretical background to this equation is discussed subsequently in Section 6.3.10.2 of this volume. Equation 1b is a refinement of the equation for λ_{rw} in AISC (2016) recommended by Subramanian and White (2017a). AISC (2016) uses Eq. 1a with a constant value for c_{rw} equal to 5.7.

AASHTO (2020) defines the compact-web limit as

$$\lambda_{pw(D_c)} = \frac{\dfrac{D_c}{D_{cp}} \sqrt{\dfrac{E}{F_{yc}}}}{\left(0.54 \dfrac{M_p}{M_y} - 0.09\right)^2} \leq \lambda_{rw} \qquad (6.3.5\text{-}2)$$

(AASHTO A6.2.2-6 & 6.2.1-2, AISC Table B4.1b)

Equation 2 accounts for the larger demands on the web required to develop the cross-section plastic moment in singly symmetric cross sections. The term D_c/D_{cp} in the numerator converts this equation from its fundamental form associated with the plastic depth of the web in compression, D_{cp}, to the form associated with the elastic depth of the web in compression, D_c. This is necessary so that a consistent web slenderness parameter, $2D_c/t_w$, may be employed for the linear interpolation between the anchor points (λ_{pw}, M_p) and (λ_{rw}, $R_h M_{yc}$) in Figure 60. For a homogeneous doubly symmetric I-section with $D_c/D_{cp} = 1.0$ and an assumed $M_p/M_y = 1.12$, Eq. 2 reduces to the limit in Eq. 6.3.3-1. The requirement of $\lambda_{pw(Dc)} \leq \lambda_{rw}$ in Eq. 2 conservatively defines the compact-web limit as $\lambda_{pw(Dc)} = \lambda_{rw}$ for singly symmetric sections with proportions such that the section is classified as slender based on the elastic depth of the web in compression and Eq. 1, but as compact based on the plastic depth of the web in compression D_{cp} and the fundamental form of Eq. 2 with the ratio D_c/D_{cp} removed from its numerator. This type of cross section is possible in negative bending regions of continuous-span I-girders having a significantly larger bottom compression flange. White (2008) shows a practical cross section for which $\lambda_{pw(Dc)} = \lambda_{rw}$.
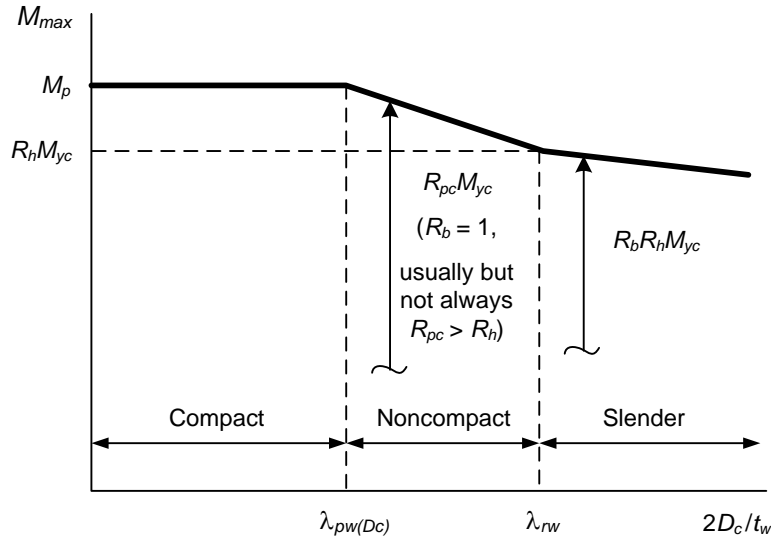
Figure 60. Variation of M_{max} versus the web slenderness $\lambda_w = 2D_c/t_w$.

The linear interpolation between (λ_{pw}, $M_{max} = M_p$) and (λ_{rw}, $M_{max} = R_h M_{yc}$) shown in Figure 60 is represented by the *web plastification factor*, R_{pc}, in AASHTO (2020) (and in AISC (2016)). This parameter is simply equal to the cross-section shape factor, M_p/M_{yc}, for a compact-web section. It may be considered as an *effective shape factor* that varies linearly between M_p/M_{yc} and R_h for noncompact-web sections. One should note that R_{pc} is greater than one in most situations for girders with noncompact webs. However, M_{yc} can be greater than M_p for some extreme singly symmetric sections having a large flange in compression and a neutral axis close to the compression flange (this is because earlier yielding in tension is generally neglected in the calculation of $M_{yc} = F_{yc}S_{xc}$). In these cases, R_{pc} can be less than one. The resistance tends to be governed by tension flange yielding (TFY) in these situations.

6.3.5.2.2 Slender-web sections and the web load-shedding strength reduction factor, R_b

For I-girders in which $2D_c/t_w > \lambda_{rw}$, the web is defined as slender and M_{max} is given by the expression $R_b R_h F_{yc} S_{xc}$ as shown in Figure 60 (i.e., $F_{max} = R_b R_h F_{yc}$). In this case, $R_b < 1$ accounts for a reduction in M_{max} or F_{max} due to shedding of flexural stresses to the compression flange associated with the post-bend buckling response of the web. The base AASHTO (2020) web load-shedding strength reduction factor for girders that do not have web longitudinal stiffeners is

$$R_b = \frac{a_{wc}}{1200 + 300a_{wc}}\left(\frac{2D_c}{t_w} - \lambda_{rw}\right) \leq 1.0 \qquad \text{(6.3.5-3) (AASHTO 6.10.1.10.2-3, AISC F5-6)}$$

where a_{wc} is given by Eq. 1c. This equation is the more general and accurate form of two equations developed by Basler and Thurlimann (1961). For composite sections in negative bending, AASHTO (2020) Article 6.10.1.10.2 specifies the use of the depth of the web in compression D_c for the section consisting of the steel girder plus the longitudinal deck reinforcement within the slab effective width in determining R_b by Eq. 3.

116

AASHTO (2020) Article 6.10.1.10.2 gives the following equation for the web load-shedding strength reduction factor for girders that have one or more continuous web longitudinal stiffeners satisfying $d_s/D_c < 0.76$:

$$R_b = 1.07 - 0.12\frac{D_c}{D} - \frac{a_{wc}}{1200 + 300a_{wc}}\left(\frac{D}{t_w} - \lambda_{rwD}\right) \leq 1.0 \qquad (6.3.5\text{-}4)$$

(AASHTO 6.10.1.10.2-2)

where

$$\lambda_{rwD} = 0.95\sqrt{\frac{Ek}{F_{yc}}} \quad \text{for homogeneous longitudinally stiffened sections} \qquad (6.3.5\text{-}5)$$

(AASHTO 6.10.1.10.2-6)

$$\lambda_{rwD} = \left(\frac{1}{2D_c/D}\right)5.7\sqrt{\frac{E}{F_{yc}}} \quad \text{for hybrid longitudinally stiffened sections} \qquad (6.3.5\text{-}6)$$

(AASHTO 6.10.1.10.2-7)

d_s = distance from the centerline of the closest plate longitudinal stiffener, or from the gauge line of the closest angle longitudinal stiffener to the inner surface or leg of the compression flange element

k = bend buckling coefficient for webs with longitudinal stiffeners, discussed in Section

D = web depth

As noted in the previous sub-section, λ_{rw} is the web slenderness at which the longitudinally unstiffened web theoretical elastic bend buckling stress is equal to the compression flange yield strength. Similarly, λ_{rwD} is the corresponding web slenderness for the web with a single continuous longitudinal stiffener located at a distance d_s from the compression flange. Hybrid longitudinally-stiffened girders exhibit significant strength reductions due to combined early web yielding and web bend buckling at smaller values of the web slenderness than that corresponding to theoretical elastic bend buckling at F_{yc}. This behavior is captured by Eq. 6. For both hybrid longitudinally unstiffened and hybrid longitudinally stiffened webs, the combined effects of load shedding to the compression flange due to web bend buckling and early web yielding are quantified by the product of R_b with the hybrid strength reduction factor, R_h, discussed in the next section. Equations 4 through 6 are based on parametric finite element test simulation studies of a wide range of girder geometries with longitudinally stiffened webs (Subramanian and White 2017c).

AASHTO (2020) Article 6.10.1.10.2 gives a separate equation for a_{wc} that conservatively approximates the beneficial effect of the concrete composite deck for calculation of R_b in composite longitudinally stiffened sections in positive bending. AASHTO (2020) Article C6.10.1.10.2 states that R_b may be taken equal to one for composite sections in positive bending that satisfy the proportioning limits of Article 6.10.2.1.1. Composite cross sections in positive bending that satisfy these limits generally have R_b values that, if calculated, are equal to or close

to 1.0. However, composite longitudinally stiffened sections in positive bending, that are classified as noncompact sections (based on the second requirement listed in Section 6.3.3.1 of this volume) will sometimes have R_b values somewhat smaller than 1.0.

6.3.5.2.3 Hybrid-web strength reduction factor

As noted above, the term R_h is the hybrid web strength reduction factor. This factor accounts for the reduced contribution of the web to the nominal flexural resistance at the first yielding of any flange element, due to earlier yielding of a lower strength hybrid web. In AASHTO (2020), this factor is defined by the single equation,

$$R_h = \frac{12 + \beta(3\rho - \rho^3)}{12 + 2\beta}$$

(6.3.5-8) (AASHTO 6.10.1.10.1-1)

for all types of composite and noncomposite members, where

$$\beta = 2D_n t_w / A_{fn}$$

(6.3.5-9) (AASHTO 6.10.1.10.1-2)

ρ = smaller of F_{yw}/f_n and 1.0

A_{fn} = sum of the flange area and the area of any cover plates on the side of the neutral axis corresponding to D_n. For composite sections in negative bending, the area of the longitudinal reinforcement may be included in calculating A_{fn} for the top flange.

D_n = larger of the distances from the elastic neutral axis of the cross section to the inside face of either flange. For sections where the neutral axis is at the mid-depth of the web, the distance from the neutral axis to the inside face of the flange on the side of the neutral axis where yielding occurs first.

f_n = for sections where yielding occurs first in the flange, a cover plate or the longitudinal reinforcement on the side of the neutral axis corresponding to D_n, the largest of the specified minimum yield strengths of each component included in the calculation of A_{fn}. Otherwise, the largest of the elastic stresses in the flange, cover plate or longitudinal reinforcement on the side of the neutral axis corresponding to D_n at first yield on the opposite side of the neutral axis.

These definitions account for all possible combinations associated with different positions of the elastic neutral axis and different yield strengths of the top and bottom flange elements. Equation 8 is adapted from a fundamental strength reduction equation, originally derived for doubly symmetric I-sections (ASCE 1968; Schilling 1968; Frost and Schilling 1964), to also handle singly symmetric and composite sections. This is accomplished by focusing on the side of the neutral axis where yielding occurs first. This side of the neutral axis has the most extensive web yielding prior to first yielding of any flange element. All of the flange elements on this side of the neutral axis are conservatively assumed to be located at the edge of the web. The original equation is also adapted by assuming that the shift in the neutral axis due to the onset of web yielding is negligible. These assumptions are similar to those used in the development of a separate R_h equation for

composite members in prior AASHTO and AISC Specifications. AISC (2016) does not address hybrid I-section members to simplify its design rules.

In lieu of the use of Eq. 8, AASHTO (2020) Article C6.10.1.10.1 allows the Engineer to determine R_h directly from an iterative strain-compatibility analysis. However, since the computed R_h values from Eq. 8 are typically close to 1.0, this refined calculation typically will provide little benefit.

6.3.5.2.4 Other considerations

For sections with $2D_c/t_w < \lambda_{rw}$, AASHTO (2020) Articles 6.10.6.2.3 and A6.1 apply two restrictions on the use of M_{max} values larger than R_hM_{yc} ($F_{max} > R_hF_{yc}$). If the compression flange of noncomposite I-sections is substantially smaller than the tension flange such that

$$I_{yc} \,/\, I_{yt} < 0.3 \qquad\qquad\qquad \text{(6.3.5-10) (AASHTO 6.10.6.2.3-2 \& A6.1-2)}$$

the Engineer is required to calculate the flexural resistance conservatively based on the slender-web member equations of Article 6.10.8. This restriction guards against the use of extremely monosymmetric sections where analytical studies indicate a significant loss in the influence of the St. Venant torsional rigidity GJ on the LTB resistance due to cross-section distortion. If the flanges are of equal thickness, this limit is equivalent to $b_{fc} < 0.67b_{ft}$. AISC (2016) requires the use of $J = 0$ in the calculation of L_r and the elastic LTB resistance for singly symmetric I-sections that satisfy Eq. 10, but expressed as $I_{yc}/I_y < 0.23$; otherwise, AISC (2016) permits the calculation of M_{max} as shown in Figure 60 for compact- and noncompact-web members. Based on the results from White and Jung (2007), the AASHTO restriction is considered more prudent.

Also, AASHTO Article 6.10.6.2.3 requires the use of the slender-web member equations and disallows the use of Appendix A6 for all bridges with kinked (chorded) continuous or horizontally curved segments. As noted previously in Section 3 of this volume, this restriction is based on the limited information about the influence of cross-section partial yielding on the response of curved bridge structural systems. The component studies on which the AASHTO (2020) curved I-girder resistances are based (White and Jung 2008; White and Kim 2008; White et al. 2008) fully support the use of Appendix A6 as well as Article 6.10.7.1 for composite and noncomposite curved I-girders. The studies by Jung and White (2010) support the use of these Articles for curved I-girder bridges. However, as noted in Section 3, further studies are needed to address the influence of partial cross-section yielding on continuous-span curved I-girder bridges.

6.3.5.3   Tension flange yielding (TFY) resistance

Prior to considering the other parameters illustrated in Figure 59, it is useful to discuss the definition of the AASHTO (2020) TFY resistance. The AASHTO TFY resistance varies with the web slenderness in a fashion similar to the variation of M_{max} and F_{max}. However, the R_b factor is not applied in determining the TFY resistance of slender-web sections since the tension flange stress is not increased significantly by the shedding of the web compressive stresses (Basler and Thurlimann 1961). Figure 61 illustrates the variation of the TFY resistance as a function of the web slenderness $2D_c/t_w$. AASHTO (2020) Article 6.8.10.3 defines the TFY resistance of slender-web sections as the nominal first yielding of the tension flange reduced by any hybrid web effects, R_hF_{yt} in terms of the tension flange stress, or $R_hF_{yt}S_{xt} = R_hM_{yt}$ in terms of the member bending

moment. However, Articles A6.2 and A6.3 define a TFY resistance that varies linearly from $R_h M_{yt}$ to the section plastic moment M_p as the web slenderness $2D_c/t_w$ varies from λ_{rw} to $\lambda_{pw(Dc)}$. Finally, for compact-web sections, the TFY resistance is equal to M_p.
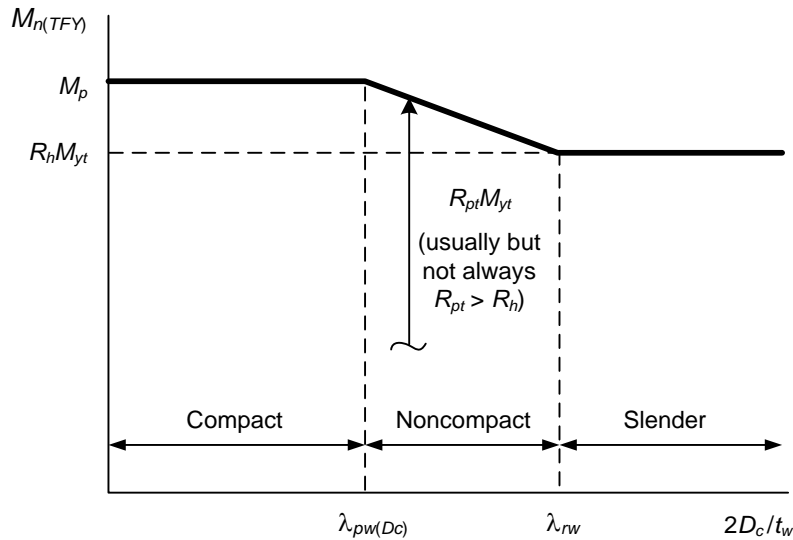
Figure 61. Variation of the tension flange yielding (TFY) resistance $M_{n(TFY)}$ versus the web slenderness $\lambda_w = 2D_c/t_w$.

Similar to the web plastification factor R_{pc} used in defining M_{max} for LTB and FLB of noncompact- and compact-web I-section members, AASHTO (2020) specifies a web plastification factor R_{pt} that corresponds to the TFY limit state. Similar to R_{pc}, R_{pt} is simply equal to the cross-section shape factor M_p/M_{yt} for compact-web sections, and it may be considered as an effective shape factor for noncompact-web sections. Also, similar to R_{pc}, R_{pt} can be less than one for extremely monosymmetric I-sections, basically sections that have a significantly larger tension flange causing the neutral axis to be very close to the tension flange (in these sections, M_{yt} can be greater then M_p due to the neglect of earlier yielding in compression when writing $M_{yt} = F_{yt}S_{xt}$). However, in these cases, R_{pc} will be greater than R_h and the LTB or FLB resistance equations will usually govern.

For sections in which $M_{yt} \geq M_{yc}$, TFY never governs and does not need to be checked.

Recent studies (Slein et al. 2021a) have confirmed that, for sections with $M_{yt} < M_{yc}$, the TFY limit state acts as an artificial and highly conservative limit on the physical ultimate strengths in flexure, and that the TFY limit state check can be removed completely from specification resistance calculations, contingent on the calculation of M_{yc} as the "actual" moment at nominal first yielding of the compression flange (considering the influence of earlier yielding in tension) and on a several related modifications to the web R_{pc} and R_b calculations. These findings are under consideration by AISC and AASHTO Technical Committees at this time (September 2021). Similar calculations have been implemented in the AASHTO (2020) Article 6.12.2 provisions for noncomposite box-section members.

6.3.5.4   Compact bracing limit, L_p

AASHTO (2020) specifies the equation

$$L_p = 1.0 r_t \sqrt{\frac{E}{F_{yc}}} \qquad\qquad \text{(6.3.5-11) (AASHTO 6.10.8.2.3-4 \& A6.3.3-4)}$$

as the compact bracing limit for all types of composite I-section members in negative bending and for all types of noncomposite I-section members. This equation is based on extensive analysis of experimental data by Yu and Sause (2002), White and Jung (2008) and White and Kim (2008). These studies demonstrate that the inelastic LTB resistance is represented accurately using this single equation, with no variation in L_p as a function of web slenderness, etc. other than via the radius of gyration r_t, combined with the expressions for the resistances M_{max} or F_{max} discussed in Section 6.3.5.2 of this volume. The radius of gyration in Eq. 11 can be calculated in all cases using the equation

$$r_t = \frac{b_{fc}}{\sqrt{12\left(1 + \frac{1}{3}\frac{D_c t_w}{b_{fc} t_{fc}}\right)}} \qquad\qquad \text{(6.3.5-12) (AASHTO 6.10.8.2.3-9 \& A6.3.3-10)}$$

This equation is precisely equal to the radius of gyration of the compression flange plus one-third of the depth of the web in compression. The web area term $D_c t_w$ in Eq. 12 accounts for the destabilizing effect of the flexural compression in the web on the member lateral-torsional stability.

In Specifications prior to AASHTO (2004) and AISC (2005), the L_p limit was based on different radii of gyration for different types of sections, including r_t, the radius of gyration of solely the compression flange itself about the cross-section y-axis, r_{yc}, and the radius of gyration of the complete cross section about its y axis, r_y. The radius of gyration r_{yc} is in general not appropriate because it neglects the destabilizing effect of the web compression. Also, the radius of gyration r_y is not appropriate for singly symmetric and composite I-section members since it does not properly account for the influence of the cross-section monosymmetry on the LTB response. The radius of gyration r_t provides the best overall characterization for all I-section types not only within the context of Eq. 11, but also within the elastic LTB calculations discussed in Section 6.3.5.7 of this volume. This statement is based on the simplicity of the equations as well as the accuracy of the predictions relative to experimental and refined analytical resistances.

Equation 11 generally gives somewhat smaller L_p values than in prior AISC and AASHTO Specifications. However, for slender-web members, if Eq. 11 is substituted into the original CRC based expression for the LTB resistance suggested by Basler and Thurlimann (1961) and summarized by Cooper et al. (1978), a strength of $0.97M_y$ is obtained for members with R_b and R_h equal to one. If L_p/r_t from Eq. 11 is substituted as an equivalent slenderness ratio into the column strength Eqs. 6.2.1-4 and 6.2.1-1a, a resistance of $0.96M_y$ is obtained.

The more liberal L_p equations in previous AASHTO and AISC Specifications are based largely on the studies by Yura et al. (1978), where the L_p limit

$$L_p = \frac{300r_y}{\sqrt{F_y}} = 1.76r_y\sqrt{\frac{E}{F_{yc}}}$$ (6.3.5-13)

was recommended for doubly symmetric steel I-section members with compact webs and compact flanges. However, the original study by Galambos and Ravindra (1976) recommended

$$L_p = \frac{240r_y}{\sqrt{F_y}} = 1.41r_y\sqrt{\frac{E}{F_{yc}}}$$ (6.3.5-14)

for these member types. Table 1 of Yura et al. (1978) reports the same resistance factors ϕ_b based on predictions of experimental results as in Galambos and Ravindra (1976), although Yura et al. (1978) propose different L_p equations. The correct L_p expression corresponding to the ϕ_b factors in Yura et al. (1978) Table 1 is Eq. 14. Furthermore, the ratio r_t/r_y ranges from 1.12 to 1.28 for rolled wide-flange sections. Therefore, in terms of r_t, Eq. 14 may be expressed as

$$L_p = 1.10r_t\sqrt{\frac{E}{F_{yc}}} \quad \text{to} \quad 1.26r_t\sqrt{\frac{E}{F_{yc}}}$$ (6.3.5-15)

Cooper et al. (1978) specified

$$L_p = 0.86r_t\sqrt{\frac{E}{F_{yc}}}$$ (6.3.5-16)

in their final recommendations for load and resistance factor design of slender-web I-section members. These recommendations were subsequently changed to

$$L_p = \frac{300r_t}{\sqrt{F_{yc}}} = 1.76r_t\sqrt{\frac{E}{F_{yc}}}$$ (6.3.5-17)

for slender-web I-section members (referred to as plate girders) in AISC (1986), apparently to match the coefficient in Eq. 13 and to produce comparable compactly-braced results to the AISC (1978) Allowable Stress Design (ASD) equations. AISC (1986) also specified Eq. 13 for singly symmetric I-section members, but AISC (1993 and 1999) subsequently changed the L_p limit for these members to

$$L_p = 1.76r_{yc}\sqrt{\frac{E}{F_{yc}}}$$ (6.3.5-18)

As discussed by White and Jung (2003b), r_{yc} can be substantially larger than r_y and r_t. Therefore, Eq. 18 liberalizes the AISC (1993 and 1999) L_p equations for singly symmetric I-section members even further. The prior AASHTO equations for L_p were largely adopted from AISC, using the coefficient of 1.76 but with radii of gyration that in some cases differed from the AISC equations.

White and Jung (2008) show that Eq. 11 with a coefficient of 1.1 gives a nearly uniform reliability index throughout the compactly- and noncompactly-braced ranges for all types of I-section members. The results using a coefficient of 1.0 in Eq. 8 are essentially the same as those using a coefficient of 1.1 (the maximum difference in the resistance predictions is approximately one percent). AISC (2016) uses Eq. 11 with a coefficient of 1.1 except for doubly symmetric compact-web I-section members, where Eq. 13 is retained from AISC (1986, 1993 and 1999). White and Chang (2007) show that Eq. 11 with a coefficient of 1.1 gives resistances are that are larger than the traditional AISC ASD values for most compact-web I-section members. The maximum difference in the predictions using Eq. 13 versus Eq. 11 with a coefficient of 1.1 is approximately six percent.

Figure 62 compares the predictions by AASHTO (2020) and AISC (2016) for a set of rolled I-beam tests in uniform bending conducted by Dux and Kitipornchai (1983) and Wong-Chung and Kitipornchai (1987). Figure 63 shows the AASHTO and AISC predictions for a suite of noncompact-web member tests in uniform bending conducted by Richter (1998). The unbraced lengths L_b are modified using the Nethercot and Trahair (1976) effective length factor K (discussed subsequently in Section 6.3.5.13 of this volume) for the Dux and Kitipornchai (1983) and Wong-Chung and Kitipornchai (1987) tests. The Nethercot and Trahair (1976) K factors are equal to 1.0 in all cases for the Richter (1998) tests.

Equation 11 provides the best combination of simplicity (one equation that applies to all I-section members) and accuracy (near uniformity of the reliability index throughout the compactly- and noncompactly-braced ranges for all I-section members). However, the differences in the results using the various incarnations of L_p are relatively small with the exception of the application of Eq. 18 to singly symmetric I-section members. The use of r_t in Eq. 11 facilitates the assessment of LTB in composite I-section members subjected to negative bending, since r_t depends only on the characteristics of the portion of the cross section subjected to flexural compression.

6.3.5.5 Compact flange slenderness limit, λ_{pf}

AASHTO (2020) and AISC (2016) define the compact-flange slenderness limit by the equation

$$\lambda_{pf} = 0.38\sqrt{\frac{E}{F_{yc}}} \qquad \text{(6.3.5-19) (AASHTO 6.10.8.2.2-4 \& A6.3.2-4, AISC Table B4.1b)}$$

for all types of I-section members. This equation is identical to the compact-flange limit in AISC (1989 and 1999) and is based largely on the original research by Lukey et al. (1969) as well as the subsequent studies by Johnson (1985).
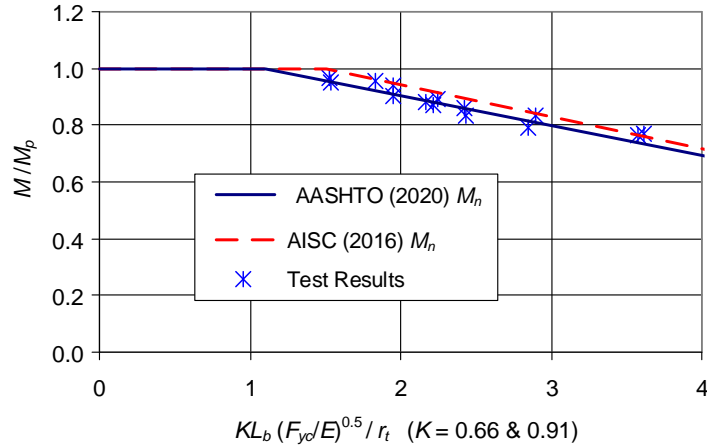
Figure 62. Comparison of rolled beam I-section uniform bending test results from Dux and Kitipornchai (1983) and Wong-Chung and Kitipornchai (1987) to the AASHTO (2020) and AISC (2016) flexural resistances (F_{yc} = 41.3 and 42.5 ksi, LTB effective length factors K = 0.66 and 0.91).
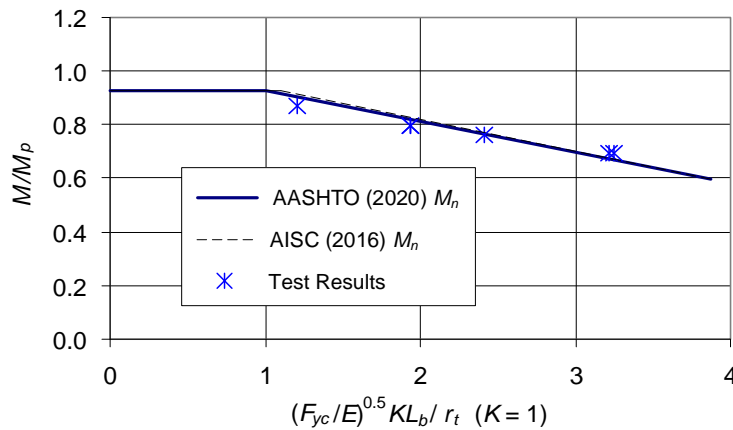
Figure 63. Comparison of compact-flange noncompact-web welded member test results for uniform bending, from Richter (1998), to the AASHTO (2020) and AISC (2016) flexural resistances ($b_{fc}/2t_{fc}$ = 8.0 to 8.1, D/t_w = 110, D/b_{fc} = 3.6, F_{yc} = 48.4 ksi.

6.3.5.6   Compression flange stress at the nominal onset of inelastic buckling, F_{yr}

AASHTO (2020) specifies $F_{yr} = 0.7F_{yc}$ with the exception of (1) highly monosymmetric compact-web and noncompact-web cross sections with the larger flange in compression, where the neutral axis is so close to the compression flange that nominal tension flange yielding occurs prior to reaching a stress of $0.7F_{yc}$ at the compression flange and (2) hybrid web members in general where $F_{yw} < 0.7F_{yc}$. To address these cases, AASHTO (2020) Articles A6.3.2 and A6.3.3 specify

$$F_{yr} = \min\left(0.7F_{yc}, F_{yt}\frac{S_{xt}}{S_{xc}}, F_{yw} \right) \geq 0.5F_{yc} \qquad (6.3.5\text{-}20)$$

124

The product $F_{yt}S_{xt}$ in the second term of this equation is the moment corresponding to nominal yielding at the tension flange. This value, divided by the section modulus to the compression flange, S_{xc}, is the compression flange stress corresponding to the onset of nominal yielding at the tension flange. The third term interprets the web yield stress as the limit corresponding to the onset of significant inelastic stability effects for hybrid sections with unusually low values for F_{yw} relative to F_{yc}. In extreme cases where $F_{yt}S_{xt}/S_{xc}$ or F_{yw} is less than $0.5F_{yc}$, AASHTO (2020) uses a minimum value of $F_{yr} = 0.5F_{yc}$.

For slender-web members, AASHTO (2020) Article 6.10.8.2 specifies

$$F_{yr} = \min\left(0.7F_{yc}, F_{yw}\right) \geq 0.5F_{yc}$$

(6.3.5-21)

That is, the second-term in Eq. 20 is not considered. This simplification is possible because the TFY resistance of slender-web members is defined as the nominal first yielding of the tension flange reduced by any hybrid web effects, R_hF_{yt}. However, since the TFY resistance for compact- and noncompact-web sections is generally larger than R_hM_{yt}, Eq. 20 is necessary to avoid significant violation of the assumption of elastic member behavior when using the AASHTO equations based on elastic LTB or FLB.

The limit $F_{yr} = 0.7F_{yc}$ is based on LTB and FLB experimental test data (White and Jung 2008; White and Kim 2008). This is a significant liberalization relative to the implicit use of $F_{yr} = 0.5F_{yc}$ for slender-web members in prior Specifications. Recent studies (Slein et al. 2021a) have shown that a corresponding moment of $0.5M_{yca}$ is needed for the ordinate of the elastic-to-inelastic transition point for the LTB of general built-up I-section members, to provide the target level of reliability for values of KL_b approaching L_r, where M_{yca} is the "actual" moment at nominal first yielding of the compression flange (considering the influence of earlier yielding in tension where applicable). These findings are under consideration by AISC and AASHTO Technical Committees at this time (September 2021). "Actual" yield moment calculations similar to these have been implemented in the AASHTO (2020) Article 6.12.2 provisions for noncomposite box-section members.

6.3.5.7 Elastic LTB stress, $F_{e.LTB}$

The AASHTO (2020) elastic LTB resistances are based on a single equation applicable for all types of I-section members. This equation gives the exact beam-theory solution for LTB of doubly symmetric I-section members, and it gives an accurate to somewhat conservative approximation for singly symmetric noncomposite members and composite members in negative bending (White and Jung 2003 a and b; White 2008). This equation may be written in terms of the compression flange flexural stress as

$$F_{cr} = F_{e.LTB} = C_b \frac{\pi^2 E}{(L_b/r_t)^2} \sqrt{1 + \frac{0.078}{X^2}(L_b/r_t)^2}$$

(6.3.5-22)

(AASHTO A6.3.3-8, AISC F2-4 & F4-5)

where

125

$$X^2 = \frac{S_{xc}h}{J} \tag{6.3.5-23}$$

r_t is approximately the radius of gyration of the compression flange plus one-third of the area of the web in compression, S_{xc} is the elastic section modulus to the compression flange, h is the distance between the centroids of the flange elements, and J is the St. Venant torsion constant of the steel I-section. Equation 23 is a simple ratio of the bending and torsional efficiencies of the cross section. For a doubly symmetric I-section, $X^2 \cong 2I_x/J$. This parameter ranges from 13 to 2500 for the complete set of ASTM A6 W shapes.

 (Note that AASHTO (2020) uses the symbol F_{cr} rather than $F_{e.LTB}$ in Eq. 22. However, for slender-web members, AASHTO (2020) multiplies the beam-theory elastic LTB stress $F_{e.LTB}$, with J taken equal to zero, by the web load-shedding parameter R_b to obtain the nominal flange stress at elastic LTB, i.e., $F_{cr} = R_b F_{e.LTB}$. The notation $F_{e.LTB}$ is used in this volume for consistency with the notation for column buckling as well as to distinguish the beam-theory based $F_{e.LTB}$ from the nominal elastic LTB resistance for slender-web members $F_{cr} = R_b F_{e.LTB}$.)

The radius of gyration r_t may be calculated exactly as

$$r_t = \frac{(I_y C_w)^{1/4}}{S_x^{1/2}} \tag{6.3.5-24} \text{ (AISC F2-7)}$$

for doubly symmetric I-sections (White and Jung 2003a). AISC (2016) gives this equation, but refers to the corresponding radius of gyration as r_{ts}, to avoid its potential erroneous use for singly symmetric I-section members. Alternately, r_t may be calculated generally for any rectangular flange I-section as

$$r_t \cong \frac{b_{fc}}{\sqrt{12\left(\dfrac{h}{d} + \dfrac{1}{3}\dfrac{D_c t_w}{A_{fc}}\dfrac{D^2}{hd}\left(1 + 6\dfrac{A_{fillet}}{D_c t_w}\right)\right)}} \tag{6.3.5-25}$$

where d is the total depth of the member, D is the depth of the web, and A_{fillet} is the area of each of the web-to-flange fillets (White and Jung 2003a). It should be noted that A_{fillet} is commonly taken equal to zero for welded I-section members. Upon substation of $A_{fillet} = 0$, this Eq. 25 reduces to AASHTO Eq. C6.10.8.2.3-1. If one assumes $d \cong h \cong D$ and $A_{fillet} \cong 0$, Eq. 25 reduces to Eq. 12 which is precisely the equation for the radius of gyration of the compression flange plus one-third of the depth of the web in compression. Equation 25 gives results that are within one percent of the exact Eq. 24 for all rolled I-sections. Due to compensating effects within the approximation of Eq. 25 by Eq. 12, Eq. 12 also tends to give an accurate but slightly conservative approximation of Eq. 24 for general doubly symmetric I-shapes.

For column-type I-sections with $D/b_{fc} \cong 1$, D/t_w less than about 50 and compact flanges, the second term under the radical in Eq. 22 tends to be significantly larger than one. As such, it would be quite uneconomical to discount this major contribution to the resistance to obtain a simpler form for Eq. 22. However, in situations involving beam- or girder-type I-sections with D/b_{fc} greater than about

two and $b_{fc}/2t_{fc}$ near the compact-flange limit λ_{pf} or larger, the contribution from the second term in Eq. 22 is relatively small (White and Jung 2003a).

For slender-web members, the contribution from the radical in Eq. 22 is neglected altogether, due to the reduction in the effective St. Venant torsional stiffness associated with web distortional flexibility (i.e., the deformation of the web into an S shape upon twisting of the cross section, and the corresponding reduction in the twist rotation of the flanges) (White and Jung 2007). In this case, Eq. 22 reduces to the form

$$F_{e.LTB} = C_b \frac{\pi^2 E}{(L_b / r_t)^2} \qquad\qquad \text{(6.3.5-26) (AISC F5-4)}$$

used traditionally by AISC and AASHTO for slender-web members. AASHTO (2020) multiplies Eq. 26 by the web load-shedding strength reduction factor, R_b, to obtain the elastic LTB flexural resistance in terms of the compression flange stress for slender-web members (AASHTO Eq. 6.10.8.2.3-8). Similarly, AISC (2016) multiplies Eq. 26 by its factor R_{pg}, which is a form of Eq. 3 previously employed with the AASHTO Specifications, as discussed in Sections 6.3.5.2.1 and 6.3.5.2.2 of this volume.

6.3.5.8 Noncompact bracing limit, L_r

The noncompact bracing limit L_r is obtained by equating the base elastic LTB resistance for uniform bending ($C_b = 1$) to the compression flange stress at the nominal onset of yielding, F_{yr}. Equation 22 results in the following succinct expression for the noncompact lateral brace spacing,

$$L_r = \frac{1.95 r_t}{X} \frac{E}{F_{yr}} \sqrt{1 + \sqrt{1 + 6.76\left(\frac{F_{yr}}{E}\right)^2 X^4}} \qquad\qquad \text{(6.3.5-27)}$$

$$\text{(AASHTO A6.3.3-5, AISC F2-6 \& F4-8)}$$

applicable for all types of compact- and noncompact-web I-section members, with X^2 given by Eq. 23, whereas Eq. 26 gives

$$L_r = \pi r_t \sqrt{\frac{E}{F_{yr}}} \qquad\qquad \text{(6.3.5-28) (AASHTO 6.10.8.2.3-5, AISC F5-5)}$$

White and Jung (2003b) give a closed-form alternative expression to Eq. 27 for compact- and noncompact-web singly symmetric I-sections, based on the rigorous application of open-section thin-walled beam theory. Unfortunately, this equation is significantly longer than Eq. 27. Also, due to the larger effects of web distortion in singly symmetric members, the rigorous beam-theory equation does not necessarily give a better representation of the physical buckling resistance (White and Jung 2007).

It should be noted that AISC (2016) writes Eq. 27 specifically as

$$L_r = 1.95r_t \frac{E}{F_{yr}} \sqrt{\frac{J}{S_{xc}h} + \sqrt{\left(\frac{J}{S_{xc}h}\right)^2 + 6.76\left(\frac{F_{yr}}{E}\right)^2}} \qquad \text{(6.3.5-29) (AISC F2-6 \& F4-8)}$$

This form of the equation accommodates the substitution of $J = 0.0$ without the problem of dividing by zero.

6.3.5.9 Elastic FLB stress, $F_{e\ell}$

The elastic plate local buckling equation defined previously by Eq. 6.2.4-1 is also the base equation for the I-section FLB resistances in AASHTO (2020). Furthermore, the FLB coefficients k_c defined by Cases 1b and 1c of Table 5 are employed for noncompact- and compact-web built-up and rolled I-sections in flexure. However, for slender-web I-section members, Article 6.10.8.2.2 implicitly assumes $k_c = 0.35$ as an accurate to conservative simplification. As noted in Section 6.2.4.1 of this volume, the FLB coefficient for simply supported edge conditions at the web-flange juncture is $k_c = 0.425$. Therefore, smaller values of k_c indicate that the web is tending to destabilize the flange. The equation for k_c in Case1c of Table 5 was developed originally by equating the results from the AISC LRFD (1993) resistance equations to measured experimental strengths for a number of tests in which the flexural resistance was governed by FLB, then back-solving for k_c (Yura 1992). The data used in these developments was predominantly from Johnson (1985). White and Jung (2008) and White and Kim (2008) discuss the correlation of the AASHTO (2020) and AISC (2016) equations with a larger updated set of experimental test results. Case 1c of Table 5 may be considered as a simple but reasonable approximate lower-bound value for the FLB coefficient for general built-up I-section members.

6.3.5.10 Noncompact flange slenderness limit, λ_{rf}

Similar to the calculation of L_r, the noncompact flange slenderness limit λ_{rf} is obtained by equating the elastic FLB stress given by Eq. 6.2.4-1 to the compression flange stress at the nominal onset of yielding, F_{yr}. The resulting equation is

$$\lambda_{rf} = 0.95\sqrt{k_c E / F_{yr}} \qquad \text{(6.3.5-30) (AASHTO A6.3.2-5, AISC Table B4.1a)}$$

By substituting the implicitly assumed value of $k_c = 0.35$ into this equation, one obtains

$$\lambda_{rf} = 0.56\sqrt{E / F_{yr}} \qquad \text{(6.3.5-31) (AASHTO 6.10.8.2.2-5)}$$

for the noncompact flange slenderness limit within the main AASHTO (2020) provisions.

6.3.5.11 Moment gradient modifier, C_b

As illustrated previously in Figure 59, the effect of any variation in the moment along an unbraced length is accounted for in AASHTO (2020) and AISC (2016) via the moment gradient modifier C_b. The C_b modifier has a base value of 1.0 when the moment and the corresponding compression flange major-axis bending stresses are uniform along the length between the brace points. Furthermore, C_b may be conservatively taken equal to 1.0 for all cases, with the exception of:

- Situations involving significant top flange loading either on unbraced cantilevers or on members with no intermediate bracing in the entire span, and

- General unbraced cantilevers with less than essentially rigid warping restraint at their fixed end due to flexible end connections or continuity with a flexible back-span (Ziemian 2010).

(For cases involving flexure in members other than in horizontal (i.e., in-plan) framing, the "top" flange should be considered as the flange opposite to the direction of the applied loads causing the major-axis bending, assuming that all the applied loads are in the same direction. Also, the "vertical" supports should be considered as the supports corresponding to the reactions associated with major-axis bending.)

The above exceptional cases are addressed after discussion of the other more routine cases below. It should be noted that whenever both ends of a cantilevered member are prevented from twisting (by cross frames or diaphragms), the behavior is effectively the same as that of an ordinary span with vertical supports and with twisting restrained at both ends.

If one or more intermediate braces are provided within either an ordinary span or a cantilever span in which the ends are prevented from twisting, load height effects do not need to be considered in the calculation of C_b. Helwig et al. (1997) discuss mitigating factors regarding load-height effects that justify this simplification. Cases in which the ends of a span are not prevented from twisting require special consideration regardless of the loading and span type.

For the above "routine" cases, AASHTO (2020) and AISC (2016) specify different equations for C_b, both of which tend to give accurate to somewhat conservative estimates. The AISC (2016) *Specification* Section F1 addresses the calculation of C_b for doubly symmetric members subjected to general moment diagrams, and for singly symmetric members subjected to reverse curvature bending. For more general cases, AISC (2016) refers the design engineer to the commentary to its Section F1. In the commentary, AISC (2016) specifies a number of alternative equations for the calculation of C_b, including the more general expression

$$C_b = \frac{12.5 M_{\max}}{2.5 M_{\max} + 3 M_A + 4 M_B + 3 M_C} R_m \le 3.0 \qquad \text{(6.3.5-32) (AISC C-F1-3)}$$

where

M_{max} = absolute value of the maximum moment in the unbraced segment

M_A = absolute value of the moment at the quarter point of the unbraced segment

M_B = absolute value of the moment at the mid-length of the unbraced segment

M_C = absolute value of the moment at the three-quarter point of the unbraced segment

R_m = cross-section monosymmetry parameter

= 1.0 for doubly symmetric members

= 1.0 for singly symmetric members subjected to single-curvature bending

$$= 0.5 + 2\left(\frac{I_{y.top}}{I_y}\right)^2 \qquad\qquad (6.3.5\text{-}33)$$

for singly symmetric members subjected to reverse curvature bending.

Conversely, AASHTO (2020) Article 6.10.8.2.3 specifies

$$C_b = 1.0 \qquad\qquad (6.3.5\text{-}34a)\ (AASHTO\ 6.10.8.2.3\text{-}6)$$

for members where $f_{mid}/f_2 \geq 1$ or $f_2 = 0$, and

$$C_b = 1.75 - 1.05\frac{f_1}{f_2} + 0.3\left(\frac{f_1}{f_2}\right)^2 \leq 2.3 \qquad (6.3.5\text{-}34b)\ (AASHTO\ 6.10.8.2.3\text{-}7)$$

for all other situations, where

f_2 = absolute value of the largest factored compressive major-axis bending stress at either end of the unbraced length of the flange under consideration, determined from the critical moment envelope value. If the stress is zero or tensile in the flange under consideration at both ends of the unbraced length, f_2 is taken equal to zero.

f_{mid} = factored major-axis bending stress at the middle of the unbraced length of the flange under consideration, calculated from the moment envelope value that gives the largest compression at this point, or the smallest tension if this point is never in compression, taken as positive in compression and negative in tension.

$$f_1 = f_o \qquad\qquad (6.3.5\text{-}35)\ (AASHTO\ 6.10.8.2.3\text{-}10)$$

when the variation in the flange stress between the brace points is concave in shape, and otherwise

$$f_1 = 2f_{mid} - f_2 \geq f_o \qquad\qquad (6.3.5\text{-}36)\ (AASHTO\ 6.10.8.2.3\text{-}11)$$

f_o = factored major-axis bending stress at the brace point opposite to the one corresponding to f_2, calculated from the moment envelope value that gives the largest compression at this point in the flange under consideration, or the smallest tension if this point is never in compression, taken as positive in compression and negative in tension.

Figure 64 shows several sample cases that illustrate the application of the AASHTO procedure. The first two cases involve a concave flange stress envelope, that is, $|f_{mid}|$ is smaller than the absolute value of the average of f_2 and f_o. For these cases, f_1 is taken equal to f_o. The second two cases involve a convex flange stress envelope. In these cases, AASHTO (2020) defines f_1 as the ordinate of a straight line that goes from f_2 at the opposite end of the unbraced length through f_{mid} at the mid-length. This definition gives $C_b = 1.30$ for the third case, and 1.51 for the fourth case, which are accurate approximations of analytical solutions for the subject nonlinear moment diagrams (Ziemian 2010). Additional sample cases are illustrated in AASHTO (2020) Article C6.4.10.
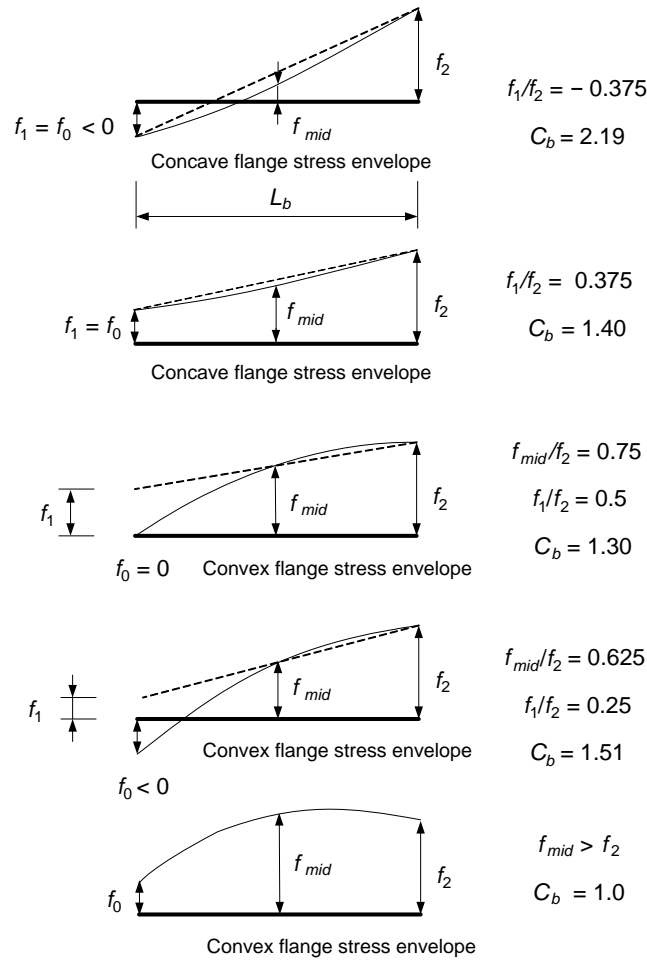
Figure 64. Sample cases for calculation of the AASHTO (2020) moment gradient modifier, adapted from AASHTO (2020) Article C6.4.10.

For reverse curvature bending, both the AISC and AASHTO procedures require the Engineer to check LTB considering the base resistance for uniform bending, causing flexural compression in the flange under consideration, scaled by an appropriate C_b value. In the AISC method, one C_b factor is calculated using Eq. 28 and is applied to both flanges. In the AASHTO method, a separate C_b factor is calculated using Eqs. 34 to 36 for each flange.

Figure 65 summarizes various C_b estimates from both of the above procedures for a number of representative examples. The results are compared to the exact LTB solutions for the I-girder cross sections shown in Figure 66. An unbraced length-to-depth ratio of $L_b/h = 12.5$ ($L_b = 75$ ft) is assumed for the first four examples, and an unbraced length-to-depth ratio of 8.0 ($L_b = 48$ ft) is assumed for the fifth example. The cross sections shown in Figure 66 are similar in terms of behavioral characteristics to those considered by Helwig et al. (1997). Both cross sections satisfy the AASHTO (2020) Article 6.10.2 proportioning requirements and, for last two examples in Figure 65, these sections are representative of potential continuous-span I-girder designs using the AASHTO Specifications. The singly symmetric cross section shown in Figure 66 is a representative extreme case with $I_{yc}/I_{yt} = 0.22$ (for positive bending), which is smaller than the Eq. 10 limit but satisfies Eq. 6.3.2-6.
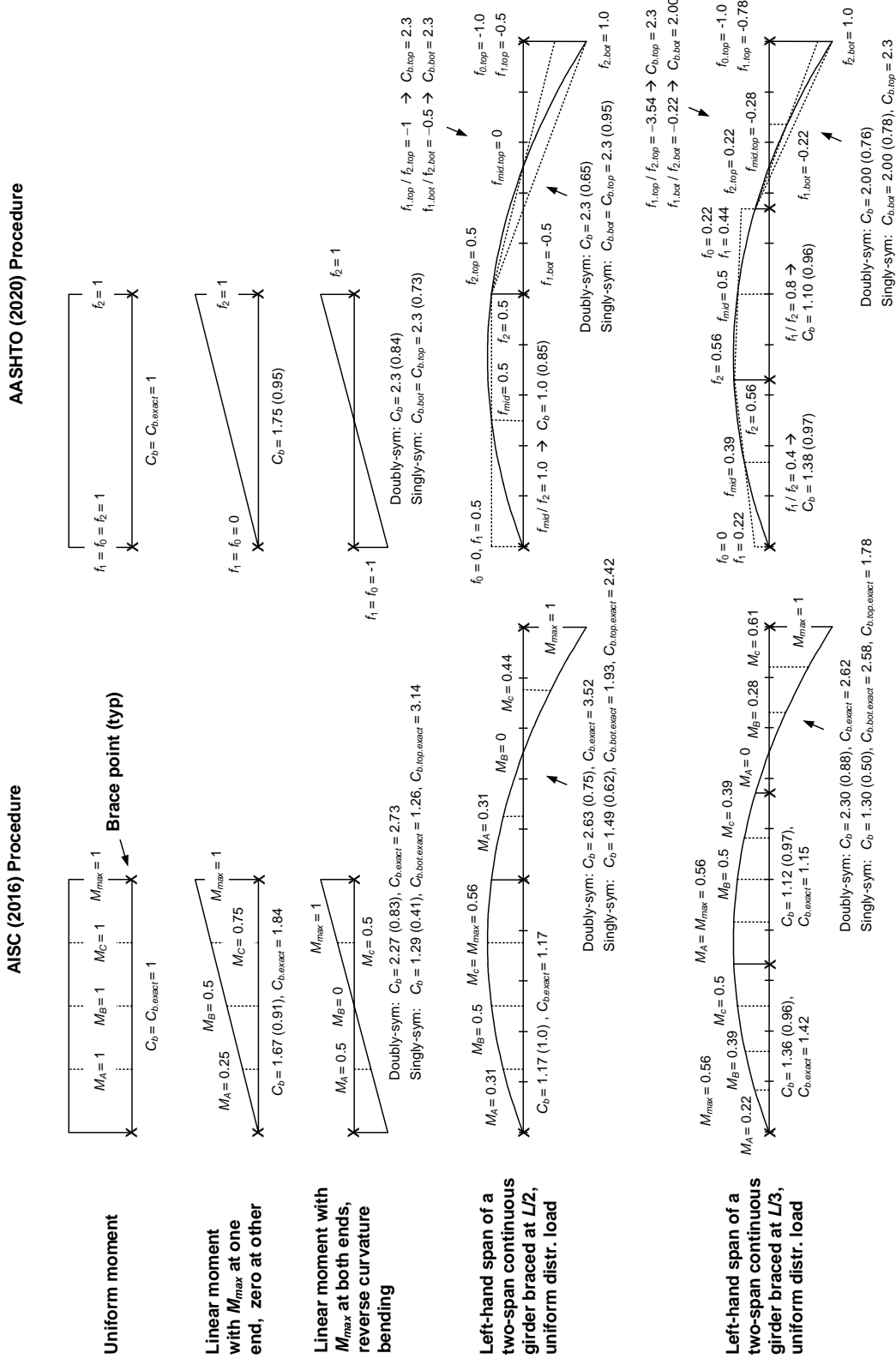
Figure 65. Calculation of C_b by AISC (2016) and AASHTO (2020) estimates for several representative design examples.
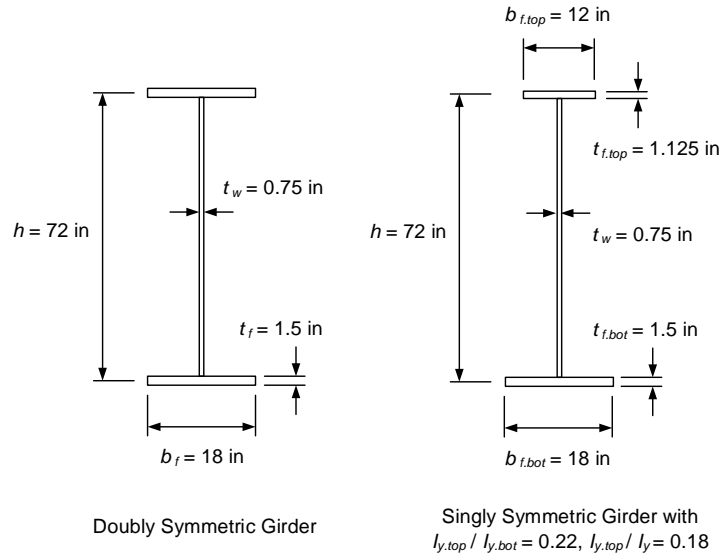
Figure 66. Cross sections used in the example C_b calculations.

For demonstration purposes, non-moving loads are assumed in Figure 65 such that the moment envelopes and the moment diagrams are the same. Also, noncomposite members are assumed to simplify, since the application of Eq. 32 is not defined for composite members. In the case of noncomposite members, the distribution of the flange stresses along the unbraced length is the same as the distribution of the member bending moments. However, for composite members, the distribution of the flange stresses and the bending moments are different due to the influence of the separate noncomposite, short-term composite and long-term composite loadings, and due to the different effective cross sections in positive and negative bending.

The exact solutions in Figure 65 are determined using the open-section thin-walled beam element in SABRE2 (White et al. 2021b). These solutions are obtained by analyzing the various unbraced lengths as isolated segments assuming torsionally simply supported end conditions (i.e., the flange lateral bending and warping are unrestrained at the ends of the isolated unbraced segments, neglecting any continuity effects with adjacent unbraced lengths). The "exact" C_b values are calculated as

$$C_{b.exact} = M_{cr} / M_{cro} \tag{6.3.5-37}$$

where

M_{cr} = buckling moment corresponding to the cross section with the largest compression stress in the flange under consideration for any of the loadings causing non-uniform moment along the unbraced length, and

M_{cro} = buckling moment corresponding to uniform compression in the flange under consideration.

This is the same as the procedure employed by Helwig et al. (1997) for the calculation of benchmark C_b values in their studies. The exact C_b results are shown with the AISC (2016)

estimates in Figure 65, to simplify the figure. Both the AISC and the AASHTO estimates can be compared to the exact solutions. The number shown in the parentheses after the reported C_b estimate is the ratio between the approximate and the exact C_b value. As noted above, for the reverse curvature bending cases, one C_b value is calculated and applied to both flanges in the AISC procedure. The LTB strength prediction is then governed by the flange that has the smallest ratio of $C_{b.AISC} / C_{b.exact}$. In the AASHTO procedure, separate C_b values are determined for each flange in the cases involving reverse curvature bending. The LTB strength prediction is again governed by the flange that has the smallest ratio of $C_{b.AASHTO} / C_{b.exact}$.

The following observations can be drawn from the results summarized in Figure 65:

- The AASHTO (2020) procedure involves fewer calculations. In cases where the flange stress diagram is concave (e.g., the bottom flange stress distribution in the right-most unbraced lengths of the two-span continuous beam examples), as well as when the variation in the stress along the length is essentially a straight line, f_1 and f_2 in Eqs. 34 are simply the flange stresses at the ends of the unbraced segment under consideration. In other cases, where the flange stress diagram is convex, the Engineer only needs to determine the maximum compressive flange stress, f_2, and the flange stress at the middle of the unbraced length, f_{mid}, from the structural analysis. The stress f_1 is simply the ordinate of a straight line that goes from f_2 at the opposite end of the unbraced length through f_{mid} at the mid-length. By defining f_1 in this way, Eq. 34b gives a good approximation of the exact C_b for these cases.

- The AASHTO (2020) procedure is more accurate for the linear moment diagram cases. Both the AASHTO and the AISC equations are lower-bound approximations to analytical solutions. As such, the larger lower-bound is the more accurate one. Helwig et al. (1997) state that Eq. 32 is quite conservative for cases with linear moment diagrams in reverse curvature bending and smaller values of $I_{y.top}/I_y$. They refer to Kitipornchai et al. (1986) for more accurate estimates of C_b in these situations. Equations 34 give accurate to somewhat conservative calculations relative to the more complex equations presented by Kitipornchai et al. (1986) for linear moment diagrams.

- For longer unbraced lengths, nonlinear moment diagrams (due to transverse load effects within the unbraced length) and single-curvature bending, Eq. 32 often gives more accurate estimates than the AASHTO method. For example, for the left-most unbraced length in the first continuous-span example of Figure 65, Eq. 32 gives $C_b = 1.17$ (versus $C_{b.exact} = 1.17$) while the AASHTO procedure gives $C_b = 1.0$. However, for the unbraced lengths in single-curvature bending in the second continuous-span example, which still has only two intermediate brace points, the C_b values are essentially the same from both methods. Both the AISC and the AASHTO C_b estimates are only slightly conservative compared to the exact solutions for the specific doubly symmetric I-girder considered in this study.

- For the continuous-span beam segments subjected to reverse curvature bending, both the AISC and AASHTO procedures give accurate to somewhat conservative results for the doubly symmetric girder. However, for the singly symmetric girder, the AISC calculation is quite conservative relative to the exact elastic LTB solutions. For cases with a smaller

top flange ($I_{y.top}/I_y < 0.5$), Eq. 33 specifies an abrupt drop in the calculated C_b value regardless of the length of the top flange subjected to compression. Furthermore, the terms M_A, M_B and M_C in Eq. 32 are blind to the sign of the bending moment. This is appropriate for doubly symmetric I-section members, but the accuracy of Eq. 32 is limited for reverse curvature bending of singly symmetric I-section members due to this simplification.

- For all the cases involving reverse curvature bending on the singly symmetric girder in Figure 65, the AISC procedure gives a more accurate estimate of $C_{b.exact}$ if R_m is taken equal to 1.0 (such that the C_b calculation is the same as that for a doubly symmetric girder). For the third example (the linear moment diagram with M_{max} at both ends and reverse curvature bending) the resulting C_b is 2.27 from the AISC procedure versus $C_{b.top.exact} = 3.14$, giving a ratio of the design estimate to the exact buckling calculation of 2.27/3.14 = 0.72 rather than the ratio 0.41 shown in the figure. For the right-most unbraced length in the fourth example, the resulting C_b is 2.63 versus $C_{b.top.exact} = 2.42$, giving a ratio of 2.63/2.42 = 1.09. This is within the range of the $C_b/C_{b.exact}$ ratios for the examples studied by Helwig et al. (1997). For the right-most unbraced length in the fifth example, the resulting C_b is 2.18 versus $C_{b.bot.exact} = 2.58$, giving a ratio of 2.18/2.58 = 0.84 rather than 0.48. However, for more extreme reverse curvature bending cases involving singly symmetric girders, such as when there are no intermediate braces within the span, the calculation of R_m by Eq. 33 is necessary to obtain an adequate solution using Eq. 32 (Helwig et al. 1997).

In addition to the above observations, White et al. (2001) show that the AASHTO (2020) approach, when used with the most critical moment envelope values as specified in the definitions of f_2, f_{mid} and f_o, always gives an accurate to conservative representation of the moment gradient effects associated with the actual concurrent loadings. There does not appear to be a way to prove this useful property for Eqs. 32 and 33. Also, Eqs. 34 focus solely on the flange under consideration. For unbraced lengths subject to single-curvature negative bending or for reverse curvature bending in composite I-girders, Eq. 34b is applied by focusing solely on the bottom flange stresses, without the need to consider any properties of the top flange. For composite sections in positive bending, AASHTO (2020) considers the compression flange to be continuously braced. If the right-most unbraced lengths in Examples 4 and 5 of Figure 65 were composite I-girders, the C_b calculations for the bottom flange would be the same as illustrated in the figure. No calculations would be required for the composite top flange. As noted above, the application of Eqs. 32 and 33 to composite I-section members has not been addressed. Sections 6.3.5.1 and 6.3.5.12 of this volume discusses the overall logic and rationale behind the AASHTO (2020) LTB calculations for composite I-girder segments in negative bending. Lastly, it is important to recognize that in most practical design situations, even with relatively large unbraced lengths, the base uniform bending resistance, F_{nc} or M_{nc}, shown by the solid curve in Figure 59 is often not significantly smaller than F_{max} or M_{max}. For example, if $L_b = L_r$, F_{nc} is equal to $0.7F_{yc}$ for uniform bending. Therefore, for corresponding slender-web members, a C_b value of 1/0.7 = 1.43 is sufficient to raise the flexural resistance to F_{max}.

Recent studies (Slein et al. 2021b) have developed and demonstrated an extension of Eq. C-F1-2b of the AISC (2016) Commentary that provides substantial improved accuracy relative to Eq. 32 and Eqs. 34 for general doubly and singly symmetric I-section members subjected to single and reverse curvature bending. The quarter-point format of this equation, similar to Eq. 32, requires additional information from the structural analysis for the calculation of C_b, compared to Eqs. 34

through 36. However, the improvements in the generality of this equation, in addition to the improvements in its accuracy, merit its consideration as a single general purpose C_b estimate.

The discussion at the beginning of this section indicates that in unusual cases involving significant top flange loading either on unbraced cantilevers or on members with no intermediate bracing within the entire span, the influence of the load height must be considered. Loads applied to the top flange cause destabilizing (tipping) effects, whereas loads applied to the bottom flange enhance the member LTB resistance. When twisting of the cross section is prevented at the ends of a cantilever or ordinary span, these effects are approximated with reasonable accuracy by the equation

$$C_b^* = 1.4^{2y/h} C_b \tag{6.3.5-38}$$

where C_b is the base moment gradient factor determined without considering load height effects (e.g., via Eq. 32 or Eqs. 34), y is the load height above the mid-depth of the cross section, negative for load applied above the mid-depth, and h is the distance between the flange centroids (Helwig et al. 1997; Ziemian 2010). Helwig et al. (1997) show that the definition of y in Eq. 38 as the distance from the mid-depth gives an accurate representation of the effect of the load height. They show that if the C_b values are derived using the cross-section shear center as the origin for y, they are sensitive to the shear center location. However, with the origin for y taken at the cross-section mid-depth, Eq. 32 gives an accurate representation of the C_b values for loadings applied at the mid-depth, regardless of the shear center location. Equation 32 generally gives a more accurate and more liberal estimate of the effects of moment gradient relative to Eqs. 34 for spans with no intermediate bracing, as long as twisting is restrained at the ends of the span.

The discussion at the beginning of this section also indicates that C_b may not necessarily be taken equal to 1.0 in general unbraced cantilevers with less than essentially rigid warping restraint at their fixed end. Ziemian (2010) suggests recommended procedures for determining the buckling load of these types of members. The reader is referred to Ziemian (2010), Dowswell (2002), Yura and Helwig (1996) and Anderson and Trahair (1972) for a range of LTB solutions applicable for unbraced cantilevers.

6.3.5.12 Other considerations specific to composite I-section members in negative bending

The AASHTO (2020) equations discussed in the above sections provide one single consistent representation of the FLB and LTB resistance of both noncomposite I-section members as well as composite I-section members in negative bending. The application of these equations to composite I-girders in negative bending is based on the following simple concept that has been used extensively for the design of experimental tests to study the behavior in the negative moment regions of composite beams. Numerous research studies have shown that the resistance of composite beams in negative bending can be approximated accurately to conservatively by using a large steel tension flange or a cover-plated tension flange. These tension flange elements provide a force equivalent to that developed by the slab reinforcing steel in the prototype composite member (White and Barth 1998; Barth and White 1997; Kemp 1996; Grubb and Carskaddan 1981 and 1979; Climenhaga and Johnson 1972). The AASHTO (2020) approach considers the contribution to the cross-section moment from the reinforcing steel as a tension flange element, and it focuses on the compressed region of the steel I-section for the stability assessment. The

lateral and torsional restraint that the concrete deck provides at the level of the tension flange is neglected. The effects of this restraint are reduced in general by web distortion, and for typical I-girder bridges, the benefits of this restraint are judged not to be worth the additional effort associated with a distortional buckling solution. This is because, for many bridge I-girders, the C_b values calculated as discussed in the previous section will place the negative bending LTB capacity on the plateau of the dashed flexural resistance curve shown in Figure 59.

In calculating the radius of gyration r_t from Eq. 12 for composite I-section members, AASHTO (2020) specifies that D_c should be determined using the steel I-section member plus the longitudinal reinforcing steel. For composite I-sections in negative bending, this value of D_c tends to be slightly conservative relative to the actual D_c under the combined composite and noncomposite loadings. This calculation also removes another dependency of the LTB resistance on the applied loadings.

For composite I-section members in negative bending, the Appendix A6 LTB and FLB resistances, which are written in terms of member moments, depend in general on the elastic section modulus to the compression flange, S_{xc}. Also, the TFY resistance depends in general on the elastic section modulus to the tension flange elements, S_{xt}. These elastic section moduli are calculated as

$$S_{xc} = M_{yc}/F_{yc} \qquad \text{(6.3.5-39a)}$$

and

$$S_{xt} = M_{yt}/F_{yt} \qquad \text{(6.3.5-39b)}$$

where M_{yc} and M_{yt} are the cross-section yield moments. The yield moments are in turn calculated using the procedure detailed in Article D6.2.2, which accounts for the separate influence of noncomposite and composite loadings on the cross-section elastic stresses. The yield moment M_{yt} is based on first yield of any top-flange elements of the steel section or of the slab reinforcing steel.

For negative bending of composite I-section members with compact or noncompact webs, the AASHTO Appendix A6 flexural resistance depends on the loading type only in the places where the elastic section moduli, S_{xc} or S_{xt}, or the yield moments, M_{yc} or M_{yt}, enter into the calculations. The composite cross section is handled as fully cracked in the section-level calculations, and hence the long-term and short-term section moduli are identical.

Article A6.3.3 specifies equations for C_b that parallel Eqs. 34 but are written in terms of the member moments rather than the flange stresses. This is consistent with the practice of neglecting the separate influence of noncomposite and composite loadings on the resistance in the limit that the I-section web, flange and unbraced length are compact. Article C6.10.8.2.3 points out that the overall effect of the different types of loading on the C_b calculation is considered negligible for compact- and noncompact-web composite I-sections in negative bending. This article also permits the use of the total moments in calculating C_b for slender-web members if it is felt in the judgment of the Engineer that the influence on the final calculated value of C_b is insignificant.

6.3.5.13 LTB effective lengths

As noted in Section 6.3.5.1 of this volume, ordinary practice is to take KL_b as the actual unsupported length between the brace points corresponding to compression flange level bracing and/or the diaphragm or cross-frame locations. That is, a LTB effective length factor of $K = 1.0$ is assumed for all the unbraced lengths. However, substantial restraint can exist at the ends of a critical unbraced length when the adjacent segments are less critically loaded, resulting in an effective length $KL_b < L_b$ for the critical segment. AASHTO (2020) allows this smaller KL_b to be used in place of L_b to increase the calculated member LTB resistance, F_{nc} or M_{nc}, in its Articles 6.10.8.2.3 and A6.3.3 and/or to reduce the calculated amplification of the compression flange lateral bending stresses in Article 6.10.1.6. Article C6.10.8.2.3 recommends a simple hand method from Ziemian (2010) and Nethercot and Trahair (1976) for estimating K. A generalized form of this procedure, which is applicable for singly- and doubly symmetric I-section members and includes the consideration of moving live loads, is outlined below. The method is based on an analogy between the buckling of a continuous beam and the buckling of an end-restrained column. As such, it uses the alignment chart for nonsway columns to determine a K factor for the critical unbraced length.

The suggested procedure involves the following steps:

1. Determine C_b for each unbraced segment in the member as discussed in Section 6.3.5.11.

2. Identify the critical segment. This segment is the one that buckles elastically at the smallest multiple of the design loadings, using the most critical moment envelope in each unbraced segment, and using the actual unbraced length L_b in the applicable elastic LTB resistance equation for each segment. The multiple of the design loadings associated with the buckling of the critical segment is denoted by γ_m. Also, the multiples of the design loadings associated with the buckling of the adjacent unbraced lengths (should they exist) are denoted by γ_{rL} and γ_{rR} respectively. For each of these segments, the following equation applies:

$$\gamma = \frac{F_{e.LTB}}{f_{bu}} \tag{6.3.5-40}$$

where $F_{e.LTB}$ is the governing elastic LTB resistance determined using Eq. 22 for compact- or noncompact-web members or Eq. 26 for slender-web I-section members, and f_{bu} is the largest value of the compression flange stress in the segment under consideration.

3. Calculate a stiffness ratio, α, for each of the above three segments. The stiffness ratio for the critical segment is written as

$$\alpha_m = \frac{2(b_{fc}t_{fc} + \frac{1}{3}D_c t_w)r_t^2}{L_{bcr}} \tag{6.3.5-41}$$

138

and the stiffness ratio for each of the adjacent "restraining" segments is written as

$$\alpha_r = \frac{n(b_{fc}t_{fc} + \frac{1}{3}D_c t_w)r_t^2}{L_b}\left(1 - \frac{\gamma_m}{\gamma_r}\right) \tag{6.3.5-42}$$

where $n = 2$ if the far end of the adjacent segment is continuous, $n = 3$ if it is simply supported (torsionally), and $n = 4$ if it is torsionally fixed. If the critical segment has a simply supported end and no adjacent unbraced length, $\alpha_r = 0$. Also, for cases involving singly symmetric I-girders and reverse curvature bending in any one of the above segments, the area $(b_{fc}t_{fc} + D_c t_w / 6)$ and r_t terms in Eqs. 41 and 42 are the values corresponding to the governing elastic LTB resistance.

4. Determine the ratios $G = \alpha_m/\alpha_r$ for each end of the critical segment.

5. Substitute the above G values into the sidesway-inhibited column alignment chart (AISC 2016; AASHTO 2020; Kavanagh 1962) to obtain the effective length factor K. As noted previously in Section 6.2.2 of this volume, AASHTO (2020) Article C4.6.2.5 gives closed form equations that provide a close fit to the alignment chart results.

The above procedure is a very practical approach in that Steps 1 and 2 are a by-product of the ordinary design calculations, where K is implicitly taken equal to 1.0 and the actual unsupported length L_b is used within the LTB resistance equations. Therefore, Steps 3 through 5 are basically an "add-on" to the ordinary design procedures that the Engineer can utilize when they deem the additional calculations to be useful to justify a more liberal calculation of the resistance. Also, the Engineer should note that in the special case where the adjacent unbraced lengths are equally critical (e.g., if all three unbraced lengths have the same length L_b, the same cross section, each segment is subjected to the same uniform bending moment, and $n = 2$ in the adjacent segments), $\alpha_r = 0$ and $G = \infty$ at each end of the critical segment. This gives $K = 1.0$ from the sidesway-inhibited column alignment chart. The above method is conservative because it is based on the assumption that the largest moment envelope values in the adjacent segments are taken from the concurrent loadings associated with buckling of the critical unbraced length. In addition, the assumption of $n = 2$ in quantifying the effect of continuity across the braced points at the far ends of the restraining unbraced segments typically is conservative in that it assumes that the unbraced lengths outside of this location are equally critical compared to the restraining segments.

The application of the above procedure can be understood best by working a representative example. Consider the prismatic simple-span girder with four equally-spaced intermediate brace points shown in Figure 67. The middle unbraced length of this beam is clearly the most critical since it contains the largest moment and all of the unbraced lengths are equal. In Step 1 of the above procedure, the moment envelope values for the middle unbraced segment give $f_{mid}/f_2 > 1$. As a result, $C_b = 1.0$ for this segment from Eq. 34a. The moment envelope values for the unbraced lengths adjacent to the central segment give $f_{mid}/f_2 = 0.875$ and thus $f_1/f_2 = 0.75$ using Eq. 36. This gives, $C_b = 1.13$ for these segments from Eq. 34b. For the end segments, $f_{mid}/f_2 = 0.56$, giving $f_1/f_2 = 0.12$ and $C_b = 1.63$.
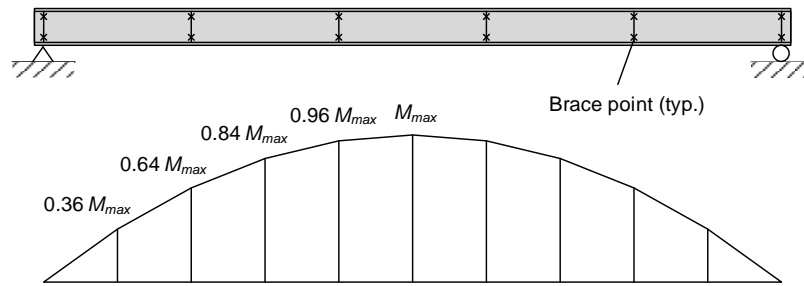
Figure 67. Simple-span I-girder and critical moment envelope for example calculation of LTB effective length factor *K*.

If the Engineer deems that the additional effort of calculating $K < 1$ is not worthwhile, they can stop at this stage and use the above C_b values along with $K = 1$ for the design. For that matter, the Engineer could base the design on $C_b = 1$ and $K = 1$ and avoid the calculations in Step 1. However, if the additional benefits of using $K < 1$ are potentially significant, the Engineer may wish to continue to Step 2. One of the excellent attributes of the suggested (Nethercot and Trahair 1976) procedure is that the subsequent steps utilize the C_b values that the Engineer has already determined based on ordinary practice.

If the Engineer continues to Step 2 for the example girder in Figure 67, they would observe that since the central segment has $C_b = 1$ and the girder is prismatic (no section transitions) with equal unbraced lengths, the central unbraced length is the most critical one. If the applied load level on the beam associated with the buckling of this segment is, for example, $\gamma_m = 10.0$, the corresponding applied load levels at the buckling of the adjacent segments (using $K = 1$), are simply $\gamma_r = C_b = (10)(1.13)/0.96 = 11.8$. (Note that one has to divide by 0.96 because at the applied load level of $\gamma_m = 1.00$, the maximum moment in the adjacent unbraced lengths is only $0.96M_{max}$.) If one uses a normalized value of $\alpha_m = 2.0$ from Eq. 41, then

$$\alpha_r = 2.0\left(1 - \frac{10.0}{11.8}\right) = 0.301 \tag{6.3.5-43}$$

from Eq. 42. This completes Step 3. In Step 4, the value of $G = \alpha_m/\alpha_r$ is $2.0/0.301 = 6.64$ at both ends of the critical segment. Given these G values, one enters the sidesway-inhibited column alignment chart (step 5) to obtain $K \cong 0.94$. This K factor can be used to obtain a slightly higher LTB resistance (roughly 13 % higher if the slender-web girder elastic LTB equations govern the strength) as well as a slightly smaller amplification of the elastic compression flange lateral bending stresses (see Section 6.3.7.2). This is a relatively small benefit in this example. However, the benefit can be larger in some cases.

When checking the resistance of the unbraced lengths adjacent to the critical segment, it is recommended that an effective length factor of $K = 1.0$ should be employed. Theoretically, the effective length factor for the adjacent unbraced lengths is actually greater than 1.0, since they are providing restraint to the critical segment. However, since these segments are the less critical ones, it is recommended that $K = 1.0$ is sufficient for the design evaluation of these segments.

An effective length factor of $K = 1.0$ should be used for other unbraced lengths that are not adjacent to the critical segment. The above procedure focuses only on the influence of end restraint on the buckling load of the critical segment. This is akin to the practice of calculating member axial compressive resistances by focusing on a subassembly within the overall structural system, rather than seeking to determine the elastic buckling load of an entire structure when assessing the different column unbraced lengths.

In cases where one or more of the unbraced lengths contains a cross-section transition, but the members are otherwise prismatic, the transition to a smaller section may be neglected in determining the γ value for the segment containing the transition, and the above procedure may be used to determine the LTB effective lengths, when:

- The critical segment or either of its adjacent segments has a cross-section transition within 20 % of the corresponding unbraced length L_b, and

- The changes in the flange moments of inertia about the plane of the web at the cross-section transition(s) are less than a factor of two for both flanges (i.e., $I_1/I_2 \geq 0.5$ where I_1 and I_2 are the moments of inertia of the smaller and larger flanges respectively).

The calculation of the LTB resistances for more general cases involving stepped, variable web-depth and other nonprismatic I-section members is addressed in Section 6.3.6 of this volume.

6.3.5.14 Inelastic redistribution of interior pier moments in continuous-span bridges

Minor yielding over the interior supports of continuous spans results in a redistribution of the girder moments. For straight continuous-span flexural members that satisfy requirements intended to ensure adequate ductility and robustness of the girder segments adjacent to the interior piers, AASHTO (2020) Appendix B6 may be used to calculate the redistribution moments at the Service II and/or Strength load levels. These provisions provide a simple calculated percentage redistribution from the interior-pier sections. The calculated redistribution moments are akin to internal moments generated by the following pre-stressing procedure:

1. The slab is cast and/or cover plates are welded to the bottom flange of pier sections with the interior supports jacked to an elevation higher than their final positions, then

2. The interior supports are lowered to their final positions after the construction is complete and the slab has attained sufficient strength.

However, the redistribution moments are generated by minor inelastic rotations in the girders over the interior supports rather than the above construction process. The interior pier sections are designed to exhibit ductile moment-rotation responses and to shake down elastically after a few passages of the maximum design loads.

Appendix B6 utilizes the elastic moment envelopes and does not require any direct use of inelastic analysis. As such, the Appendix B6 procedures are substantially simpler and more streamlined than inelastic analysis procedures of previous AASHTO Specifications. For the types of bridges and girder requirements where they are allowed, these provisions make it possible to potentially use prismatic sections along the entire length of the bridge or between field splices without

requiring excess material. This practice can improve the overall fatigue resistance and provide significant fabrication economies. The development of the Appendix B6 provisions is documented in a number of comprehensive reports (Barker et al. 1997; Schilling et al. 1997; White et al. 1997) and in a summary paper by Barth et al. (2004).

The provisions of Appendix B6 account for the fact that the compression flange slenderness, $b_{fc}/2t_{fc}$, and the cross-section aspect ratio, D/b_{fc}, are the predominant factors that influence the ductility of the moment-rotation response at adequately braced interior-pier sections. As such, these provisions apply to all compact compression-flange pier sections with compact, noncompact or slender webs up to $D/t_w = 150$, as long as the following restrictions are satisfied:

- The bridge must be straight.

- The support lines shall not be skewed more than 10 degrees.

- None of the cross-frame lines may be staggered.

- The largest girder specified minimum yield strength in the unbraced lengths immediately adjacent to the interior piers shall not exceed 70 ksi.

- The tension flange shall not have any holes over a distance of two times the web depth on each side of interior pier sections from which moments are redistributed.

- Moments shall be redistributed only from interior pier sections that have bearing stiffeners and for which the immediately adjacent unbraced lengths are prismatic and satisfy the requirements

$$\frac{2D_c}{t_w} \leq 6.8\sqrt{\frac{E}{F_{yc}}} \qquad\qquad \text{(6.3.5-41) (AASHTO B6.2.1-1)}$$

$$D_{cp} \leq 0.75D \qquad\qquad \text{(6.3.5-42) (AASHTO B6.2.1-3)}$$

$$b_{fc} \geq \frac{D}{4.25} \qquad\qquad \text{(6.3.5-43) (AASHTO B6.2.2-2)}$$

$$L_b \leq \left[0.1 - 0.06\frac{M_1}{M_2}\right]\frac{E}{F_{yc}}r_t \qquad\qquad \text{(6.3.5-44) (AASHTO B6.2.4-1)}$$

and

$$V_u \leq \phi_v \, V_{cr} \qquad\qquad \text{(6.3.5-45) (AASHTO B6.2.5-1)}$$

where

M_1 = the bending moment at the brace point with the smaller moment due to the factored loads, taken as the value from the moment envelope that produces the smallest permissible unbraced length,

M_2 = the bending moment at the brace point with the larger moment due to the factored loads, taken as the critical moment envelope value,

V_u = the shear in the web due to the factored loads, and

V_{cr} = the shear buckling resistance specified in AASHTO (2020) Article 6.10.9.2 for unstiffened webs and in AASHTO Article 6.10.9.3 for transversely-stiffened webs.

The above limits ensure that the pier sections exhibit significant ductility and limit the application of the AASHTO Appendix B6 procedures to designs supported by the background research.

The main provisions of AASHTO (2020) Articles B6.3 and B6.4 utilize the concept of an effective plastic moment

$$M_{pe} \leq M_n \qquad\qquad (6.3.5\text{-}46)\ (\text{AASHTO B6.5.1-2 \& B6.5.2-2})$$

at the interior pier sections, where M_n is the pier section flexural resistance calculated as discussed in the above sub-sections of this volume, and the reduction in M_{pe} relative to M_n is based on simplified lower-bound estimates of the pier section inelastic moment-rotation responses. The differences between the maximum moments from the factored elastic moment envelopes, M_e, and the effective plastic moments, M_{pe}, are redistributed from the pier sections to the positive moment regions up to a maximum of $0.2M_e$.

6.3.6   Stepped, Variable Web Depth and Other Nonprismatic I-Section Members

Section 6.2.6 of this volume outlines how AISC Design Guide 25 (White et al. 2021a) extends the AASHTO (2020) and AISC (2016) column resistance equations to address general nonprismatic members loaded in nonuniform axial compression. Design Guide 25 also details procedures for calculation of the flexural resistance of general nonprismatic I-section members. The following is a summary of the basic concepts and methods.

The equations for composite members in positive bending, discussed in Sections 6.3.3 and 6.3.4 of this volume, as well as the FLB and TFY equations for composite members in negative bending and noncomposite members, outlined in Section 6.3.5, are effectively cross-section based checks. Hence, these equations may be applied directly for all types of members on a cross-section by cross-section basis. One determines the required moment, M_u, or the required flange stress, f_{bu}, at all the cross sections along the member length. Typically, it is possible to identify one or a few potentially critical cross sections that need to be checked.

In contrast to the above limit states checks, the LTB resistance cannot be assessed solely on a cross-section by cross-section basis. This is because the LTB resistance depends on the cross-section properties along the entire unbraced length as well as the loading configuration (e.g., moment gradient) and the end conditions (e.g., continuity with adjacent unbraced lengths). These factors are very similar to the factors that influence the member buckling resistance in axial compression. As such, similar to the approach outlined in Section 6.2.6 of this volume, the LTB resistance of a general nonprismatic I-section member may be determined by focusing on:

1. The ratio of the moments (or compression flange stresses) at elastic LTB to the corresponding factored moments (or stresses)

$$\gamma_{e.LTB} = \frac{M_{e.LTB}}{M_u} = \frac{F_{e.LTB}}{f_{bu}}$$ (6.3.6-1)

and

2. The maximum ratio of the moments (or compression flange stresses) at the various cross sections to the cross-section strength. This ratio may be written as

$$\rho_{o.max} = \left(\frac{f_{bu}}{R_b R_h F_{yc}} \right)_{max}$$ (6.3.6-2a)

for slender-web I-section members, and

$$\rho_{o.max} = \left(\frac{M_u}{R_{pc} M_{yc}} \right)_{max}$$ (6.3.6-2b)

for compact- and noncompact-web I-section members.

Similar to the parameter γ_e discussed in Section 6.2.6, the elastic buckling load ratio, $\gamma_{e.LTB}$, is the same value throughout a given member, equal to the minimum eigenvalue obtained from an elastic buckling analysis if a computational solution is employed. Conceptually, for a given factored load moment diagram along the member length, the elastic buckling load level is obtained simply by scaling up all the applied loads, thus scaling the internal values of the moment, M_u, and the elastic stresses, f_{bu}, until elastic LTB occurs. The member LTB slenderness effects are captured by $\gamma_{e.LTB}$. The second main parameter, $\rho_{o.max}$, focuses specifically on the cross-section by cross-section flexural demands relative to the cross-section "plateau" resistances.

Generally speaking, the governing LTB flexural capacity ratio for nonprismatic I-section members, $f_{bu}/\phi_b F_{nc}$ or $M_u/\phi_b M_n$, is the largest value of the demand to the capacity obtained by dividing the cross-section demand by the following resistance equations at different locations along the member length (White et al. 2021a):

1. For $\dfrac{\gamma_{e.LTB} f_{bu}}{F_{yc}} \geq \dfrac{\pi^2}{1.0^2} = 9.87$ (where the term 1.0 in the denominator on the right-hand side of the inequality is the coefficient in Eq. 6.3.5-11 for L_p), the LTB resistance is governed by the plateau resistance. In this case, the LTB resistance may be expressed as

$$F_{nc} = R_b R_h F_{yc}$$ (6.3.6-3a)

for slender-web members and

$$M_n = R_{pc} M_{yc}$$ (6.3.6-3b)

for compact- and noncompact-web members.

2. For $9.87 > \dfrac{\gamma_{e.LTB} f_{bu}}{F_{yc}} \ge \dfrac{F_{yr}}{F_{yc}}$, the LTB resistance is governed by the inelastic LTB strength

and may be written as

$$F_{nc} = R_b R_h F_{yc} \left[1 - \left(1 - \dfrac{F_{yr}}{R_h F_{yc}} \right) \left(\dfrac{\pi \sqrt{\dfrac{F_{yc}}{\gamma_{e.LTB} f_{bu}}} - 1}{\pi \sqrt{\dfrac{F_{yc}}{F_{yr}}} - 1} \right) \right] \le R_b R_h F_{yc} \qquad (6.3.6\text{-}4a)$$

for slender-web members and

$$M_{nc} = R_{pc} M_{yc} \left[1 - \left(1 - \dfrac{F_{yr} S_{xc}}{R_{pc} M_{yc}} \right) \left(\dfrac{\pi \sqrt{\dfrac{F_{yc}}{\gamma_{e.LTB} f_{bu}}} - 1}{\pi \sqrt{\dfrac{F_{yc}}{F_{yr}}} - 1} \right) \right] \le R_{pc} M_{yc} \qquad (6.3.6\text{-}4b)$$

for compact- and noncompact-web members.

3. For $\dfrac{\gamma_{e.LTB} f_{bu}}{F_{yc}} < \dfrac{F_{yr}}{F_{yc}}$, the LTB resistance is governed by the elastic LTB strength and may

be written as

$$F_{nc} = R_b \gamma_{e.LTB} f_{bu} \qquad (6.3.6\text{-}5a)$$

for slender-web members and

$$M_n = \gamma_{e.LTB} f_{bu} S_{xc} = \gamma_{e.LTB} M_u \qquad (6.3.6\text{-}5b)$$

for compact- and noncompact-web members.

AISC Design Guide 25 actually writes the above equations in an overall unified form involving just a single equation within each of the ranges of the LTB response, recognizing that nonprismatic girders often involve a combination of slender, noncompact and/or compact webs within the same member.

If one performs a detailed parametric evaluation of the behavior pertaining to the LTB strength ratios, $f_{bu}/\phi_b F_{nc}$ or $M_u/\phi_b M_n$, given the above equations, it can be shown that:

- If the strength is governed by elastic LTB throughout the unbraced length under consideration (Case 3 above), the value $1/(\phi_b \gamma_{e.LTB})$, is obtained at all cross-section locations for compact- and noncompact-web members. Similarly, the maximum LTB strength ratio is obtained as $1/(\phi_b R_b \gamma_{e.LTB})$ at the cross section having the smallest R_b for slender-web members.

- If the strength is governed by the plateau resistance throughout the unbraced length under consideration (Case 1 above), the maximum LTB strength ratio for slender-web members is $f_{bu}/(\phi_b R_b R_h F_{yc})$, and this ratio is of course obtained at the cross section having this value. Similarly, for compact- and noncompact-web members, the maximum LTB strength ratio is $M_u/(\phi_b R_{pc} M_{yc})$, and is obtained at the cross section having this value.

- If the strength is governed by inelastic LTB throughout the unbraced length under consideration, and if the web is compact or noncompact, the largest LTB strength ratio is obtained at the cross section having the largest $M_u/(R_{pc} M_{yc})$. Furthermore, if one employs the minimum R_b for all the cross sections within the unbraced length within Eq. 4a, the largest LTB strength ratio is obtained at the cross section having the largest $f_{bu}/(R_h F_{yc})$ (this simplification can be employed to streamline the evaluation of the LTB strength ratios). For all other cases, the maximum LTB strength ratio can occur theoretically at any location. However, the maximum $f_{bu}/\phi_b F_{nc}$ or $M_u/\phi_b M_n$ from the locations that have the largest $M_u/(R_b R_{pc} M_{yc})$ (combining the slender-web and the compact- and noncompact-web member equations into a single unified equation as discussed in Design Guide 25), or the smallest R_b will be very close to or equal the governing (largest) LTB strength ratio.

For unbraced lengths with constant F_{yc}, the smallest R_b occurs generally at the location where the effective web bend-buckling slenderness, $2D_c/t_w$, is largest. This typically occurs where the web D/t_w is largest. However, it is not as straightforward to determine the cross section with the largest $M_u/(R_b R_{pc} M_{yc})$ by inspection. Given the above attributes, White et al. (2021a) recommend that it is sufficient to sample at the following locations for the calculation of $f_{bu}/\phi_b F_{nc}$ or $M_u/\phi_b M_n$:

- For linearly tapered members, the middle and ends of the unbraced length;

- For cases involving a continuously-varying web taper, such as parabolic haunches within the negative moment region of continuous-span girders, the above locations plus the cross sections at the quarter points of the unbraced length;

- Any taper change or plate change;

- Locations of maximum flexural stress.

Once the critical cross section is identified, the corresponding LTB strength check can be conceptualized as being performed on an equivalent uniformly-loaded prismatic unbraced length that has the same overall $\gamma_{e.LTB}$ as well as the same $\rho_{o.max} = M_u/(R_b R_{pc} M_{yc})$ as the critical cross section. This concept is illustrated in Figure 68.
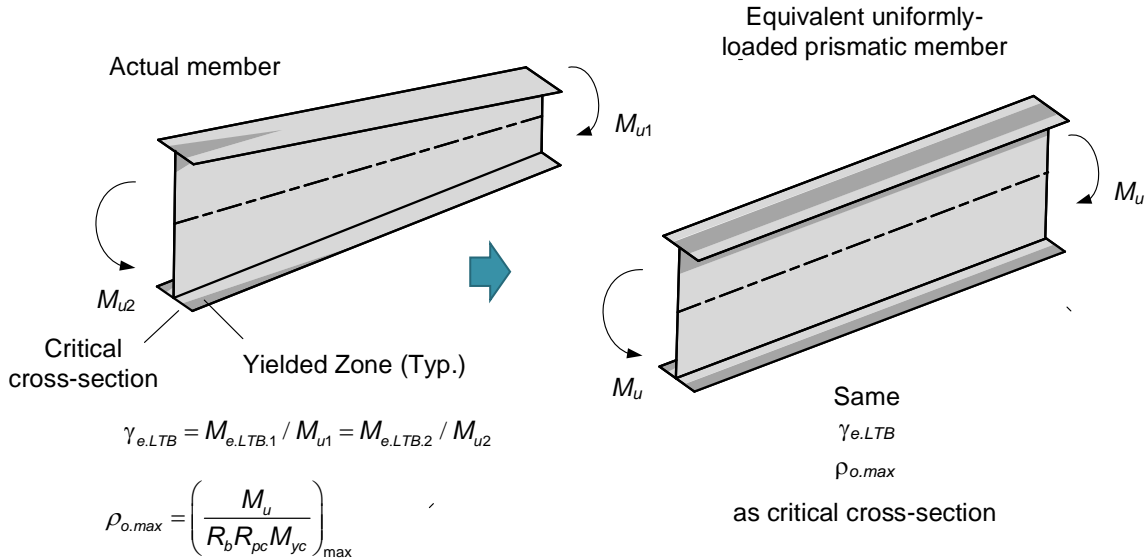
Figure 68. Equivalent uniformly-loaded prismatic member concept.

Based on the above concepts, Design Guide 25 recommends the following basic approach for calculating the LTB strength ratio, $f_{bu}/\phi_b F_{nc}$ or $M_u/\phi_b M_n$:

1. Calculate the elastic LTB load ratio, $\gamma_{e.LTB}$, for the unbraced length under consideration. Design Guide 25 provides a single generalized approach for the manual estimation of $\gamma_{e.LTB}$ considering web taper and/or steps in the cross-section geometry. This type of solution is sufficient for most problems; however, more accurate, larger values of $\gamma_{e.LTB}$ can be obtained from elastic eigenvalue buckling analysis using thin-walled open-section beam theory. Design Guide 25 provides guidance for this type of computational solution as well.

2. Determine F_{yr}. This is calculated from Eq. 6.3.5-20 or Eq. 6.3.5-21 as applicable.

3. At each of the potentially critical cross sections along the unbraced length, calculate F_{nc} or M_n from Eqs. 3 through 5 as applicable.

4. Divide f_{bu} by $\phi_b F_{nc}$, or M_u by $\phi_b M_n$ at each of the potential critical cross sections. The largest ratio is the LTB strength ratio for the entire unbraced length.

White and Grubb (2003) recommend the following approximate solution for the calculation of $\gamma_{e.LTB}$ in unbraced lengths composed of prismatic segments with a single cross-section transition within the unbraced length. The solution is adapted from Carskaddan and Schilling (1974) and Dalal (1969):

1. Calculate C_b using Eqs. 6.3.5-34 assuming that the unbraced length is prismatic.

2. Calculate the elastic LTB stress corresponding to the section with the largest end moment M_2 as

$$F_{e.LTB.2} = \chi \frac{C_b \pi^2 E}{(L_b / r_{t.2})^2}$$ (6.3.6-12)

where $r_{t.2}$ is the radius of gyration of the compression flange plus one-third of the depth of the web in compression for the cross section corresponding to M_2 and χ is determined from the chart shown in Figure 69. (This procedure is based on the assumption that M_2 is the largest moment within the unbraced length under consideration, and that this moment occurs in the larger of the two cross sections.)

3. Calculate $\gamma_{e.LTB}$ as $F_{e.LTB.2}/f_{bu.2}$, where $f_{bu.2}$ is the compression flange factored stress at the cross section corresponding to M_2.

The parameter χ is the ratio $P_e/(\pi^2 E I_2/L_b^2)$ shown in Figure 69, where P_e is the estimated elastic buckling load for the stepped column. This ratio gives a slightly conservative estimate of the elastic LTB resistance for a stepped I-section member subjected to moment gradient with the larger moment applied to the larger end cross section. Based on the behavior illustrated in Figure 69, AASHTO (2020) Articles C6.10.8.2.3 and CA6.3.3 allow transitions to a smaller cross section to be neglected in determining F_n (or M_n) for unbraced lengths having a step in the cross section when

* $L_1/L_b \leq 0.2$,
* $I_1/I_2 \geq 0.5$ and
*   the maximum f_{bu}/F_{yc} occurs in the unbraced length corresponding to the larger cross section.

where L_1 is the length of the segment with the smaller cross section, and I_1 and I_2 are the individual compression flange moments of inertia about the plane of the web for the smaller and larger flanges respectively (to be checked for both flanges).
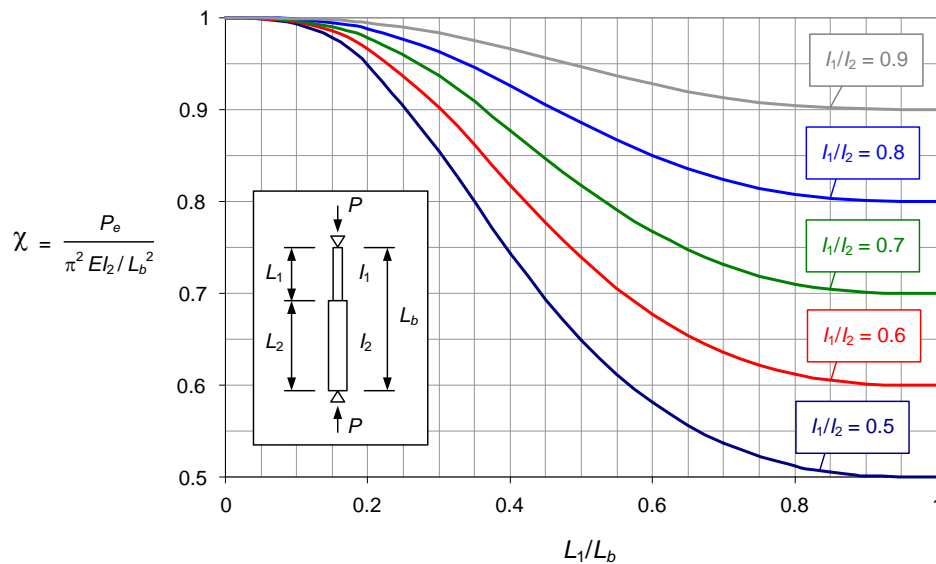
Figure 69. Ratio of elastic LTB stress at the section with the largest moment M_2 to the LTB stress determined assuming the member is prismatic with the larger cross section through- out the unbraced length (adapted from Carskaddan and Schilling (1974) and Dalal (1969)).

6.3.7 Combined Major-Axis Bending, Minor-Axis Bending and Torsion

6.3.7.1 General

AASHTO (2020) Article 6.10 and its Appendices A6 and B6 provide a unified approach for consideration of I-girder major-axis bending, minor-axis bending and torsion from any source. Similar to prior Guide Specifications for curved steel bridge design, such as AASHTO (2003), the AASHTO (2020) provisions focus on the flange lateral bending caused by the warping (i.e., cross-bending) of the flanges as the primary response associated with the torsion of I-section members. Significant flange lateral bending may be caused by wind, by eccentric concrete deck overhang loads acting on forming brackets placed along exterior girders, and by the use of discontinuous cross-frame lines in bridges with skew angles larger than about 20°. For the majority of straight non-skewed bridges, flange lateral bending effects tend to be the most significant during construction and tend to be insignificant in the final constructed condition. However, for horizontally curved bridges, in addition to the effects from the above sources, flange lateral bending due to the curvature must be considered at all limit states and during construction. The intent of the Article 6.10 provisions is to provide a straightforward approach for the Engineer to account for the above effects in design in a direct and rational manner whenever these effects are significant. When the various flange lateral bending effects are judged negligible or incidental, the provisions reduce to the design of I-section members subjected to major-axis bending alone (outlined in Sections 6.3.5 and 6.3.6 of this volume).

The basic form of the AASHTO (2020) resistance equations that account for the combined effects of major-axis bending and flange lateral bending is

$$f_{bu} + \frac{1}{3} f_\ell \leq \phi_f F_n \qquad\qquad (6.3.7\text{-}1)$$

$$(\text{AASHTO } 6.10.3.2.1\text{-}2, 6.10.3.2.2\text{-}1, 6.10.7.2.1\text{-}2, 6.10.8.1.1\text{-}1 \,\&\, 6.10.8.2\text{-}1)$$

for members in which the major-axis bending resistance is expressed in terms of the corresponding flange stress and

$$M_u + \frac{1}{3} f_\ell S_x \leq \phi_f M_n \qquad (6.3.7\text{-}2) \ (\text{AASHTO } 6.10.7.1.1\text{-}1, \text{A}6.1.1\text{-}1 \,\&\, \text{A}6.1.2\text{-}1)$$

for members in which the major-axis bending resistance is expressed in terms of the bending moment, where

f_{bu} = the elastically-computed flange major-axis bending stress,

f_ℓ = the elastically-computed flange lateral bending stress,

$\phi_f F_n$ = the factored flexural resistance in terms of the flange major-axis bending stress,

M_u = the member major-axis bending moment,

S_x = the elastic section modulus about the major-axis of the section to the flange under consideration, taken as the short-term section modulus for composite members in positive bending or the section modulus of the composite section to the bottom flange for composite members in negative bending, and

$\phi_f M_n$ = the factored flexural resistance in terms of the member major-axis bending moment.

Equations 1 and 2 are referred to in AASHTO (2020) as the one-third rule. These equations are simple, yet they do an excellent job of characterizing the various strength limit states that can govern the resistance of I-section members. Equations 1 and 2 address the combined major-axis and flange lateral bending effects basically by handling the flanges as equivalent beam-columns.

Equation 1 is targeted specifically at checking of slender-web noncomposite members, slender-web composite members in negative bending, and noncompact composite members in positive bending. In the limit that the flange lateral bending stress f_ℓ is equal to zero, Eq. 1 reduces to the basic member check $f_{bu} \leq \phi_f F_n$ for major-axis bending alone. The maximum potential value of F_n is the flange yield strength F_{yf}, but F_n can be less than F_{yf} due to slender-web bend buckling and/or hybrid-web yielding effects, or due to compression flange lateral-torsional (LTB) or local buckling (FLB) limit states.

Equation 2 may be used for checking the strength limit states of straight noncomposite members or composite members in negative bending that have compact or noncompact webs, and for checking of compact composite members in positive bending. For these member types, $\phi_f M_n$ can be as large as $\phi_f M_p$, where M_p is the section plastic moment resistance. The reader is referred to Sections 6.3.3 through 6.3.5 of this volume for definitions of the terms slender, noncompact and compact and for an overview of the calculation of $\phi_f F_n$ and $\phi_f M_n$. Equation 1 may be used as a simple conservative resistance check for all types of I-section members. AASHTO (2020) Article 6.10 emphasizes this fact by relegating the use of Eq. 2 for straight compact and noncompact web noncomposite members and composite members in negative bending to its Appendix A6. The definition of S_x as the short-term modulus to the bottom flange for composite sections in positive bending, and as the section modulus to the bottom flange of the composite section for composite sections in negative bending, is a conservative simplification. This simplification is consistent with the precedent of neglecting the influence of the different types of loading on the resistance for compact composite members in positive bending, and with the limited dependency of the different loading types for compact- and noncompact-web composite members in negative bending, as discussed previously in Sections 6.3.3 and 6.3.5 of this volume.

In the application of Eqs. 1 and 2, the stresses f_ℓ and f_{bu}, and the moment M_u, are taken as the largest values throughout the unbraced length when checking against the base flexural resistance $\phi_f F_n$ or $\phi_f M_n$ associated with lateral-torsional buckling. This is consistent with the application of the AASHTO and AISC interaction equations for a general beam-column subjected to combined axial load and bending. The stress f_{bu} in Eq. 1 and the moment M_u in Eq. 2 are analogous to the axial load in a general beam-column, and the stress f_ℓ is analogous to the beam-column bending moment. The moment M_u is analogous to axial loading since it produces axial stresses in the flanges. When checking compression flange local buckling or tension flange yielding, f_ℓ, f_{bu} and M_u may be determined as the corresponding values at the cross section under consideration. Generally, Eq. 1

or 2, as applicable, must be checked for each flange, and both the FLB and LTB based resistances must be checked for the compression flange in calculating F_{nc} or M_{nc}. The check providing the largest ratio of the left-hand side to the right-hand side of these equations governs.

The Engineer is permitted to use $f_\ell = 0$ when checking the top flange of composite I-girders, once the section is composite, since the composite slab tends to restrain the top flange lateral bending. AASHTO (2020) Article 6.10.7.2.1 requires that the concrete slab flexural stress shall be checked in addition to the use of Eq. 1. However, except in shored construction and in unusual cases of unshored construction discussed in the commentary to this article, the concrete flexural stress is typically much less than f_c' at the Eq. 1 strength limit, and therefore the concrete stress check does not govern.

As noted above, for curved bridges, AASHTO (2020) restricts the I-girder design in all cases to the use of Eq. 1. This restriction is due to the lack of a comprehensive understanding of the implications of significant member yielding and the concomitant inelastic redistribution on the forces and moments in curved bridge structural systems at the time that these provisions were implemented. Otherwise, Eqs. 1 and 2 are valid generally for all types of I-section members that satisfy the limits

$$L_b/R \leq 0.1 \qquad\qquad \text{(6.3.7-3) (AASHTO 6.7.4.2-1)}$$

within the final constructed configuration, where L_b is the unsupported length between the cross-frame locations and R is the horizontal radius of curvature,

$$L_b \leq L_r \qquad\qquad \text{(6.3.7-4) (AASHTO 6.7.4.2-1)}$$

where L_r is the unbraced length limit beyond which the base lateral-torsional buckling limit state is elastic, and

$$f_\ell \leq 0.6\ F_{yf} \qquad\qquad \text{(6.3.7-5) (AASHTO 6.10.1.6-1)}$$

The first of these limits is a practical upper bound for the subtended angle between the cross-frame locations (for constant R). It ensures that the I-girder webs will not have a d_o/R larger than 0.1, where d_o is the spacing of the transverse stiffeners. Equations 1 and 2 have been observed to perform adequately in a number of cases with L_b/R larger than 0.2 (White et al. 2001). However, the development of these equations as well as the validation of the AASHTO (2020) Article 6.10.9.3 tension-field action shear strength equations for curved web panels focused predominantly on members designed up to the limit specified by Eq. 3. Equation 4 is a practical upper bound for the unbraced length L_b beyond which the second-order amplification of the flange lateral bending stresses tends to be particularly severe. The reason for Eq. 5 is discussed below in Section 6.3.7.3 of this volume.

Prior AASHTO Specifications have required L_b to be less than 25 ft. AASHTO (2020) Article C6.7.4.1 explains that this requirement has been replaced by the requirement for a rational analysis. Nevertheless, typical curved I-girders will not have unbraced lengths exceeding this former limit.

6.3.7.2   Calculation of flange lateral bending stresses

Various methods may be used for calculating the flange elastic lateral bending stresses f_ℓ. AASHTO (2020) Article 6.10.1.6 gives simple equations for estimating the first-order lateral bending stresses due to the torsion associated with horizontal curvature (see Eq. 2.2.1-1 of this volume and AASHTO (2020) Article 4.6.1.2.4b), the torsion from eccentric concrete deck overhang loads acting on cantilever forming brackets placed along exterior girders (see AASHTO (2020) Article C6.10.3.4), and due to wind load (see AASHTO (2020) Article 4.6.2.7). These equations are based on the assumption of unbraced lengths other than at the ends of the bridge, where the flange is continuous with adjacent unbraced lengths, as well as equal length adjacent unbraced segments. Based on these idealized assumptions, the ends of the unbraced lengths are effectively torsionally and laterally fixed due to approximate symmetry boundary conditions. The Engineer should consider other more appropriate idealizations, or the use of computer analysis methods, when these assumptions do not approximate the actual conditions. Implications of various types of computer analysis on the calculation of f_ℓ are addressed by Jung et al. (2005) and Chang et al. (2005).

Similar to the amplification of internal bending moments in beam-column members, flange lateral bending stresses generally are amplified due to stability effects. However, it is impractical to calculate second-order live load stresses for moving live loads. Therefore, when Eq. 1 is applied for checking the compression flange, AASHTO (2020) Article 6.10.1.6 provides the following simple lateral bending amplification equation to account in an approximate fashion for these second-order effects:

$$f_\ell = \left(\frac{0.85}{1 - \dfrac{f_{bu}}{F_{cr}}} \right) f_{\ell 1} \geq f_{\ell 1} \qquad\qquad \text{(6.3.7-6) (AASHTO 6.10.1.6-4 \& 6.10.1.6-5)}$$

where

F_{cr} = the compression flange elastic lateral-torsional buckling resistance from Eq. 6.3.5-22 for compact- or noncompact-web members or Eq. 6.3.5-26 times R_b for slender-web members,

$f_{\ell 1}$ = the first-order compression flange lateral bending stress at the section under consideration (for checking of FLB), or the largest first-order compression flange lateral bending stress within the unbraced length (for checking of LTB), and

f_{bu} = the largest value of the compression flange major-axis bending stress within the unbraced length under consideration.

Amplification of the tension flange lateral bending stresses is not required, since this effect on the girder strength tends to be relatively minor compared to the compression flange response. White et al. (2001) show that Eq. 6 gives accurate to conservative estimates of the flange second-order lateral bending stresses. The purpose of Eq. 6 is to guard conservatively against large unbraced lengths in which second-order lateral bending effects are significant. The Engineer should be

152

particularly mindful of the amplified compression flange lateral bending in exterior girders due to eccentric concrete deck overhang loads during construction. In situations where the amplification given by these equations is large, the Engineer may wish to consider using an effective length factor $K < 1$ in the calculation of $F_{e.LTB}$ from Eq. 6.3.6-22 or 6.3.5-26 (using the procedure outlined in Section 6.3.5.13 of this volume).

When determining the amplification of $f_{\ell 1}$ in horizontal curved I-girders with $L_b/R \geq 0.05$, AASHTO (2020) Article C6.10.1.6 recommends that F_{cr} in Eq. 6 may be calculated using $KL_b = 0.5L_b$. The use of $KL_b = 0.5L_b$ for girders with $L_b/R \geq 0.05$ gives a better estimate of the amplification of the bending deformations associated with the boundary conditions for the flange lateral bending at the intermediate cross-frame locations, which are approximately symmetrical, and assumes that an unwinding stability failure of the compression flange is unlikely for this magnitude of the horizontal curvature.

In cases where the amplification of construction stresses is large, a second alternative is to conduct a direct geometric nonlinear analysis to determine the second-order effects within the superstructure more accurately. In the final constructed condition, the above amplification typically is applied only to the bottom flange in negative moment regions of continuous spans. In this case, $F_{e.LTB}$ is increased significantly due to the moment gradient in these regions, via the moment gradient modifier C_b (see Section 6.3.5.11).

6.3.7.3 One-third rule concept

Figure 70 compares the result from Eq. 2 to the theoretical fully plastic resistance for several doubly symmetric noncomposite compact-flange, compact-web cross sections. Figure 71 shows a sketch of a typical fully plastic stress distribution on this type of cross section. The equations for the fully plastic cross-section resistances are based on the original research by Mozer et al. (1971) and are summarized by White and Grubb (2005). The specific stress distribution shown in Figure 71 is associated with equal and opposite lateral bending in each of the equal-size flanges (i.e., warping of the flanges due to nonuniform torsion). However, the solution is the same if one considers equal flange lateral bending moments due to minor-axis bending.

One can observe that, within the limit given by Eq. 5, the one-third rule equation (Eq. 2) provides an accurate to somewhat conservative estimate of the theoretical cross-section resistances for the different web-to-flange area ratios, A_w/A_f, shown in Figure 70. In the limit that A_w/A_f is taken equal to zero, the same approximation is provided by both Eq. 2 and Eq. 1. The comparison of the theoretical and approximate equations shown in Figure 70 is useful for gaining a conceptual understanding of the one-third rule equations in the limit of compact-flange, compact-web, compactly-braced noncomposite members. Also, Schilling (1996) and Yoo and Davidson (1997) present other useful cross-section yield interaction relationships. However, cross-section yield interaction equations are limited in their ability to fully characterize the combined influence of distributed yielding along the member lengths along with the various stability effects (FLB, LTB and web bend buckling). Furthermore, yield interaction equations generally do not reduce to the resistance equations for straight members subjected to major-axis bending in the limit that $f_\ell = 0$.
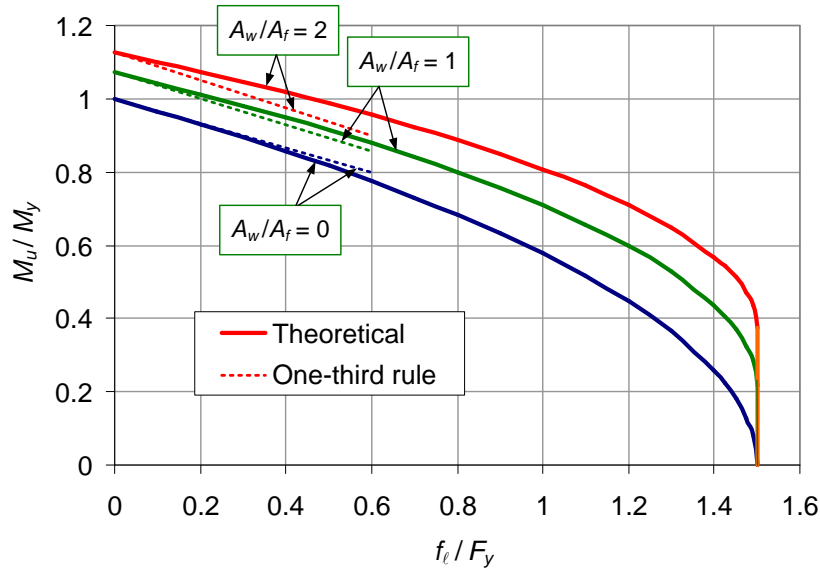
Figure 70. Comparison of the AASHTO (2020) one-third rule equation to the theoretical fully-plastic cross-section resistance for several doubly symmetric noncomposite compact-flange, compact-web I-sections (adapted from White and Grubb (2005)).
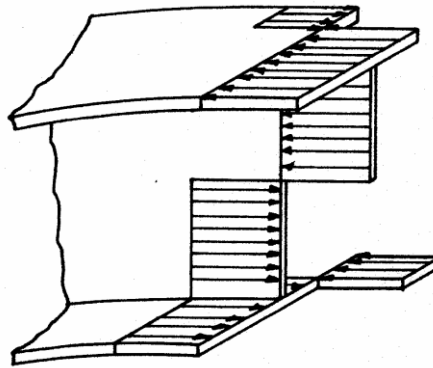
Figure 71. Sketch of a fully plastic stress distribution, including flange lateral bending.

Equations 1 and 2 are a basic extension of the one-third rule approximation of the above theoretical cross-section resistances to address the influence of general yielding and stability limit states on the member resistance. The basic extension is accomplished simply by changing the flange yield strength, F_{yf}, to $\phi_f F_n$ in Eq. 1 and by changing the section plastic moment resistance, M_p, to $\phi_f M_n$ in Eq. 2. The 1/3 coefficient accurately captures the strength interaction including the various yielding and stability effects (White et al. 2001). The extension from cross-section equations to member equations is ad hoc, but it is similar in many respects to the development of the AISC (2016) and AASHTO (2020) general beam-column interaction relationships. The shape of the interaction (i.e., the slope of the line relating f_{bu} and f_ℓ in Eq. 1 or M_u and f_ℓ in Eq. 2) is based on curve fitting. Equations 1 and 2 are thus semi-analytical and semi-empirical. White and Grubb (2005) provide a summary of the correlation of Eqs. 1 and 2 with analytical, numerical and experimental results.

154

6.3.8 Shear Strength

6.3.8.1 General

For transversely stiffened webs, AASHTO (2020) Article 6.10.9.3 bases the I-section member shear resistance either (conservatively) on the web shear buckling capacity or an idealized additive contribution of the web shear buckling and postbuckling resistances. The classification of webs as stiffened or unstiffened is addressed in the following discussions. The web elastic shear buckling capacity may be expressed generally as

$$V_{cr} = \tau_{cr} D t_w = \frac{\pi^2 E k}{12\left(1-v^2\right)\left(\dfrac{D}{t_w}\right)^2} D t_w = \frac{0.90 E k}{\left(\dfrac{D}{t_w}\right)^2} D t_w \qquad (6.3.8\text{-}1)$$

which is the classical plate buckling equation multiplied by the web area, $D t_w$, but with the buckling coefficient, k, corresponding to pure shear loading. This coefficient is taken as

$$k = 5 + \frac{5}{\left(\dfrac{d_o}{D}\right)^2} \qquad (6.3.8\text{-}2a)\ (\text{AASHTO } 6.10.9.3.2\text{-}7)$$

for stiffened webs, i.e., webs with transverse stiffeners (referred to as transversely-stiffened) or with transverse and longitudinal stiffeners (referred to as longitudinally-stiffened) and in which the transverse stiffeners are spaced within specified maximum limits, and it is taken as

$$k = 5 \qquad (6.3.8\text{-}2b)$$

for unstiffened webs. These equations are a simple approximation of analytical buckling solutions for isolated panels with ideal simply supported edge conditions subjected to pure shear loading (Ziemian 2010). They are applied based on the average web shear stress. Therefore, the ratio of the AASHTO (2020) elastic shear buckling strength to the web plastic shear capacity may be written as

$$C_{el} = \frac{\tau_{cr}}{\tau_{yw}} = \frac{V_{cr}}{V_p} = \frac{1.57 E k}{\left(\dfrac{D}{t_w}\right)^2 F_{yw}} \qquad (6.3.8\text{-}3)$$

where

$$V_p = \tau_{yw} Dt_w = \frac{F_{yw}}{\sqrt{3}} Dt_w = 0.58 F_{yw} Dt_w \qquad \text{(6.3.8-4) (AASHTO 6.10.9.2-3)}$$

is the fully plastic resistance of the web based on the von Mises yield criterion and $\tau_{yw} = F_{yw} / \sqrt{3}$.

Inelastic buckling is assumed to occur when the web average shear stress is larger than 80 % of the shear yield stress, i.e., inelastic shear buckling is assumed for $C_{el} > 0.8$. The corresponding AASHTO (2020) Article 6.10.9.3 web shear buckling resistance (elastic or inelastic) is expressed as a fraction of the fully plastic shear strength (C) as follows:

For $C_{el} \leq 0.8$ or $\dfrac{D}{t_w} \geq 1.40 \sqrt{\dfrac{Ek}{F_{yw}}}$ (elastic buckling)

$$C = C_{el} \qquad \text{(6.3.8-5a) (AASHTO 6.10.9.3.2-6)}$$

and for $C_{el} > 0.8$

$$C = \sqrt{0.8 C_{el}} = \frac{1.12}{\dfrac{D}{t_w}} \sqrt{\frac{Ek}{F_{yw}}} \quad \text{(inelastic buckling)} \qquad \text{(6.3.8-5b) (AASHTO 6.10.9.3.2-5)}$$

Lastly, the above inelastic shear buckling equation gives

$$C = 1 \text{ (full web plastification)} \qquad \text{(6.3.8-5c) (AASHTO 6.10.9.3.2-4)}$$

at $C_{el} \geq 1.25$ or $\dfrac{D}{t_w} \leq 1.12 \sqrt{\dfrac{Ek}{F_{yw}}}$.

AASHTO (2020) requires that webs without longitudinal stiffeners, and with transverse stiffeners spaced at $d_o > 3D$, shall be considered as unstiffened. In these cases, the shear resistance is limited to the shear buckling design resistance

$$\phi_v V_n = 1.0 \; C \; V_p \qquad \text{(6.3.8-6) (AASHTO 6.10.9.2-1)}$$

However, webs with closer transverse stiffener spacing are considered as stiffened. (AASHTO (2020) Article 6.10.11.1.1 requires transverse stiffeners spaced at $d_o \leq 2D$ for webs containing longitudinal stiffeners, whether or not they are required for shear, to provide support to the longitudinal stiffeners along their length; therefore, longitudinally stiffed webs always may be considered as stiffened for calculation of their shear resistance.) The ultimate shear resistance of stiffened webs may be taken as the additive combination of the above shear buckling resistance with a representation of the shear postbuckling strength from Basler's (1961) seminal research. For members where the ratio of the web area to the average flange area is smaller than 2.5, i.e.,

$$\frac{2Dt_w}{(b_{fc}t_{fc}+b_{ft}t_{ft})} \leq 2.5 \qquad\qquad \text{(6.3.8-7) (AASHTO 6.10.9.3.2-1)}$$

the sum of the web buckling and postbuckling design resistances is expressed as

$$\phi_v V_n = 1.0 \left[C + \frac{0.87(1-C)}{\sqrt{1+\left(\dfrac{d_o}{D}\right)^2}} \right] V_p \qquad\qquad \text{(6.3.8-8) (AASHTO 6.10.9.3.2-2)}$$

whereas for members that have smaller flanges relative to the web area, this sum is written as

$$\phi_v V_n = 1.0 \left[C + \frac{0.87(1-C)}{\sqrt{1+\left(\dfrac{d_o}{D}\right)^2}+\dfrac{d_o}{D}} \right] V_p \qquad\qquad \text{(6.3.8-9) (AASHTO 6.10.9.3.2-8)}$$

The second term inside the square brackets in each of the above equations is the web postbuckling contribution to the strength based on Basler's (1961) theory. Both of the above equations are based on the assumption that the web develops tensile postbuckling stresses (i.e., a tension field) along a diagonal in the web panels as shown in Figure 72, in addition to the shear buckling stresses. In determining the slope of this tension field, θ, Basler assumes that only an effective band, *s*, takes part in transmitting the additional tension (i.e., the flanges are assumed to provide zero anchorage to the theoretical tension field). The maximum resistance is obtained when yielding occurs due to the combination of the tension field stress plus the initial web shear buckling stress. The angle θ is determined to maximize the predicted postbuckling contribution. However, when the ultimate shear force given by Eq. 8 is determined, a complete tension field is assumed at the orientation θ throughout the entire web. Basler (1963) acknowledges this inconsistency, and explains that the flanges are actually not loaded to the extent required by his theory in physical tests. Nevertheless, he argues that his theory still provides an acceptable characterization of I-girder shear strengths.

Equation 9 is referred to in the literature as the "true Basler" shear resistance (e.g., see Porter et al. (1975) and Wolchuk and Mayrbaurl (1980)). This equation is determined by consistently applying the idealization shown in Figure 72 throughout the formulation. (There is a typographical error in the equation for the true Basler shear strength in Porter et al. (1975); the correct expression is as provided in Eq. 9.)

It should be obvious to the reader that the above idealizations are only a very simplified representation of the true web response. Numerous additional web shear failure theories have been postulated since Basler's original research (e.g., see Ziemian (2010)). The large number of these idealizations in itself is evidence of the fact that the corresponding behavior is complex and tends to defy explanation by basic plane stress strength of materials models. Studies such as Yoo and Lee (2006), Kim et al. (2007) and Jha (2016) have provided further insight into the detailed force

157

transfer mechanisms associated with the web ultimate shear resistance. These studies show that the force transfer mechanisms can differ substantially from the various failure theories. Nevertheless, the ability of Eqs. 8 and 9 to provide a reasonable prediction of experimental test results is irrefutable. White and Barker (2008) studied the predictions by 12 different models using a data set of 129 experimental high-shear low-moment tests, including 30 hybrid and 11 horizontally curved I-girders. They concluded that Basler's model provides the best combination of accuracy and simplicity of the models considered.
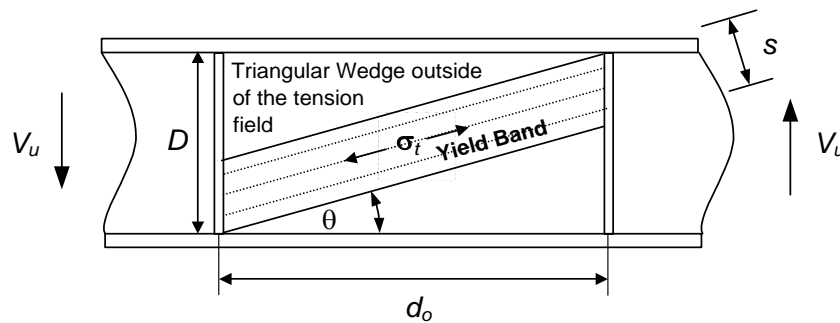
Figure 72. Assumed tension field used in determining the angle θ implicit in Basler's (1961) shear postbuckling strength (Eq. 8), and used in determining the "true Basler" shear resistance (Eq. 9).

White et al. (2008) studied the predictions for the above 129 tests plus an additional 57 tests involving combined high-shear and high-moment, including 21 additional hybrid girders. Their results indicated that within the limit defined by Eq. 7 plus the AASHTO (2020) proportioning limits discussed in Section 6.3.2 of this volume, the combination of Eq. 8 for the shear resistance and the AASHTO (2020) equations outlined in Sections 6.3.3 through 6.3.5 for the flexural resistance gives a sufficient representation of the high-shear high-moment resistance without the consideration of moment-shear strength interaction. In other words, the same resistance factor $\phi_v = 1.0$ is justified for both high-shear low-moment and high-shear high-moment, and the same resistance factor $\phi_f = 1.0$ is justified for both high-moment low-shear and high-moment high-shear. Also, White et al. (2008) showed that for girders with small flanges that violate Eq. 7, the capacities tend to be smaller but are predicted adequately when Eq. 9 is used for the shear resistance. Extensive finite element parametric studies have been conducted by Hash (2001), White et al. (2001), Aydemir et al. (2004), Jung and White (2006), Kim et al. (2007) and others that support the above conclusions and help address the complete range of potential I-girder designs including hybrid and curved I-girders with combined high-moment and high-shear.

One important condition associated with the above conclusions is that the members must be checked in general using the maximum shear within a given web panel for V_u, the maximum moment (or flange stress) within the web panel for M_u or f_{bu} when the flexural resistance is governed by FLB or TFY, and the maximum moment (or flange stress) within the unbraced length under consideration for M_u or f_{bu} when the flexural resistance is governed by LTB. Some of the developments in the past have suggested that the moment should be checked at the smaller of $D/2$ or $d_o/2$ from a transverse stiffener location. The use of M_u at min $(D/2, d_o/2)$ in plotting the experimental results leads to a false indication of significant M-V interaction. At regions of high shear, the moment drops rapidly as one moves away from the peak moment position. This drop is

required for equilibrium, i.e., *dM/dx = V*. It is not due to *M-V* interaction. Use of the maximum moment or flange stress for the flexural resistance check in regions of combined high-moment and high-shear is consistent with the established procedures for checking of regions subjected to high-moment low-shear (White et al. 2008).

6.3.8.2 Members with longitudinally-stiffened webs

The contribution of the longitudinal stiffeners to the shear resistance is neglected in AASHTO (2020). Longitudinal stiffeners divide a web panel into sub-panels. Cooper (1967) calculates the full web shear resistance for these member types by summing the shear resistance of the subpanels. However, when a single longitudinal stiffener is located near its optimum position for flexure, the corresponding enhancement of the shear capacity is relatively small. Furthermore, the longitudinal stiffener requirements in AASHTO (2020) Article 6.10.11.3 are not sufficient to develop the general shear postbuckling resistance of the web panels. Subramanian and White (2017b) show that the calculated shear resistance, neglecting any contribution from web longitudinal stiffeners, correlates well with the results from refined finite element test simulations. Since any contribution from longitudinal stiffeners to the shear resistance is neglected, it can be concluded that moment-shear interaction may be neglected for longitudinally-stiffened I-girders on the same basis that it is neglected for girders without web longitudinal stiffening.

6.3.8.3 Variable web depth members

AASHTO (2020) Article C6.10.1.4 discusses the positive or negative contribution of the force within an inclined flange to the I-girder shear resistance. Also, Article C6.10.1.4 suggests that this flange contribution is difficult to calculate in general, since numerous sets of concurrent moments and shears must be evaluated to determine the critical combination. Therefore, this contribution is commonly neglected. However, the vertical component of the inclined flange force can provide a substantial contribution to the overall shear resistance, reducing the shear force that the web must resist near the interior supports in continuous-span I-girders. For cases in which the increase in moment is in the same direction as the increase in the web depth along the length, the tapered web geometry results in a reduction in the web shear demands. (The web shear demands are increased in the opposite case; this can occur for example in regions of positive flexure in which the web taper is decreasing toward the supports.) AISC Design Guide 25 (White et al. 2021a) provides a detailed analysis of the web shear demands in variable web depth member, as well as the recommended application/adaptation of the web shear strength equations for members with variable web depth.

AASHTO (2020) Article C6.10.1.4 suggests that the bottom flange normal stress is increased due to the bottom flange slope within a haunch, and that this increase can be estimated as

$$f = \frac{P_h}{A_f \cos\theta}$$
(6.3.8-10a) (AASHTO C6.10.1.4-1)

where

$$P_h = \frac{M_u}{S_x} A_f$$
(6.3.8-10b) (AASHTO C6.10.1.4-2)

is the horizontal component of the flange force required to develop the bending moment M_u,

A_f =   area of the inclined bottom flange

θ =   angle of inclination of the bottom flange, and

S_x =   elastic section modulus to the inclined bottom flange

Equation 10b assumes that the member does not resist any applied axial force. If the member axial force is non-zero, the corresponding girder axial stress should also be included in the calculation of P_h.

At the "kink" where an inclined bottom flange is changed to horizontal, the vertical component of the inclined flange force is transferred into the web as a concentrated load. At these locations, the web is sufficient without additional stiffening if the provisions of Article D6.5.2 are satisfied for the factored vertical component of the inclined flange force using a length of bearing N equal to zero (see Section 6.3.10.5 of this volume). Otherwise, partial or full-depth bearing stiffeners should be provided at these locations.

6.3.8.4   Web transverse stiffeners

AASHTO (2020) Article 6.10.11.1 addresses the design requirements for web transverse stiffeners. Numerous research studies have observed that the bending rigidity is the dominant parameter that governs the performance of transverse stiffeners. This is true both for developing the shear buckling as well as the combined shear buckling and postbuckling resistance of stiffened webs (Kim et al. 2007; Yoo and Lee 2006; Lee et al. 2003; Stanway et al. 1996; Rahal and Harding 1990; Horne and Grayson 1983). Although there is some evidence of axial stresses in the transverse stiffeners due to tension field action, these effects are relatively minor compared to the lateral loading on the stiffeners due to the postbuckling response of the web panels. Furthermore, several research studies have shown that prior AASHTO stiffener area requirements were more than adequate in certain cases and less than adequate in others in maintaining a line of near zero lateral deflection along the line of the stiffener (Kim et al. 2007; Lee et al. 2003; Xie 2000). Also, the studies have shown that different types of transverse stiffeners with comparable moments of inertia, but with widely different areas, have essentially the same strength performance. Webs with transverse stiffeners attached such that the stiffeners only provide lateral restraint perform similarly to webs in which a load path exists to transfer tension-field axial forces into the stiffeners. Lastly, Kim et al. (2007) observe that the demands on the transverse stiffeners are very similar in comparable straight and curved I-girders that satisfy the AASHTO (2020) proportioning requirements. Based on these research results, AASHTO (2020) Article 6.10.11.1 no longer specifies any area requirement for transverse stiffeners in stiffened webs. Rather, several equations are specified for the transverse stiffener lateral rigidity that apply equally to straight and curved I-section members.

For stiffeners adjacent to web panels in which neither panel supports shear forces larger than the shear buckling resistance, the stiffener moment of inertia, taken about the edge in contact with the web for single stiffeners and about the mid-thickness of the web for stiffener pairs, is required to satisfy the *smaller* of the following limits:

$$I_t \geq \left(I_{t1} = bt_w^3 J \right) \qquad\qquad \text{(6.3.8-11) (AASHTO 6.10.11.1.3-1 \& 6.10.11.1.3-3)}$$

$$I_t \geq \left[I_{t2} = \frac{D^4 \rho_t^{1.3}}{40} \left(\frac{F_{yw}}{E} \right)^{1.5} \right] \qquad\qquad \text{(6.3.8-12) (AASHTO 6.10.11.1.3-2 \& 6.10.11.1.3-4)}$$

where

b = the smaller of d_o and D

$$J = \frac{2.5}{\left(d_o / D \right)^2} - 2.0 \geq 0.5 \qquad\qquad \text{(6.3.8-13) (AASHTO 6.10.11.1.3-5)}$$

ρ_t = the larger of F_{yw}/F_{crs} and 1.0

$$F_{crs} = \frac{0.31E}{\left(b_t / t_p \right)^2} \leq F_{ys} \qquad\qquad \text{(6.3.8-14) (AASHTO 6.10.11.1.3-6)}$$

b_t = the width of a rectangular plate stiffener

t_p = the thickness of the rectangular plate stiffener

F_{ys} = the specified minimum yield strength of the stiffener.

Equation 11 is the fundamental stiffener rigidity necessary to develop the calculated AASHTO web shear buckling resistance. For webs proportioned to develop their full plastic shear capacity (i.e., $C = 1$ in Eq. 6.3.8-5c), the rigidity requirement based on this equation becomes excessive as the web is made more and more stocky. Equation 12 generally gives a required rigidity that is slightly larger than that required by Eq. 11 at the web slenderness D/t_w just sufficient to achieve $C = 1$. For webs in which the I_t requirement from Eq. 11 is larger than that from Eq. 12, the requirement from Eq. 12 is sufficient to develop the web plastic shear capacity ($C = 1$) (Kim et al. 2007). For webs in which the nominal shear buckling capacity is less than V_p (i.e., $C < 1$), Eq. 11 typically gives a smaller requirement than Eq. 12. The rigidity requirement defined by this equation is constant for $d_o/D > 1.0$, but increases substantially for $d_o/D < 1$ as shown by Figure 73. That is, the demand on the transverse stiffeners to hold a line of near zero lateral displacement at the web shear buckling load is substantially larger when the stiffeners are spaced at $d_o < D$.

For transverse stiffeners adjacent to web panels in which the shear force is larger than the shear buckling resistance, such that the web tension-field resistance is required in one or both panels, AASHTO (2020) specifies that the moment of inertia of the transverse stiffeners must satisfy the following requirements:
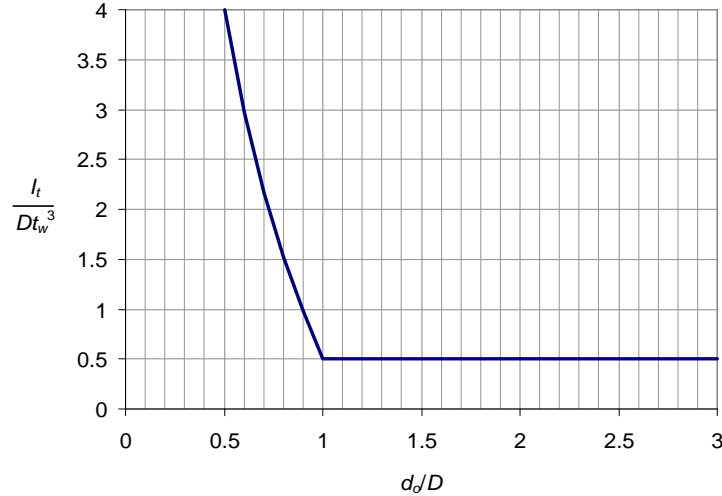
Figure 73 Normalized transverse stiffener bending rigidity I_t / Dt_w^3 necessary to develop the AASHTO (2020) web shear buckling resistance V_{cr}.

If $I_{t2} > I_{t1}$, then

$$I_t \geq I_{t1} + \left(I_{t2} - I_{t1}\right)\rho_w \qquad\qquad \text{(6.3.8-15) (AASHTO 6.10.11.1.3-7)}$$

Otherwise,

$$I_t \geq I_{t2} \qquad\qquad \text{(6.3.8-16) (AASHTO 6.10.11.1.3-8)}$$

where, if both web panels adjacent to the stiffener are subject to tension field action, ρ_w is the maximum value of

$$\frac{V_u - \phi_v V_{cr}}{\phi_v V_n - \phi_v V_{cr}} \qquad\qquad \text{(6.3.8-17)}$$

calculated from the two web panels, and if only one panel is subject to tension field action, ρ_w is calculated from Eq. 17 for that panel. The term $\phi_v V_{cr}$ in Eq. 17 is the web shear buckling strength calculated from Eq. 6.

As noted above, Eq. 12 generally requires a stiffener size slightly larger than that necessary to develop the web fully plastic shear capacity, were the web to be made thick enough such that $C = 1$ for a given panel aspect ratio d_o/D, web yield strength F_{yw} and web depth D. Kim et al. (2007) observed that this stiffener size is always accurate to somewhat conservative compared to the size necessary to develop the web shear postbuckling resistance for thinner webs. The term ρ_t in Eq. 12 accounts conservatively for the effect of early yielding in transverse stiffeners with $F_{ys} < F_{yw}$ and for the effect of potential local buckling of plate stiffeners having a relatively large width-to-thickness ratio b_t/t_p. The stiffener local buckling stress F_{crs} is given by Eq. 14. Kim and White (2013) provide additional discussion of the background to these requirements.

Equation 15 provides a conservative linear variation in the transverse stiffener rigidity requirement between the value I_{t2} required for development of the full shear resistance including tension field action, $\phi_v V_n$, and the value I_{t1} required for development of the shear buckling resistance, $\phi_v V_{cr}$. As a simplification, transverse stiffeners supporting web panels with $V_u > \phi_v V_{cr}$ can be sized based on the assumption of $\rho_w = 1.0$, which gives the requirement specified by Eq. 12. The more elaborate calculation by Eq. 15 typically is not necessary except for long-span girders with relatively deep webs.

For girders with longitudinally stiffened webs, Article 6.10.11.1.3 also requires that the transverse stiffeners satisfy

$$I_t \geq \left(\frac{b_t}{b_\ell}\right)\left(\frac{D}{3d_o}\right)I_\ell = \left(\frac{b_t}{b_\ell}\right)\left(\frac{1}{3(d_o/D)}\right)I_\ell \qquad \text{(6.3.8-18) (AASHTO 6.10.11.1.3-11)}$$

This equation is a liberalization (by a factor of three) of the transverse stiffener section modulus recommended by Cooper (1967). Equation 18 tends to govern the transverse stiffener size only for horizontally curved I-girders with longitudinal stiffeners, relatively large d_o/R values (such that the curvature parameter Z in the Article 6.10.11.3.3 provisions for the longitudinal stiffener requirements approaches its maximum value of 12), d_o/D close to its maximum value of 2.0, and D/t_w is relatively small compared to the maximum limit of 300.

Equation 12 facilitates the selection of a single size for all the transverse stiffeners in a given girder or set of girders, since it is independent of D/t_w and d_o/D. AASHTO (2020) also specifies several other transverse stiffener dimensional requirements that ensure that the stiffener width is not overly small relative to the widest compression flange or the largest web depth within the field section under consideration. These basic dimensional requirements govern in a number of practical cases.

6.3.9 Shear Connectors

AASHTO (2020) Article 6.10.10 addresses the design of the shear connectors between the deck and the steel I-sections for composite construction. Both fatigue and strength limit states must be considered in selecting the number, type and size of the shear connectors. This section focuses on the strength behavior of the shear connectors in horizontally curved I-girders. In horizontally curved girders, the shear connectors can be subjected to significant lateral (i.e., radial) shear forces in addition to longitudinal shear forces. In the limit that the girder is straight, the lateral shear forces are relatively small and are generally neglected. The calculation of the longitudinal shear forces is the same in both straight and curved I-girders. Therefore, the behavior of the shear connectors in straight composite I-girders may be considered as a special case of the behavior in curved I-girders.

Figure 74 shows idealized free-body diagrams of the slab and the steel I-section for a single I-girder taken from approximately one-half of the span of a hypothetical simple-span composite I-girder bridge. All the forces acting on each of the elements are indicated in the figure, with the exception of:

1. Dead loads and vertical live loads applied directly to the I-girder,

2. Slab membrane and plate bending forces and moments transferred from adjacent I-girders along the circumferential cuts made through the slab thickness to isolate the effective width of the slab over the I-girder being considered, b_s, from the remainder of the slab, and

3. Vertical forces transferred between the slab and the I-girder, including any vertical forces associated with the torsional restraint of the I-girder provided by the slab.
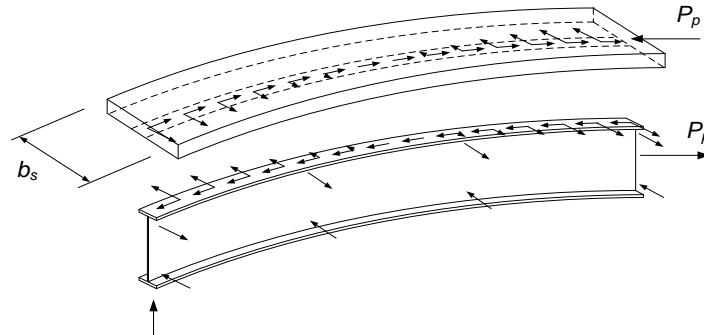
Figure 74. Idealized free-body diagrams of the slab and the steel I-section for a single I-girder taken from approximately one-half of the span of a hypothetical simple-span composite I-girder bridge.

The force labeled P_p in the figure is the total force developed in the slab by a maximum positive major-axis bending moment equal to the corresponding cross-section plastic moment M_p. AASHTO Article 6.10.10.4.2 assumes that the maximum positive bending moment is located approximately at the position of the maximum positive live load plus impact moment. This position is selected because it is easier to locate than the position of the total maximum dead plus live load moment. The force P_p is calculated as

$$P_p = \min \begin{pmatrix} 0.85\, f_c'\, b_s\, t_s, \\ F_{yw}\, D\, t_w + F_{yt}\, b_{ft}\, t_{ft} + F_{yc}\, b_{fc}\, t_{fc} \end{pmatrix} \tag{6.3.9-1}$$

(AASHTO 6.10.10.4.2-2 & 6.10.10.4.2-3)

Any reduction in the cross-section major-axis positive bending moment associated with Eqs. 3-2, 6.3.3-3, 6.3.4-1 and 2, 6.3.7-1 and/or 6.3.7-2 is neglected.

For straight I-girders, Article 6.10.10.4.2 requires that the shear connectors located between the maximum moment cross section and the simply supported end of the girder must develop the total force P_p. No other forces acting on the shear connectors need to be considered for these member types. Furthermore, only a slight deformation around more heavily stressed shear connectors is needed to redistribute the horizontal shear forces to less heavily stressed connectors. Therefore, the total required number of connectors within the above I-girder length may be calculated as

$$n = \frac{P_p}{Q_r}$$
<div align="right">(6.3.9-2) (AASHTO 6.10.10.4.1-2)</div>

where

$$Q_r = \phi_{sc}Q_n = 0.85Q_n$$
<div align="right">(6.3.9-3) (AASHTO 6.10.10.4.1-1)</div>

is the factored shear resistance of a single connector.

For the horizontally curved I-girder illustrated in Figure 74, potentially significant radial shear forces must be accounted for in addition to the above longitudinal forces. Colville (1972) suggested the simplified model for calculation of these forces illustrated in Figures 75 and 76. Figure 75 is a plan view of the slab free-body diagram from Figure 74. Note that the subtended angle between the ends of this free-body diagram is $\theta = L_p/R$, where L_p is the arc length from the girder simply-supported end to the position of the maximum positive live load plus impact moment. Figure 76 is an idealization of this free-body diagram explained below. One can observe that the force P_p developed at the maximum moment cross section is not collinear with the shear connectors. This creates a secondary radial loading effect on the connectors. The connector radial loads are estimated based on the following idealizations:

1. The influence of the slab forces and moments within the circumferential cut through the slab thickness to isolate the effective width b_s from the remainder of the slab are neglected. That is, the shear connectors are assumed to be the only components available to equilibrate the force P_p within the plan view of Figure 75.

2. Any differences in the slab stresses across the cut at the maximum moment location, which would give an eccentricity to the force P_p on this cross section, are neglected.

3. The shear connectors are assumed to be spaced uniformly along a straight chord between the ends A and B shown in Figure 75. This idealization is illustrated in Figure 76. The shear connectors are actually located along the curved axis AB in Figure 75. By assuming that they are located along the straight chord AOB (see Figure 76), the equations are simplified and the resulting connector forces are estimated conservatively. Also, since the radius R is typically large compared to the length $R\theta$, the error caused by this assumption is small.

4. The radial forces in the shear connectors are taken as normal to the line AOB in Figure 76 and they are assumed to be proportional to the distance of the connectors from point O.

Based on these idealizations and considering equilibrium of the free-body diagram in Figure 76, the resultant of the connector forces must be equal to the force P_p acting at the center of the group of connectors (point O), plus the moment of P_p about the vertical axis through point O, equal to $P_p R (1 - \cos \theta) / 2$. Correspondingly, the total force in the connectors at the locations A and B is equal to the vector sum of two components, namely the longitudinal force

$$\bar{P} = P_p / n$$
<div align="right">(6.3.9-4)</div>
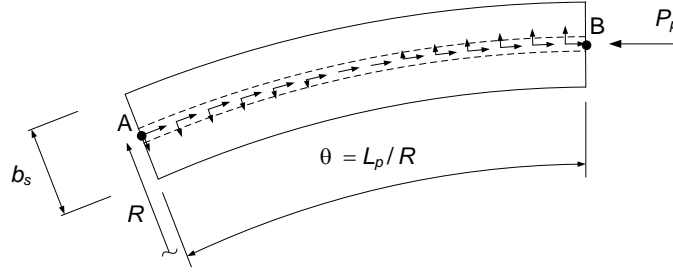
Figure 75. Plan view of the slab in the idealized free-body diagram of Figure 74.
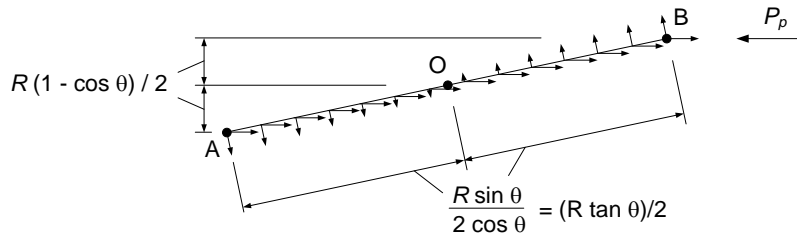
Figure 76. Plan view simplification of the free-body diagram of the slab in Figure 75.

where n is the total number of connectors along the girder length under consideration, and the lateral force (perpendicular to AOB)

$$\bar{F} \cong \frac{P_p\, R(1-\cos\theta)/2}{[(n/n*-1)\, n*\ \tan\theta]/6} \tag{6.3.9-5a}$$

where $n*$ is the number of shear connectors placed at each cross section ($\bar{F}$ times the denominator in Eq. 5a is the moment generated by the connector forces perpendicular to AOB, which balances the moment from P_p about point O). If $n/n*$ is assumed to be large compared to one, Eq. 5a simplifies to

$$\bar{F} \cong \frac{3P_p\,(1-\cos\theta)}{n\ \tan\theta} \tag{6.3.9-5b}$$

Furthermore, for practical (small) values of the subtended angle θ between the maximum moment location and the simply supported end of the girder, $\cos\theta$ may be approximated as $1-\theta^2/2$, $\tan\theta$ may be approximated as θ, and Eq. 5b may be written as

$$\bar{F} \cong \frac{1.5\,P_p\,\theta}{n} \tag{6.3.9-5c}$$

where θ is expressed in radians. AASHTO (2020) Article 6.10.10.4.2 neglects the 1.5 coefficient in Eq. 5c. This is justified by the conservative nature of the assumption that the connectors are all

located along AOB. Also, Article 6.10.10.4.2 idealizes $\bar{F}$ as perpendicular to $\bar{P}$ in writing the vector sum of the shear forces. This leads to a total force

$$P = \sqrt{P_p^2 + F_p^2}$$
(6.3.9-6) (AASHTO 6.10.10.4.2-1)

that replaces P_p in Eq. 2, where

$$F_p = n\,\bar{F} = P_p\theta = P_p\,\frac{L_p}{R}$$
(6.3.9-7) (AASHTO 6.10.10.4.2-4)

Colville (1972) discusses other contributions to the shear connector radial forces that come from the uniform St. Venant and nonuniform warping torsion of the composite I-girder between the brace points, where the brace points are indicated by the larger radial arrows on the free-body diagram of the steel I-section in Figure 74. He concludes that these forces are small compared to the above forces $\bar{P}$ and $\bar{F}$. Nevertheless, the assumption that the connector radial forces increase linearly with their distance from point O in Figure 76 is inconsistent with Colville's open-section thin-walled beam theory analysis of the composite I-section member to determine the connector forces due to St. Venant and warping torques. The above calculation of the connector radial loading effect from Eqs. 6 and 7 should be considered as no more than a reasonable but coarse approximation of the true radial loading effects on the shear connectors. The above equations are based on a constant radius of curvature R between the maximum moment location and the simply supported girder ends. For more general girder geometries, R may be taken conservatively as the minimum girder radius over the length under consideration.

A more conservative estimate of the shear connector radial force is used in Article 6.10.10.1.2 for calculating the connector radial fatigue shear range for horizontally curved bridges and in straight bridges with skews exceeding 20°. If written in terms of the forces under strength load conditions (which is the focus of the discussions in this volume), these estimates would be

$$\bar{F} \cong A_{bot}\,f_{bu.bot}\,\frac{L_b}{R}\,\frac{1}{n_w}$$
(6.3.9-8)

and

$$\bar{F} \cong \frac{F_c}{n_w}$$
(6.3.9-9)

where

$\quad$ A_{bot} $\quad=\quad$ area of the bottom flange

$\quad$ $f_{bu.bot}$ $\quad=\quad$ elastically computed bottom flange stress

$\quad$ L_b $\quad=\quad$ distance between brace points

$\quad$ R $\quad=\quad$ horizontal radius of curvature at the brace point under consideration

F_c = cross-frame or diaphragm force at the top flange, taken as the total radial force transferred to the I-girder from all the components of the cross frames or diaphragms on each side of the girder at the location under consideration (the assumption associated with this calculation is that this total radial force must be balanced by a shear that is transferred to the slab by the shear connectors)

n_w = number of shear connectors within an effective length of the deck over which the total radial force from the cross frames is developed, taken as 48 inches at interior locations and 24 inches at end supports for calculation of the connector radial fatigue shear range in Article 6.10.10.1.2

AASHTO (2020) Article 6.10.10.4 takes Eqs. 6 and 7 as a sufficient estimate of the shear connector radial loads under strength conditions. It uses formulas related to Eqs. 8 and 9 for checking the fatigue shear force range in the shear connectors in horizontally curved bridges and in bridges with skews exceeding 20°.

Colville (1972) also discusses a conservative calculation of the vertical (uplift) forces on shear connectors due to the restraint provided to twisting of the steel I-girders from the bridge deck. His equations for estimating these forces tend to be small compared to the vector sum of the longitudinal and radial forces. Furthermore, the downward dead and live loads located above the I-girder-to-slab interface counteract these local uplift forces. Therefore, AASHTO (2020) Article 6.10.10 does not require any consideration of uplift forces on the shear connectors. Article 6.10.10.1.1 simply specifies that the connectors shall be capable of resisting both horizontal and vertical movement between the concrete and the steel.

AASHTO (2020) Article 6.10.10.4.3 specifies the nominal shear resistance of a single stud shear connector embedded in a concrete deck as

$$Q_n = 0.5 A_{sc} \sqrt{f_c' E_c} \le A_{sc} F_u \qquad \text{(6.3.9-10) (AASHTO 6.10.10.4.3-1, AISC I3-3)}$$

where

A_{sc} = cross-sectional area of the stud shear connector,

E_c = modulus of elasticity of the deck concrete,

f_c' = compressive strength of the deck concrete,

F_u = specified minimum tensile strength of the stud shear connector.

Also, an alternate equation is specified for the strength of less commonly used channel shear connectors. Channel shear connectors should not be used in curved bridges or bridges with skews larger than 20° due to the combined longitudinal and radial loading effects.

The above calculations of P_p and F_p apply only to simple span bridges, and to the length between the position of the maximum positive moment (taken as the maximum live load plus impact moment) and the adjacent point of zero moment in continuous-span bridges that are noncomposite for negative flexure in the final condition. For I-girders in continuous-span bridges that are composite for negative flexure in the final condition, a larger total longitudinal force must be

developed in the length between the maximum positive moment position and the centerline of an adjacent interior support. This is handled by replacing P_p in Eqs. 1, 2, 6 and 7 by

$$P_T = P_p + P_n \qquad \text{(6.3.9-11) (AASHTO 6.10.10.4.2-6)}$$

where P_n is an estimate of the total force developed in the negative moment cross section of the concrete deck over the interior support. That is, the model of Figure 75 is replaced by the one shown in Figure 77. The force P_n is calculated as

$$P_n = \min \begin{pmatrix} 0.45\, f_c'\, b_s\, t_s, \\ F_{yw}\, D\, t_w + F_{yt}\, b_{ft}\, t_{ft} + F_{yc}\, b_{fc}\, t_{fc} \end{pmatrix} \qquad \text{(6.3.9-12)}$$

$$\text{(AASHTO 6.10.10.4.2-7 \& 6.10.10.4.2-8)}$$

at the interior support cross section. The first term in this equation is intended as a conservative estimate of the combined contribution of both the longitudinal reinforcement and the concrete that remains effective in tension at the maximum negative moment cross section.
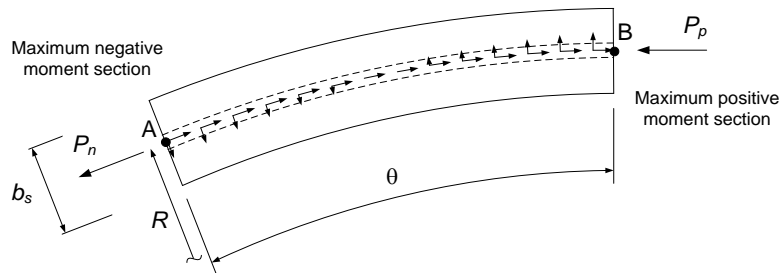
Figure 77. Plan view free-body diagram of the slab between the maximum positive moment and maximum negative moment positions.

6.3.10 Other Limit States

This section highlights a number of strength limit states pertaining to I-section flexural members that are somewhat separate from the overall flow and logic of the behavioral considerations discussed in the previous sections. Nevertheless, all strength limit states are essential to the proper structural performance.

6.3.10.1 Net section fracture

AASHTO (2020) Article 6.10.1.8 addresses the potential fracture through the net section of tension flanges containing holes typically used for connectors such as bolts. This article implements the check

$$f_t \le 0.84 \frac{A_n}{A_g} F_u \le F_{yt} \qquad \text{(6.3.10-1) (AASHTO 6.10.1.8-1)}$$

where

f_t = the elastically computed stress on the gross area of the tension flange, not including flange lateral bending but presumably including the stress due to tensile axial force if it exists,

A_n = the net tension flange area at the holes, calculated as discussed in Section 6.1.1 of this volume,

A_g = the gross area of the tension flange, and

F_u = the specified minimum tensile strength of the tension flange.

By multiplying each of the expressions in Eq. 1 by A_g and noting that $0.84 \cong \phi_u / \phi_y = 0.80 / 0.95$, one can observe that this equation effectively considers the tension flange as a tension member according to AASHTO Article 6.8 (discussed in Section 6.1.1) and ensures that tension yielding will govern relative to tension fracture based on these provisions. Dexter and Altstadt (2004) indicated that due to the constraint provided by the web, net section fracture of the tension flange is less critical than the tension member equations imply. Therefore, Eq. 1 is expected to provide a conservative evaluation of potential net section fracture. Further research may justify some liberalization of this requirement.

6.3.10.2 Web bend buckling

The web bend buckling resistance does not enter directly into the flexural resistance of I-section members at strength load levels except in the context of influencing when the web load-shedding parameter R_b is less than one, via Eqs. 6.3.5-3 through 6.3.5-6. However, the AASHTO (2020) Article 6.10.3 and 6.10.4.2 provisions for constructability and for the Service II permanent deflection limit states directly restrict the elastically computed compression flange stress to the nominal web bend buckling stress as a simple device to help limit web plate bending and transverse displacements under these conditions. As noted in AASHTO Article C6.10.5.3 on special fatigue requirements for webs, the Article 6.10.4.2 provisions with respect to web bend buckling under the Service II load combination always govern relative to a comparable check of web bend buckling using the fatigue load combinations of this article. Therefore, theoretical web bend buckling is effectively prevented also under the AASHTO (2020) factored fatigue loading.

AASHTO Article 6.10.1.9.1 defines the web bend buckling resistance as

$$F_{crw} = \frac{0.9Ek}{\left(D / t_w\right)^2} \qquad\qquad \text{(6.3.10-2) (AASHTO 6.10.1.9.1-1)}$$

which is again the classical elastic plate buckling equation shown previously as Eqs. 6.2.4-1 and 6.3.8-1, but with another expression for the buckling coefficient k. AASHTO Article 6.10.1.9.1 defines the web bend buckling coefficient as

$$k = \frac{9}{(D_c / D)^2} \qquad\qquad \text{(6.3.10-3) (AASHTO 6.10.1.9.1-2)}$$

for webs without longitudinal stiffeners. Article 6.10.1.9.2 defines the web bend buckling coefficient as

$$k = \frac{5.17}{\left(d_s / D\right)^2} \geq \frac{9}{\left(D_c / D\right)^2} \qquad \text{(6.3.10-4a) (AASHTO 6.10.1.9.2-1)}$$

for longitudinally-stiffened webs with $d_s/D_c \geq 0.4$ and by

$$k = \frac{11.64}{\left(\dfrac{D_c - d_s}{D}\right)} \qquad \text{(6.3.10-4b) (AASHTO 6.10.1.9.2-2)}$$

for other longitudinally-stiffened webs, where d_s is the depth between the compression flange and the longitudinal stiffener.

It should be noted that the bend buckling resistance for webs without longitudinal stiffeners is actually based on the slenderness $2D_c/t_w$, and that the corresponding bend buckling coefficient is $k = 36$ when c_{rw} in Eqs. 6.3.5-1 is equal to 5.7. The Eq. 2 form is specified so that a single equation can be applied for webs with and without longitudinal stiffeners. For a doubly symmetric I-section without longitudinal stiffeners, the above constant $k = 36$ is approximately equal to $k_{ss} + 0.8(k_{sf} - k_{ss})$, where $k_{ss} = 23.9$ and $k_{sf} = 39.6$ are the bend buckling coefficients for simply supported and fully-restrained longitudinal edge conditions respectively (Timoshenko and Gere 1961). For singly symmetric I-sections, Eqs. 2 and 3 provide a reasonably accurate approximation of the theoretical bend buckling resistance (Ziemian 2010) consistent with $k = k_{ss} + 0.8(k_{sf} - k_{ss})$.

A value of $c_{rw} = 4.6$ in Eqs. 6.3.5-1 corresponds to a bend buckling coefficient of $k = k_{ss} = 23.9$.

For webs without longitudinal stiffeners, Eqs. 2 and 3 predict $F_{crw} = F_{yc}$ at $2D_c/t_w = \lambda_{rw}$ given by Eq. 6.3.5-1. The potential use of $F_{crw} > F_{yw}$ in hybrid members is justified since the flange tends to restrain the longitudinal and plate bending strains associated with web bend buckling for nominal compression flange stresses up to $R_h F_{yc}$. ASCE (1968) recommends that web bend buckling does not need to be considered in hybrid sections with F_{yc} up to 100 ksi as long as the web slenderness does not exceed $5.87\sqrt{E/F_{yc}}$. AASHTO Article 6.10.1.9 adopts a more conservative approach than recommended by ASCE (1968) for $F_{yw}/F_{yc} < 0.7$ by limiting F_{crw} to the smaller of $R_h F_{yc}$ and $F_{yw}/0.7$ in its explicit web bend buckling checks.

Equation 2 generally gives $F_{crw} = F_{yc}$ at $D/t_w = 0.95\sqrt{Ek/F_{yc}}$ as defined by Eq. 6.3.5-5. Equations 4, developed by Frank and Helwig (1995), account for the influence of the location of a single longitudinal stiffener with respect to the compression flange on the web bend buckling resistance. The optimum stiffener position is given by $d_s/D_c = 0.4$, in which case both Eqs. 4a and 4b give $k = 129$ for a doubly symmetric girder. For longitudinally-stiffened webs with $d_s/D_c \geq 0.4$, the web bend buckling deformations occur predominantly within the height d_s between the longitudinal stiffener and the compression flange. Equation 4a results in a web bend buckling stress that is constant with respect to d_s/t_w in this case. For longitudinally-stiffened webs with $d_s/D_c < 0.4$, the web bend buckling deformations occur predominantly within the height $(D - d_s)$ between the longitudinal stiffener and the tension flange. Equations 4 assume simply supported boundary conditions at the flanges. Equation 4a is limited to a minimum value equal to the k for webs without

longitudinal stiffeners (Eq. 3) to recognize the nominal restraint from the flanges in the limit that Eq. 4a would otherwise predict a smaller F_{crw} than if the web did not have a longitudinal stiffener.

Aside from its implicit use in determining when load shedding due to the postbuckling actions of the web must be considered via the R_b factor, the theoretical web bend buckling stress given by Eq. 2 has little significance with respect to the maximum flexural resistance. Article C6.10.1.9.1 emphasizes:

"In many experimental tests, noticeable web plate bending deformations and associated transverse displacements occur from the onset of load application due to initial web out-of-flatness. Because of the stable postbuckling behavior of the web, there is no significant change in the rate of increase of the web transverse displacements as a function of the applied loads as the theoretical web bend-buckling stress is exceeded (Basler et al. 1960). Due to unavoidable geometric imperfections, the web bend-buckling behavior is a load-deflection rather than a bifurcation problem. The theoretical web-buckling load is used in these Specifications as a simple index for controlling the web plate bending strains and transverse displacements."

6.3.10.3 Web longitudinal stiffeners

The AASHTO (2020) Article 6.10.11.3 provisions specify the following requirements for the design of web longitudinal stiffeners in I-girders subjected to flexure:

1. Web longitudinal stiffeners nominally must not yield when subjected to the idealized stress due to major-axis bending, i.e.,

$$f_s \leq \phi_f R_h F_{ys} \qquad\qquad\qquad (6.3.10\text{-}5) \text{ (AASHTO 6.10.11.3.1-1)}$$

   where

   f_s = the elastic stress at the longitudinal stiffener due to major-axis bending, calculated assuming a linear variation in the flexural stress through the depth of the web and

   F_{ys} = the specified minimum yield strength of the stiffener.

   The yield strength of the stiffener is multiplied by the hybrid strength reduction factor to account conservatively for the influence of early web yielding on the stiffener stress in hybrid members. Article C6.10.11.3 suggests that R_h in Eq. 5 should be taken as the value applied to the flanges at the strength limit state. Lateral bending of longitudinal stiffeners due to eccentricity of the stiffener with respect to the web plate, and/or due to horizontal curvature, is neglected in Eq. 5.

2. Web longitudinal stiffeners must not buckle locally prior to reaching their yield strength in uniform axial compression. This is achieved by satisfying the following slenderness limit, assuming rectangular plate longitudinal stiffeners

$$b_s \leq 0.48 t_s \sqrt{\frac{E}{F_{ys}}}$$
(6.3.10-6) (AASHTO 6.10.11.3.2-1)

which corresponds to the Γ_r from Case 1c of Table 5 with an assumed plate local buckling coefficient of $k_c = 0.56$.

3. Web longitudinal stiffeners and a portion of the web adjacent to them, acting as an equivalent column, must not fail by flexural buckling prior to development of the yield strength of the compression flange. This is achieved by:

- Assuming that the equivalent column fails by inelastic buckling,

- Using the traditional CRC column inelastic buckling formula, and

- Assuming a linear variation in the flexural stress through the depth of the web as in the first requirement above.

These combined idealizations give

$$R_h F_{ys} \left[1 - \frac{1}{4} \left(\frac{d_o}{r} \right)^2 \left(\frac{F_{ys}}{E} \right) \frac{1}{\pi^2} \right] \geq \left(1 - \frac{d_s}{D_c} \right) F_{yc}$$
(6.3.10-7a)

The stiffener yield strength is multiplied by the hybrid factor, R_h, on the left-hand side of this equation, but the hybrid factor is not included in the reduction for column inelastic buckling in the square brackets on the left-hand side. The longitudinal stiffener is taken as a simply supported column with an effective length equal to the spacing between the transverse stiffeners, d_o, within the reduction for column inelastic buckling. The right-hand side of this equation is simply the elastic stress at the location of the longitudinal stiffener when the compression flange reaches its yield strength F_{yc}. If Eq. 7a is solved for the required radius of gyration of the equivalent column, one obtains

$$r \geq \frac{0.16 d_o \sqrt{\dfrac{F_{ys}}{E}}}{\sqrt{1 - \left(1 - \dfrac{d_s}{D_c} \right) \dfrac{F_{yc}}{R_h F_{ys}}}}$$
(6.3.10-7b)

The Engineer is required to include an effective width of the web of $18t_w$ with the longitudinal stiffener in calculating the radius of gyration r. Also, it is required that the radius of gyration shall be calculated about the neutral axis of the combined effective cross section (one is not allowed to assume that the neutral axis is located at the edge of the stiffener in contact with the web, as specified for transverse stiffeners). This requirement is based on the recommendations by Cooper (1967). Cooper recommended the use of a mean effective width of $20t_w$ based on the results of strain measurements reported by Massonnet (1960). The effective width of $18t_w$ is specified to conform to traditional assumptions in American bridge design, as discussed by Vincent (1969). Lastly, AASHTO

(2020) invokes one additional simplification that is justified given all the above idealizations and assumptions utilized in arriving at Eq. 7b. Rather than make the required radius of gyration a function of d_s/D_c, AASHTO Article 6.10.11.3 addresses the influence of the location of the longitudinal stiffener solely via Eq. 5 and assumes the optimum location $d_s/D_c = 0.4$ in Eq. 7b to obtain

$$r \geq \frac{0.16d_o\sqrt{\dfrac{F_{ys}}{E}}}{\sqrt{1-0.6\dfrac{F_{yc}}{R_hF_{ys}}}} \qquad\qquad \text{(6.3.10-7c) (AASHTO 6.10.11.3.3-2)}$$

4. Web longitudinal stiffeners must be stiff enough to maintain a line of near zero lateral deflection at their juncture with the web plate for load levels up to the calculated bend buckling resistance of the web. This is achieved by satisfying

$$I_\ell \geq Dt_w^3 \left[2.4\left(\frac{d_o}{D}\right)^2 - 0.13 \right]\beta \qquad\qquad \text{(6.3.10-8) (AASHTO 6.10.11.3.3-1)}$$

where

I_ℓ = moment of inertia of the longitudinal stiffener including an effective width of the web equal to $18t_w$ taken about the neutral axis of the combined section. If F_{yw} is smaller than F_{ys}, the strip of the web included in the effective section shall be reduced by the ratio F_{yw}/F_{ys}.

β = correction factor for horizontal curvature, taken as 1.0 for straight I-girders.

Equation 8 with $\beta = 1$ gives a good fit to the results from Dubas (1948) for the required lateral rigidity of longitudinal web stiffeners in doubly symmetric I-girders with $0.5 \leq d_o/D \leq 1.6$, a single longitudinal stiffener located at the optimum position $d_s = D/5$, an effective width of the web acting with the stiffener of $20t_w$, and an upper-bound stiffener-to-web area ratio $A_s/A_w = A_s/Dt_w$ of 0.1. Dubas (1948) accounted for the fact that the necessary rigidity depends not only on the panel aspect ratio d_o/D, but also on the ratio of the stiffener area to the total web area A_s/A_w. The required I_ℓ is smaller for lesser values of A_s/A_w, and hence Eq. 8 may be considered as a reasonable upper bound for the necessary moment of inertia of the combined stiffener and web effective width (conservatively taken as $18t_w$).

It is important to recognize that the true web bend buckling resistance is a continuous function of the longitudinal stiffener properties. For stiffener I_ℓ values larger than specified by Eq. 8, the web bend buckling resistance asymptotes gradually to a maximum value as I_ℓ approaches infinity. For I_ℓ values somewhat smaller than specified by Eq. 8, the web bend-buckling resistance starts to reduce significantly due to increasing participation of stiffener lateral deformations in the web buckling mode. Also, it is important to note that the theoretical web bend buckling stress is not necessarily the maximum limit of the flexural resistance.

Equation 8 neglects any influence of the stiffener location, d_s/D, or the fraction of the web depth in compression, D_c/D, on the required I_ℓ. Frank and Helwig (1995) showed that Eqs. 2 and 4 give an accurate to slightly conservative estimate of F_{crw} values determined from finite element analysis for a wide range of doubly and singly symmetric web panels with $d_o/D = 1$ using minimum-size longitudinal stiffeners based on the AASHTO (1998) requirements. For $\beta = 1$, Eqs. 6 and 8 are identical to the AASHTO (1998) requirements except that AASHTO (1998) specified that I_ℓ should be calculated about the edge of the stiffener in contact with the web. AASHTO (2020) specifies that I_ℓ is to be calculated about the true neutral axis for the combined stiffener and effective width of the web ($18t_w$) based on Cooper (1967). For $F_{ys} = F_{yc}$ and $R_h = 1$, Eq. 7c requires an eight percent larger radius of gyration, r, relative to d_o, as well as the calculation of $r = \sqrt{I_\ell / \left(b_s t_s + 18 t_w^2\right)}$ using I_ℓ determined as specified above. Therefore, the minimum size longitudinal stiffeners studied by Frank and Helwig (1995) had I_ℓ values that range from 72 to 81 percent of the AASHTO (2020) requirement from Eq. 8, and they had r values that range from 64 to 131 percent of the AASHTO (2020) requirement from Eq. 7c. Frank and Helwig (1995) pointed out that one source of conservatism in their study is the fact that the longitudinal stiffeners participate in resisting the overall bending applied to the I-girder. That is, they do not apply flexural stresses directly to the longitudinal stiffeners in their study, but the longitudinal stiffeners tend to attract stress due to their compatibility with the web plate. Subramanian and White (2017c) show that it is acceptable and appropriate to include the contribution from the longitudinal stiffeners to the moment of inertia and elastic section moduli of the overall girder section.

It is important to note that Eq. 8 and the results from Dubas (1948) are based only on linear buckling analysis. Therefore, Eq. 8 gives an I_ℓ that guarantees only the development of the web bend-buckling resistance given by Eqs. 2 and 4. Longitudinal stiffener rigidities as much as seven times larger have been found to be necessary to ensure the integrity of the longitudinal stiffeners within the postbuckling range of the web response, e.g., see Ziemian (2010) and Owen et al. (1970).

For horizontally curved girders, AASHTO (2020) requires an increase in the required I_ℓ to account for the tendency of the web to bow and the tendency of the longitudinal stiffeners to bend laterally. This is accomplished via the parameter β, given by

$$\beta = Z/6 + 1 \qquad\qquad\qquad \text{(6.3.10-9a) (AASHTO 6.10.11.3.3-3)}$$

for cases where the longitudinal stiffener is on the side of the web away from the center of curvature, and

$$\beta = Z/12 + 1 \qquad\qquad\qquad \text{(6.3.10-9b) (AASHTO 6.10.11.3.3-4)}$$

for cases where the longitudinal stiffener is on the side of the web toward the center of curvature, where

$$Z = \frac{0.95 d_o^2}{R t_w} \qquad\qquad\qquad \text{(6.3.10-10) (AASHTO 6.10.11.3.3-5)}$$

is referred to as the curvature parameter. This parameter is limited to a maximum value of 12. When a longitudinal stiffener is placed on the side of the web away from the center of curvature, the eccentricity of the stiffener with respect to the web plate gives a bending effect that is additive with the effect of the horizontal curvature. Conversely, when the longitudinal stiffener is placed on the side of the web toward the center of curvature, the eccentricity of the stiffener gives a bending effect that counteracts the effect of the horizontal curvature.

Equations 9 are a simplification of the Hanshin (1988) provisions for longitudinal stiffeners developed by Hall et al. (1999). The reader is referred to Nakai and Yoo (1988) for a summary of the Hanshin (1988) equations. A comparison of the AASHTO (2020) and Hanshin (1988) requirements gives the following results:

- For $d_o/D = 0.5$, Eqs. 8 through 10 give a net I_ℓ requirement ranging from about 0.3 to 1.0 of that from the Hanshin provisions.

- For $d_o/D = 1.0$, the AASHTO equations give a net requirement ranging from about 1.0 to 2.0 times that from the Hanshin provisions.

- For $d_o/D = 1.5$, Eqs. 8 through 10 give a net requirement ranging from about 1.0 to 3.0 times that of the Hanshin provisions.

The Hanshin provisions are based on preventing nominal yielding of the longitudinal stiffener and a portion of the web acting together as a beam-column. These provisions assume that longitudinal stiffeners are continuous across the transverse stiffener locations; hence, it is imperative that the detailing of the longitudinal stiffeners is consistent with this assumption. The reason for the more liberal nature of the AASHTO equations for small d_o/D stems predominantly from the fact that the Hanshin provisions require a larger I_ℓ for straight I-girders with small d_o/D.

The behavior of stiffened plate assemblies is one of the areas of greatest complexity in the analysis and design of steel structures. The AASHTO (2020) Article 6.10.11.3 provisions for longitudinal stiffeners are a basic set of criteria for proper proportioning of longitudinal stiffeners in the webs of I-girders subjected solely to flexure. These provisions are not intended for members that are subjected to combined flexure and axial compression. The reader is referred to Section 7 of this volume for discussion of the broader problem of combined flexure and axial compression in members with longitudinally-stiffened webs.

6.3.10.4 Bearing stiffeners

AASHTO (2020) Article 6.10.11.2 addresses the design of bearing stiffeners. AASHTO Article 6.10.11.2.1 requires full-depth bearing stiffeners on built-up sections at all bearing locations. This is consistent with the AISC (2016) provisions for unframed ends of beams and girders, and helps ensure adequate member torsional restraint at support locations. At bearing locations on rolled shapes and at other locations on built-up sections or rolled shapes where the concentrated loads are not transmitted through a deck or deck system, either bearing stiffeners must be provided or the web must satisfy the provisions of Article D6.5 (discussed below).

Bearing stiffeners are designed using the AASHTO Article 6.9.2.1 column strength equations and assuming an effective length equal to 0.75D. Also, bearing stiffeners are required to satisfy the

same limit as Eq. 6 to ensure against local buckling, the areas at the ends of the stiffeners (where the stiffeners are clipped to clear the web-to-flange fillet weld) must be sufficient to accept the bearing loads, and the connection of the stiffeners to the web must be sufficient to transmit the full bearing force to the web. AASHTO Article 6.10.11.2.1 requires plates or angles bolted or welded on both sides of the web, the intent being that the bearing stiffeners should be symmetric about the plane of the web.

With the exception of the restrictions described below, a strip of the web extending not more than $9(F_{yw}/F_{ys})\ t_w \le 9\ t_w$ on each side of the stiffener elements may be included as part of the effective column area. If multiple stiffener pairs are used, the effective column section may include the web area extending up to $9(F_{yw}/F_{ys})\ t_w \le 9t_w$ on each side of the outer projecting elements of the web. If the stiffeners are bolted to the web or if F_{yw} is less than 70 % of the specified minimum yield strength of the higher strength flange at interior supports of continuous-span members, only the stiffener elements may be included in the effective column cross section. The first of these conditions guards against the loss of compatibility between the web and the stiffeners due to slip within the bolted connection.   The second of these conditions guards against the loss of effectiveness of a hybrid web due to early yielding caused by longitudinal flexural stresses.

6.3.10.5 Web yielding and web crippling

Webs of built-up sections and rolled shapes subjected to concentrated loads at locations that do not have bearing stiffeners, and where the loads are not transmitted through a deck or deck system, must be designed to prevent transverse web yielding or web crippling at the concentrated loads. If the loads are transmitted through a deck or deck system, they are assumed to be adequately distributed to the web such that these failure modes do not occur. AASHTO (2020) Article D6.5 specifies the same web yielding and web crippling limit state equations as in AISC (2016) to guard against these secondary failure modes. The web yielding and web crippling limit states can be important in some cases during construction, for example during incremental launching over supports, where temporary concentrated loads may be applied to the members at locations that do not have bearing stiffeners.

6.4   Composite Box-Section Flexural Members

6.4.1   Introduction

The design of composite box-girder bridges is generally more involved than the design of I-girder bridges. AASHTO (2020) Articles 6.7.4.3, 6.7.5.3 and 6.11 address various considerations specific to composite box-girder bridge design. Coletti et al. (2006 and 2005) provide useful summaries of the broad analysis and design considerations for tub girder bridges, which as noted in Section 2.3 of this volume are the predominant type of box-girder construction in the United States. Composite box-girder bridges require a number of unique considerations tied to the design of the individual girder elements. Also, they contain a number of components other than just the box girders themselves, components that are essential to the behavior of the girders and the corresponding overall structural system. These include:

- Diaphragms inside the individual girders at points of support, to transmit the girder vertical reactions and torques to the support bearings, which generally are not located directly under the girder webs.

- Intermediate cross frames inside the individual boxes at certain intervals along their span to maintain the shape of the cross section, and in tub girders, to help brace the narrow top flanges prior to placement of the deck.

- External diaphragms between the box girders at supports to transmit the torsional reactions across the entire bridge width between the inside and outside bearings, and to restrain individual girder torsional rotations at the support lines (such rotations tend to impact the girder torsional rotations throughout the span length). Also, at end support lines, these diaphragms provide support for an expansion joint.

- For tub girders, lateral bracing inside the individual boxes near the top flanges to make the girders act as a pseudo-closed section prior to composite action of the slab. After composite slab action is achieved, the slab itself acts predominantly as the top flange of the box, rendering the lateral bracing redundant for subsequent loading. Nevertheless, the top lateral bracing system still can be an important element during future redecking.

In spite of the unique attributes of composite box girders and box-girder bridges, many of the requirements for their design can be taken directly from the requirements for I-girder bridges. For instance, the general requirements for analysis of the composite structure and for consideration of slab reinforcing in negative bending regions, hybrid webs, variable web depth, lateral bending stresses in the top flanges of tub girders during construction, net section fracture at cross sections containing holes in a tension flange, and web bend buckling are largely the same as the I-girder requirements. As such, Article 6.11 refers back to Article 6.10 in numerous places rather than duplicate the I-girder provisions.

AASHTO (2020) specifies several broad restrictions intended to limit its scope to the most common types of composite box-girder bridges:

- Only single-cell box girders are addressed. Multiple-cell box girders require additional considerations.

- Only moderate span lengths less than or equal to 350 ft are considered. Article C6.11.1 states that the AASHTO provisions may be applied to larger spans "based on a thorough evaluation of the application of the bridge under consideration consistent with basic structural fundamentals." This article references the Wolchuk and Mayrbaurl (1980) straight box-girder specification for additional information regarding the design of long-span steel box-girder bridges.

- Only box-girder bridges that have a composite concrete deck throughout their length in their final constructed configuration are addressed. Articles 2.5.2.6, 4.6.2.6.4, 6.14.3 and 9.8.3 address the design of orthotropic steel decks and orthotropic deck superstructures in general. However, AASHTO (2020) does not address the design of the other components

of box girders in combination with the use of an orthotropic deck. Orthotropic deck box-girder bridges are typically longer than the above moderate length definition.

- Only composite top flanges are addressed. The behavior and design of composite bottom flanges is not considered.

Section 6.4 of this volume provides an overview of the behavior of composite box-girder bridges and the corresponding AASHTO (2020) design provisions. Section 6.4.2 first focuses on several overriding system behavioral considerations. AASHTO (2020) categorizes composite box-girder bridges into two main groups, one for which various analysis and design simplifications are allowed and a second for which more detailed analysis and design procedures are necessary. Section 6.4.2 summarizes the restrictions applied to bridges classified in the first of these groups as well as the specific simplified analysis and design procedures allowed for these types of bridges. Section 6.4.2 then summarizes the more detailed procedures required for bridges not satisfying these restrictions. Sections 6.4.3 and 6.4.4 then outline additional general AASHTO (2020) requirements applicable to all types of composite box-girder bridges as well as requirements for several specific composite box-girder bridge types respectively. The remaining sections of Section 6.4 focus on the strength behavior and design of the box girders themselves. The discussions in these sections largely parallel those in the previous Sections 6.3.2 through 6.3.9 on I-section flexural members. In places where the I-girder provisions are applicable, Sections 6.4.5 through 6.4.14 refer back to the previous discussions.

Prior to discussing the behavior and design of composite box girders in detail, it is useful to establish the following definitions, adapted from AASHTO Article 6.2:

Tub section – An open-top steel girder composed of a bottom flange plate, two inclined or vertical web plates, and an independent top flange attached to the top of each web. The Specifications require that the top flanges of straight tub girders must be connected with either a partial- or a full-length lateral bracing system, with due consideration of the lateral stability of the top flanges and the overall stability of the members. A full-length lateral bracing system is required for curved tub girders.

Closed-box section – A member having a cross section composed of two vertical or inclined webs and top and bottom stiffened or unstiffened steel plate flanges. In the context of Article 6.11, the top flange of a closed-box section is always composite with a concrete deck in the final constructed configuration.

Box flange – A flange that is connected to two webs. The flange may be a flat unstiffened plate, a stiffened plate or a top flat plate with reinforced concrete attached with shear connectors. In this section, "stiffened" means that longitudinal and/or transverse stiffeners are attached to the plate, whereas "unstiffened" means that the plate does not have any longitudinal or transverse stiffeners. This is consistent with the AASHTO (2020) terminology in Article 6.9.4, discussed previously in Section 6.2.4 of this volume, but differs from the AISC (2016) approach of referring to plates that are supported on one or two longitudinal edges as unstiffened or stiffened, respectively.

Diaphragm – A vertically oriented solid-web transverse member connecting adjacent longitudinal flexural members, or placed inside of a closed-box or tub section to transfer and distribute vertical

and lateral loads, to provide stability to the compression flanges, and to limit the cross-section distortion to acceptable levels.

Cross frame – A transverse truss assembly connecting adjacent longitudinal flexural members, or placed inside of a closed-box or tub section to transfer and distribute vertical and lateral loads, to provide stability to the compression flanges, and/or to limit the cross-section distortion to acceptable levels.

6.4.2   Categorization of Composite Box-Girder Bridges in AASHTO (2020)

6.4.2.1   Straight multiple-box-girder bridges satisfying the restrictions in AASHTO Article 6.11.2.3 and having fully effective flanges

AASHTO Article 6.11.2.3 specifies the following restrictions that are first stated as being necessary for the applicability of line girder analysis using the live-load lateral distribution factor equations of Article 4.6.2.2.2 for multiple steel box girders with a concrete deck. However these restrictions, combined with additional limits, also form the basis for a number of other analysis and design simplifications. The additional limits and the corresponding analysis-design simplifications are discussed subsequently. The specific requirements for use of the above basic live-load distribution factor equations are:

- The bridge cross section must consist of two or more single-cell box sections.

- The bridge should not have any horizontally curved segments (the influence of horizontal curvature generally extends beyond the horizontally curved segments and into other straight spans of the structure).

- The bridge shall not have any support skew.

- At midspans, $0.8w \leq a \leq 1.2w$, where w is the center-to-center distance between the top flanges of the box girders and a is the center-to-center distance between the flanges of adjacent box sections (see Figure 21).

- For nonparallel box girders, $0.65w \leq a \leq 1.35w$ must be satisfied at the supports.

- The value of w must be the same for all of the girders.

- The inclination of the webs with respect to a plane normal to the bottom flange shall not exceed 1 to 4.

- The width of concrete deck cantilever overhangs, w_o, including curbs and parapets, shall satisfy $w_o \leq \min (0.6\, a_{avg}, 6\,\text{ft})$, where a_{avg} is the average a dimension along the span length.

These restrictions are based on the range of bridge characteristics considered in the original development of the composite box-girder lateral load distribution factors by Johnston and Mattock (1967).

In addition to the above restrictions, AASHTO Article 6.11.1.1 specifies that a box flange may be considered to be fully effective in resisting flexure (i.e., no reduction in resistance due to shear lag effects) when $b_f \leq L/5$, where L is taken as the span length for simple spans and the distance between points of permanent load contraflexure or between a simple support and a point of permanent load contraflexure for continuous spans. For negative moment regions in continuous-span box girders, L is taken as the distance between the points of permanent load contraflexure on each side of the support.

The above simplified rule comes from studies of simple-span bridges with L/b_f ranging from 5.65 to 35.3 (Goldberg and Leve 1957). The effective flange width ranged from 0.89 for the bridge with the smallest L/b_f to 0.99 for the bridge with the largest L/b_f in these studies. Dowling and Harding (1992) also indicate that box flanges may be considered as fully effective except in cases with particularly large aspect ratios (i.e., large b_f/L), or cases with particularly slender edge panels or stiffeners. AASHTO 4.6.2.6.4 gives the same basic rules for simplified analysis of box girders employing orthotropic steel decks.

Various AASHTO (2020) articles specify analysis and design simplifications for box-girder bridges that: satisfy all of the above requirements for (1) use of the simple live-load distribution factor equations and (2) consideration of the box flange or flanges as fully effective. These analysis and design simplifications are as follows:

- Stresses due to distortion of the box cross section (when it is subjected to torsion) may be neglected (Article C6.11.2.3). These are the shear, warping and plate bending stresses illustrated previously in Figure 20. AASHTO (2020) allows these stresses to be neglected both for consideration of strength as well as for consideration of fatigue (see Article 6.11.5).

- If several other requirements are also satisfied (discussed subsequently), composite box girder sections in positive flexure may be designed as "compact" sections using the provisions of Article 6.11.7.1 (this is specified in Article 6.11.6.2.2).

- Shear stresses due to St. Venant torsion may be neglected (Article C6.11.2.3).

- The shear connectors between the slab and the steel girders need be designed only for flexural shear (Article 6.11.10).

- The Engineer may consider reducing the number of intermediate internal cross frames to a minimum of: (1) points of maximum moment in the span, (2) points adjacent to field splices, and (3) points required to avoid excessive stresses during transportation and lifting of shipping pieces (Article C6.7.4.3). Article C6.7.4.3 also indicates that internal bracing members inserted for transportation, lifting and/or construction may be handled as temporary members. Nevertheless, Article C6.7.4.3 also states that additional cross-frame members may be required for construction. This statement either requires the use of judgment about potential construction conditions, such as eccentric loading causing torsion, and/or analysis of potential construction conditions to check the St. Venant shear and distortional stresses and deformations. Furthermore, Article C6.7.4.3 states that in tub sections with inclined webs, additional intermediate cross frames, diaphragms or struts may

be required to reduce the lateral bending in the discretely-braced top flanges during construction. Lastly, Article C6.11.1.3 states that at least two intermediate internal cross frames or diaphragms are necessary to reduce the magnitude of the secondary stresses due to distortion of the cross section at the web-to-flange welds to an extent (i.e., by more than 80 %) such that fillet welds on both sides of the web designed according to Article 6.13.3.4 may be assumed to be adequate. In short, although it is possible to reduce the number of internal cross frames in bridges satisfying the above restrictions, there are a number of additional considerations that must be addressed.

6.4.2.2 Composite box-girder bridges not satisfying one or more of the above requirements

AASHTO (2020) specifies the following more detailed analysis and design procedures for composite box-girder bridges not satisfying one or more of the above requirements:

- The bridge should be analyzed using a refined analysis, i.e., an analysis that captures the three-dimensional responses of the structure (Article C6.11.2.3).

- For wide bridges in which the box flanges are not considered fully effective, the box-flange width is to be taken as $L/5$ in calculating the major-axis bending stresses (Article 6.11.1.1). However, the full box flange width is to be used in the applicable resistance equations.

- Internal diaphragms or cross frames shall be provided to control the cross-section distortion, with the spacing not to exceed 40 ft (Article 6.7.4.3). Article C6.7.4.3 elaborates that internal diaphragms and cross frames: (1) "must" be spaced to limit the plate bending stresses due to distortion (see Figure 20) to 20 ksi at the strength limit state (this is stated as a requirement in Article 6.11.1.1), and (2) should be spaced to limit the longitudinal warping stresses (see Figure 20) to 10 % of the normal stresses due to major-axis bending at the strength limit state (Article 6.11.1.1 states that these stresses may then be ignored at the strength limit state). These plate bending stresses can be estimated using a beam-on-elastic-foundation (BEF) analogy developed by Wright and Abdel-Samad (1968). In this method, the internal cross-braces are analogous to intermediate supports and the resistance to distortion provided by the box cross section is analogous to a continuous elastic foundation. Sample calculations using this method are presented by Heins and Hall (1981), AASHTO (2003) and Grubb et al. (2015). The longitudinal warping stresses due to cross-section distortion also can be determined using the BEF analogy. Given the provision of adequate internal diaphragms and cross frames using these rules, AASHTO (2020) neglects the influence of the plate bending and warping stresses due to cross-section distortion for checking of strength limit states.

- As noted subsequently in Section 6.4.3 of this volume, Article C6.7.4.3 also states that in tub sections with inclined webs, additional intermediate cross frames, diaphragms or struts may be required to reduce the flange lateral bending in discretely-braced top flanges. Furthermore, the following statement from Article C6.11.1.3 still applies: at least two intermediate internal cross frames or diaphragms are necessary to reduce the magnitude of the secondary stresses due to distortion of the cross section at the web-to-flange welds to an extent (i.e., by more than 80 %) such that fillet welds on both sides of the web designed according to Article 6.13.3.4 may be assumed to be adequate.

- In designing the webs for shear, the web shear force shall be taken as the sum of the forces due to flexure and due to the St. Venant torsional shear (Article 6.11.9).

- The top flange shear connectors shall be designed for the sum of the shear forces due to flexure and due to the St. Venant torsion (Article 6.11.10).

- Web splices shall be designed for the sum of the above shears (Article 6.13.6.1.4b).

- The longitudinal warping stresses due to cross-section distortion shall be considered when checking bolted flange splices for slip and for fatigue (Article 6.13.6.1.3c).

- Article C6.11.11.2 indicates that for rare cases where a box flange is exceptionally wide and more than two longitudinal stiffeners may be required, transverse flange stiffeners should be considered to reduce the required size of the longitudinal stiffeners. AASHTO (2020) does not suggest any other conditions requiring a transverse member or transverse stiffener attached to a box flange.

- Article 6.11.5 states that the need for a bottom transverse member within internal cross frames shall be considered. Article 6.11.5 indicates that this member may be needed to limit the plate bending stress range for fatigue in the bottom box flange at the termination of fillet welds connecting cross-frame connection plates to the flange. This article also states that: (1) where provided, the transverse member shall be attached to the box flange unless flange stiffeners are used, in which case the transverse member shall be attached to the longitudinal stiffeners by bolting, and (2) the moment of inertia of these transverse cross-frame members shall be greater than or equal to the moment of inertia of the largest connection plate for the internal cross frame under consideration, taken about the edge in contact with the web. The intent of these provisions is to ensure that the shape of the cross section is maintained, i.e., to limit the transverse bending of the bottom flange due to cross-section distortion at the internal cross-frame locations.

6.4.3 Other General Requirements Applicable to All Types of Composite Box-Girder Bridges

In addition to the above rules and procedures, which differ depending on whether the bridge satisfies the restrictions for simplified analysis and design listed in Section 6.4.2 of this volume or not, AASHTO (2020) specifies other general requirements that apply to all types of composite box-girder bridges. These requirements are summarized in the following subsections.

6.4.3.1 Diaphragm requirements at supports (AASHTO Article 6.7.4.3)

AASHTO Article 6.7.4.3 specifies the following diaphragm requirements at the bridge supports:

- Internal diaphragms or cross frames shall be provided at each support to resist transverse rotation, displacement and cross-section distortion and shall be designed to transmit the torsional moments and lateral forces from the box to the bearings.

- External cross frames or diaphragms shall be used between the boxes at end supports.

- Where box or tub girders are supported on only one bearing, the need for external cross frames between girders at interior supports should be evaluated to ensure torsional stability (these components are also key in controlling the torsional rotations of the individual girders, particularly during construction).

- Diaphragms that are provided for continuity or to resist torsion shall be connected to the webs and flanges of the box section. (It should be noted that studies by Zhou (2006) and Helwig et al. (2007) indicate that it is not essential to connect the diaphragms to the girder flanges when the length to depth ratio of the diaphragm is less than five; fit-up of external diaphragms with the girders during construction is facilitated by not providing a connection to the flanges,)

- The influence of access holes on the stresses in diaphragms should be investigated to determine if reinforcement is required

6.4.3.2   Bearing requirements (AASHTO Article 6.11.1.2)

AASHTO Article 6.11.1.2 specifies the following requirements at bearings:

- Single or double bearings may be used. Double bearings provide a restoring couple on each box, whereas single bearings require bearings on other girders to provide the torsional reactions required for equilibrium.

- Single bearings shall be aligned with the shear center of the box.

Furthermore, Article 6.11.11.1 states that stiffeners are to be designed using the I-girder provisions of Article 6.10.11.2 plus the following additional requirements:

- The bearing stiffeners should be attached to the diaphragms and not to the inclined webs, so that the stiffeners are perpendicular to the sole plate.

- At expansion bearings, the bearing stiffeners and diaphragms should be designed for eccentricity due to the thermal movement. This may be handled by designing the bearing stiffener assembly as a beam-column.

6.4.3.3   Top lateral bracing requirements in tub girders (AASHTO Article 6.7.5.3)

AASHTO Article 6.7.5.3 addresses the top lateral bracing system requirements for tub girders. This article requires a full-length lateral bracing system for curved boxes. Its commentary states that a full-length system should be provided for all straight tub girders with spans greater than about 150 ft, and that a full length system should be considered for general cases in which the torques acting on the steel section are deemed particularly significant (e.g., tubs in which the deck is unsymmetrically placed, and tub girders with skewed supports). Article 6.7.5.3 indicates that the objective is to ensure that the overall stability of the girders is provided and the deformations of the tub sections are adequately controlled during erection and placement of the concrete deck. For the other very limited situations, the Engineer is allowed to consider providing a partial length lateral bracing system. However, if the bracing system is partial length, the local and global

stability of the top flanges and the tub-girder members must be investigated for the Engineer's assumed construction sequence. Also, Article C6.7.5.3 states that for spans less than about 150 ft, at least one panel of horizontal lateral bracing should be provided on each side of a lifting point. Furthermore, this article indicates that cross-section distortion and additional top-flange lateral bending stresses due to warping of the cross section may need to be considered when a tub with a partial-length bracing system is subjected to a net torque.

Article C6.7.5.3 suggests the following equation as a guideline to ensure that a reasonable minimum area is provided for the diagonal bracing members of a top lateral bracing system:

$$A_d \geq 0.03w \hspace{3cm} \text{(6.4.3-1) (AASHTO C6.7.5.3-1)}$$

where

    A_d = the minimum required cross-sectional area of one diagonal, expressed in in.^{2}

    w = the center-to-center distance between the top flanges, expressed in inches.

This equation was recommended by Heins (1978) based on studies of straight and curved steel composite box-girder bridges with spans between 50 and 250 ft. Tub sections with vertical webs and ratios of the section width-to-depth between 0.5 and 2.0, and an X-type top lateral bracing system with the diagonals placed at an angle of 45° relative to the longitudinal axis of the flanges were assumed in these studies. Heins found that an equivalent solid plate thickness for the top lateral bracing system of

$$t_{eq} = 0.05 \text{ in} = \frac{E}{G} \frac{2A_d}{w} \cos^2 \alpha \ \sin \alpha \hspace{3cm} \text{(6.4.3-2)}$$

was sufficient to limit the section warping stresses to less than 10 % of the major-axis bending stresses in all cases, where α is the angle of the X-bracing diagonals with respect to the plane of the box cross section. Equation 2 is obtained from Kollbrunner and Basler (1969) by assuming rigid truss chords (i.e., the tub girder top flanges) relative to the diagonal members. By substituting $\alpha = 45°$ into this equation and solving for A_d, one obtains Eq. 1.

AASHTO Article C6.7.5.3 acknowledges that Eq. 1 is not necessarily applicable to general bracing configurations and cross-section geometries. However, it suggests that this equation may be used as a guide to ensure that a reasonable minimum area is provided for the bracing members. If the underlying $t_{eq} = 0.05$ in. were generally applicable, the equations given by Kollbrunner and Basler (1969) could be used to determine the necessary bracing member areas for various bracing configurations. It is suggested that the requirement of $t_{eq} = 0.05$ in. should be revisited to ascertain its applicability for a complete range of modern tub girder designs, including spans up to 350 ft. Pending such further studies, it is recommended that $t_{eq} = 0.05$ in. may be used as an implementation of the Article C6.7.5.3 suggestion to ensure that a reasonable minimum area is provided for top flange bracing members.

Lastly, Article 6.7.5.3 requires that the top lateral bracing system shall be designed for the combined forces due to the shear flow in the pseudo-box section plus the forces associated with

the flexure of the tub due to the factored loads before the concrete deck has hardened or is made composite.

6.4.4 Additional Requirements for Specific Composite Box-Girder Bridge Types

In addition to the above general requirements, specific types of box girders are addressed by different Articles of the AASHTO (2020) provisions. These requirements are summarized below.

6.4.4.1 Horizontally curved boxes (multiple or single)

AASHTO Article C6.11.1 emphasizes that for horizontally curved tub girders, top flange lateral bending due to curvature must be considered during construction. Also, it points out that the effects of the St. Venant torsional shear must always be considered at all limit states and during construction in horizontally curved boxes.

6.4.4.2 Single boxes

The following specific AASHTO (2020) requirements pertain to single composite box section bridges:

- Article 6.11.1 states that single box sections shall be positioned in a central position with respect to the cross section, and that the center of gravity of the dead load shall be as close to the shear center of the box as possible. This requirement is intended to minimize the torsion that must be resisted by the box.

- Article C6.11.1 indicates that items such as sound barriers on one side of the bridge may be critical on single-box sections.

- Article C6.11.1.1 states that the live load should be positioned separately to evaluate both the maximum flexure and the maximum torsion in single-box-girder bridges, since the loads causing the critical torsion may be different than those causing the critical flexure.

- Article C6.11.1.2 emphasizes that the bearing arrangement dictates how torsion is resisted at supports and that this is especially critical for single box sections.

6.4.4.3 Closed boxes

The following specific AASHTO (2020) requirements pertain to composite closed-box section bridges:

- Article 6.11.3.2 states that for loads applied to a composite box flange before the concrete has hardened or is made composite, the flange shall be designed as a noncomposite box flange.

- Article 6.11.3.2 states that the maximum vertical deflection of a noncomposite box flange relative to its edges due to the unfactored permanent loads plus the unfactored construction loads is limited to $b_f/360$.

- Article 6.11.3.2 specifies that the through thickness bending stress in the noncomposite box flange due to the factored permanent loads plus the factored construction loads shall not exceed 20 ksi. The box flange may be assumed to be simply supported at the webs in making this calculation and in the above calculations.

6.4.5 Proportioning Limits

AASHTO Article 6.11.2 defines the following proportioning limits unique to box girders:

- A 1 to 4 limit on the inclination of the web plates is recommended relative to an axis normal to the bottom flange. Larger web inclination is allowed, but the effects of changes in the St. Venant and/or flexural web shears on lateral bending of the top flanges will be larger during construction (see the discussion in Section 2.3 of this volume). Also, highly inclined webs are generally less efficient in transmitting shear. However, the width of the bottom flange may be reduced by using a larger web inclination.

- The webs shall be attached to the mid-width of the top flanges. Attachment of the webs other than at the top flange mid-widths would cause additional flange lateral bending that would require special investigation.

- Article C6.11.2.2 indicates that the extension of the box flanges at least one inch beyond the outside of each web is recommended to facilitate welding of the webs to the flange.

Otherwise, the web and top flange proportioning requirements for box girders are the same as those for I-girders (discussed previously in Section 6.3.2 of this volume), with the exception that Eq. 6.3.2-6 (Section 6.3.2 of this volume) is not applicable. AASHTO Article 6.11.2 specifies that the inclined distances along the web are to be used in checking the web proportioning limits as well as all other pertinent design requirements.

6.4.6 Compact Composite Sections in Positive Flexure

The AASHTO Article 6.11.6.2.2 requirements for composite sections in positive flexure to be considered as compact are the same as in Article 6.10.6.2.3 for I-sections (see Section 6.3.3 of this volume), except that the bridge must also satisfy the requirements of AASHTO Article 6.11.2.3 for use of the simplified live load distribution factor (see Section 6.4.2.1 of this volume) and the box flange must be fully effective based on the provisions of AASHTO Article 6.11.1.1 (also discussed in Section 6.4.2 of this volume).

The corresponding AASHTO Article 6.11.7.1 resistance calculations and ductility requirements are the same as for compact composite I-sections in positive flexure (see Section 6.3.3 of this volume) except that, for continuous spans, the nominal flexural resistance is always subject to the limitation of Eq. 3-2 (AASHTO Eq. 6.10.7.1.2-3). Either Eq. 3-2 or Eq. 6.3.3-3 (AASHTO Eq. 6.10.7.1.2-2) will usually govern, thus limiting the nominal flexural resistance to a value less than the full plastic moment of the cross section but larger than the cross-section yield moment.

6.4.7 Noncompact Composite Sections in Positive Flexure

AASHTO (2020) Article 6.11.6.2.2 specifies that all box sections in positive bending that do not meet the restrictive requirements discussed above must be designed as noncompact composite sections. As such, the flexural resistance is always taken as less than or equal to the cross-section yield moment. Similar to the procedures for noncompact composite I-sections in positive flexure, discussed previously in Section 6.3.4 of this volume, the resistances are expressed in terms of the elastically computed flange stresses.

For tub sections, the AASHTO Article 6.11.7.2 calculation of the resistance based on the top flange stress is the same as that for noncompact composite I-sections in positive flexure (see Section 6.3.4 of this volume). However, for closed-box sections, the nominal resistance of the top (compression) flange is taken as

$$F_{nc} = R_b R_h F_{yc} \Delta \qquad\qquad \text{(6.4.7-1) (AASHTO 6.11.7.2.2-2)}$$

where

$$\Delta = \sqrt{1 - 3\left(\frac{f_v}{F_{yc}}\right)^2} \qquad\qquad \text{(6.4.7-2) (AASHTO 6.11.7.2.2-3)}$$

f_v = the St. Venant torsional shear stress in the flange due to the factored loads at the section under consideration, calculated as

$$f_v = \frac{T}{2A_o t_{fc}} \qquad\qquad \text{(6.4.7-3) (AASHTO 6.11.7.2.2-4)}$$

R_b = the web load-shedding strength reduction factor specified in Article 6.10.1.10.2, with the top flange area taken as one-half of the effective area of the box flange, including the contribution of the concrete deck, and

R_h = the hybrid web strength reduction factor specified in Article 6.10.1.10.1, with the bottom flange area taken as one-half of the effective area of the box flange. (Note that yielding will practically always occur first in the bottom flange of these section types.)

Also, in Eq. 3,

T = the torque due to the factored loads and

A_o = the enclosed area within the box section.

Equation 2 reduces the effective yield resistance of the top flange accounting for the influence of the St. Venant torsional shear stress via the von Mises yield criterion. The participation of the concrete deck in transferring the shear stresses is neglected by using just the thickness of the steel

top flange for t_{fc} in Eq. 3. Also, the flange shear stress due to flexure is considered negligible and is not included in Eq. 2.

The term Δ appears in numerous places in the box flange resistance equations presented in this section. In all cases, this term gives a reduction in the effective yield strength under longitudinal tension or compression due to the St. Venant torsional shear stress.

Similar to the above, the nominal resistance of the bottom tension flange is taken as

$$F_{nt} = R_h F_{yt} \Delta \qquad \text{(6.4.7-4) (AASHTO 6.11.7.2.2-5)}$$

(with Δ calculated using Eq. 2 but with the St. Venant shear stress in the tension flange, and with the yield strength taken as F_{yt}).

AASHTO Article 6.11.1.1 requires that box flanges also must generally satisfy

$$f_v \leq 0.75 \phi_v \frac{F_{yf}}{\sqrt{3}} \qquad \text{(6.4.7-5) (AASHTO 6.11.1.1-1)}$$

This magnitude of torsional shear stress is rarely, if ever, encountered in practical box girder designs. However, this limit ensures that Δ (Eq. 2) will never be smaller than 0.66.

The AASHTO Article 6.11 provisions imply that box flange shear stresses associated with flexure do not need to be considered in any situation. However, for cases with t_f only slightly larger than t_w, consideration of these shear stresses is prudent. The elastic shear flow $f = VQ/I$ in a box flange at the web-flange junctures is essentially the same as the corresponding elastic shear flow in the webs at these locations.

As a refinement on Eq. 3, for composite box flanges, the St. Venant torsional shear in the steel plate may be determined by multiplying the shear on the top of the composite box section by the ratio of the transformed concrete deck to the total thickness of the top flange plus the transformed deck. The St. Venant torsional shear in the concrete deck may be determined similarly. Adequate transverse reinforcing should be provided in the concrete deck to resist the shear forces due to St. Venant torsion.

The requirements for checking the slab stresses in shored construction are the same as those for I-section members

6.4.8 Evaluation of Noncomposite Sections During Construction

AASHTO (2020) Article 6.11 assumes that box-girder bridges always have a composite concrete deck throughout their length in their final constructed condition. The resistance of composite box sections under noncomposite loadings during construction is addressed within Article 6.11.3, Constructability. This article requires the checking of noncomposite box flanges in tension as well as continuously-braced (top) box flanges in tension or compression using Eq. 6.4.7-4 (Section 6.4.7 of this volume) but with the yield strength of the flange under consideration substituted for

F_{yt}. Noncomposite box flanges in compression are checked under the factored construction loads for

$$f_{bu} \leq \phi_f F_{nc} \qquad \text{(6.4.8-1) (AASHTO 6.11.3.2-1)}$$

where

f_{bu} = the longitudinal flange stress due to the factored loads at the section under consideration, calculated without consideration of cross-section warping, and

F_{nc} = the nominal compressive resistance, defined in the Article 6.11.8.2 provisions for sections in negative flexure (discussed in the next section of the volume).

The top flanges of tub-girders are checked in their noncomposite condition under construction loadings using the I-section member provisions of AASHTO Articles 6.10.3.2.1 through 6.10.3.2.3. As such, the design of these elements in tub and I-girders is handled in the same unified fashion across all of the AASHTO (2020) provisions. The top flange unbraced length is taken as the distance between the panel points of the top lateral bracing system. The flange strength check under construction loadings is given by Eq. 6.3.7-1 of this volume, which includes the influence of flange lateral bending due to any source. The following actions contribute generally to the lateral bending of the top flanges in tub girders in their noncomposite condition prior to the concrete slab becoming composite:

- forces from overall action of top lateral bracing system in resisting major-axis flexure and torsion,

- changes in shear along the length of the girder, causing a horizontal distributed load on the top flanges of the tub,

- eccentric loads from cantilever overhangs acting on forming brackets,

- horizontal curvature, and

- typically to a minor extent, wind.

The top flanges of tub girders are assumed to be continuously braced after the concrete slab has hardened or is made composite. As such, the top flange lateral bending effects are negligible and are no longer considered once the flanges have reached this state.

6.4.9 Composite Sections in Negative Flexure

As noted in the previous section, AASHTO (2020) Article 6.11 assumes that box-girder bridges always have a composite concrete deck in their final constructed condition. As a result, resistance checks for flange lateral bending and/or member lateral-torsional buckling are no longer a consideration once the slab is made composite. Flange lateral bending is not a consideration because the top flange elements are continuously supported by the concrete deck. Sufficient internal cross frames and diaphragms are required such that lateral bending stresses due to warping are negligible in box flanges at the strength limit states during construction and after the

completion of the structure. Lateral-torsional buckling is not a consideration for composite boxes because of their large torsional stiffness and lateral-torsional buckling resistance.

For the continuously-braced top flanges of box girders in the final constructed condition, AASHTO Articles 6.11.8.1.2 and 6.11.8.3 specify

$$f_{bu} \leq \phi_f R_h F_{yt} \qquad\qquad (6.4.9\text{-}1) \text{ (AASHTO 6.11.8.1.2-1 and 6.11.8.3-1)}$$

for tub sections and Eq. 6.4.7-4 (Section 6.4.7 of this volume) for closed box sections. For the bottom box flange in compression under negative flexure, AASHTO Article 6.11.8.1.1 specifies

$$f_{bu} \leq \phi_f F_{nc} \qquad\qquad (6.4.9\text{-}2) \text{ (AASHTO 6.11.8.1.1-1)}$$

where F_{nc} is the nominal compressive resistance, in terms of the average compression stress, defined in Article 6.11.8.2. The influence of St. Venant torsional shear stress in the compression flange, f_v, is accounted for in the calculation of F_{nc} using the equation

$$F_{nc} = F_{cb} \sqrt{1 - \left(\frac{f_v}{\phi_v F_{cv}} \right)^2} \qquad\qquad (6.4.9\text{-}3) \text{ (AASHTO 6.11.8.2.2-1)}$$

where

F_{cb} = nominal buckling resistance in axial compression, in units of stress, for the flange subjected to compression alone

F_{cv} = nominal shear buckling resistance, in units of stress, for the flange under shear alone

ϕ_v = 1.00

Equation 3 is a circular interaction equation between the plate strengths in axial compression and shear. This interaction form is an accurate characterization of the plastic strength interaction between normal and shear stresses, based on the von Mises yield criterion. Furthermore, this form is commonly accepted as an accurate characterization of the inelastic buckling strength interaction between the axial and shear stresses in rectangular plates (Ziemian 2010). However, Eq. 3 is slightly aggressive as a representation of the elastic buckling strength interaction in axial compression and shear. This equation, written without taking the square root of the last term, is a well-accepted representation of the corresponding elastic buckling strength interaction (Ziemian 2010). The form without the square root is applied by AASHTO Article 6.9.2.2.2 to account for axial-shear interactions in various general types of noncomposite members (see Section 6.6.3 of this volume).

The shear resistance, F_{cv}, in Eq. 3 is based on the theoretical web shear buckling resistance equations detailed in Section 6.3.8.1 of this volume, but using the flange width-to-thickness ratio, b_f/t_f, instead of D/t_w, using the flange yield strength, F_{yc}, rather than the web yield strength, and with the shear resistance in terms of stress obtained by dividing the shear force equations in Section 6.3.8.1 by Dt_w. In addition, the shear buckling coefficient is denoted by the variable k_s in AASHTO

Article 6.11.8.2.2, and k_s is taken as the more precise curve-fit value for a long unstiffened plate, $k_s = 5.34$, rather than the value of $k = 5.0$ employed when writing the shear resistance of member webs. The resulting equations are

$$F_{cv} = 0.58 F_{yc} \quad \text{for} \quad \frac{b_f}{t_f} \le 1.12 \sqrt{\frac{Ek_s}{F_{yc}}} \qquad\qquad \text{(6.4.9-4a) (AASHTO 6.11.8.2.2-5)}$$

$$F_{cv} = \frac{0.65\sqrt{F_{yc}Ek_s}}{b_f/t_f} \quad \text{for} \quad 1.12\sqrt{\frac{Ek_s}{F_{yc}}} < \frac{b_f}{t_f} \le 1.40\sqrt{\frac{Ek_s}{F_{yc}}} \quad \text{(6.4.9-4b) (AASHTO 6.11.8.2.2-6)}$$

$$F_{cv} = \frac{0.91Ek_s}{\left(b_f/t_f\right)^2} \quad \text{for} \quad \frac{b_f}{t_f} > 1.40\sqrt{\frac{Ek_s}{F_{yc}}} \qquad \text{(6.4.9-4c) (AASHTO 6.11.8.2.2-7)}$$

AASHTO Article 6.11.8.2 is subdivided into two subarticles addressing the cases of unstiffened box flanges and longitudinally stiffened box flanges. The base axial compressive and shear resistance equations for unstiffened box flanges in compression are specified in Article 6.11.8.2.2 along with the plate buckling coefficients k and k_s for uniform axial compression and uniform shear on unstiffened flanges respectively. Article 6.11.8.2.3 addresses stiffened flanges by employing the same resistance equations, but using the panel width (defined below) rather than the total flange width in its definition of the flange slenderness. Also, this article redefines the plate buckling coefficients k and k_s accounting for the influence of the flange stiffeners. The subsection below explains the Article 6.11.8.2.2 strength equations for unstiffened flanges. This is followed by a second subsection that explains the modifications to these equations for stiffened flanges.

6.4.9.1 Strengths of unstiffened box flanges under flexural compression and under shear alone

Although the above definition of F_{cb} given by AASHTO (2020) Article 6.11.8.2.2 is "under compression alone," the corresponding equations for F_{cb} include an additional term, Δ, which applies a second von Mises type strength reduction. However, this reduction is applied only to the "plateau" of the plate strength curve under uniform axial compression. This is clearly a double-counting of the strength interaction between axial compression and shear. Equation 3 is sufficient to capture the axial-shear strength interaction without any further adjustments associated with the applied shear stress, f_v, albeit the circular interaction is slightly aggressive for elastic buckling interaction as noted above. A simpler approach that is more consistent with AASHTO Article 6.9.2.2.2 would be to employ Eq. 3 without taking the square root of the last term for the calculation of F_{nc} and to set $\Delta = 1.0$ in the following equations. This equation accounts fully for all the axial-shear interaction effects, elastic buckling, inelastic buckling, and yield interactions. Nevertheless, the equations specified by AASHTO Article 6.11.8.2.2 tend to provide a conservative result relative to this recommendation. These equations are presented below including the Δ term.

The AASHTO Article 6.11.8.2.2 axial compressive strength, F_{cb}, is expressed as a theoretical buckling strength using the three-part compact, noncompact and slender representation as

illustrated previously by Figure 59 for the flange local buckling strength I-section members. However, for box flanges in compression, Article 6.11.8.2.2 defines the flange slenderness as b_{fc}/t_{fc}, where b_{fc} is the compression flange width between the webs As discussed previously, these three parts of the strength curve correspond to plastic buckling at a "plateau" strength level for a flange slenderness smaller than λ_p, an inelastic buckling strength curve that varies linearly between two anchor points λ_p and λ_r, and an elastic buckling strength curve for flange slenderness larger than λ_r.

AASHTO Article 6.11.8.2.2 defines the plate's plateau strength in axial compression as

$$F_{cb} = R_b R_h F_{yc} \Delta \qquad \text{(6.4.9-5) (AASHTO 6.11.8.2.2-2)}$$

where R_b and R_h are the web load-shedding factor and the hybrid factor, respectively, defined as discussed in Sections 6.3.5.2.2 and 6.3.5.2.3 of this volume, except that a_{wc} is to be determined with $b_{fc}t_{fc}$ taken as one-half of the flange area in the calculation of R_b and A_{fn} is to be determined using one-half of the corresponding flange area in the calculation of R_h (it should be noted that the definitions of R_b and R_h at the end of AASHTO Article 6.11.8.2.2 are in error in that they do not include these adjustments in the determination of the flange areas). AASHTO Article 6.11.8.2.2 specifies

$$\Delta = \sqrt{1 - 3\left(\frac{f_v}{F_{yc}}\right)^2} \qquad \text{(6.4.9-6) (AASHTO 6.11.8.2.2-11)}$$

Again, the recommended approach discussed above is to set $\Delta = 1.0$ in the AASHTO equations, and to account for the axial-shear strength interaction solely using Eq. 3 without the square root.

AASHTO Article 6.11.8.2.2 specifies

$$\lambda_p = 0.57 \sqrt{\frac{Ek}{F_{yc}\Delta}} \qquad \text{(6.4.9-7a) (AASHTO 6.11.8.2.2-9)}$$

for the compact flange limit. Taking $\Delta = 1.0$, and substituting the specified plate local buckling coefficient of 4.0 for k, this equation reduces to

$$\lambda_p = 1.14 \sqrt{\frac{E}{F_{yc}}} \qquad \text{(6.4.9-7b)}$$

This limit may be compared to the corresponding compact-flange limit for flanges of box sections in AISC (2016), which is Eq. 7b with a coefficient of 1.12, and to a coefficient of 1.09 with this equation for welded box section members in AASHTO (2020) Article 6.12.2.2c (see Table 5 in Section 6.2.4 of this volume).

AASHTO Article 6.11.8.2.2 specifies the noncompact flange limit for a box flange subjected to axial compression as

$$\lambda_{rf} = 0.95\sqrt{Ek / F_{yr}} \qquad\qquad \text{(6.4.9-8) (AASHTO 6.11.8.2.2-10)}$$

which is the same form as Eq. 6.3.5-30 of this volume for I-section members, obtained simply by setting the elastic local buckling stress equal to F_{yr} and then solving for the flange slenderness parameter. In addition, AASHTO Article 6.11.8.2.2 specifies

$$F_{yr} = (\Delta - 0.3) F_{yc} \qquad\qquad \text{(6.4.9-9) (AASHTO 6.11.8.2.2-13)}$$

Again, taking $\Delta = 1.0$ in this equation, the coefficient on F_{yr} is 0.7, which is the same as that employed most commonly for the AASHTO (2020) calculation of λ_{rf} in I-section members (see Section 6.3.5-6 of this volume). After substituting $F_{yr} = 0.7 F_{yc}$ and $k = 4.0$ into Eq. 8, one obtains

$$\lambda_{rf} = 2.27\sqrt{E / F_{yc}} \qquad\qquad \text{(6.4.9-10)}$$

For unstiffened noncompact box flanges subjected to flexural compression, AASHTO Article 6.11.8.2.2 provides the following expression for the interpolation between the anchor points $(\lambda_p, R_b R_h F_{yc} \Delta)$ and $(\lambda_r, R_b (\Delta - 0.3) F_{yc})$ at the compact and noncompact flange limits:

$$F_{cb} = R_b R_h F_{yc} \left[\Delta - \left(\Delta - \frac{\Delta - 0.3}{R_h} \right) \left(\frac{\lambda_f - \lambda_p}{\lambda_r - \lambda_p} \right) \right] \qquad \text{(6.4.9-11) (AASHTO 6.11.8.2.2-3)}$$

where again, $\lambda_f = b_f / t_f$ for the box flange application. Lastly, AASHTO Article 6.11.8.2.2 specifies

$$F_{cb} = \frac{0.9 E R_b k}{\lambda_f^2} \qquad\qquad \text{(6.4.9-12) (AASHTO 6.11.8.2.2-4)}$$

This is identical to the theoretical Eq. 6.2.4-1 discussed in Section 6.2.4.1 of this volume, multiplied by the web load-shedding factor, R_b.

Figure 78 compares the box flange F_{cb} curve for $\Delta = 1.0$ to the more general unstiffened plate strength curves from Cases 4 and 6 of Table 5 (Section 6.2.4 of this volume). Case 4 from Table 5 corresponds to flanges of nonwelded built-up box section members, and Case 6 from Table 5 corresponds to general unstiffened flange plates in welded built-up box section members. One can observe that the F_{cb} curve falls between the Case 4 and 6 curves within its inelastic buckling range from b_f/t_f of 27.5 to 54.7, but then drops significantly below the other strength curves for larger flange slenderness values. This is consistent with the results from Dwight and Little (1974) as discussed by Wolchuk (1997). The Case 4 curve is slightly aggressive compared to the results shown by Wolchuk (1997) for unwelded plates, and the Case 6 curve is slightly aggressive compared to the results shown by Wolchuk (1997) for heavily welded plates.
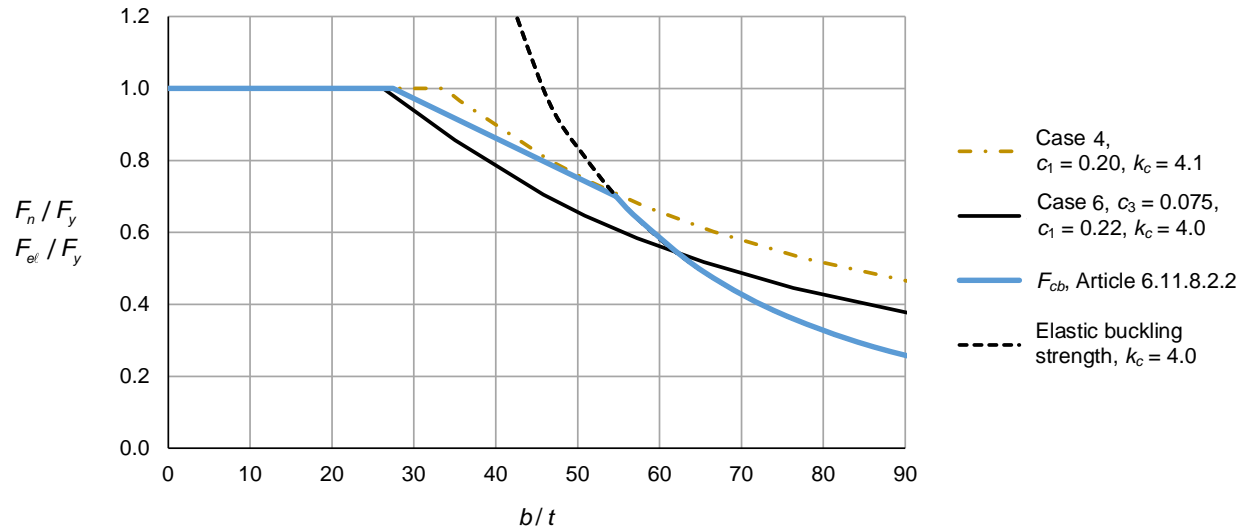
Figure 78. Comparison of F_{cb} from AASHTO Article 6.11.8.2.2 with $\Delta = 1.0$ to the plate strength curves from Cases 4 and 6 of Table 1 for $F_y = F_{yc} = 50$ ksi.

Regarding the box flange shear strength, AASHTO Article 6.11.8.2.2 basically employs the shear buckling strength curves given by Eqs. 6.3.8-5 of this volume for the normalized strength $F_{cv}/(0.58F_{yc})$, except it uses b_f/t_f as the width-to-thickness ratio rather than D/t_w, and it uses a shear buckling coefficient of $k_s = 5.34$ rather than the value $k = 5.0$ as discussed previously. The C value from Eqs. 6.3.8-5 is multiplied by the shear yield strength, $0.58F_{yc}$, to obtain the shear buckling strength in terms of stress.

6.4.9.2 Strengths of stiffened box flanges under flexural compression and under shear alone

For stiffened flanges, k and k_s are typically smaller than the values discussed in the previous section due to the finite rigidity (i.e., flexibility) of the longitudinal stiffeners. In this case, the AASHTO (2020) equations are formulated in terms of the longitudinal stiffener moment of inertia I_s necessary to develop a certain value of $k \leq 4.0$. The base equation is

$$I_s \geq \psi w t_{fc}^3 \qquad\qquad \text{(6.4.9-13) (AASHTO 6.11.11.2-2)}$$

where

ψ	$=$	$0.125k^3$ for $n = 1$	(6.4.9-14a)
	$=$	$1.120k^3$ for $n = 2$	(6.4.9-14b)

I_s is taken as the moment of inertia of the longitudinal flange stiffener about an axis parallel to the flange located at the base of the stiffener, w is the larger of the width of the flange between the longitudinal stiffeners or the distance from a web to the nearest longitudinal stiffener, and n is the number of equally spaced longitudinal flange stiffeners.

AASHTO (2020) Articles 6.11.8.2.3 and 6.11.11.2 require I_s to be large enough to develop a value of at least $k = 1.0$, although a value of at least $k = 2.0$ is recommended. Equations 14a and b, which

originate from Vincent (1969), are approximate equations that give values close to theoretical elastic buckling solutions for infinitely long, longitudinally stiffened plates from Goldberg and Levy (1957). In AASHTO Article 6.11.8.2.3, the above equations are solved algebraically for the k values corresponding to a given I_s. AASHTO Article C6.11.11.2 suggests that the number of longitudinal flange stiffeners should not exceed one for economy in boxes of typical proportions.

AASHTO (2020) Article C6.11.11.2 gives the following more general equation for ψ, from Vincent (1969), applicable for $n = 2, 3, 4$ and 5:

$$\psi = 0.07k^3n^4 \tag{6.4.9-14c}$$

For $n > 2$, the required moment of inertia from Eqs. 13 and 14c is excessive. This is due to the fact that these equations are based on the idealization of an infinitely long plate. Therefore, for the rare cases where an exceptionally wide box flange is required and n may need to exceed 2, AASHTO Article C6.11.11.2 suggests that transverse flange stiffeners be provided to reduce the required size of the longitudinal stiffeners to a more practical value. This Article also suggests that transverse flange stiffeners should be considered for $n = 2$ if a k value larger than about 2.5 is needed and it is desired to reduce the required size of the longitudinal stiffeners relative to that given by Eq. 13. AASHTO Article C6.11.11.2 provides equations for the proportioning of the transverse and longitudinal stiffeners as well as the resulting value of the plate buckling coefficient k applicable for these exceptional cases. The longitudinal stiffeners are sized using $\psi = 8.0$ in these situations, which is approximately the same as the requirement to develop $k = 2.0$ in Eq. 14b. Transverse and longitudinal flange stiffeners sized by these requirements give a value of $k \cong 4.0$ when the transverse flange stiffeners are spaced at a distance less than or equal to $4w$ for $n \leq 5$.

AASHTO (2020) Article 6.11.8.2.3 specifies the coefficient for the elastic shear buckling of a longitudinally stiffened flange as

$$k_s = \frac{5.34 + 2.84\left(\dfrac{I_s}{wt_{fc}^3}\right)^{1/3}}{(n+1)^2} \leq 5.34 \tag{6.4.9-15 (AASHTO 6.11.8.2.3-3)}$$

This equation and Eq. 14c originate from Culver (1972).

It should be noted that the above equations address the design of the key components carrying the axial compression, i.e., the longitudinal stiffeners, in a very indirect manner. The longitudinal stiffeners in wide plates with multiple stiffeners tend to behave as unconnected compression struts. The key property influencing the compressive resistance of these types of plates is the moment of inertia of the longitudinal stiffeners. However, for these types of plates, the plate buckling coefficient in AASHTO (2020) Articles 6.11.8.2, 6.11.11.2 and C6.11.11.2 is selected independent of this key property, followed by a calculation of the stiffener moment of inertia required to develop the selected plate buckling coefficient based on theoretical elastic buckling equations for the stiffened plate. Furthermore, AASHTO (2020) Article C6.11.11.2 requires a spacing of the transverse stiffeners less than or equal to three times the width of the stiffened plate for the transverse stiffeners to be considered effective. It would be better to provide design engineers with more flexibility in choosing the transverse stiffener spacing.

Appendix E of AASHTO (2020) provides numerous advances that facilitate the direct, efficient and accurate calculation of design resistances for longitudinally stiffened plates in noncomposite box section members (see Section 7 of this volume). These advances are a substantial improvement on the conservatism and lack of usability of the above longitudinally stiffened flange provisions for composite box section members. It is anticipated that these advances will be integrated into AASHTO Article 6.11 in the future.

The longitudinal stiffeners act integrally with the flange in resisting flexural compression in stiffened box flanges. As can be noted from the above discussions, AASHTO (2020) generally does not count upon any postbuckling resistance of box flange elements in composite box girders. It is recommended that the area of these stiffeners generally should be included in calculating the moment of inertia, elastic section modulus and other properties of the box section. In addition, web longitudinal stiffeners are sized using the same philosophy as for I-section members (see Section 6.3.10 of this volume). That is, the web longitudinal stiffeners are sized to maintain a line of near zero lateral deflection at their juncture with the web plate for load levels up to the calculated bend buckling resistance of the web. As discussed previously in Section 6.3.10 of this volume, it is also recommended that web longitudinal stiffeners should be included in determining the member cross-section properties.

AASHTO Article 6.11.11.2 requires that the specified minimum yield strength of the flange longitudinal stiffeners shall not be less than the specified minimum yield strength of the box flange to which they are attached. This is similar to the previously discussed requirement pertaining to Eq. 6.3.10-5 of this volume. Also, this article specifies that the projecting widths of the flange longitudinal stiffener elements must satisfy the same limit as defined by Eq. 6.3.10-6. As noted in Section 6.3.10 of this volume, this limit is intended to prevent local buckling of the flange longitudinal stiffeners. For structural tee stiffeners, this limit is to be applied to one-half of the tee flange width.

6.4.10 Bottom Box Flange at Interior Pier Sections

AASHTO (2020) Article C6.11.8.1.1 addresses the complex biaxial stress conditions in bottom box flanges at interior pier sections. At these locations, the bottom flange is subjected to the stresses from major-axis bending of the box section as well as major-axis bending of the internal diaphragm over the bearings. In addition the flange is subjected to shear stresses due to the internal diaphragm vertical shear as well as, when it is non-negligible, the St. Venant torsional shear in the box section. The flexural and shear stresses due to the bending of the internal diaphragm can be particularly significant for boxes supported on single bearings. AASHTO Article C6.11.8.1.1 provides the following equation for checking the bottom box flange at interior pier sections under the strength limit states:

$$\sqrt{f_{bu}^2 - f_{bu}f_{by} + f_{by}^2 + 3(f_d + f_v)^2} \le \phi_f R_b R_h F_{yc} \qquad \text{(6.4.10-1) (AASHTO C6.11.8.1.1-1)}$$

where

f_{bu} = the longitudinal flange stress due to major-axis bending of the box section,

f_{by} = the flexural stress in the flange caused by major-axis bending of the internal diaphragm over the bearings,

f_d = the shear stress in the flange caused by the internal diaphragm vertical shear, and

f_v = the St. Venant torsional shear stress in the box flange.

Equation 1 is simply a statement of the von Mises yield criterion (Ugural and Fenster 2020) for a plate subjected to biaxial normal stress plus shear. AASHTO Article C6.11.8.1.1 suggests the use of a flange width equal to $18t_f$ with the internal diaphragm for simplified calculation of the stresses f_{by} and f_d. The shear stress f_d may be estimated as

$$f_d = \frac{VQ}{It_{fc}}$$ (6.4.10-2) (AASHTO C6.11.8.1.1-2)

where

V = the maximum vertical shear in the internal diaphragm,

Q = the first moment of one-half of the effective box flange area ($9t_f^2$) about the neutral axis of the effective internal diaphragm section, and

I = the moment of inertia of the effective internal diaphragm section.

The shear stress f_v may be estimated using Eq. 6.4.7-3 of this volume.

AASHTO Article C6.11.8.1.1 points out that for a box supported on two bearings, f_{by} and f_d in Eq. 1 are typically small and can often be neglected. In these cases, Eq. 6.4.9-2 (Section 6.4.9 of this volume) will govern the resistance of the bottom box flange at an interior support. Theoretically, in cases where the bottom box flange is governed by Eq. 1, the top flange (i.e., the concrete slab in a tub girder or the top composite box flange in a closed-box section girder) should also be checked for its adequacy under the related biaxial and shear loading conditions.

6.4.11 Concrete Slab

AASHTO (2020) Article 6.11.1.1 states that the shear due to St. Venant torsion should be considered when designing the reinforcing steel for the concrete slab. Article 6.11.10 suggests a simple method for determining the torsional shear in the slab of closed box sections. For tub sections, Article 6.11.1.1 indicates that the slab should be considered to resist all the torsional shear acting on the top of the composite box section.

6.4.12 Stepped, Variable Web Depth and Other Nonprismatic Box-Section Members

With the exception of:

1. Potential overall lateral-torsional buckling of tub girders during construction, and

2. Potential lateral-torsional buckling of the top flanges between their brace points for tub girders subjected to positive bending under construction conditions (prior to the hardening or the concrete slab or the slab being made composite),

all of the resistance checks for composite box section members are effectively cross-section based. For stepped, variable web depth and other general nonprismatic box-section members, the above two cases can be handled as discussed for I-section members in Section 6.3.6 of this volume. For other cases, the resistance calculations for stepped, variable web depth and other nonprismatic box-section members may be handled on a cross-section by cross-section basis as discussed in the above Sections 6.4.6 through 6.4.11.

6.4.13 Web Shear Strength

The provisions of AASHTO Article 6.10.9 (discussed in Section 6.3.8 of this volume) are applied separately for checking each of the webs of box girders. These provisions have been discussed previously in Section 6.3.8 of this volume. In applying these provisions, D is taken as the depth of the web along the slope of the web for inclined webs. Also, the factored shear force in each web is determined generally as

$$V_{ui} = V_u / \cos \theta \qquad\qquad (6.4.13\text{-}1)\ (\text{AASHTO } 6.11.9\text{-}1)$$

where

V_u = vertical shear due on the inclined web under consideration and

θ = the angle of inclination of the web plate with respect to the vertical direction.

For box girders in bridges not satisfying the requirements of AASHTO Article 6.11.2.3, or with box flanges that are not fully effective according to the provisions of Article 6.11.11.1, V_u is to be taken as the sum of the flexural and St. Venant torsional shears.

In checking Eq. 6.3.8-7 (Section 6.3.8 of this volume) to determine whether the full or true Basler shear resistance is applicable for transversely stiffened webs designed utilizing the web postbuckling shear strength, the effective flange width b_{fc} or b_{ft} of box flanges should be taken as the smaller of:

- One-half the flange width between the webs plus the outside extension of the flange beyond the centerline of the web, or

- $18t_f$ plus the outside extension of the flange beyond the centerline of the web.

The above $18t_f$ limit ensures that the I-section member web shear postbuckling resistance equations of AASHTO Article 6.10.9 may be applied equivalently to box-section members.

AASHTO Articles 6.11.9 and 6.11.11.1 require that intermediate transverse web stiffeners shall be designed using the I-girder provisions of AASHTO Article 6.10.11.1 (see Section 6.3.8 of this volume).

6.4.14 Shear Connectors

AASHTO Article 6.11.10 points to the I-girder provisions of Article 6.10.10 for design of shear connectors and provides the following additional supplementary requirements:

- Shear connectors are required in negative moment regions. This is because these components are necessary to resist any significant St. Venant torsional shears that exist in composite box sections. Also, the simplified live load distribution factors of AASHTO Article 4.6.2.2.2b were developed for straight box sections that had shear connectors throughout the negative flexure regions.

- For box girders in bridges not satisfying the requirements of AASHTO Article 6.11.2.3 (for use of the simplified live load distribution factors), or with box flanges that are not fully effective according to the provisions of AASHTO Article 6.11.11.1, the shear connectors are to be designed for the sum of the flexural and St. Venant torsional shears. For tub girders, the St. Venant shear increases the connector force on one flange and decreases it on the other. AASTHO Article 6.11.10 requires that the same connector pitch shall be used on both flanges. AASHTO Article C6.11.10 points out the conservatism of adding both the maximum flexural and torsional shears, since these are typically not produced by concurrent loads, but indicates that the calculation of the critical concurrent shear forces is not practical using current analysis tools.

- The total area of the steel box section and the effective area of the concrete deck associated with the box are to be used in calculating the longitudinal force requirements in Eqs. 6.3.9-1 and 6.3.9-12 of this volume.

- The shear connectors on composite box flanges shall be distributed uniformly across the width of the flange. The transverse spacing between shear connectors on composite box flanges, s_t, shall satisfy

$$\frac{s_t}{t_f} \le 0.57 \sqrt{\frac{kE}{F_{yf}}} \tag{6.4.14-1}$$

  (with k taken equal to 4.0) to help prevent local buckling of the flange plate subjected to compression. This limit is equal to the value of $\lambda_f = b/t_f$ corresponding to Eq. 6.4.9-6b of this volume.

- In composite box flanges, in addition to satisfying the requirements of AASHTO Article 6.10.10, which require consideration of a radial force component in the shear connectors due to horizontal curvature, the vector sum of the longitudinal and St. Venant torsional shears must be considered. The St. Venant torsional shear may be determined by multiplying the shear on the top of the composite box section by the ratio of the transformed concrete deck to the total thickness of the top flange plus the transformed deck.

6.5 Miscellaneous Flexural Members

6.5.1 Introduction

Article 6.12 of AASHTO (2020) addresses the flexural resistance of various rolled, built-up noncomposite and composite members used in trusses, frames, arches, and other diverse applications subjected to bending, often in combination with axial loads. In many cases, the Article 6.12 provisions are based on the AISC (2016) Specification provisions. However, there are a number of important differences. This section provides a succinct overview of the corresponding AASHTO (2020) and AISC (2016) provisions.

6.5.2 I-Section Members in Weak-Axis Bending

The nominal flexural resistance of I-section members subjected to weak-axis bending is defined by AASHTO (2020) Article 6.12.2.2.1 as the corresponding fully-plastic resistance

$$M_n = M_p = F_{yf} Z_y \qquad\qquad \text{(6.5.2-1) (AASHTO 6.12.2.2.1-1)}$$

for cross sections in which the largest flange slenderness $b_f/2t_f$ is less than or equal to the compact-flange limit λ_{pf} given by Eq. 6.3.5-19 of this volume. For unusual cases where the flanges have different yield strengths, the smaller of these yield strengths should be used in checking the flange compactness and in calculating M_p. The web contribution to M_p is generally small, and hence hybrid web effects are ignored. For cross sections with the largest flange slenderness greater than λ_{pf} but less than the noncompact flange limit λ_{rf} given by Eq. 6.3.5-30 of this volume, with F_{yr} taken equal to the smaller F_{yf} and k_c taken equal to 0.76, the flexural resistance is assumed to be governed by inelastic flange local buckling (FLB). For $F_{yr} = F_{yf}$ and $k_c = 0.76$, Eq. 6.3.5-30 becomes

$$\lambda_{rf} = 0.83 \sqrt{\frac{E}{F_{yf}}} \qquad\qquad \text{(6.5.2-2) (AASHTO 6.10.2.2.1-5)}$$

The theoretical elastic FLB coefficient for a linear stress distribution across the flange width, with the maximum compressive stress at the flange tip and zero stress at the web-flange juncture, is 0.57 for simply supported conditions and 1.61 for fixed edge conditions at the web-flange juncture (Ziemian 2010). The value $k_c = 0.76$ is taken as a reasonable value given some restraint from the web and from the portion of the flange loaded in flexural tension on the opposite side of the web. In setting $F_{yr} = F_{yf}$, the influence of residual stresses is neglected. This is justified due to the strain gradient across the flange width, as well as the relatively small value of $k_c = 0.76$ compared to potential theoretical values. Therefore, the moment capacity corresponding to $F_{yr} = F_{yf}$ is the nominal yield moment $M_y = F_{yf} S_y$, where S_y is the elastic section modulus for minor-axis bending. If the above values are substituted into the linear equation representing the inelastic buckling resistance between Anchor Points 1 and 2 in Figure 59 (with R_b taken equal to 1.0 since the web flexural stress is zero), one obtains

$$M_n = M_p - \left(M_p - M_y\right)\left(\frac{\lambda_f - \lambda_{pf}}{0.45\sqrt{E/F_{yf}}}\right)$$ (6.5.2-3)

where λ_f = larger $b_f/2t_f$ of the two flanges. AASHTO (2020) gives the following form for this equation:

$$M_n = \left[1 - \left(1 - \frac{S_y}{Z_y}\right)\left(\frac{\lambda_f - \lambda_{pf}}{0.45\sqrt{E/F_{yf}}}\right)\right]F_{yf}Z_y$$ (6.5.2-4) (AASHTO 6.12.2.2.1-2)

where

S_y = elastic section modulus about the weak axis,

Z_y = plastic section modulus about the weak axis, and

F_{yf} = specified minimum yield strength of the lower-strength flange.

Equation 2 gives $\lambda_{rf} = 14.1$ for $F_{yf} = 100$ ksi, which is larger than the maximum $b_f/2t_f = 12$ permitted for I-sections in AASHTO Article (6.10.2.2) (see Eq. 6.3.2-3). Therefore, Article 6.12.2.2 does not define a weak-axis bending resistance based on elastic FLB.

The inelastic FLB resistance is slightly different in AISC (2016). AISC (2016) uses $k_c = 0.76$ and $F_{yr} = 0.7F_y$ in its calculation of λ_{rf}. The resulting AISC inelastic FLB resistance approaches the AASHTO FLB resistance as the flange slenderness approaches the compact limit given by Eq. 6.3.5-19 (Section 6.3.5 of this volume). However, it tends to be significantly more conservative than the AASHTO resistance for more slender flanges.

It is important to note that for I-section members subjected to major-axis bending combined with flange lateral bending due to minor-axis flexure or torsion, the one-third rule equations discussed in Section 6.3.7 of this volume apply as long as Eq. 6.3.7-5 is satisfied. The one-third rule equations provide a more accurate representation of the resistance and should be utilized rather than the above equations in these cases.

6.5.3 Noncomposite Box-Section and Square and Rectangular HSS Members

AASHTO (2020) Article 6.12.2.2.2 addresses the flexural resistance of all types of noncomposite box-section members. This includes the consideration of:

- Compact, noncompact and slender flanges. Consideration of all three of these flange classifications is important for general applications involving biaxial bending, since a relatively thin web in one principal axis bending direction becomes a flange for bending about the other principal axis.

- Compact, noncompact and slender webs, recognizing the ability box-section or HSS members to develop the plastic moment capacity of the cross section when the webs and the compression flange are sufficiently stocky and the member is sufficiently braced.

- Hybrid webs.

- Single symmetry of the box section.

- Lateral-torsional buckling (LTB) of narrow doubly and singly symmetric box-section members.

- Local flange, local web and global lateral-torsional buckling interaction.

- Longitudinal stiffening of the webs and/or the flanges.

These considerations are addressed by adopting an approach that parallels to some extent the provisions for design of general noncomposite I-section members in Article 6.10 and Appendix A of the AASHTO (2020) Specifications. However, there are also significant differences compared to the AASHTO noncomposite I-section member provisions. The following discussions provide a brief summary of the AASHTO (2020) Article 6.12.2.2.2 provisions with the exception of the consideration of longitudinally stiffened compression flanges. The consideration of longitudinally stiffened box-section compression flanges is addressed subsequently in Section 7 of this volume.

It should be noted that in rectangular box-section members subjected to biaxial bending, the flange plates in one direction of principal-axis bending serve as web plates in the other direction of principal-axis bending. Therefore, the consideration of a given set of plates as web plates or as flange plates depends on the axis of bending.

AASHTO (2020) Article 6.12.2.2.2e expresses the overall box-section and rectangular HSS member flexural resistance by the single equation

$$M_n = R_b R_{pc} R_f M_{yce}$$
(6.5.3-1) (AASHTO 6.12.2.2.2e-1)

for unbraced lengths, L_b, less than or equal to L_p, where

L_p = limiting unbraced length, or first anchor point, at which the flexural resistance under uniform bending starts to reduce due to the influence of lateral-torsional buckling

M_{yce} = yield moment to the compression flange of the cross section, using an effective width based on the equations discussed in Section 6.2.4.2 of this volume, and using the flange yield strength, F_{yf}, for f. For singly symmetric box sections having a larger effective compression flange, such that early yielding occurs in flexural tension, M_{yce} is calculated as the yield moment to the effective compression flange including the influence of early yielding in tension. Closed-form equations are provided in AASHTO Article C6.12.2.2.2c for this calculation.

R_b = web bend buckling (load-shedding) strength reduction factor, adapted from the I-section member provisions of AASHTO Article 6.10.1.10.2 for slender-web sections (see Section 6.3.5.2.2 of this volume) by using an equivalent flange

area corresponding to each of the member webs, taken equal to 1.0 for compact- and noncompact-web sections.

R_{pc} = web plastification factor, which varies from the shape factor for the effective cross section, M_{pe}/M_{ye}, for a compact-web section to the hybrid web factor, R_h, for a slender-web section; the effective plastic moment, M_{pe}, is calculated where needed based on an idealization of the fully-plastic cross section using the effective width of the compression flange. This factor, and the above web load-shedding factor, are evaluated as functions of the effective depth of the web in compression associated with the calculation of M_{yce}.

R_f = compression flange slenderness factor, which varies from 1.0 for a compact flange to 0.85 for a slender flange. This factor accounts for the limited ability of a thinner compression flange to develop large inelastic strains without a reduction in the flange force contribution, when the webs are compact or noncompact, as well as the limited ability of a thinner compression flange to accept stresses shed from slender webs due to web bend buckling.

For unbraced lengths, L_b greater than L_p, the flexural resistance is expressed for all types of box-section and rectangular HSS members using the single equation

$$M_n = C_b R_b \left[R_{pc} R_f M_{yce} - \left(R_{pc} R_f M_{yce} - F_{yr} S_{xce} \right) \frac{L_b - L_p}{L_r - L_p} \right] \le R_b R_{pc} R_f M_{yce} \qquad \text{(6.5.3-2)}$$

(AASHTO 6.12.2.2.2e-2)

where

C_b = moment gradient factor, calculated using the same procedures discussed for I-section members (see Section 6.3.5.11 of this volume)

F_{yr} = compression flange flexural stress defining the second anchor point of the inelastic portion of the LTB strength curve at a large unbraced length, L_r; taken as $0.5F_{yc}$

S_{xce} = elastic section modulus to the compression flange, considering the compression flange effective width

L_r = large unbraced length defined the second anchor point of the inelastic portion of the LTB strength

The length limits L_p and L_r are derived using the theoretical equations for elastic LTB of a general box-section, similar to the development of the equations for these terms in the case of I-section members. The length L_p is the unbraced length at which the elastic LTB critical moment is equal to 15 times the plastic moment M_p, which is equivalent to the basis for this limit in the AISC (2016) Section F7 provisions for square and rectangular HSS and box sections, but with M_p taken equal to $1.3M_{yce}$ as a simplification. This magnitude of the elastic LTB critical moment defines the limiting condition at which the "plateau" resistance, Eq. 1, can just be achieved. The length L_r is

defined as 0.3 of the length corresponding to theoretical elastic LTB at a compression flange stress of F_{yr}. The Eq. 2 resistance curve gives results comparable to the applicable Eurocode 3 (CEN 2005) resistance curve for LTB of box-section members (Lokhande and White 2018).

In Lokhande and White (2018), the elastic LTB equations for a general singly symmetric box-section member are presented. These equations were employed initially in the development of the above flexural resistance provisions. However, for all box-section members within the practical extreme limits permitted by AASHTO (2020) Article 6.12.2.2.2, the simpler elastic LTB equations based on the assumption of a doubly symmetric box cross section give predictions that are always within one percent of the exact elastic LTB equations. In addition, it should be noted that the elastic LTB equations appear solely in the derivation of the L_p and L_r limits in the developments by Lokhande and White (2018). The lengths required for elastic LTB of even the most extreme box-section members are so large that members having these lengths are not possible. Therefore, only the simpler doubly symmetric box-section LTB equations were employed for the development of the L_p and L_r expressions in AASHTO (2020) Article 6.12.2.2.2e. The resulting equations for L_p and L_r are

$$L_p = 0.10 E r_y \frac{\sqrt{JA}}{M_{yce}} \qquad \text{(6.5.3-3) (AASHTO 6.12.2.2.2e-4)}$$

and

$$L_r = 0.60 E r_y \frac{\sqrt{JA}}{F_{yr} S_{xce}} \qquad \text{(6.5.3-4) (AASHTO 6.12.2.2.2e-5)}$$

where

r_y = radius of gyration of the gross box cross section about its minor principal axis

J = St. Venant torsional constant of the gross box cross section

A = gross area of the box cross section

F_{yr} = compression flange stress at the onset of nominal yielding within the cross section, including residual stress effects, for moment applied about the axis of bending, taken as $0.5F_{yc}$

Upon substituting $F_{yr} = 0.5F_{yc}$ into Eq. 4, it can be observed that $L_r = 12L_p$.

Lateral-torsional buckling will not occur in square box-sections or in box-sections bent about their minor axis. Furthermore, HSS members are typically governed by service deflection limits before there is any significant reduction in flexural strength due to LTB. AASHTO (2020) Article C6.12.2.2.2e provides specific guidance regarding general box-section member designs for which the reduction in strength due to LTB is of importance. The reduction in the flexural resistance under uniform bending is never more than approximately 10 percent for longitudinally unstiffened box-section members with $D/b_{fo} < 2.0$ and $L_b/D < 20$ that satisfy the cross-section proportion limits

of AASHTO Article 6.12.2.2.2b, where b_{fo} is the outside width of the box-section. The maximum reduction in the flexural resistance under uniform bending is approximately one-half of this value, i.e., 5 percent, for these types of members with $D/b_{fo} < 2.0$ and $L_b/D < 10$. Members that have stocky compression and tension flanges combined with webs proportioned at the maximum limit of AASHTO Eq. 6.12.2.2.2b-1 ($D/t_w = 150$) exhibit the largest reduction in strength associated with the LTB limit state. In designs where the moment gradient modifier, C_b, is greater than 1.10, this reduction is nonexistent.

The compact-flange limit of the AASHTO (2020) Article 6.12.2.2.2 provisions is taken as the nonslender plate limit for uniform axial compression, i.e., the slenderness limit at which the flange effective width, calculated from the appropriate equations discussed in Section 6.2.4.2 of this volume, is equal to the total gross flange width. In terms of a b/t limit on the compression flange, this limit is given by Eq. 6.2.4-10a, with Γ_r defined in Case 6 of Table 5 for welded box-sections, Case 5 of Table 5 for square and rectangular cold-formed HSS, and Case 4 of Table 5 for non-welded built-up box-sections. The limit given by Eq. 6.2.4-10a for Case 6 of Table 5 is comparable to the Class 1 flange limit in Eurocode 3 (CEN 2005), which is intended to ensure that the section can form a plastic hinge with a rotation capacity sufficient for plastic analysis. The limit given by Eq. 6.2.4-10a for Case 5 is comparable to the Eurocode 3 Class 2 flange limit, which is intended to ensure that the plastic moment of the cross section can be developed. The limit given by Eq. 6.2.4-10a for Case 4 is slightly larger than the Eurocode 3 Class 2 flange limit. These limits are intended to recognize the different conditions associated with each of the above section types.

It is important to note that the different forms of the plate effective width equations are often based on the idealization of simply supported edge conditions, i.e., no rotational restraint from the adjacent plates. Clearly, if one has a box-section member with a noncompact or slender flange in flexure, combined with a compact web for instance, some rotational restraint at the longitudinal edges of the flange might be anticipated from the compact web. This helps explain, conceptually, along with the influence of the R_f factor, how the M_{pe}-based model works to characterize the strength of a member with a noncompact or slender flange and a compact web.

The noncompact flange slenderness limit in flexure, which in the AASHTO (2020) Article 6.12.2.2.2 provisions has the function only of defining the slenderness beyond which R_f is reduced to a constant value of 0.85, is taken as $1.56\lambda_{pf}$, where λ_{pf} is the compact-flange limit.

The compact-web slenderness limit in AASHTO (2020) Article 6.12.2.2.2 is somewhat larger than the corresponding value for doubly symmetric box-sections in AISC (2016), and tends to be slightly larger than the Class 2 limit for noncomposite box-sections specified in Eurocode 3 (CEN 2005). The recommended equation for this limit, which is used with the web effective slenderness $2D_{ce}/t_w$ for the classification of box-section webs, is

$$\lambda_{pw} = 3.1 \frac{D_{ce}}{D_{cpe}} \sqrt{\frac{E}{F_{yc}}} \leq \lambda_{rw} \qquad (6.5.3\text{-}5)\ (\text{AASHTO } 6.12.2.2.2c\text{-}3)$$

where D_{ce} is the depth of the web in compression corresponding to first nominal yielding of the effective compression flange, and D_{cpe} is the depth of the web in compression at the plastic

moment, determined considering the box cross section with the effective width of the compression flange.

The AASHTO (2020) Article 6.12.2.2.2 noncompact-web slenderness limit, which is the value of $2D_{ce}/t_w$ beyond which R_{pc} is a constant value equal to R_h, and beyond which R_b reduces below 1.0, is taken as

$$\lambda_{rw} = 4.6\sqrt{\frac{E}{F_{yc}}} \qquad\qquad \text{(6.5.3-6) (AASHTO 6.12.2.2.2c-6)}$$

The theoretical background to the coefficient of 4.6 in this equation is discussed in Section 6.3.10.2 of this volume. This limit is based on the assumption of simply supported edge conditions at the web-flange juncture, and is the same as the noncompact web limit for I-sections in cases where the area of the I-section flanges is small relative to the web area (see Section 6.3.5.2.1 of this volume). This limit is slightly larger than the Class 3 limit for noncomposite box-sections specified by Eurocode 3 (CEN 2005).

The AISC (2016) Section F7 provisions have a substantial flaw in their formulation for members having a slender compression flange combined with noncompact or slender webs. There is a significant discontinuity in the flexural resistance predicted by the AISC (2016) Eqs. F7-6 and F7-9 when the webs transition from noncompact to slender. This flaw has been eliminated in draft provisions for the 2022 AISC *Specification* by removing the provisions for box-section members with slender webs and slender flanges, and by inserting a user note stating that box-sections with slender webs and slender flanges are not addressed. However, AISC (2016) and the draft 2022 AISC *Specification* provisions still quantify the flexural resistance as the minimum value from four independent limit state checks – full plastification of the cross section in flexure (corresponding to the plastic moment resistance, M_p), web local buckling, compression flange local buckling, and lateral-torsional buckling. There is evidence that these limit states interact in certain cases, and that quantifying the flexural resistance as the smallest of these four independent limit states checks has limited accuracy (Lokhande and White 2018).

It should be noted that AASHTO (2020) Article 6.12.1.2.3a points to AASHTO Article 6.10.9 for the web shear resistance calculations in noncomposite box-section members, using an equivalent flange area for determining whether Basler's complete tension field action equation or the true Basler partial tension field action equation applies for calculating the ultimate shear resistance (see Section 6.3.8 of this volume).

6.5.4 Circular Tubes and Round HSS

AASHTO (2020) Article 6.12.2.2.3 adopts the following equations directly from AISC (2016) for the nominal flexural resistance of noncomposite circular tubes having *D/t* ratios less than $0.45E/F_y$:

$$M_n = M_p \text{ for } D/t \leq 0.07 \; E/F_y \qquad \text{(6.5.4-1) (AASHTO 6.12.2.2.3-1, AISC F8-1)}$$

$$M_n = \left(\frac{0.021E}{D/t} + F_y \right) S \quad \text{for } 0.07 \ E/F_y < D/t \le 0.31 \ E/F_y \tag{6.5.4-2}$$

<div align="right">(AASHTO 6.12.2.2.3-2, AISC F8-2)</div>

$$M_n = \frac{0.33ES}{D/t} \quad \text{for } D/t \le 0.31 \ E/F_y \tag{6.5.4-3}$$

<div align="right">(AASHTO 6.12.2.2.3-3 & 6.12.2.2.3-4, AISC F8-3 & F8-4)</div>

The failure modes and postbuckling behavior of these types of members can be grouped into the following three categories (Sherman 1992; Ziemian 2010):

1. For D/t less than about $0.05E/F_y$, a long inelastic plateau occurs in the moment-rotation curve. The cross section gradually ovalizes, then eventually local buckling waves eventually form, after which the moment resistance slowly decays. The flexural resistance may exceed the theoretical plastic moment due to strain hardening.

2. For $0.05E/F_y \le D/t \le 0.10E/F_y$, the plastic moment is nearly achieved but a single local buckle develops and the moment decays slowly with little or no inelastic plateau.

3. For $D/t > 0.10E/F_y$, multiple buckles form suddenly with little ovalization, and the bending moment drops rapidly to a more stable level.

The above equations reflect the above regions of behavior for specimens with long constant moment regions and little restraint against ovalization at the failure location. They are based on five North American studies involving hot-formed seamless pipe, electric-resistance-welded pipe and fabricated tubing (Sherman 1992; Ziemian 2010).

Circular tubes and round HSS are apt to be used in certain applications involving significant torsion. As such, their strength may be governed by a limit state involving combined shear due to torsion plus shear due to bending. The consideration of these strengths is addressed in AASHTO (2020) Article 6.12.1.2.3. The torsional resistance of these types of members is taken as

$$T_n = F_{cv}C \tag{6.5.4-4} \quad \text{(AASHTO 6.12.1.2.3b-4)}$$

where

$$C = \frac{\pi(D-t)^2 t}{2} \tag{6.5.4-5} \quad \text{(AASHTO 6.1.1.2.3b-5)}$$

F_{cv} = torsional shear buckling resistance, taken as the larger of

$$F_{cv1} = \frac{1.23E}{\sqrt{L/D}\,(D/t)^{5/4}} \le 0.58F_y \tag{6.5.4-6} \quad \text{(AASHTO 6.12.1.2.3b-6)}$$

and

$$F_{cr2} = \frac{0.60E}{(D/t)^{3/2}} \leq 0.58F_y \qquad \text{(6.5.4-7) (AASHTO 6.12.1.2.3b-7)}$$

D =   outside diameter

L =   length of the member

and

t =   wall thickness (for round HSS, the provisions of AASHTO Article 6.12.1.2.4 are referenced for the definition of t for the design calculations)

In addition, the shear resistance of these types of members is taken as

$$V_n = 0.5F_{cr}A_g \qquad \text{(6.5.4-8) (AASHTO 6.12.1.2.3b-1)}$$

where

A_g =   gross area of the section based on the design wall thickness

F_{cr} =   flexural shear buckling resistance, taken as the larger of 1.3 times the critical stress values for torsion given by Eqs. 6 and 7, but with the length L_v substituted for L, where L_v is the distance between points of maximum and zero shear, or the full length of the member if the shear does not go to zero within the member length

The critical buckling stress F_{cr} used with Eq. 8 is taken as 1.3 times the critical stress for torsion and the length term is in the Eq. 6 is taken as L_v since the flexural shear typically has a gradient (Brockenbrough and Johnston 1981; Ziemian 2010). The nominal flexural shear resistance is based on the assumption that the shear stress at the neutral axis, $V/\pi Rt$, is at F_{cr}, where V is the cross-section shear force and $R = D/2$.

Given the factored applied torque and flexural shear and, T_u and V_u, and the above resistances T_n and V_n, the shear strength limit state under combined torsion and flexural shear is expressed as

$$\frac{V}{\phi_v V_n} + \frac{T}{\phi_T T_n} \leq 1.0 \qquad \text{(6.5.4-9) (AASHTO 6.12.1.2.3a-5)}$$

where ϕ_v and ϕ_T are defined by AASHTO Article 6.5.4.2 as 1.0. The influence of the flexural and torsional shear on the combined axial compressive and flexural strength of circular tubes and round HSS also must be considered. This strength check is addressed subsequently in Section 6.6.3.2 of this volume.

6.5.5   Tees and Double Angles Loaded in their Plane of Symmetry

AASHTO (2020) Article 6.12.2.2.4 adopts the model defined in the AISC (2016) *Specification* for the calculation of the flexural resistance of tees and double angles loaded in their plane of

symmetry. This model takes the nominal flexural strength as the smallest value obtained considering the limit states of yielding, i.e., the plateau strength, lateral-torsional buckling, flange local buckling, and local buckling of the tee stem or the side-by-side double angle web legs. The side-by-side double angle web legs may either be in continuous contact or connected with separators. For angles connected by separators, connectors should be placed at an interval a along the member length such that the a/r_i of each of the angles between the connectors does not exceed ¾ of the governing slenderness ratio of the double angle member, where r_i is the minimum slenderness ratio of each angle (this basic requirement is stated in AASHTO Article 6.9.4.3 and is discussed in Section 6.2.5 of this volume). Each of the flexural strength limit states is discussed below.

Important applications involving flexure of tee sections in bridge construction include loading of struts in eccentric tension or compression via a flange connection to gusset plate, as well as the transverse loading on double angles used as a cross-frame top chord that also supports a deck joint at bridge abutments.

6.5.5.1   Yielding

The flexural resistance associated with the yielding limit state depends significantly on whether the tee stem or double angle web legs are in flexural tension or flexural compression. AISC (2016) uses the symbol M_p in its Section F9-1 to define an overall equivalent plastic moment of sorts, and takes this moment as the yielding (plateau) resistance. That is, for the limit state of yielding, AISC (2016) writes

$$M_n = M_p$$
(6.5.5-1) (AISC F9-1)

where M_p is as defined below. AASHTO (2020) Article 6.12.2.2.4b writes the yielding resistance directly based on the equations below without defining the equivalent plastic moment of the section, M_p. It then uses the symbol M_p without defining the term in writing the strengths for the other limit states. The intent in AISC (2016) is that the equivalent plastic moment is used for M_p, as defined below, when M_p is employed in the description of the other limit states. This is an important distinction, since the true theoretical plastic moment of the section can be substantially larger than the following equivalent plastic moments.

For cases with tee stems or web legs in tension, the equivalent plastic moment is expressed as the true plastic moment, but not larger than 1.6 times the yield moment:

$$M_p = F_y Z_x \leq 1.6 M_y$$
(6.5.5-2) (AASHTO 6.12.2.2.4b-1; AISC F9-2)

where the yield moment is expressed as

$$M_y = F_y S_x$$
(6.5.5-3) (AISC F9-3)

and

S_x =   elastic section modulus about the x-axis with respect to the tip of the tee stem or the double angle web legs.

The limit of $1.6M_y$ is intended to indirectly preclude potential significant yielding under service loading conditions.

The smallest shape factor of all the ASTM A6 WT, MT and ST shapes is $Z_x/S_x = 1.75$. In addition, the smallest shape factor listed for all the double angles in the AISC shapes database (AISC 2021) is $Z_x/S_x = 1.73$. Therefore as a practical matter, one can always use $1.6M_y$ as the equivalent plastic moment, or plateau strength, for rolled tee and double angle sections when the tee stem or the web legs are in tension.

Tee sections are relatively weak and unaccommodating of the onset of yielding of their stem in flexural compression. Therefore, the equivalent plastic moment is taken as

$$M_p = M_y \qquad\qquad\qquad \text{(6.5.5-4) (AASHTO 6.12.2.2.4b-2; AISC F9-4)}$$

when the stem is in flexural compression.

For double angles with the web legs in flexural compression, the equivalent plastic moment is taken as

$$M_p = 1.5M_y \qquad\qquad\qquad \text{(6.5.5-5) (AASHTO 6.12.2.2.4b-3; AISC F9-5)}$$

This equivalent plastic moment comes from the recommendations by Earls and Galambos (1997) for single angles.

6.5.5.2   Lateral-torsional buckling

The AISC (2016) and AASHTO (2020) provisions for tees and double angles utilize a simplified elastic LTB equation developed by Kitipornchai and Trahair (1980). This equation is based on the characteristics of tee and double angle sections in that their warping constant, C_w, is essentially zero, and their shear center is located at the juncture of the mid-thickness of the flange or flange elements, and the step or web elements of the cross section (Ziemian 2010). Ellifritt et al. (1992) reviewed this equation and other prior AISC equations for tees and compared the results to experimental tests. The AISC (2016) and AASHTO (2020) elastic LTB resistances are expressed as

$$M_{cr} = \frac{1.95E}{L_b}\sqrt{I_y J}\left(B + \sqrt{1+B^2}\right) \qquad \text{(6.5.5-6) (AASHTO 6.12.2.2.4c-5; AISC F9-10)}$$

where

$$B = 2.3\frac{d}{L_b}\sqrt{\frac{I_y}{J}} \qquad\qquad \text{(6.5.5-7) (AASHTO 6.12.2.2.4c-6; AISC F9-11)}$$

when the tee stem or web legs are in flexural tension, and

211

$$B = -2.3 \frac{d}{L_b} \sqrt{\frac{I_y}{J}}$$ (6.5.5-8) (AASHTO 6.12.2.2.4c-10; AISC F9-12)

when the tee stem or web legs are in flexural compression.

For cases with the stem or the web legs subjected to flexural tension, the overall AISC and AASHTO LTB strength curve for tee and double angle members has the same general form as illustrated previously for I-section members in Figure 59. The compact bracing limit is defined as

$$L_p = 1.76 r_y \sqrt{\frac{E}{F_y}}$$ (6.5.5-9) (AASHTO 6.12.2.2.4c-3; AISC F9-8)

which is the same form as the compact bracing limit given by Eq. 6.3.5-13 (Section 6.3.5 of this volume) for doubly symmetric compact web and compact flange I-section members from AISC (2016). It should be noted, however, that the r_y of a tee section is essentially only one-half of the r_y of the corresponding rolled I-section.

The noncompact bracing limit for cases with the stem or the web legs in flexural tension is derived the same way as the L_r equation for I-section members (Eq. 6.3.5-29 of this volume) except that the ordinate for the inelastic-to-elastic buckling transition, Anchor point 2 in Figure 59, is taken as the cross section first-yield moment, M_y. This gives

$$L_r = 1.95 \frac{E}{F_y} \frac{\sqrt{I_y J}}{S_x} \sqrt{2.36 \left(\frac{F_y}{E} \right) \frac{d\, S_x}{J} + 1}$$ (6.5.5-10) (AASHTO 6.12.2.2.4c-4; AISC F9-9)

where

d	=	depth of the tee or width of the double angle web leg
I_y	=	moment of inertia about the y-axis
J	=	St. Venant torsional constant
L_b	=	unbraced length
r_y	=	radius of gyration about the y-axis

The smallest value of L_r/d for all the ASTM A6 WT sections is 22. Therefore, WT members with their stems in tension are not usually long enough to be governed by elastic LTB.

Where the tee stem or web legs are loaded in flexural compression at any location along the unbraced length, the LTB resistance is substantially smaller at these locations than in the above case there they are in tension. Where a stem is in flexural compression, the LTB resistance of a tee section member is written simply as

$$M_n = M_{cr} \leq M_y \qquad (6.5.5\text{-}11) \text{ (AASHTO 6.12.2.2.4c-7; AISC F9-7)}$$

where M_{cr} is defined by Eqs. 6 and 8. For this case with double angles, the LTB resistance is written as follows:

If $\dfrac{M_y}{M_{cr}} \leq 1.0$:

$$M_n = \left(1.92 - 1.17\sqrt{\dfrac{M_y}{M_{cr}}}\right) M_y \leq 1.5 M_y \quad (6.5.5\text{-}12) \text{ (AASHTO 6.12.2.2.4c-8; AISC F10-2)}$$

If $\dfrac{M_y}{M_{cr}} > 1.0$:

$$M_n = \left(0.92 - 0.17\dfrac{M_{cr}}{M_y}\right) M_{cr} \leq 1.5 M_y \quad (6.5.5\text{-}13) \text{ (AASHTO 6.12.2.2.4c-8; AISC F10-2)}$$

where M_{cr} is determined as specified by Eqs. 6 and 8. Equations 12 and 13 are based on the AISC (2016) provisions for the LTB resistance of single angles without continuous lateral-torsional restraint along the length.

The C_b factor used for I-section members is unconservative for tee beams with the stem in compression. For such cases, $C_b = 1.0$ is appropriate. When these types of beams are bent in reverse curvature, the portion with the stem in compression may control the LTB resistance even though the moments in this portion may be small compared to those at other locations along the unbraced length. Since the buckling strength is sensitive to the moment diagram, C_b is conservatively taken as 1.0 in all of the LTB calculations for tees and double angles loaded in the plane of symmetry. The commentaries of AASHTO Article C6.12.2.2.4c and AISC Section F9 state that for cases where a tee stem is in tension, connection details should be designed to minimize end restraint moments that may cause the stem to be in flexural compression at the ends of the member.

Some of the wording of the AISC Section F9.2 and the AASHTO Article 6.12.2.2.4c provisions implies that one should use the LTB resistance equations for the stem or the double angle web legs in compression to check the resistance to a maximum moment causing tension in the stem or double angle web legs whenever there is a moment causing flexural compression in the stem or double angle web legs at any location along the length. This interpretation is believed to be unnecessarily conservative. The LTB resistance for the case with the step or double angle webs in flexural tension should be checked when these elements are in flexural tension, and LTB resistance for the step or double angle webs in flexural compression should be checked for the other case, both using $C_b = 1.0$.

6.5.5.3 Flange local buckling

The general form of the flange local buckling resistance (FLB) strength curves for tees and double angles loaded in the plane of symmetry is the same as that shown for I-section members in Figure 59. For flanges of tees, the compact and noncompact flange limits, λ_{pf} and λ_{rf}, are identical to those for rolled I-section members. Furthermore, the implicit value for k_c employed within the elastic FLB strength equation is the same as that employed for rolled I-section beams in AISC (2016), i.e., $k_c = 0.76$. This results in a net coefficient in the elastic FLB equation of 0.901 (0.76) = 0.687, considering the theoretical form shown in Eq. 6.2.4-1, which AISC and AASHTO round to 0.7.

For double angles with the flange legs subjected to flexural compression, the FLB limit state is not applicable when $b/t \leq \lambda_{pf}$, where

$$\lambda_{pf} = 0.54\sqrt{\frac{E}{F_y}}$$

(6.5.5-14) (AASHTO 6.12.2.2.4d-7; AISC Table B4.1b)

For $\lambda_{pf} < b/t \leq \lambda_{rf}$, inelastic FLB governs and the FLB resistance is written as

$$M_n = F_y S_{xc}\left(2.43 - 1.72\frac{b}{t}\sqrt{\frac{F_y}{E}}\right)$$

(6.5.5-15)

(AASHTO 6.12.2.2.4d-3; AISC F10-6 & Section F9.3(b))

where

$$\lambda_{rf} = 0.91\sqrt{\frac{E}{F_y}}$$

(6.5.5-16) (AASHTO 6.12.2.2.4d-9; AISC Table B4.b)

It should be observed that for the double angle members listed in the AISC section property tables, the smallest value of $F_y S_{xc}$ is 1.09 times $1.5 F_y S_x$, the average value of $F_y S_{xc}$ is 1.67 times $1.5 F_y S_x$, and the maximum value of $F_y S_{xc}$ is 2.55 times $1.5 F_y S_x$. At $b/t = \lambda_{pf}$, Eq. 15 gives an $M_n = 1.50 F_y S_{xc}$, but this value is moderately to substantially larger than $1.5 F_y S_x$. The smallest value of $F_y S_{xc}$ is 0.76 times $F_y Z_x$, the average value of $F_y S_{xc}$ is 1.39 times $F_y Z_x$, and the maximum value of $F_y S_{xc}$ is 2.13 times $F_y Z_x$. Therefore, it is recommended that S_{xc} in Eq. 15 should be taken as the smaller elastic modulus value, S_x.

The values of λ_{pf} and λ_{rf} are somewhat liberal compared to the compact and noncompact limits for flanges in other types of sections, and are based on Earls and Galambos (1997).

For $b/t > \lambda_{rf}$, the FLB resistance of double angle sections is expressed as

$$M_n = \frac{0.7 E S_{xc}}{(b/t)^2}$$

(6.5.5-17)

(AASHTO 6.12.2.2.4d-4; AISC F10-7 & F10-8 & Section F9.3(b))

At $b/t = \lambda_{rf}$, both Eqs. 17 and 15 give $M_n = 0.86F_yS_{xc}$. However, based on the above observations, this value will be larger than F_yZ_x in many cases. Therefore, it is recommended that S_{xc} in Eq. 17 should also be taken as the smaller elastic modulus value, S_x. This is more consistent with the definition of the elastic section modulus in AISC (2016) Section F10.3(c). The above anomalies are due to the use of elastic section moduli in defining the resistances of members where early yielding in tension at the opposite extreme fiber invalidates the assumption of elastic cross-section stresses.

6.5.5.4 Local buckling of tee stems and double angle web legs in flexural compression

For calculation of the local buckling strength of tee stems in flexural compression, the width-to-thickness ratio is taken as the total depth of the section divided by the thickness of the stem, d/t_w. The general form for the characterization of this strength limit state follows that shown in Figure 59. For calculation of the compact limit pertaining to this strength limit state, AISC (2016) and AASHTO (2020) base their characterization of the local buckling strength of tee stems in flexural compression on an underlying assumed value of $k_c = 1.61$ and a corresponding elastic buckling stress of $2.0F_y$. This gives the compact limit

$$\lambda_{pw} = 0.84\sqrt{\frac{E}{F_y}}$$

(6.5.5-18) (AISC Table B4.1b)

Furthermore, for calculation of the noncompact limit as well as the elastic buckling strength, AISC (2016) and AASHTO (2020) base their characterization of the local buckling strength on $k_c = 1.68$ and a corresponding elastic buckling stress of $0.65F_y$. This gives the noncompact limit

$$\lambda_{rw} = 1.52\sqrt{\frac{E}{F_y}}$$

(6.5.5-19) (AISC Table B4.1b)

and the elastic buckling strength

$$M_n = \frac{1.52ES_x}{\left(d/t_w\right)^2}$$

(6.5.5-20) (AASHTO 6.12.2.2.4e-4; AISC F9-19)

For double angles with the web legs subjected to flexural compression, the local buckling resistance of the web legs is taken the same as that described by Eqs. 14 to 16, with S_{xc} taken as the elastic section modulus about the x-axis with respect to the tip of the double angle web legs.

The AISC (2016) Commentary also provides guidelines for calculating the resistance of tees and double-angles bent about their y-axis. This case is not addressed in this volume, since it is expected to be rare for bridge applications.

6.5.6 Channels in Strong- and Weak-Axis Bending

AASHTO (2020) adopts the AISC (2016) provisions for calculation of the flexural resistance of channels. AISC (2016) uses a generalized form of the compact I-section member equations for channels subjected to major-axis bending. This generalized form simply uses

$$X^2 = \frac{S_x h}{J c} \qquad (6.5.6-1)$$

where

$$c = \begin{cases} 1 & \text{for doubly-symmetric I-shapes} \\ \dfrac{h}{2}\sqrt{\dfrac{I_y}{C_w}} & \text{for channels} \end{cases} \qquad (6.5.6-2)$$

in place of Eq. 6.3.5-23 of this volume. This equation simply provides a conversion from the implicit warping constant C_w for doubly symmetric I-section members to the C_w for channel sections. This generalized form also uses Eq. 6.3.5-24 from Section 6.3.5 of this volume for the radius of gyration term r_t. The LTB resistance equations, i.e., Eqs. 6.3.5-22, 6.3.5-27, etc., are otherwise unchanged. The AISC (2016) equations for channels assume compact flanges and webs. All of the ASTM A6 channels have compact flanges and webs for $F_y \leq 65$ ksi. As such, the flanges and webs of fabricated channels must satisfy Eqs. 6.3.5-19 and

$$\frac{D}{t_w} \leq 3.76 \sqrt{\frac{E}{F_y}} \qquad (6.5.6-3)$$

respectively.

The AISC (2016) resistance equations for channels in major-axis bending are based on the assumption that the other members that frame into the channel are sufficient to restrain the twisting of the member (Johnston 1976; McGuire 1968). Based on this assumption, bending without twisting occurs between the supports.

AASHTO (2020) also bases its provisions for weak-axis bending of channels on the corresponding AISC (2016) Section F6 provisions. For channel-section members subjected to minor-axis flexure, AISC (2016) uses its equations for minor-axis flexure of I-section members (see Section 6.5.2 of this volume). AISC (2016) places a limit of $1.6F_yS_y$ on the maximum minor-axis bending flexural resistance. For I-section members, the shape factor Z_y/S_y is nearly always less than 1.6 (only four ASTM A6 W-shapes have a $Z_y/S_y > 1.6$). However, for channel-sections, Z_y/S_y is generally greater than 1.6. Similar to the $M_{max} = 1.6M_y$ limit for tee-sections with the stem in tension, the use of $M_{max} = 1.6F_yS_y$ for channel sections is intended to indirectly prevent substantial yielding at service load levels. Interestingly, the AISC (2016) Section F6 provisions do not give any restriction on the slenderness of the web for channels in weak-axis bending. However, if the web is loaded in flexural compression, the AISC Section F6 provisions are based implicitly on a compact web response. The slenderness limit

$$\frac{D}{t_w} \le 1.12\sqrt{\frac{E}{F_y}} \tag{6.5.6-4}$$

may be taken as a sufficient requirement to ensure the compact behavior of the web in this case. AASHTO (2020) specifies Eq. 3 instead, which is in error since this equation is for a web bent about an axis normal to its plane.

6.5.7 Rectangular Bars and Rounds

In addition, AASHTO (2020) uses the AISC (2016) for calculation of the flexural resistance of rectangular bars and rounds. For rectangular bars bent about their major-axis, the AISC (2016) resistances are based on lateral-torsional buckling and have the same form as shown previously in Figure 59. For these member types, the maximum potential resistance is

$$M_{max} = M_p \tag{6.5.7-1 (AASHTO 6.12.2.2.7-1, AISC F11-1)}$$

Anchor Point 1 has the abscissa

$$L_p = 0.08\frac{t^2}{d}\frac{E}{F_y} \tag{6.5.7-2}$$

where d and t are the section depth and width respectively, and Anchor Point 2 has the abscissa

$$L_r = 1.9\frac{t^2}{d}\frac{E}{F_y} \tag{6.5.7-3}$$

and an ordinate of M_y (i.e., residual stress effects are neglected at the elastic-to-inelastic LTB transition point). Furthermore, the nominal elastic LTB capacity may be expressed for these sections in terms of the bending moment or in terms of the maximum bending stress, respectively, as:

$$M_{e.LTB} = C_b\frac{\pi}{L_b}\sqrt{EI_y GJ} = C_b\frac{\pi}{L_b}\frac{E}{\sqrt{2.6}}\sqrt{\frac{dt^3}{12}\frac{dt^3}{3}} = 0.32C_b E\frac{dt^3}{L_b} \tag{6.5.7-4}$$

$$F_{e.LTB} = \frac{M_{e.LTB}}{S_x} = C_b\frac{1.9E}{L_b d/t^2} \qquad \tag{6.5.7-5 (AASHTO 6.12.2.2.7-3, AISC F11-3 \& F11-4)}$$

For solid rounds and rectangular bars bent about their minor axis, AISC and AASHTO give the flexural resistance as

$$M_n = M_p \le 1.6M_y \tag{6.5.7-6}$$

One might note that AISC (2016) and AASHTO (2020) also specify the limit of $1.6M_y$ with Eq. 6.5.7-1. However, since the shape factor for a rectangular bar is equal to 1.5, the limit $1.6M_y$ is never reached for these sections.

6.5.8 Single Angles

Single angles are generally not intended as flexural members in bridge construction. Furthermore, the practical condition of flexure due to eccentric axial compression is addressed via the equivalent slenderness, *KL/r*, expressions discussed in Section 6.2.3 of this volume, and the practical condition of flexure due to eccentric axial tension is addressed via the shear lag coefficient *U* (see Section 6.5.1). Therefore, the calculation of the flexural resistance of single-angle members is not addressed in this document. The reader is referred to AISC (2016) and the references provided in the commentary of the AISC Specification for flexural resistance equations and discussion of the flexural behavior of single-angle members.

6.5.9 Concrete-Encased and Concrete-Filled Tube Members

6.5.9.1 Overview

AASHTO (2020) Articles 6.12.2.3.1 and 6.12.2.3.2 specify the AISC (1999) LRFD Specification approach as the base AASHTO method to quantify the flexural resistance of concrete-encased and concrete-filled tube members. In addition, the AASHTO (2020) Specifications provide a separate Article 6.12.2.3.3 detailing alternative calculation procedures recognizing the enhanced strength characteristics of circular concrete-filled steel tubes (CFSTs) that satisfy the restrictions specified by Article 6.9.6.2 (discussed previously in Section 6.7.2.4 of this volume). AASHTO (2020) Article 6.12.2.3.3 refers to two methods of performing the flexural strength calculations for CFSTs:

- The plastic stress distribution method (PSDM), and
- The strain compatibility method (SCM).

However, the guidance provided in AASHTO Article C6.12.2.3.3 is focused on the PSDM. The PSDM simply involves the assumptions that (1) the steel tube and any longitudinal reinforcing steel bars are stressed to their specified minimum yield strength throughout their areas, either in tension or in compression, (2) the concrete portion of the cross section is stressed at $0.95f_c'$ everywhere on the compression side of the neutral axis, where f_c' is the specified minimum 28-day compressive strength of the concrete, and (3) the concrete is fully cracked and the concrete stresses are entirely zero on the tension side of the neutral axis. The SCM is more akin to typical reinforced concrete section calculations in which (1) a linearly-varying strain distribution is assumed through the cross section, (2) all the steel stresses are then calculated based a specified steel stress-strain response (typically elastic-perfectly plastic), (3) the concrete contribution on the compression side of the neutral axis follows some specified stress-strain curve (or an idealization akin to the Whitney stress block), and (4) the concrete stresses in tension are again entirely neglected.

For the case of bending under zero axial compression, the PSDM cited in AASHTO (2020) Article 6.12.2.3.3 and discussed in Article C6.12.2.3.3 is the same as the procedure specified in AISC (2016) for "compact" filled composite sections (although AASHTO Article C6.9.6.1 states that CFSTs should not be used as pure flexural members).

Section 6.5.9.2 below explains the background to the AASHTO (2020) Article 6.12.2.3.1/ 6.12.2.3.2 - AISC (1999) approach. This is followed by Section 6.5.9.3, which discusses a number

of important qualifications pertaining to the AISC (2016) and AASHTO (2020) Article 6.12.2.3.3 PSDM procedures. The subsequent Section 6.6.4 of this volume addresses the broader consideration of combined axial force and flexure in composite column-type members.

6.5.9.2 AASHTO (2020) Article 6.12.2.3.1/6.12.2.3.2 - AISC (1999) approach

For concrete-encased shapes that satisfy the specific detailing requirements on the lateral and longitudinal reinforcement defined in AASHTO Article 6.9.5.2.3, AASHTO Article 6.12.2.3.1 defines the flexural resistance for members that are not subjected to any axial compression as the smaller of:

1. The plastic moment resistance of the steel section alone, M_{ps}, and
2. The yield moment of the composite section, M_{yc}, determined accounting for the different moments applied to the noncomposite, long-term composite, and short-term composite cross sections, and neglecting any of the concrete loaded in tension.

The concrete is assumed to prevent local buckling of the steel, and hence concrete-encased shapes are not subject to the width/thickness limitations of AASHTO Article 6.9.4.2 (discussed in Section 6.2.4 of this volume).

Furthermore, for concrete-encased shapes subjected to combined compression and flexure with $P_u/\phi_c P_n \geq 0.3$, AASHTO Article 6.12.2.3.1 specifies that the flexural resistance may be calculated as

$$M_n = Z\,F_y + \frac{(H_c - 2c)A_r F_{yr}}{3} + \left(\frac{H_c}{2} - \frac{A_w F_y}{1.7\,f_c'\,B_c}\right)A_w F_y \quad \text{(6.5.9-1) (AASHTO 6.12.2.3.1-3)}$$

where

A_r = total area of the longitudinal bar reinforcement in the composite column cross section,

A_w = the web area of the structural steel section, i.e., $d\,t_w$ for an I-section member, where d is the total depth of the steel section and t_w is the thickness of the web,

B_c = the total width of the composite cross section perpendicular to the plane of bending (AASHTO uses the variable b; B_c is employed herein to emphasize this is the width of the composite section, and to be consistent with the use of H_c below).

F_y = the yield strength of the structural steel section,

F_{yr} = the yield strength of the reinforcing steel,

H_c = the total depth of the composite cross section in the plane of bending (AASHTO uses the variable d; H_c is employed herein to emphasize this is the depth of the composite cross section and to avoid conflict with the common definition of d as the total depth of the steel section),

Z = plastic section modulus of the steel section about the axis of bending ($M_{ps} = Z\,F_y$),

c = the average distance from the compression face to the longitudinal reinforcement adjacent to that face and the distance from the tension face to the longitudinal reinforcement adjacent to that face, and

f_c' = the specified minimum 28-day compressive strength of the concrete.

Equation 1 gives a simplified estimate of the appropriate fully-plastic flexural resistance for use with the AASHTO (2020) beam-column strength interaction equations. The first, second and third terms of this equation are the estimated plastic moment contributions from the steel shape, the reinforcing bars, and the reinforced concrete, respectively. In the second term, it is assumed that at least one-third of the longitudinal bars in the cross section can be considered to be located at the distance c from the tension and compression faces of the cross section. To obtain the third term, the web of the encased shape is taken as the tension reinforcement for the concrete cross section with a flexural depth equal to half the overall depth of the composite section in the plane of bending.

If $P_u/\phi_c P_n$ is less than 0.3, AASHTO Article 6.12.2.3.1 requires that the flexural resistance shall be determined by a straight-line transition between the value obtained from Eq. 1 at $P_u/\phi_c P_n = 0.3$ and the flexural resistance at $P_u = 0$ (defined above as $M_{ps} = Z F_y$ or M_{yc}).

The above approach is supported by comparisons to 44 beam-column tests with concrete-encased steel shapes (Galambos and Chapuis 1980). This approach is essentially the same as the method detailed in AISC (1999). The only difference is that the AASHTO procedure does not allow for any consideration of the influence of shear connectors. The AISC (1999) provisions allowed the flexural resistance at $P_u = 0$ to be taken as the corresponding beam fully-plastic composite section resistance if adequate shear connectors were provided and the concrete longitudinal and lateral bars met specific requirements. Also, when shear connectors were not provided, AISC (1999) specified that either the steel section plastic moment resistance or the composite section yield resistance at $P_u = 0$ could be used in determining the nominal flexural capacity.

For concrete-filled sections, AASHTO (2020) Article 6.12.2.3.2 assumes the use of circular tubes and specifies the following flexural resistance equations:

$$M_n = M_{ps} \quad \text{for} \quad \frac{D}{t} < 2.0\sqrt{\frac{E}{F_y}} \qquad \text{(6.5.9-2) (AASHTO 6.12.2.3.2-1)}$$

and

$$M_n = M_{yc} \quad \text{for} \quad 2.0\sqrt{\frac{E}{F_y}} \leq \frac{D}{t} \leq 8.8\sqrt{\frac{E}{F_y}} \qquad \text{(6.5.9-3) (AASHTO 6.12.2.3.2-2)}$$

where M_{ps} and M_{yc} are defined at the beginning of this section. These equations are a simplification of the AISC (1999) provisions. For filled sections, AISC (1999) specified the use of the same approach as defined above for encased sections, but with A_w taken equal to zero in Eq. 1. This approach is supported by comparisons to 48 beam-column tests of concrete-filled pipe and tubing (Galambos and Chapuis 1980).

AISC (1999) Section I2.4 specified a number of shear connector requirements for transfer of the axial force from the steel to the concrete and vice-versa, to ensure that the steel and the concrete work compositely. For concrete-encased members, AISC (1999) Section I2.4 required that an adequate number of shear connectors must be provided along the length of the member to develop the axial forces into the composite cross section. The maximum spacing of these connectors was not allowed to exceed 16 in, and connectors were required on at least two faces of the steel shape in a configuration symmetrical about the cross section. The commentary of AISC (1999) indicated that force transfer by bond is generally disregarded in encased members, but is commonly used in concrete-filled HSS members as long as the connections are detailed to limit local deformations. However, it noted that no guidelines were available for structures other than fixed offshore platforms. No specific guidelines were provided for the shear connector requirements in concrete-filled members in the AISC (1999) Specification. Also, no specific shear connector requirements were provided for development of the bending moments into the composite cross section of concrete-encased or filled members.

6.5.9.3   AISC (2016) and Alternative AASHTO Article 6.12.2.3.3 Approaches

The AISC (2016) provisions for the nominal flexural resistance of concrete-encased members are essentially the same as AISC (1999) for the case of $P_u = 0$. Also, presumably, Eq. 1 and the linear interpolation between this equation and the strength at $P_u = 0$ is still allowed for concrete encased members where the shear transfer between the concrete and the steel is not provided according to the Specification requirements. However, for filled composite members, AISC (2016) emphasizes a direct plastic stress distribution based approach (the PSDM) that provides significantly enhanced strength estimates for members, assuming adequate shear transfer between the concrete and the steel. Section 6.6.3 of this volume explains this enhanced procedure in more detail for the general case of combined flexure and axial compression. In addition, AISC (2016) provides additional equations that quantify a reduced flexural resistance for filled composite sections where the steel section is classified as noncompact or slender in flexural compression (see Section 6.2.7 of this volume for a description of these and other definitions of "compact," "noncompact," and "slender" in the AISC (2016) and AASHTO (2020) Specifications).

AISC (2016) provides substantial information about force transfer mechanisms and concrete anchorage and shear connector requirements for composite members.

As noted in the above Section 6.5.9.1 of this volume, the AASHTO (2020) Article 6.12.2.3.3 and C6.12.2.3.3 procedures are the same as the AISC (2016) procedures for the ideal case of flexure under zero axial load, and they utilize and highlight the plastic stress distribution method (PSDM). Section 6.6.4 of this volume addresses the broader consideration of combined axial force and flexure in composite column-type members.

6.6   Combined Axial Load, Uniaxial and/or Biaxial Flexure, Shear and Torsion

6.6.1   Introduction

Section 6.1 of this volume addresses the resistance of members under concentric axial tension, Section 6.2 addresses the resistance of members under concentric axial compression, and Sections 6.3 through 6.5 address the flexural resistance of I- and box-section members and members with

other miscellaneous cross-section profiles. For members subjected to combined bending and axial load, commonly referred to as beam-columns, the AASHTO (2020) and AISC (2016) Specifications define the resistance by interaction equations that reduce to the above resistances in the limit of pure axial loading (with zero flexure) or flexure about a single principal axis (with zero axial load).

Strength interaction equations addressing axial tension or compression in combination with uniaxial or biaxial bending and other loading effects generally involve significant simplification.

Section 6.6.2 summarizes the base strength interaction equations defined in AASHTO (2020) and in the primary AISC (2016) beam-column provisions. Section 6.6.3 then provides an overview of how the AASHTO (2020) Article 6.9.2.2.2 and 6.8.2.3.2 provisions supplement these base beam-column interaction equations to account for the combined influence of torsional and/or flexural shear.

Section 6.6.4 provides an overview of an approach for separate checking of cross sections that may be vulnerable to tension rupture, implemented in AASHTO (2020) Article 6.8.2.3, which accounts for the additive effects of axial tension and flexure as well as the beneficial effects of axial compression when combined with flexural tension.

Section 6.6.5 then discusses further details of the fundamental background to the equations presented in Section 6.6.2 and 6.6.3 and summarizes extensions to and enhancements of these equations for a number of specific cases.

Finally, Section 6.6.6 outlines the interaction relationships for composite steel-concrete beam-columns and Section 6.6.7 provides concluding remarks.

6.6.2 Primary AASHTO (2020) and AISC (2016) Beam-Column Interaction Equations

AASHTO (2020) Articles 6.8.2.3 and 6.9.2.2 specify the following bilinear relationship defining the resistance of members subjected to combined axial tension and uniaxial or biaxial flexure, and for members subjected to axial compression and flexure in which all the cross-section elements are classified as compact for flexure:

$$\frac{P_u}{2\phi_c P_n} + \frac{M_{ux}}{\phi_f M_{nx}} + \frac{M_{uy}}{\phi_f M_{ny}} \leq 1.0 \quad \text{for} \quad \frac{P_u}{\phi_c P_n} < 0.2 \tag{6.6.2-1a}$$

(AASHTO 6.8.2.3-1 & 6.9.2.2-1, AISC H1-1b)

$$\frac{P_u}{\phi_c P_n} + \frac{8}{9}\left(\frac{M_{ux}}{\phi_f M_{nx}} + \frac{M_{uy}}{\phi_f M_{ny}}\right) \leq 1.0 \quad \text{for} \quad \frac{P_u}{\phi_c P_n} \geq 0.2 \tag{6.6.2-1b}$$

(AASHTO 6.8.2.3-2 & 6.9.2.2-2, AISC H1-1a)

where

P_u = the maximum axial force along the member unbraced length under consideration resulting from the factored loads,

M_{ux} and M_{uy} = the maximum second-order elastic moments along the member unbraced length under consideration, taken respectively about the cross-section x- and y-axes,

$\phi_c P_n$ = the factored tensile or compressive axial resistance corresponding to the unbraced length under consideration (AASHTO (2020) uses the term P_r for $\phi_c P_n$ in its interaction equations; this term is written directly as $\phi_c P_n$ herein, to avoid conflict with the definition of P_r as the required strength in AISC (2016)), and

$\phi_f M_{nx}$ and $\phi_f M_{ny}$ = the factored flexural resistance about the cross-section x- and y-axes corresponding to the unbraced length under consideration (AASHTO (2020) uses the terms M_{rx} and M_{ry} for $\phi_f M_{nx}$ and $\phi_f M_{ny}$ in its equations; these terms are written directly as $\phi_f M_{nx}$ and $\phi_f M_{ny}$ herein, to avoid conflict with the definition of M_r as the required strength in AISC (2016)).

Figure 79 illustrates the shape of the strength envelope represented by Eqs. 1. It should be noted that all the terms in these equations are taken as positive values in all cases.
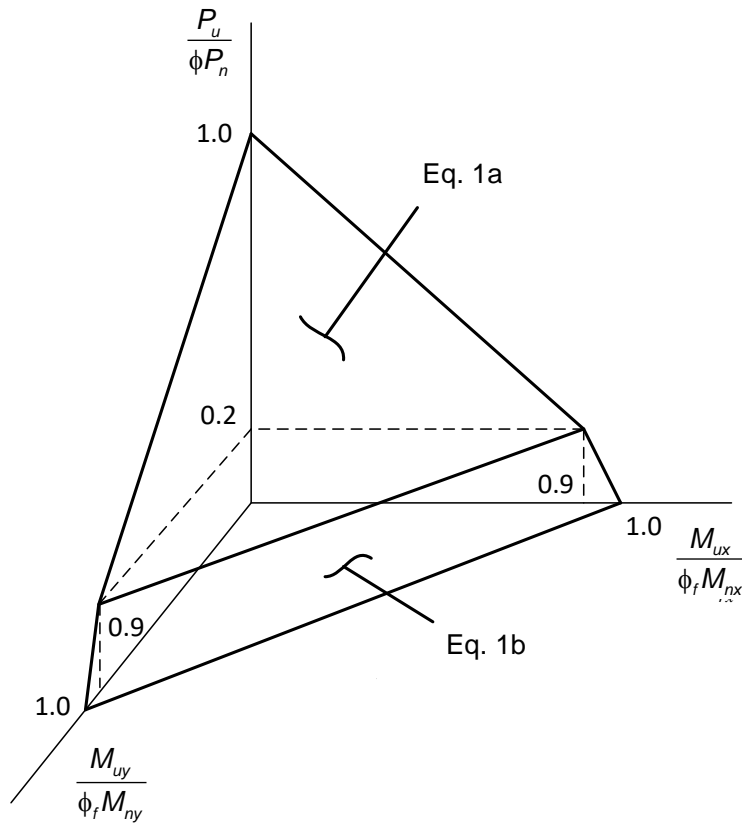
Figure 79. Interaction between axial tension or compression and biaxial bending according to Eqs. 1.

Equations 1 are also intended as being applicable to quantify the resistance of encased and filled composite members, although this application is inadvertently omitted in the AASHTO (2020)

provisions. For all other types of members, AASHTO (2020) specifies the following linear interaction equation:

$$\frac{P_u}{\phi_c P_n} + \frac{M_{ux}}{\phi_f M_{nx}} + \frac{M_{uy}}{\phi_f M_{ny}} \leq 1.0 \qquad\qquad \text{(6.6.2-2) (AASHTO 6.9.2.2.1-3)}$$

Similar to the application of Eqs. 1 above, all the terms in Eq. 2 are taken as positive values in all cases.

Members with compact cross-section elements are potentially able to develop significant distributed yielding within their cross sections for small axial compression and predominant flexural loading. As such, these types of members are able to develop a "knee" in the interaction between their axial compressive and flexural resistances. Noncomposite members with other cross-section types typically have limited capability to develop such a "knee."

In addition to Eqs. 1, AASHTO Article 6.8.2.3.1 provides an alternative set of equations that provide some recognition of the benefits of concurrent axial tension on the flexural resistances associated with compression buckling. These alternative equations are discussed in Section 6.6.5.3 below.

The above definitions are strictly applicable only for prismatic members. For nonprismatic members, P_u and $\phi_c P_n$ should be based generally on the cross section having the largest value of $P_u/\phi_c P_n$, utilizing the equivalent prismatic member concept discussed in Section 6.2.6. Similarly, M_{ux}, M_{uy}, $\phi_f M_{nx}$ and $\phi_f M_{ny}$ should be based generally on the cross sections having the largest $M_{ux}/\phi_f M_{nx}$ and $M_{uy}/\phi_f M_{ny}$ for checking the lateral-torsional buckling limit state (in cases where this limit state is applicable), again utilizing an equivalent prismatic member concept (see Section 6.3.6). It should be noted that the largest values of $P_u/\phi_c P_n$, $M_{ux}/\phi_f M_{nx}$ and $M_{uy}/\phi_f M_{ny}$ may occur at different cross sections along the length of the unbraced segment under consideration. As such, the above interaction equations are in general a conservative simplification. The buckling limit states strictly do not correspond to an individual cross section. They depend on the loadings, properties and boundary conditions along the full x- and y-axis unbraced lengths. Cross-section by cross-section application of the strength interaction equations is applicable *only* for situations where *all* of the corresponding strengths are cross-section based. AASHTO (2020) Article C6.9.2.2.1 discusses this attribute of the member strength interaction equations in detail. For bridge engineering, the applied moments, M_{ux} and M_{uy}, are obtained in the vast majority of cases by applying amplification factors to first-order elastic moments obtained from structural analysis involving the various required factored loadings.

Strictly speaking, the $P_u/\phi_c P_n$, $M_{ux}/\phi_f M_{nx}$ and $M_{uy}/\phi_f M_{ny}$ ratios used in Eqs. 1 should be concurrent values taken from a given factored loading combination. However, this requires that the above process be applied separately for each factored load combination, including all the appropriate positions of live load on the structure. Although this is theoretically not a problem for computerized assessment, such an approach would be computationally prohibitive. This is particularly true when one realizes that the concurrent loadings giving the maximum value of the unity check in Eqs. 1 may actually occur for a situation where none of the above strength ratios are at their individual

maximum values. Conversely, the maximum envelope values of $P_u/\phi_c P_n$, $M_{ux}/\phi_f M_{nx}$ and $M_{uy}/\phi_f M_{ny}$ may be combined conservatively to achieve practical member strength evaluations.

As noted above, AASHTO (2020) takes Eqs. 1 as being applicable for all types of members loaded in tension and flexure, and for all members loaded in compression and flexure in which the cross-section elements are classified as compact for flexure, including all doubly and singly symmetric section members, rolled I-sections, channels, tee-shapes, round, square and rectangular HSS, solid rounds, squares or rectangles, and any of the many possible combinations of doubly or singly symmetric members fabricated from plates and/or shapes by welding or bolting. They are also intended as being applicable to quantify the resistance of encased and filled composite members. Nevertheless, Eqs. 1 were developed predominantly based on studies of noncomposite compact I-section members subjected to combined axial loading and flexure. Therefore, in Section 6.6.4, the relationship between these equations and the physical responses of compact I-section beam-columns is summarized first. This is followed by a discussion of the predictions from Eqs. 1 versus the physical responses for other member types.

6.6.3 Adjustments to Address Interaction with Torsional and/or Flexural Shear

AASHTO (2020) Article 6.9.2.2.2 provides the following adjustment factors for general noncomposite members, which are applied multiplicatively to the factored axial and flexural resistances within Eqs. 1, to account for the influence of torsional shear and/or flexural shear on member resistances:

$$\Delta = 1 - \left(\frac{f_{ve}}{\phi_T F_{cv}}\right)^2 > 0 \qquad\qquad \text{(6.6.3-1) (AASHTO 6.9.2.2.2-1)}$$

$$\Delta_x = 1 - \left(\frac{f_{vex}}{\phi_T F_{cvx}}\right)^2 > 0 \qquad\qquad \text{(6.6.3-2) (AASHTO 6.9.2.2.2-2)}$$

$$\Delta_y = 1 - \left(\frac{f_{vey}}{\phi_T F_{cvy}}\right)^2 > 0 \qquad\qquad \text{(6.6.3-3) (AASHTO 6.9.2.2.2-3)}$$

where

ϕ_T = resistance factor for torsion, specified as 1.0 in Article 6.5.4.2

f_{ve} = total factored shear stress due to torsion and/or flexure, as applicable, calculated in a cross-section element oriented parallel to the x- or y-axis of the cross section

f_{vex} = total factored shear stress due to torsion and/or flexure, as applicable, calculated in a cross-section element oriented parallel to the x-axis of the cross section

f_{vey} = total factored shear stress due to torsion and/or flexure, as applicable, calculated in a cross-section element oriented parallel to the y-axis of the cross section

F_{cvx}, F_{cvy} = nominal shear resistance of a cross-section element under consideration, taken as the F_{cv} for that element as defined below

F_{cv} = for noncomposite rectangular box-section members, including square and rectangular HSS, and for webs of I- and H-section members, the nominal shear buckling resistance of the cross-section element under consideration, under shear alone, calculated as detailed by Eqs. 6.4.9-4, using the appropriate width-to-thickness ratio for the plate under consideration. For noncomposite circular tubes, including round HSS, the flexural or torsional shear buckling resistance as defined by Eqs. 6.5.4-4 through 6.5.4-8, as applicable, or where consideration of additive torsional and flexural stresses is required, the torsional shear buckling resistance as defined by Eqs. 6.5.4-4 through 6.5.4-7.

The member tensile or axial compressive resistance, ϕP_n, is multiplied by Δ, the bending resistance $\phi_f M_{nx}$ is multiplied by Δ_x, and the bending resistance $\phi_f M_{ny}$ is multiplied by Δ_y in Eqs. 6.6.2-1 and 6.6.2-2. The additional following details apply to these calculations:

- The smallest Δ determined from each of the cross-section elements is used for Δ, the smallest Δ_x from the flange elements of the cross section parallel to the x-axis and contributing to $\phi_f M_{nx}$ is used for Δ_x, and the smallest Δ_y from the flange elements of the cross section parallel to the y-axis and contributing to $\phi_f M_{ny}$ is used for Δ_y.

- For noncomposite circular tubes, including round HSS, only one calculation of Δ is required based on the cross-section torque and/or the vector combination of cross-section shears V_{ux} and V_{uy}, and this Δ is applied to each of the terms in the applicable member strength interaction equation.

- For I-section members, the cross-section shear stresses due to torque are neglected. For these member types, Δ_x and Δ_y are taken equal to 1.0 in all cases, and only the flexural shear stresses in the web are considered in the calculation of Δ.

For small values of $f_{ve}/\phi_T F_{cv}$, the effect of the torsion on the member strength may be considered as inconsequential. AASHTO (2020) Article 6.9.2.2.2 allows these torsional effects to be neglected for noncomposite rectangular box-section members, square and rectangular HSS, and circular tubes including round HSS, when $f_{ve}/\phi_T F_{cv}$ is less than or equal to 0.2.

For all types of noncomposite members, when $P_u/\phi P_n$ is less than or equal to 0.05, the influence of the factored flexural shear stresses on the strength interaction equations, Eqs. 6.6.2-1 and 6.6.2-2, is considered as inconsequential.

Figure 80 shows a representative rectangular box-section profile subjected to biaxial bending moments, M_{ux} and M_{uy}, biaxial flexural shears, V_{ux} and V_{uy}, and torque, T_u, illustrating the terms employed in Eqs. 1 through 3. The box-section component plates potentially can all have different thicknesses. In the unusual case where the plates have different thicknesses, it is recommended that the pair of plates subjected to the larger shear stresses due to V_{ux} and V_{uy} should be assumed to both have the smaller thickness of these two plates. As, such, the principal axes of the idealized cross section are aligned with the walls of the box.

In Figure 80, the shear force V_{ux} contributes to the shear stresses f_{vex1} and f_{vex2} in the plates that are parallel to the x-axis. The shear V_{uy} contributes to the shear stresses f_{vey1} and f_{vey2} in the plates parallel to the y-axis. Furthermore, the torque, T_u, contributes to the shear stresses in all the plates. Equation 1 recognizes that the interaction between the axial strength and the shear strength can be based conservatively on the maximum f_{ve}/F_{cv} from all the component plates. Equations 2 and 3 recognize that the interaction between the flexural strength about a given principal axis and the corresponding shear strength is predominantly due to the f_{vex}/F_{cvx} or f_{vey}/F_{cvy} values for $\phi_f M_{nx}$ and $\phi_f M_{ny}$, respectively. The ratio f_{vex}/F_{cvx} has a predominant impact on the flexural resistance $\phi_f M_{nx}$, and the ratio f_{vey}/F_{cvy} has a predominant impact on the flexural resistance $\phi_f M_{ny}$. The impact of the web shear ratios in either bending direction on the associated flexural resistance, i.e., f_{vex}/F_{cvx} on $\phi_f M_{ny}$ and f_{vey}/F_{cvy} on $\phi_f M_{nx}$, is taken to be negligible.
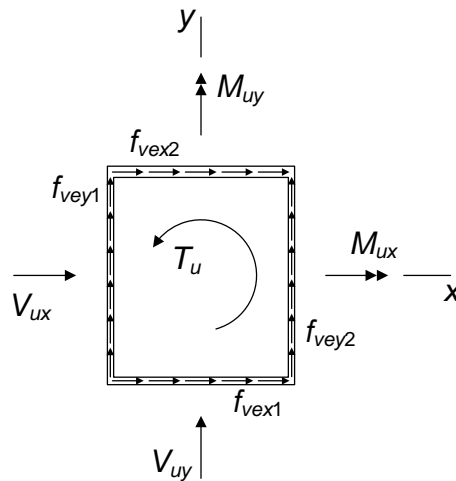
Figure 80. Representative box-section profile showing cross-section forces and corresponding plate element stresses.

Figure 81 shows a comparable illustration to Figure 80 for a representative circular tube section. In this case, the shears can be added vectorially and the resultant shear can be applied to the cross section to calculate the maximum contribution to the shear strength ratio from the flexural shears. The shear stresses from torsion are constant throughout the circumference of the tube, assuming constant thickness of the tube, and can be added to the maximum flexural shear stress to obtain the maximum total stress due to combined flexure and torsion. The corresponding f_{ve}/F_{cv} ratio is applied conservatively to ϕP_n, $\phi_f M_{nx}$ and $\phi_f M_{ny}$. As discussed in Section 6.5.4 of this volume, circular tube members subjected to flexural shear and torsion must be checked using Eq. 6.5.4-9 in addition to checking the interaction of the member axial, flexural and torsional resistances using the above equations.

Figure 82 shows an illustration of a representative I- or H-section member, subjected to biaxial bending, M_{ux} and M_{uy}, biaxial shear, V_{ux} and V_{uy}, and torque, T_u. For these member types, the shear stresses due to torsion, and the flange shear stresses due to flexure, tend to be small and are assumed to be negligible. However, thin-web I-section members can be subject to significant web shear stresses. These stresses may have a significant influence on the member axial load resistance.

For instance, the interaction between axial compression and web shear may be measurable in edge girders of cable-stayed bridges. Equation 1 captures this strength limit state response.
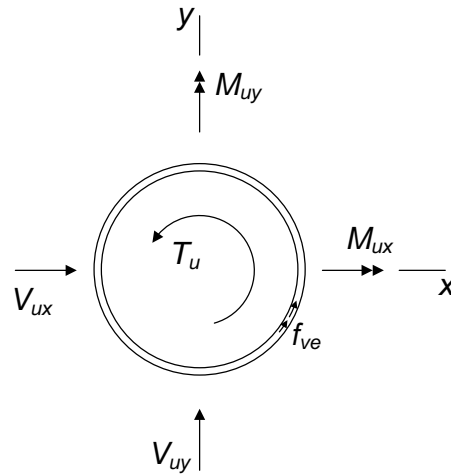
Figure 81. Representative circular tube cross-section profile showing cross-section forces and corresponding element stresses.
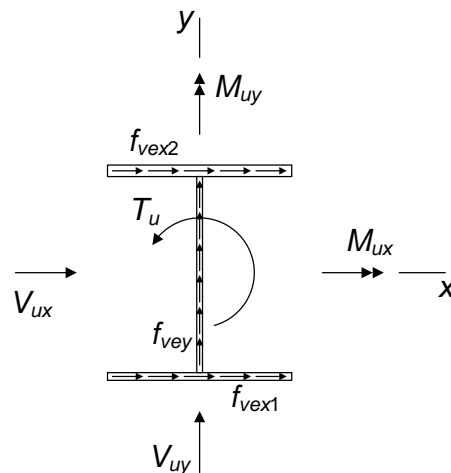
Figure 82. Representative I- or H-section profile showing cross-section forces and corresponding plate element stresses.

For I-section and H-section members subjected to torsion, the flanges may be subjected to significant additional lateral bending due to the restraint of warping. This additional flange lateral bending may be considered by calculating $M_{uy}/\phi_f M_{ny}$ considering each of the individual flanges as a separate component, then combining the larger of these $M_{uy}/\phi_f M_{ny}$ values with the other strength ratios in the appropriate strength interaction equation from Eqs. 6.6.2-1 and 6.6.2-2. Alternatively, for I-section members subjected to major- and minor-axis bending plus torsion, the one-third rule provisions discussed in Section 6.3.7.3 may be employed to assess these combined effects.

The interaction of flange flexural shear stresses with the axial and flexural resistances of the member is assumed to be negligible for I- and H-section members in AASHTO (2020). The weak-axis shear resistance of these members is checked using Article 6.12.1.2.3a.

The theoretical basis for Eqs. 1 through 3 is as follows. The strength interaction defined by these equations gives an accurate to moderately conservative representation of the plastic strength interaction between the normal and shear stresses obtained from the von Mises yield criterion, the inelastic buckling interaction in plates subjected to combined uniform axial compression and shear, and the elastic buckling interaction in plates subjected to combined bending within the plane of the plate and shear (Ziemian 2010). The theoretical interaction curve between the normalized strength ratios is circular for each of these cases, which would result in the expressions within Eqs. 1 to 3 being taken to the ½, or square root, power. However, the plate elastic buckling interaction between uniform axial compression and shear is approximated more closely by an interaction equation involving a linear term for the axial compressive strength ratio and a quadratic term for the shear strength ratio (Ziemian 2010). This results in the form given by Eqs. 1 to 3. The largest difference between the overall strengths predicted by the circular interaction and the interaction using a linear term for the axial compressive strength ratio and a quadratic term for the shear strength ratio is 15 percent, corresponding to a shear strength ratio of 0.707. In addition, the ultimate shear resistance in the theoretical elastic shear buckling range is larger than the theoretical elastic shear buckling resistance due to postbuckling action. The interaction based on using a linear term for the axial compressive and flexural strength ratios is adopted to characterize the strengths for all of the types of loading considered. This is consistent with the form of the interaction equations in AISC (2016) Section H3.2 for torsion combined with axial force and flexure in HSS members. The strength interactions with torsional and flexural shear are expressed as the Δ, Δ_x and Δ_y equations to provide a clear separation between the application of the equations when torsional and/or flexural shear effects are significant, and when they are not.

Although the interaction between the shear resistance and the axial and flexural resistances for box-section members is based largely on the theoretical strength interactions for the individual component plates, these interaction relationships are conflated into an overall member interaction relationship. This is comparable to the handling of the strength interactions for these types of members in AISC (2016) Section H3.2. Schilling (1965) shows that an interaction equation with the axial and moment strength ratios combined linearly, and with the shear strength ratio combined as a quadratic term, gives a conservative estimate of the overall member resistance for noncomposite circular tube members governed by overall member elastic or inelastic buckling (Ziemian 2010). Schilling's results provide additional justification for the use of Eqs. 1 to 3 for these types of members.

6.6.4 Tension Rupture under Axial Tension or Compression Combined with Flexure

Strength interaction equations such as Eqs. 6.6.2-1 and 6.6.2-2 have traditionally been applied for checking of the strength interaction between axial tension and flexure both for cases where the member strength under axial tension alone is governed by general yielding as well as when it is governed by tension rupture at a given critical cross section. AISC (2016) Section H4 provides a separate strength interaction equation that captures the beneficial subtractive effects of axial and/or flexural compression in checking tension rupture. However, AISC (2016) Section H1 also still

specifies that Eqs. 6.6.2-1 must be checked for members subjected to axial tension, as well as for members where the flexural resistance is governed by the AISC (2016) Section F13.1 provisions.

AASHTO (2020) Article 6.8.2.3.3 specifies a separate cross-section strength interaction check, focused on evaluation of the tension rupture resistance under axial tension or compression combined with flexure at potentially critical cross sections. This article is intended as a generalization of the AISC (2016) Section H1 and H4 provisions. Article 6.8.2.3.3 indicates that the following cross sections should be checked for tension rupture:

- Cross sections containing bolt holes in one or more flanges that are subjected to tension under combined axial tension or compression and flexure,

- Cross sections subjected to axial tension and flexure and containing bolt holes in other cross-section elements, and

- Cross sections at welded connections subjected to axial tension and flexure.

At these locations, Article 6.8.2.3.3 specifies that the following equation shall be satisfied:

$$\frac{P_u}{\phi P_n} + \frac{M_u}{\phi_f M_n} \leq 1.0 \qquad\qquad \text{(6.6.4-1) (AASHTO 6.8.2.3.3-1)}$$

where

M_u = factored moment about the principal axis of bending under consideration at the cross section under consideration, positive for tension and negative for compression in the cross section element being evaluated for tension rupture

M_n = nominal tension rupture flexural resistance about the axis of bending under consideration, calculated by multiplying the resistance in terms of stress given by Eq. 6.3.10-1 of this volume by the minimum elastic section modulus of the gross cross section for the principal axis of bending under consideration

P_u = maximum magnitude factored tensile axial force, or smallest magnitude compressive axial force, at the cross section under consideration, taken as positive in tension and negative in compression

P_n = for cross sections subjected to axial tension, nominal tensile rupture resistance of the net section based on Eq. 6.1.1-2; for cross sections subjected to axial compression, nominal tensile yield resistance of the cross section based on Eq. 6.1.1-1.

ϕ = $\phi_u = 0.8$ when P_n is calculated as the tensile rupture resistance; $\phi_y = 0.95$ when P_n is calculated as the tensile yield resistance

The above definition of M_n using the minimum elastic section modulus is a conservative approximation consistent with the AISC (2016) Section H4 provisions.

Related to the above considerations, it should be noted that AASHTO (2020) Article C6.8.2.3.3 states that angle members and light structural tee members loaded eccentrically in axial tension are to be designed only for axial tension. This is because the moment effects due to the connection eccentricities are addressed in the calculation of the shear lag reduction factor, U, when calculating the resistance of these types of members, as discussed in Section 6.1.1 of this volume.

6.6.5 A More Detailed Look Under the Hood at Strength Interactions in Noncomposite Members

6.6.5.1 In-plane resistance of doubly symmetric I-section members subjected to axial load and major- or minor-axis bending

Figure 83 shows representative nominal first-yield and "exact" fully-plastic axial force-moment strength envelopes for two short compact doubly symmetric I-section members subjected to major-axis bending moment. These envelopes are identical for axial tension or compression or for positive or negative bending moment. Therefore, only one quadrant of the strength envelopes is shown. One of the sections considered is a W40x167, which is representative of a "beam-type" wide-flange section (deep web and relatively narrow flanges). The other section is a W14x257, which is representative of a "column-type" wide-flange section (web depth and flange width nearly the same). The fully-plastic strength envelope is slightly less convex for the column-type section. However, the normalized initial-yield envelopes are essentially the same.

Figure 83 also shows the result from Eqs. 6.6.2-1 with ϕ_c and ϕ_f taken equal to 1.0. For these ideal short compact-section members, the nominal axial resistance P_n is equal to the cross-section yield load P_y (assuming that net section fracture does not govern the resistance in tension) and the nominal flexural resistance is equal to the section plastic moment capacity M_p (again assuming that the tension flange fracture flexural limit state does not govern the resistance). One can observe that Eqs. 6.6.2-1 of this volume provide a reasonable lower-bound fit to the exact fully-plastic strength envelopes.

The nominal first yield curves in Figure 83 may be expressed simply as

$$\frac{P_u}{P_y} + \frac{M_u}{M_y} = 1 \tag{6.6.5-1a}$$

in terms of the axial force and moment, or equivalently as

$$\frac{f_a}{F_y} + \frac{f_{bu}}{F_y} = 1 \tag{6.6.5-1b}$$

in terms of the corresponding additive elastic axial and flexural stresses, neglecting residual stress effects. If nominal residual stresses of f_r are assumed in compression at the flange tips and in tension at the mid-width of the flanges, the corresponding first yield condition is given by these equations with P_y, M_y and F_y replaced by $(1 - f_r/F_y)P_y$, $(1 - f_r/F_y)M_y$ and $F_y - f_r$.
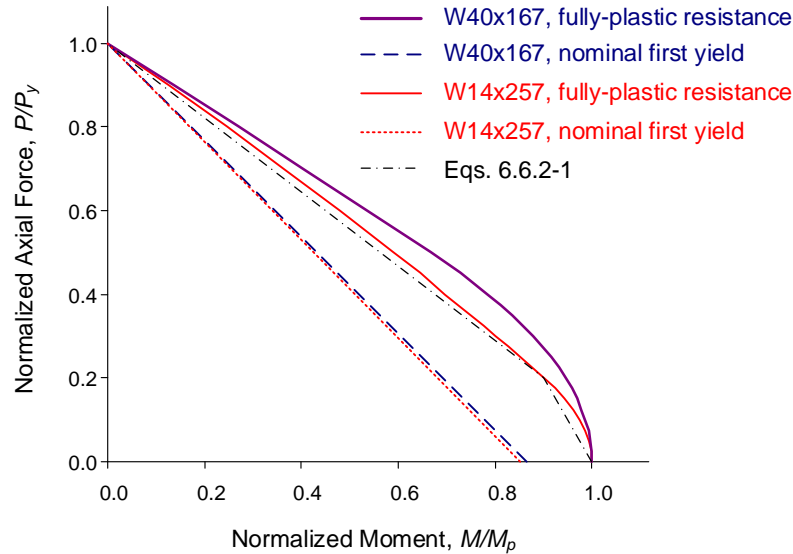
Figure 83. Representative first-yield and fully-plastic axial force-moment strength envelopes for short compact doubly symmetric I-section members subjected to major-axis bending.

Figure 84 compares the nominal first yield and fully-plastic axial force-moment strength envelopes for the same two short compact doubly symmetric I-section members to Eqs. 6.6.2-1 for the case of combined axial loading and weak-axis flexure. The W40x167 fully-plastic strength curve is again more convex than the corresponding W14x257 curve. However, the normalized first-yield envelope is slightly smaller for the W40x167 compared to that for the W14x257. In this case, one can observe that both of the theoretical fully-plastic resistance envelopes are significantly more convex than Eqs. 6.6.2-1, and that Eqs. 6.6.2-1 appear to provide a rather conservative estimate of the true capacity. Although this observation is correct, it applies only to short "stub-columns" or to members loaded in weak-axis flexure and axial tension.

Figure 85 compares the maximum in-plane strength envelopes for strong- and weak-axis bending and axial compression on representative finite-length column-type wide-flange members with *L/r* = 80, taken from Maleck (2001), to the nominal resistance predictions from Eqs. 6.6.2-1. Although the stub-column (i.e., cross-section) strength envelope for weak-axis bending is significantly more convex than either of the Eqs. 6.6.2-1, or the exact fully-plastic strength envelopes for *strong-axis* bending, the beam-column resistances for all but very short members are similar regardless of the axis of bending. This is because the weak-axis flexural rigidity of an I-section reduces dramatically once yielding starts at the flange tips. The spread of yielding through the flanges has a less dramatic effect on the flexural rigidity as the first-yield strength is exceeded and the cross-section fully-plastic resistance is approached in major-axis bending. However, the larger reduction in the member stiffness that occurs for combined compression and weak-axis bending leads to larger inelastic stability (*P-δ*) effects, which in turn reduces the finite-length member resistance to a strength envelope far below the idealized stub-column strength.
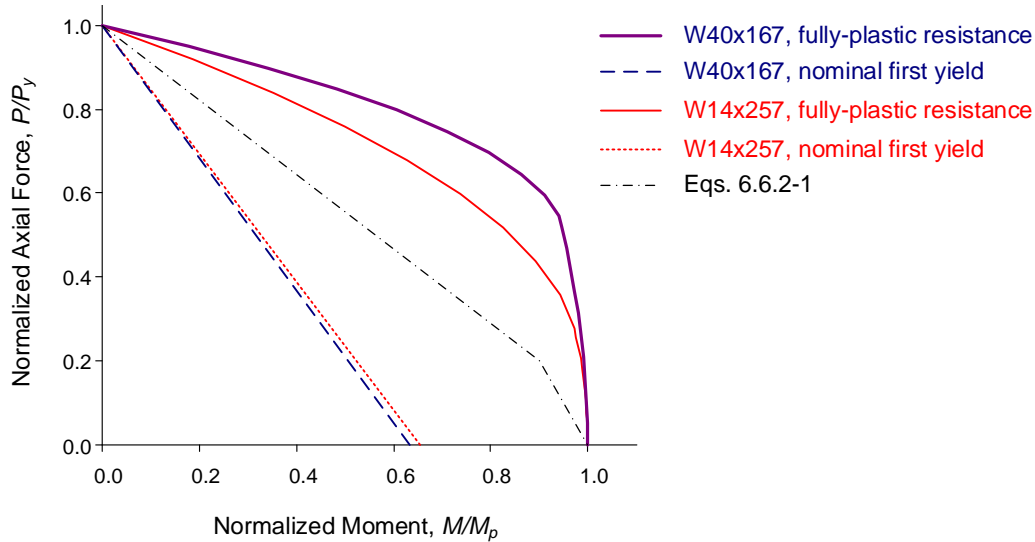
Figure 84. Representative first-yield and fully-plastic axial force-moment strength envelopes for short compact doubly symmetric I-section members subjected to minor-axis bending.
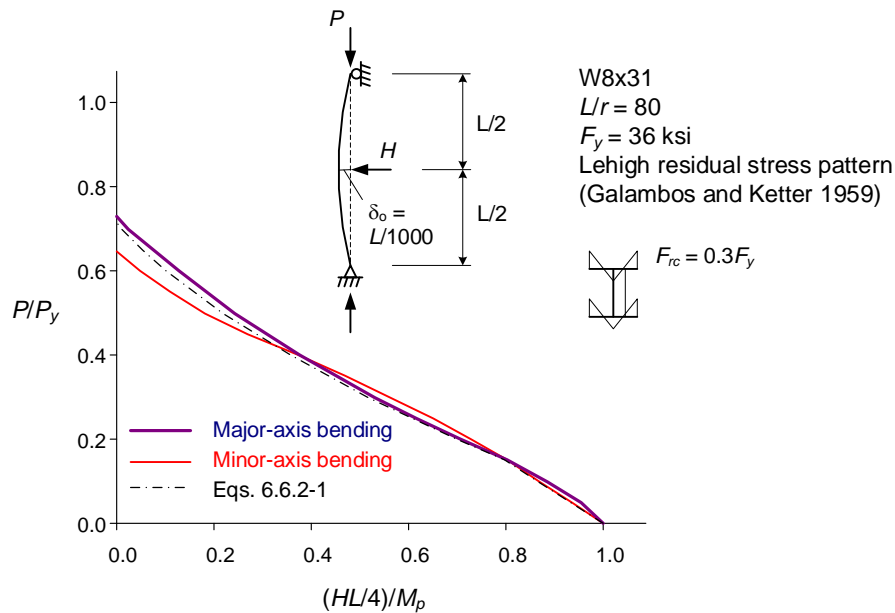
Figure 85. Representative maximum in-plane strength envelopes for strong- and weak-axis bending and axial compression on finite length column-type wide-flange members, from Maleck (2001).

Figure 86 illustrates the behavior for the above weak-axis bending example in greater detail. This figure shows the strength envelope from Figure 85, where the moment is defined as the first-order moment $M_1 = HL/4$ at the maximum load capacity of the member, the corresponding internal maximum *second-order inelastic* moment at the midspan of the member, $M_{2.inelastic} = M_1 + P\delta_{2.inelastic}$, and the corresponding internal maximum *second-order elastic* moment $M_{2.elastic} = M_1 + P\delta_{2.elastic} = AF\,M_1$. In these expressions, $\delta_{2.inelastic}$ is the "*true*" second-

order inelastic lateral deflection relative to a straight chord at the midspan of the beam-column at the maximum load capacity of the member, including a nominal initial out-of-straightness of $\delta_o = L/1000$ as well as the influence of initial residual stresses, $\delta_{2.elastic}$ is the idealized second-order elastic displacement at the midspan for the nominally-elastic ideally-straight member, obtained from any legitimate second-order elastic analysis (e.g., a first-order elastic analysis combined with a second-order elastic amplification factor), and AF is the second-order elastic amplification factor for the member maximum internal moment.
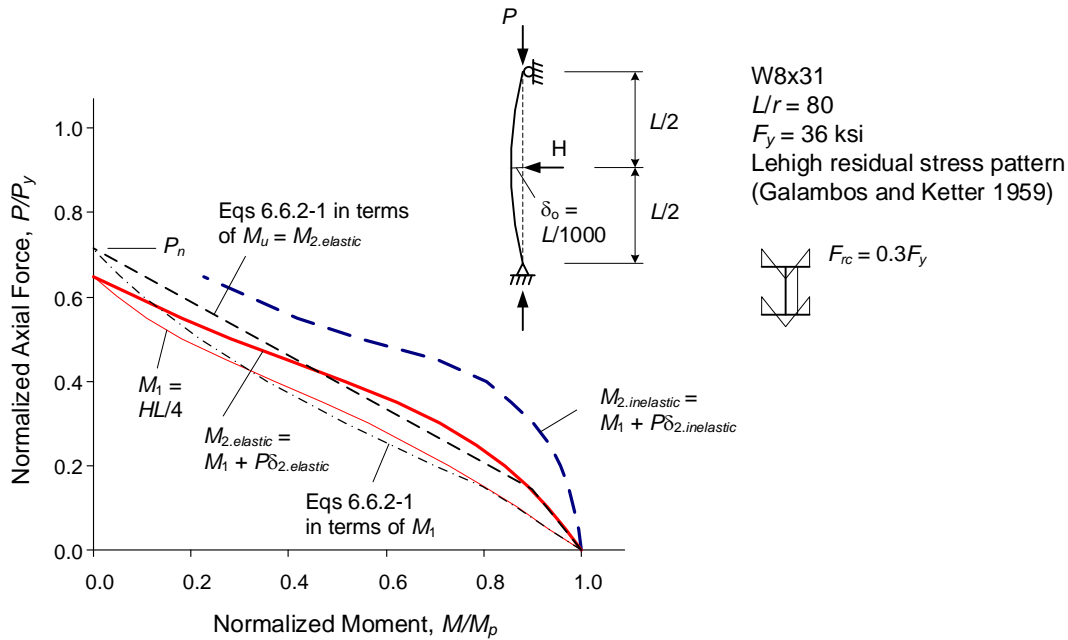
Figure 86. Strength interaction curves in terms of different calculated moments, $M_1 = HL/4$, $M_u = M_{2.elastic} = M_1 + P\delta_{2.elastic}$ and $M_{2.inelastic} = M_1 + P\delta_{2.inelstic}$ for the Figure 85 example beam-columns subjected to minor-axis bending.

The P-M_1 and P-$M_{2.inelastic}$ curves in Figure 86 are obtained from refined distributed plasticity analyses of the beam-column. This type of analysis tracks the spread of yielding through the cross sections and along the length of the member, including residual stress and initial geometric imperfections effects, and the corresponding gradual reduction in the member stiffness, with increases in the applied loads. Conversely, the P-$M_{2.elastic}$ curve is obtained by applying the second-order elastic amplification factor AF to the member maximum first-order moments $M_1 = HL/4$. The P-$M_{2.inelastic}$ curve falls inside of the bounds of the fully-plastic strength curve for the cross section (not shown but similar to the W14x257 fully-plastic resistance curve in Figure 84). This is because the maximum load capacity of the member is reached due to a combination of yielding and stability effects prior to full plastification of the midspan cross section. Part of the differences between the curves based on Eqs. 6.6.2-1 and the "exact" strength curves in Figure 85 and Figure 86 is due to the use of a single column strength curve for P_n. In general, the P_n from the AASHTO (2020) and AISC (2016) single column curve strength equations tends to fall between the major- and minor-axis column strengths obtained from distributed plasticity analysis (see Figure 85). The accuracy of the fit by Eqs. 6.6.2-1 is generally improved if P_n is set to the corresponding column strength obtained from the distributed plasticity solutions.

The AASHTO (2020) and AISC (2016) Eqs. 6.6.2-1 were established in large part based on curve fitting to the results from a large number of beam-column solutions similar to those illustrated in Figure 86. Based on the definition of the internal moment M_u as the maximum second-order elastic moment within the unbraced length under consideration, determined from an analysis of the nominally-elastic ideally-straight member (i.e., $M_u = M_{2.elastic}$), the P-$M_{2.elastic}$ curve in Figure 86 is the appropriate "exact" curve that the beam-column strength interaction equation represents. Equations 6.6.2-1 provide an accurate to conservative fit to the rigorous P-$M_{2.elastic}$ curves for all of the strong- and weak-axis bending cases studied in their development (LeMessurier 1985; Liew et al. 1992; ASCE 1997; Maleck and White 2003). In general, Eqs. 6.6.2-1 give a superb fit for strong-axis bending and L/r from 0 to 100. They are increasingly conservative for the weak-axis case when L/r is less than about 40. This is due to the large shape factor and significant convexity of the cross-section fully-plastic strength for weak-axis bending of I-shapes. They are moderately conservative for both axes when L/r is greater than 120. Also, for sidesway-inhibited cases, Eqs. 6.6.2-1 tend to be somewhat more conservative for beam-columns subjected to reverse curvature bending than for cases involving single-curvature bending (Clarke and Bridge 1992). This is due to the fact that Eqs. 6.6.2-1 do not account for the influence of moment gradient on the shape of the strength envelope.

A few additional attributes of Eqs. 6.6.2-1 deserve highlighting:

- By curve fitting to the P-$M_{2.elastic}$ strength envelopes, the calculation of second-order effects via structural analysis (or by amplification of the first-order elastic internal moments) is clearly separated from the calculation of the member internal resistances P_n and M_n. Many prior steel design standards do not provide a clear separation between the consideration of second-order effects in the elastic structural analysis and the calculation of the member resistances. The separation of these two calculations facilitates the use of an explicit second-order elastic analysis to achieve a more accurate characterization of stability effects in cases where these effects are significant.

- The bilinear form given by Eqs. 6.6.2-1, which provides an accurate characterization of the fully-plastic resistance for a short I-section member subjected to major-axis bending, also provides an accurate fit to the majority of the strong- and weak-axis P-$M_{2.elastic}$ strength envelopes.

- The bilinear form given by Eqs. 6.6.2-1 combines the consideration of "member strength" and "member stability" into one single beam-column interaction curve. Many other prior and current steel design standards worldwide quantify the in-plane strength of steel beam-column members by a combination of two curves, one that addresses a member stability (or strength) limit and the other which addresses a member cross-section strength limit. However, all beam-columns of finite length fail physically by a combination of inelastic bending and stability effects. Equations 6.6.2-1 provide a simpler representation of member strengths that is truer to the fundamental attributes of the beam-column resistance (at least for members that fail by in-plane bending).

The reader is referred to Liew et al. (1992), ASCE (1997), and Maleck and White (2003) for further discussion of the in-plane strength interaction behavior of doubly symmetric I-section members subjected to axial loading and major- or minor-axis bending.

The application of Eqs. 6.6.2-1 to other types of beam-column members and other types of strength limit states is ad hoc. Nevertheless, as noted in the previous section, within certain restrictions, these equations provide an accurate to conservative characterization of the member strength envelopes for all types of beam-column members. For instance, the in-plane beam-column resistance of compact square and rectangular welded box or HSS sections is very similar to that for I-section members in major-axis bending. The in-plane behavior of these types of members is much the same as an I-section member with a single web thickness equal to the sum of the box or HSS section web thicknesses. The next section discusses the relationship between Eqs. 6.6.2-1 and the true in-plane and out-of-plane strength interaction curves for singly symmetric members and/or members with noncompact or slender cross-section elements.

Figure 87 shows representative first-yield and fully-plastic axial force-moment strength envelopes for a short compact singly symmetric I-section member. Interestingly, these envelopes are not symmetric. The strength interaction curves have a bulge in the quadrants where the axial and flexural stresses are additive either in compression or in tension on the larger flange. Of course, similar to the above results for doubly symmetric I-section members, the fully-plastic cross-section strength is only an upper-bound theoretical limit. The actual resistance for a general singly symmetric finite-length beam-column can be influenced by a combination of yielding, overall member stability and/or local member and cross-section distortional stability effects.

The dark solid curve in Figure 88 shows a representative strength envelope for a hypothetical simply supported finite-length beam-column with noncompact and/or slender cross-section elements and a singly symmetric cross-section profile. Also shown as dashed lines in the figure are the base strength interaction curves given by Eqs. 6.6.2-1. White and Kim (2003) discuss the behavior of various strength interaction equations and review the limited experimental test results for prismatic doubly and singly symmetric I-section beam-columns with noncompact and/or slender webs and compact, noncompact and slender flanges. They conclude that the bilinear strength curves given by Eqs. 6.6.2-1 provide an accurate to conservative characterization of the in-plane and out-of-plane resistances from the available tests. Galambos (2001a and b) proposes a refined procedure for determining the resistance of prismatic singly symmetric compact I-section members and makes similar observations pertaining to Eqs. 6.6.2-1. Typically, Eqs. 6.6.2-1 provide an accurate to slightly conservative characterization of the in-plane resistance of singly symmetric I-section members when the smaller flange is subjected to additive flexural and axial stresses. However, these equations tend to be somewhat conservative relative to the physical beam-column in-plane and out-of-plane resistances in many cases involving singly symmetric I-section members when the larger flange is subjected either to additive axial and flexural compression or tension. The studies by Lee and Hsu (1981) and Lee et al. (1981) provide evidence of this conclusion for tapered web singly symmetric I-section members.
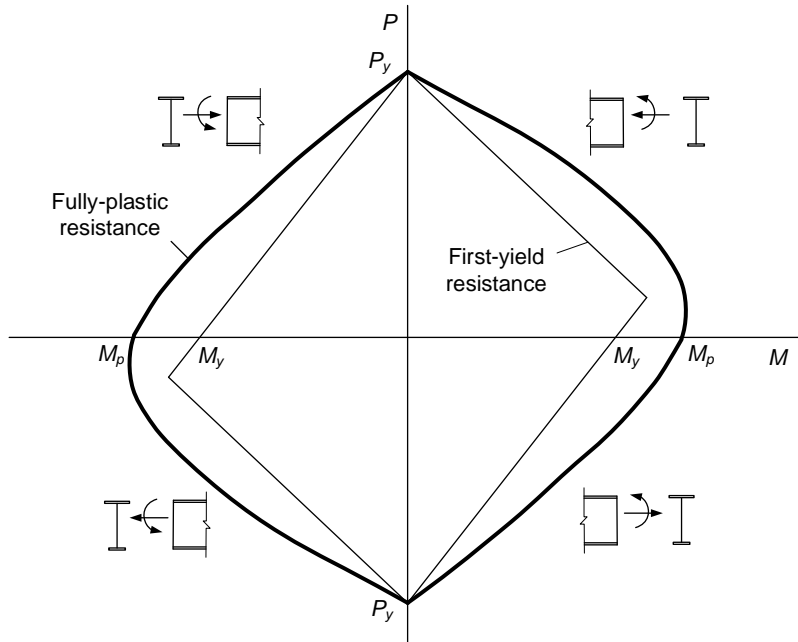
Figure 87. Representative first-yield and fully-plastic axial force-moment strength envelopes for a short compact singly symmetric I-section member.
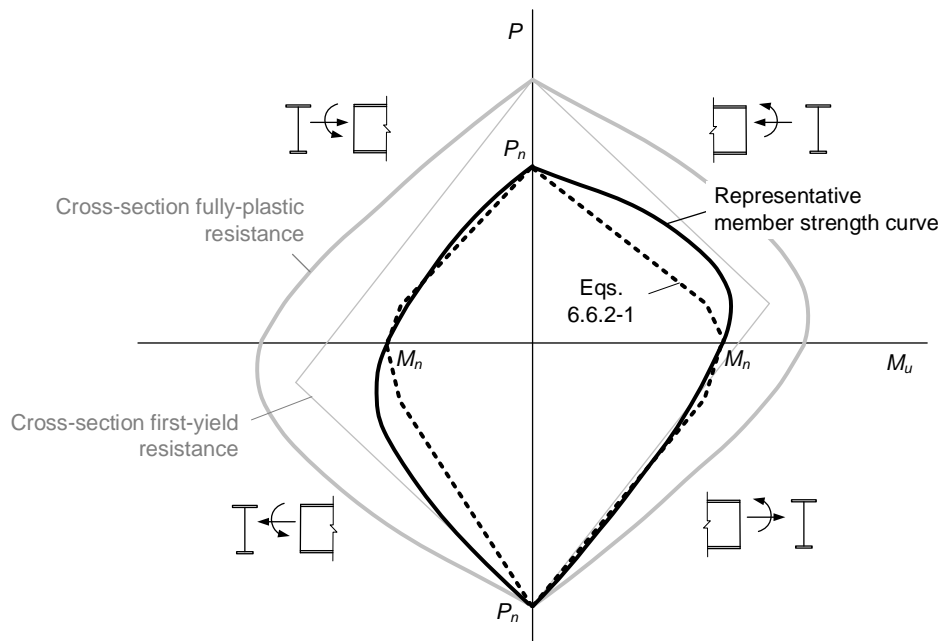
Figure 88. Comparison of a representative strength envelope for a hypothetical simply supported finite-length beam-column with noncompact and/or slender cross-section elements, the AISC (2016) strength interaction curves (Eqs. 6.6.2-1), and the cross-section yield and fully-plastic strength.

The behavior for finite-length tee- and double-angle beam columns is similar to that shown in Figure 88. However, particularly for members of these types with intermediate and longer lengths, the lack of symmetry of the interaction curves is highly accentuated. Figure 89 illustrates this behavior along with the corresponding AASHTO (2020) - AISC (2016) strength for a representative simply supported tee-section member, loaded within the plane of symmetry (Galambos 2001a). The two different solid curves in the figure denote capacities based on the in-plane strength limit states. The two dashed curves denote out-of-plane strength envelopes. Furthermore, the heavy lines illustrate the results obtained from refined calculations performed by Galambos (2001a) whereas the thin lines indicate the resistances calculated by the AASHTO (2020) - AISC (2016) equations. One can observe that the bulge in the upper-right and lower-left quadrants is substantial for this member, and that the true strength along a radial line taken from the origin of the plot can be more than two times the strength estimate based on Eqs. 6.6.2-1 for some of the combinations of axial force and bending moment. However, in the lower-right and upper-left quadrants, where the stem of the tee-section is loaded in additive axial and flexural tension or compression, Eqs. 6.6.2-1 provide an accurate estimate of the "true" member strength.
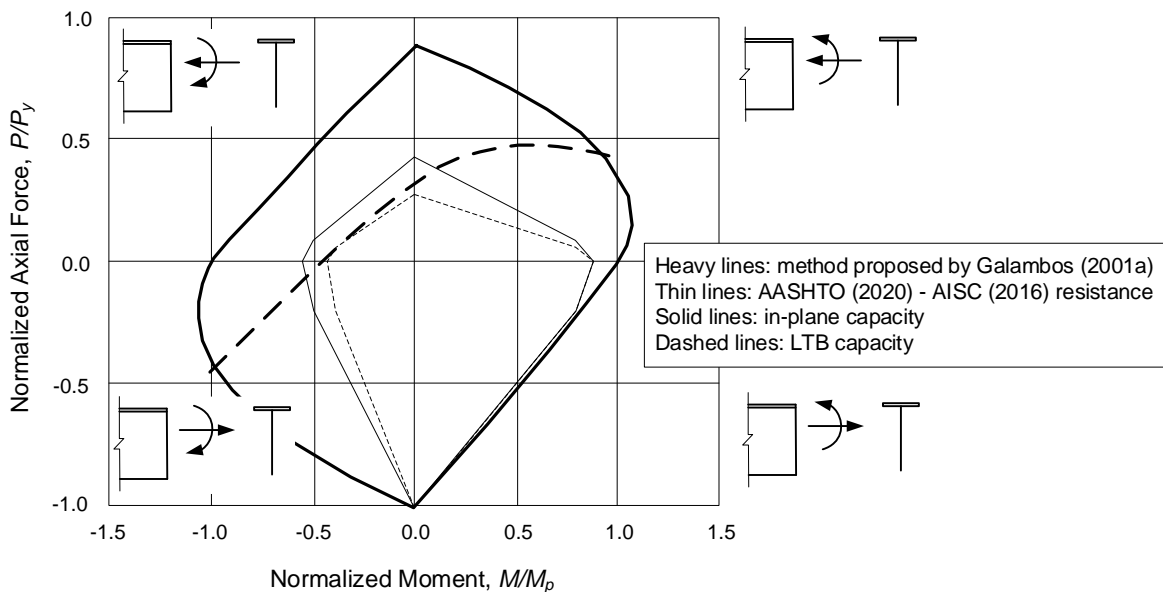
Figure 89. Representative simply supported tee-section member studied by Galambos (2001a) (WT18x67.5, F_y = 50 ksi, L = 20 ft).

Practical connections for tee-section struts used as bracing or cross-frame members are typically made to the flange. The corresponding bending moment due to the eccentricity of the connection generally places the member design in the upper-right or lower-left quadrants of Figure 89. Furthermore, the moment due to the eccentricity often places the design in the region of the strength envelopes that exhibit the largest bulge relative to Eqs. 6.6.2-1.

Although Figure 89 indicates substantial additional capacity compared to that predicted by the AASHTO (2020) - AISC (2016) procedures in the upper-right and lower-left quadrants of the response, one must be careful in utilizing these additional strengths. The conservatism in the lower-left quadrant is largely due to the fact that the AISC and AASHTO provisions for tees limit the maximum flexural resistance to $M_n = M_y$ (where M_y corresponds to first yielding at the tip of the

stem, neglecting residual stress effects) for cases where the stem is loaded in flexural compression (see Section 6.5.5 of this volume). For typical eccentric connections to tee-struts, the compressive elastic flexural stress at the tip of the stem, M/S_x, is larger than the corresponding axial tension, P/A_g. Therefore, some conservatism may be merited to protect against significant inelastic LTB distortion of the tee stem. Also, in the upper-right quadrant, the axial compressive resistance P_n is reduced due to local buckling effects (via reduced effective widths, see Section 6.2.4) for a large number of rolled tee-sections. This is the case for the WT18x67 member considered in Figure 89. However, in the upper-right quadrant, if the elastic flexural stress due to the eccentric loading, $M/S_x = Pe/S_x$, is larger than the corresponding axial compression stress, P/A_g, the tee stem is completely in tension. As such, the influence of the slenderness of the stem, d/t_w, on the beam-column resistance is expected to be minor. Furthermore, the AASHTO (2020) - AISC (2016) flexural resistances in this quadrant are limited to $M_n = 1.6M_y$ to avoid potential significant yielding at service load levels (see Section 6.5.5).

Unfortunately, no simple method has been established at the present time (2021) for determining the strength envelopes for singly symmetric members, accounting for the bulges in the upper-right and lower-left quadrants illustrated in Figure 87 and Figure 88. In fact, it is possibly fair to say that no simple manual method will ever exist for this calculation.

6.6.5.2 Enhanced strength interaction curves for singly symmetric members loaded in their plane of symmetry

AISC (2016) Section H2 gives a separate beam-column interaction equation, which can be written for the case of bending within the plane of symmetry of a singly symmetric member as

$$\left| \frac{f_a}{F_a} + \frac{f_b}{F_b} \right| \leq 1.0 \tag{6.6.5-2} \text{ (AISC H2-1)}$$

This equation is intended to capture some of the bulge in the upper right and lower left quadrants of Figure 89. The term f_a in this equation is the required axial stress, F_a is the axial capacity in terms of stress, f_b is the required flexural stress at the point under consideration, and F_b is the flexural capacity in terms of stress at the point under consideration, taken as $\phi_f M_n/S$ in LRFD where S is the corresponding elastic section modulus corresponding to the specific point in the cross section under consideration.

The implied advantage of Eq. 2 is that the Engineer is allowed to consider the sign of the axial and flexural stresses, which are additive on one side of the cross section and subtractive on the other. Unfortunately, this equation does not provide any advantage relative to Eqs. 6.6.2-1 for singly symmetric members subjected to bending in the plane of symmetry. This is because, generally, the Engineer must check all the applicable points within the cross section. Hence, *the extreme fiber where the axial and flexural stresses are additive always governs the resistance* when the axial and flexural resistance terms F_a and F_b are calculated as specified in AISC (2016), i.e., $F_a = \phi_c P_n/A$ or $\phi_t P_n/A$ and $F_b = \phi_f M_c/S$.

White and Kim (2006) discuss a variation on Eq. 6.6.5-2, proposed by Sherman (2005), that provides some of the intended benefits for cases where the M_n associated with yielding or buckling

of the smaller flange (or tee stem) is substantially smaller than M_p. However, Eqs. 6.6.2-1 always provide a more liberal estimate of the capacities for members where $M_n = M_p$.

The commentary to AISC (2016) Section H2 acknowledges the above problem and then discusses several ad hoc checks, similar to but different from Eq. 2. The last paragraph in the AISC (2016) Section H2 suggests that these checks are justified by the statement, "A more detailed analysis of the interaction of flexure and tension is permitted in lieu of Equation H2-1."

Galambos (2001a) details a procedure that accomplishes the intended objective of Eq. 2, i.e., capturing the bulge in the upper-right and lower-left quadrants of the strength envelope, for prismatic singly symmetric compact-section members loaded in their plane of symmetry. Galambos' procedure also is applicable for doubly symmetric I-section members as a special case. In these cases, it provides an enhanced assessment of the out-of-plane resistance for members subjected to major-axis bending. Galambos uses separate formulations for the in-plane and out-of-plane resistance to achieve these objectives. For the nominal in-plane resistance, Galambos uses the theoretical cross-section fully-plastic strength curve, but with an adjusted yield strength that varies from F_y at $P = 0$ to F_n at $P = P_n$, where F_n is the in-plane column resistance in terms of the axial stress and P_n is the in-plane column resistance in terms of the axial load. For the nominal out-of-plane strength, Galambos uses the fundamental equation for the elastic torsional-flexural buckling of a singly symmetric member under combined axial load and uniform major-axis bending,

$$(P_{ey} - P_e)(\bar{r}_o^2 P_{ez} - \bar{r}_o^2 P_e + \beta_x M) = (M + P_e y_o)^2 \tag{6.6.5-3}$$

to solve for the value of P_e at elastic torsional-flexural buckling corresponding to a given applied moment M. He then calculates the ordinate (i.e., the axial resistance) for the nominal out-of-plane strength curve at this moment by substituting $P_e/P_o = P_e/P_y$ into Eqs. 6.2.1-1. The terms P_{ey}, $\bar{r}_o$, P_{ez} and y_o are defined in Section 6.2.3 of this volume. The term β_x is a cross-section monosymmetry parameter (Galambos 2001a; Ziemian 2010; White and Jung 2003b).

The above approach works well for characterizing the resistance of prismatic compact doubly and singly symmetric I-section, tee and double-angle members in cases where $M_n = M_p$ at $P = 0$. However, for longer unbraced lengths, this approach predicts a lateral-torsional buckling resistance equal to the elastic critical moment $M_{e.LTB}$ in the limit of $P = 0$. This prediction is overly optimistic with respect to the *Specification* inelastic LTB flexural resistances (e.g., see Figure 59). Galambos (2001b) suggests capping the nominal flexural resistance at $M = M_n$ in these cases, where M_n is calculated using the applicable inelastic LTB resistance equations. This adjustment assumes that the member inelastic LTB resistance is unaffected by the presence of axial load, either positively for axial tension or negatively for axial compression.

The AISC (2016) Specification provides simplified procedures that accomplish the objective of the above approach for doubly symmetric rolled compact I-section members with $KL_z \leq KL_y$ subjected to major-axis bending and axial tension or compression, i.e., an enhanced characterization of the out-of-plane resistance. Section 6.6.5.3 summarizes these procedures.

Ultimately, the simplest and most reliable determination of the strengths for the above types of beam-columns may be the use of carefully validated numerical procedures that give explicit maximum strength solutions, including the influence of appropriate nominal residual stresses and geometric imperfections. Such calculations are explicitly permitted by Appendix 1 of the AISC (2016) Specification. However, these types of analysis tools are not readily available for professional practice at the present time (2021).

6.6.5.3 Out-of-plane strength of doubly symmetric rolled compact I-section members with $KL_z \leq KL_y$ subjected to axial load and major-axis bending

AISC (2016) specifies the following equation as an enhanced description of the out-of-plane resistance of doubly symmetric rolled compact-element I-section beam-columns subjected to major-axis bending and axial compression:

$$1.5\frac{P_u}{\phi_c P_{ny}} - 0.5\left(\frac{P_u}{\phi_c P_{ny}}\right)^2 + \left(\frac{M_{ux}}{C_b \phi_b M_{nx(Cb=1)}}\right)^2 \leq 1.0 \qquad \text{(6.6.5-4) (AISC H1-2)}$$

where P_{ny} is the nominal column strength for weak-axis flexural buckling in the out-of-plane direction, and $M_{nx(Cb=1)}$ is the governing major-axis flexural resistance of the member based on the idealized case of uniform bending. The term "compact-element" is intended as a requirement that the flange and web plates must be compact for flexure of the member. Although AISC (2016) restricts this equation to "rolled" sections, the equation should provide an appropriate characterization of the resistance of doubly symmetric compact welded I-section members as well.

The analytical basis for Eq. 4 comes from the solution of the differential equations of equilibrium for a simply supported elastic member subjected to axial compression and unequal end moments (McGuire 1968). This solution yields the equation

$$\frac{M^2}{C_b^2 r_o^2 P_{ey} P_{ez}} = \left(1 - \frac{P}{P_{ey}}\right)\left(1 - \frac{P}{P_{ey}}\frac{P_{ey}}{P_{ez}}\right) \qquad \text{(6.6.5-5)}$$

where P_{ey} is the out-of-plane column flexural buckling load (see Eq. 6.2.3-3), P_{ez} is the column torsional buckling load (see Eq. 6.2.3-1) and

$$r_o = \sqrt{\frac{I_x + I_y}{A_g}} \qquad \text{(6.6.5-6)}$$

is the polar radius of gyration of the cross section. The term in the denominator on the left side of Eq. 5 is the square of the elastic lateral-torsional buckling resistance of the member, i.e.,

$$M_e = \sqrt{C_b^2 r_o^2 P_{ey} P_{ez}} = C_b \frac{\pi}{L}\sqrt{\left(\frac{\pi E}{L}\right)^2 I_y C_w + E I_y G J} \qquad \text{(6.6.5-7)}$$

where C_b is the moment gradient modifier (see Section 6.3.5.11 of this volume). Equation 4 is obtained by assuming $P_{ez} = 2.0P_{ny}$, which is a lower-bound value for all the ASTM A6 rolled wide-flange section members with $KL_z \leq KL_y$, and by replacing $M_{e(Cb=1)}$ and P_{ey} by the design resistances $\phi_c P_{ny}$ and $\phi_b M_{nx(Cb=1)}$. The resulting equation provides a much improved assessment of the out-of-plane resistance of typical rolled column-type I-sections, particularly in cases where the design resistances are governed by inelastic buckling and/or yielding limit states.

Equation 4 is a simplified version of a comparable equation implemented in the Australian AS4100 Standard (SAA 1998) based on research conducted by Cuk and Trahair (1986) and Cuk et al. (1986). The simplifications relative to AS4100 are:

- The use of $P_{ez} = 2.0P_{ny}$ to remove the need for the calculation of P_{ez}, and

- The use of an appropriate C_b expression for flexure alone, whereas AS4100 provides a separate moment gradient modifier that captures enhanced moment gradient benefits for beam-columns subjected to moment and axial compression.

The AS4100 equations are reviewed and compared to other beam-column strength calculations by White and Clark (1997a and b). It is emphasized that the flexural resistance anchor point $C_b \phi_b M_{nx(Cb=1)}$ is permitted to be greater than $\phi_b M_{px}$. The resulting out-of-plane resistance is "capped" by the in-plane resistance determined using Eqs. 6.6.2-1 but considering only the in-plane strength, i.e., neglecting the potentially smaller values of $\phi_c P_{ny}$ based on minor-axis flexural buckling and $C_b \phi_b M_{nx}$ based on lateral-torsional buckling. This "cap" is similar in concept to the way that the plateau strength M_{max} serves as a cap on the general LTB strength of I-section beams subjected to moment-gradient conditions ($C_b > 1$).

Figure 90 shows the shape of Eq. 5 for several values of P_{ez}/P_{ey}. For ASTM A6 wide-flange sections, P_{ez}/P_{ey} is generally greater than 2.0 when $KL_z \leq KL_y$. However, it is not uncommon for this parameter to be only slightly larger than 2.0. In this case, one can observe that Eqs. 6.6.2-1, with $\phi_c P_{ny}$ and $\phi_f M_{nx(Cb=1)}$ replaced by P_{ey} and $M_{e(Cb=1)}$, provide a slightly liberal characterization of the theoretical beam-column elastic buckling resistance for small values of P/P_{ey}. Interestingly, Eq. 6.6.2-1a nearly matches Eq. 5 for $P/P_{ey} \leq 0.2$ when Eq. 5 is used with $P_{ez}/P_{ey} = \infty$. The base bilinear AISC (2016) beam-column strength curve defined by Eqs. 6.6.2-1 tends to be slightly conservative for large P/P_{ey} when P_{ez}/P_{ey} is close to 2.0, whereas it is significantly conservative relative to Eq. 5 for large P_{ez}/P_{ey}.

It is useful to note that Eqs. 4 through 7 are usually considered in the context of assumed torsionally-simply supported end conditions, i.e., twisting of the member ends is prevented but the member ends are free to warp and bend laterally. In cases where I-section members are continuous across brace points with less critical adjacent unbraced segments, the adjacent segments may provide substantial warping and weak-axis bending restraint at the ends of the critical unbraced length. This restraint potentially can increase the true member capacity substantially, but it is typically neglected in design practice.

There is no implicit intent in the development of the AISC provisions to disallow the use of doubly symmetric welded I-sections that have geometries comparable to rolled wide-flange sections. However, the ratio P_{ez}/P_{ny} can be smaller than 2.0 for some thin-web welded I-sections.
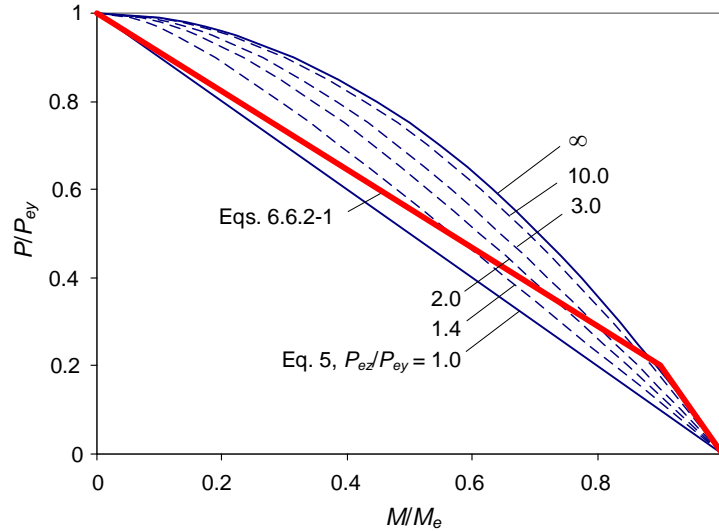
Figure 90. Theoretical elastic out-of-plane strength envelope for simply supported doubly symmetric I-section beam-columns versus the base AISC (2016) beam-column strength interaction curve.

There is no precedent for applying Eq. 4 to beam-columns having noncompact or slender cross-section elements, or to any type of tapered-web or generally nonprismatic beam-column members. It appears that there are no experimental or analytical solutions at the present time (2021) that substantiate the use of Eq. 4 for these cases.

Some enhancement relative to Eqs. 6.6.2-1 is possible in certain situations. However, the precise shape of the beam-column strength envelope depends on the mode of failure (FLB, LTB or TFY in the limit of zero axial force, weak- or strong-axis flexural buckling, or torsional buckling about a centroidal axis or a constrained axis in the limit of zero moment, and variations between these limits for combined axial load and flexure). Stated more directly, the precise shape of the beam-column strength envelope depends on the specific member parameters that influence the resistance in the various axial and flexural modes of failure as well as the different interactions between these various failure modes. Further research is needed to determine how to best characterize these resistances. In the absence of further refinements, of the simple use of Eqs. 6.6.2-1 is recommended for general cases that go beyond the applicability of Eq. 4.

AISC (2016) Section H1 gives the following modification of the moment gradient modifier C_b for doubly symmetric members subjected to axial tension:

$$C_b^* = C_b \sqrt{1 + P_u / P_{ey}} \qquad (6.6.5\text{-}8)$$

This modified C_b factor, with the tension force P_u taken as a positive number, accounts for the beneficial influence of axial tension on the lateral-torsional buckling resistance and is to be applied with Eqs. 6.6.2-1. Equation 8 can be inferred from a version of Eq. 5 with the second term on the right-hand side taken equal to 1.0. Its application in the context of Eqs. 6.6.2-1 is ad hoc, but gives a reasonable estimate of the bulge within the lower quadrants of the strength envelope for these types of members.

243

Figure 91 illustrates the combined influence of Eqs. 4 and 8 for a simply supported wide-flange beam-column subjected to uniform bending. The example W16x57 member has an unbraced length $L_b = KL_x = KL_y = KL_z = 18.3$ ft, which is equal to L_r. Therefore, $M_n = M_{e(Cb=1)} = 269$ ft-kips is governed by elastic LTB at $F_{e.LTB} = F_{yr}$ (see Eqs. 6.3.5-20, 6.3.5-22, and 6.3.5-27 of this volume). Also, the out-of-plane compressive resistance P_n is governed by elastic flexural buckling at $P_{ny} = 0.877P_{ey} = 255$ kips, and $P_{ez} = 850$ kips $= 3.33P_{ny}$ for this member. The resistance for pure axial tension with zero applied bending moment is taken as $P_y = 835$ kips, the in-plane axial compressive resistance is $P_{nx} = 777$ kips, and the in-plane flexural resistance is $M_p = 438$ ft-kips.
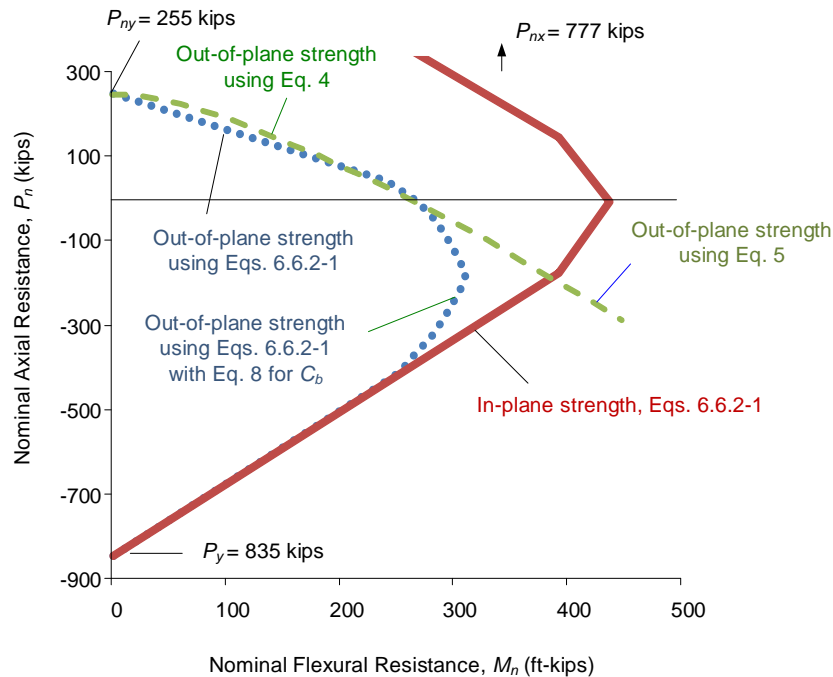
Figure 91. Beam-column resistances under tensile and compressive axial force (tension is shown as negative) and uniform primary bending (W16x57, $F_y = 50$ ksi, $L_b = 18.3$ ft, $C_b = 1.0$).

Three important sets of curves are shown in Figure 91:

- The in-plane member strength determined using Eqs. 6.6.2-1 with the resistances P_{nx}, M_p and P_y, denoted by the outer-most bold strength curves,

- The out-of-plane strength determined using Eqs. 6.6.2-1 with the resistances P_{ny} and $M_{n(Cb=1)}$ for the case of axial compression, and, for the case of axial tension, determined using Eqs. 6.6.2-1 with the resistances P_y and $M_{n(Cb=1)}$, but with $M_{n(Cb=1)}$ increased by C_b from Eq. 8 and capped by $C_b M_{n(Cb=1)} \leq M_p$. This strength is shown by the dotted curves.

- The "enhanced" "rigorous" out-of-plane strength determined using Eq. 4 with the resistances P_{ny} and $M_{n(Cb=1)}$ for the case of axial compression (with ϕ_f and ϕ_c taken equal to 1.0), and, for the case of axial tension, determined using Eq. 5 with the resistance P_{ey} replaced P_{ny} in the terms on the right-hand side of the equation, and $M_e^2 = M_{e(Cb=1)}^2 = $

$M_{nx(Cb=1)}{}^2$ in the denominator on the left-hand side of the equation. This strength is shown by the dashed curves.

For the third set of curves, Eq. 4 is only slightly more conservative compared to Eq. 5 for the case of axial compression, since $P_{ez}/P_{ny} = 3.33$ for the subject member whereas Eq. 4 uses the lower-bound value of $P_{ez}/P_{ny} = 2.0$. However, Eq. 5 is used for the axial tension case for this set of strength curves because Eq. 4 is slightly liberal relative to the exact analytical out-of-plane strength equation for tensile axial force.

One can observe that Eqs. 4 and 5 give a more liberal assessment of the out-of-plane strength, relative to the second set of curves, for the cases with high axial compression, although the increase in the strength for this uniform bending problem is relatively small for axial compression case. Conversely, for I-section members with column-type sections (i.e., $b_f \cong d$) subjected to moment-gradient loading, the benefits can be substantial. In fact, when these types of members are subjected to double-curvature, the out-of-plane resistance typically does not govern the strength. The most effective application of Eq. 4 is for this situation. In these cases, the most streamlined approach for member proportioning is to design the member assuming the out-of-plane strength does not govern, then check the resulting design using Eq. 4.

The C_b given by Eq. 8 captures some enhancement in the flexural resistance due to concurrent axial tension, as evidenced by the dotted curve, but not as substantial as the result from Eq. 5. However, the more liberal strength provided by Eq. 5 for the axial tension case is not specified in AISC (2016). One can observe that the dotted curve asymptotes to the in-plane axial tension strength from the first set of curves at approximately 400 kips axial tension. Equation 5 is more abruptly "capped" by the in-plane axial tension resistance at an axial tension slightly larger than $0.2P_y$, the axial tension force corresponding to the knee of the bilinear interaction curve.

AASHTO (2020) Article 6.8.2.3.1 provides an alternative set of strength interaction equations for combined axial tension and flexure on I- and box-section members that approximates the beneficial effect of axial tension on the LTB resistance represented by the above AISC (2016) approach. AASHTO (2020) provides the following equations that may be applied, in combination, in lieu of Eqs. 6.6.2-1:

$$\frac{P_u}{\phi_y P_{ny}} + \left(\frac{M_{ux}}{\phi_f M_{pex}} + \frac{M_{uy}}{\phi_f M_{pey}} \right) \leq 1.0 \qquad \text{(6.6.5-9) (AASHTO 6.8.2.3.1-3)}$$

$$\frac{M_{ux}}{\phi_f M_{ncx}} + \frac{M_{uy}}{\phi_f M_{ncy}} \leq 1.0 \qquad \text{(6.6.5-10) (AASHTO 6.8.2.3.1-4)}$$

where

P_{ny} = nominal resistance based on tension yielding

P_u = factored tensile axial force

M_{ncx} = nominal flexural resistance about the *x*-axis considering compression buckling

M_{ncy} = nominal flexural resistance about the *y*-axis considering compression buckling

M_{pex} = for I-section members, plastic moment about the *x*-axis; for noncomposite box-section members, effective plastic moment about the *x*-axis

M_{pex} = for I-section members, plastic moment about the *y*-axis; for noncomposite box-section members, effective plastic moment about the *y*-axis

M_{ux} = factored moment about the *x*-axis

M_{uy} = factored moment about the *y*-axis

ϕ_f = 1.0

ϕ_y = 0.95

Note that AASHTO (2020) writes the factored resistance terms in Eqs. 9 and 10 succinctly as P_{ry} for $\phi_y P_{ny}$, M_{rxpe} for $\phi_f M_{pex}$, M_{rype} for $\phi_f M_{pey}$, M_{rxc} for $\phi_f M_{ncx}$ and M_{ryc} for $\phi_f M_{ncy}$. The factored resistances are written directly herein, to avoid conflicts with the use of the subscript *r* for the required strengths in AISC (2016).

Similar to the application of Eqs. 6.6.2-1 and 6.6.2-2, all the terms in Eqs. 9 and 10 are taken as positive. Figure 92 illustrates the shape of the interation curve defined by these equations.
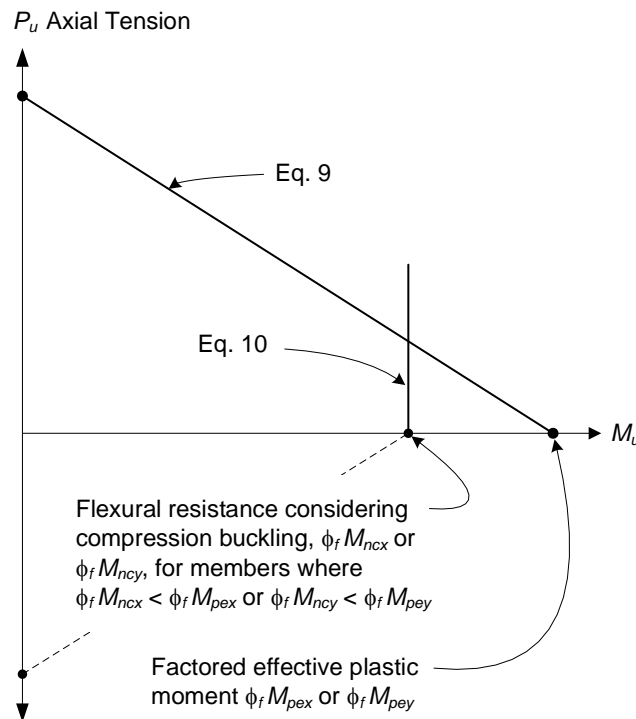
Figure 92. Interaction between axial tension and flexural yielding and buckling in flexural compression corresponding to Eqs. 9 and 10.

6.6.5.4 Other types of beam-columns, general loading conditions

The above subsections of Section 6.6.5 focus on the in-plane resistance of various types of beam-columns loaded about either their major or minor principal axis of bending, as well as the out-of-plane resistance of doubly or singly symmetric open-section members subjected to bending within their plane of symmetry. These applications constitute the vast majority of beam-column design situations in bridge construction.

The out-of-plane resistance of closed-section beam-columns bent about their strong-axis and subjected to axial compression, e.g., a beam-column with a box cross section, is represented accurately to conservatively by Eqs. 6.6.2-1 with P_n taken as the smaller of the member axial resistances for flexural buckling about the strong- or weak-axis. Equations 6.6.2-1 may be applied to the design of arch ribs, which often are rectangular box sections (see Wright and Bunner (2011) and White et al. (2019a)). In cases where a refined buckling analysis is utilized to evaluate the stability of the arch, P_n may be calculated using Eqs. 6.2.1-1 with P_e taken as the axial force at the governing buckling condition.

In some cases, bridge members are subjected to biaxial bending in combination with axial tension or axial compression. In these cases, extensive research shows that the equations presented in the above sections generally provide an accurate to somewhat conservative representation of the true strength envelope for compact I- and box-section members (Ziemian 2010; White et al. 2019a). The true shape of the strength envelope between the major- and minor-axis bending moments can be highly convex. AISC (1999) Appendix H provides nonlinear interaction equations for compact I- and box-section members in braced frames that provide the best known estimate of the true resistances. These equations no longer appear in AISC (2016), apparently due to their infrequent usage in design practice.

6.6.6 Composite Members

This section addresses the axial force-moment interaction for steel-concrete composite members. Two main types of members are considered: (1) I- and box-section members with a composite concrete deck, and (2) Concrete-encased sections and concrete-filled steel tubes.

6.6.6.1 I- and box-section members with a composite concrete deck

I-section members with a composite concrete deck behave in a fashion similar to singly symmetric steel I-sections with a large top flange, as discussed in Section 6.6.3 of this volume. The flexural resistance in positive bending is based on the plastic section response or flange yielding depending on whether the section is classified as compact or noncompact (see Section 6.3.3 and 6.3.4). The member resistance in axial compression is based either on flexural buckling about the major-axis or on torsional buckling about an enforced axis of rotation located at the depth of the shear connectors (see Section 6.2.7). The member resistance in combined axial compression and positive bending may be obtained conservatively by applying Eqs. 6.6.2-1 (see Section 6.6.2). However, a more liberal estimate may be obtained potentially by estimating the bulge in the strength envelope for loading within the upper-right quadrant of the beam-column strength curves (see Section 6.6.3). The appropriate calculations for this estimate are not readily apparent if the cross section is noncompact in positive bending, and/or if the I-section web is slender in uniform axial

compression. The behavior of box-section members with a composite concrete deck is similar, except that, as noted previously in Section 6.6.3, torsional buckling of the steel section is not a consideration.

6.6.6.2 Concrete-encased sections and concrete-filled boxes and tubes

The commentary to AISC (2016) Section I5 provides guidelines for calculation of the resistance for encased composite columns and concrete infilled sections subjected to combined axial compression and bending moment. Four separate approaches are outlined that vary in their level of conservatism and amount of calculation effort. All of the methods take advantage of the strength determination for a limited number of loading cases, establishing anchor points, and then utilize interpolation or interaction equations between the anchor points to calculate the strengths for other cases.

The AASHTO (2020) provisions utilize a form of each of the first two methods discussed in the AISC (2016) Section I5 commentary. Therefore, only these first two methods are discussed here.

The first approach is the base AASHTO method and is specified in AASHTO (2020) Article 6.9.2.2.1. This approach involves the use of Eqs. 6.6.2-1 to define the interaction between the axial compressive resistance calculated as discussed in Section 6.2.7.2 and the flexural resistance calculated as discussed in Section 6.5.9.2. As indicated in the AISC (2016) Section I5, this approach applies strictly only to doubly symmetric cross-section members. For these types of members, Eqs. 6.6.2-1 provide a conservative estimate of the member resistance for combined axial compression and flexure, given the axial resistance, P_n, and the flexural resistance, M_n, calculated as discussed above. The degree of conservatism depends on the extent of the concrete contribution to the strength, relative to that of the steel. Equations 6.6.2-1 are generally more conservative for members that have a larger contribution from the concrete.

The AASHTO (2020) 9th Edition Article 6.9.2.2.1 provisions specify the use of only a linear interaction between the axial compressive and flexural resistances. This is an inadvertent change in the AASHTO provisions from the 8th to the 9th Edition. Equations 6.6.2-1 are the intended interaction equations for composite members in combined axial compression and flexure.

Also, the above approach may be used for combined tension and flexure (although the AASHTO Article 6.8.2.3 provisions do not explicitly address composite members subjected to axial tension; the AISC (2016) Section I2.1c provisions specify the sum of the yield strengths of the steel section and the reinforcing steel as the axial strength in tension).

The second approach starts with a plastic analysis to determine the cross-section strength under combined bending and axial force. The preferred base calculation in this approach is the plastic stress distribution (PSDM) method discussed pertaining to flexure in the absence of axial loading in Section 6.5.9.1 and 6.5.9.3. This approach is specified by AASHTO Articles 6.12.2.3.3 and 6.9.6.3.4 specifically as an enhanced strength calculation procedure specifically for circular concrete-filled steel tube (CFST) members that satisfy the restrictions of AASHTO Article 6.9.6.2. The AISC (2016) Section I5 applies a form of this approach more broadly to doubly symmetric encased and *compact* filled beam-column members (as long as anchors are provided between the steel section and the concrete for encased members); AISC (2016) Sections I6 and I8 provide

detailed guidance on force transfer mechanisms and anchorage; AISC Section I6.3 states specifically that the force transfer mechanism of direct bond interaction shall not be used for encased composite members).

The second approach can be illustrated by considering the strength behavior for an encased I-section bent about its major axis and having only four bars as longitudinal reinforcement (see Figure 93). The "exact" cross-sectional strength interaction curve, shown by the bold solid curve in Figure 94, is obtained by a strain-compatibility analysis. The flexural strength, M, and axial load, P, may be estimated for various points along this curve by assuming a position of the plastic neutral axis, PNA, drawing the corresponding fully-plastic stress distributions, and summing their moments about the cross-section reference axis. The concrete under tension is neglected. Strain continuity is assumed between the steel and the concrete portions of the cross section. This assumption, although not supported well by the data from experimental tests where the interface was monitored, has a negligible influence on the ultimate strength and a minor influence on the stiffness of the cross section (Ziemian 2010).
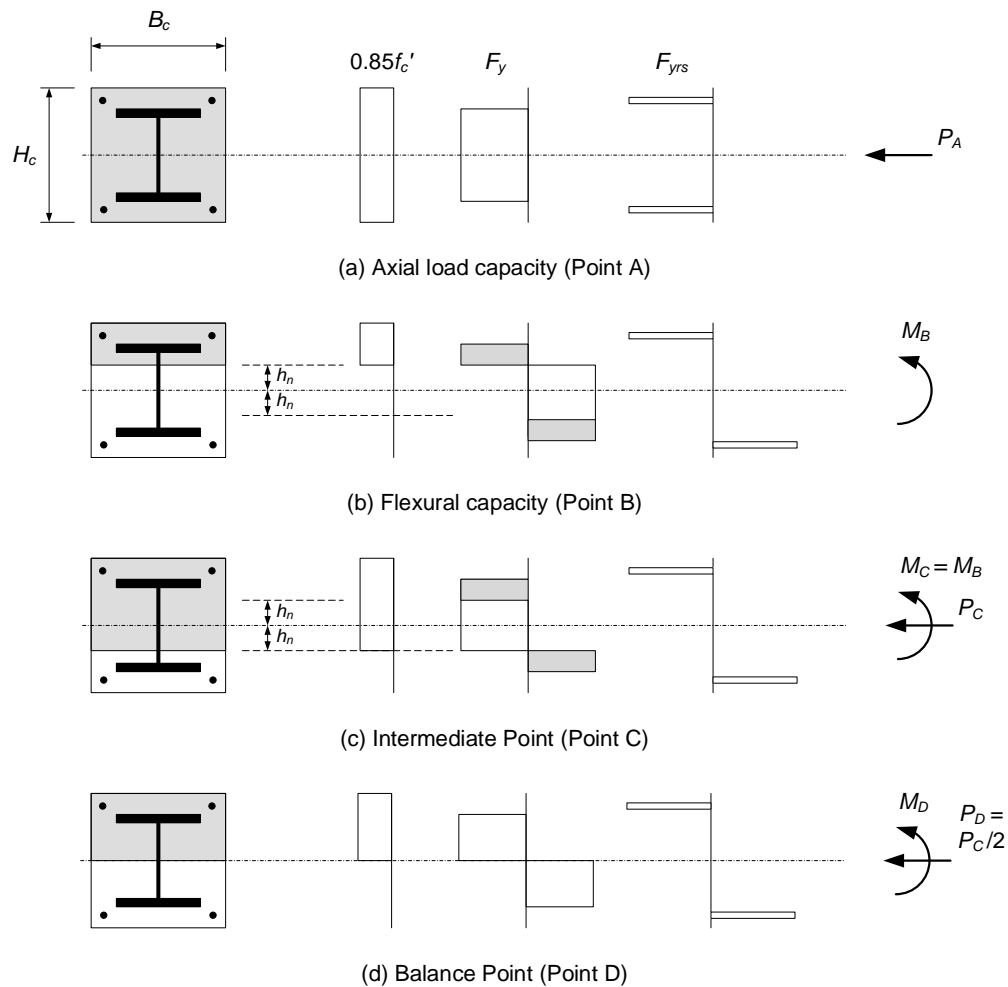
Figure 93. Stress distributions corresponding to key points on the beam-column strength envelope.
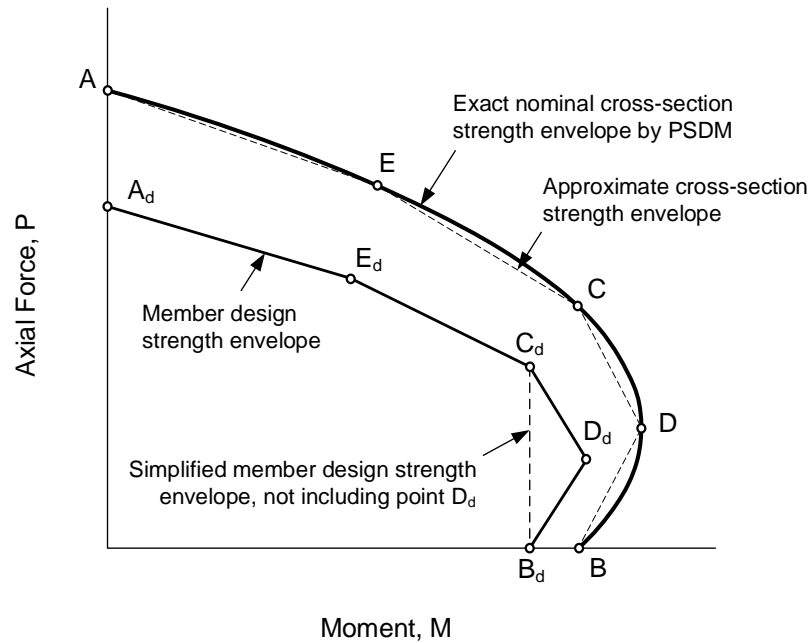
Figure 94. Cross section and member strength envelopes for an encased or filled composite beam-column.

Rather than determine a continuous locus of points to define the cross-section plastic strength curve, it is sufficient to define the cross-section strength by locating the five points labeled A through E in Figure 94 (Roik and Bergmann 1992; Ziemian 2010; AISC 2016). The commentary of AISC (2016) Section I1.2a suggests that only four points, A through D, are sufficient for typical cases in major-axis bending. Other strengths are determined by linear interpolation for cases that fall between these points. The strengths corresponding to these five anchor points may be determined as follows:

- Point A is the strength under concentric axial compression, determined as the value P_o in Section 6.2.7 of this volume.

- Point B is the plastic cross-section flexural resistance for zero axial force.

- Point C corresponds to the PNA location that gives the same flexural capacity as point B but with a nonzero axial compression. Assuming that the PNA lies in the web of the steel I-section for Points B and C, and that it is located at a distance h_n above the mid-depth of the I-section for Point B, the corresponding PNA for Point C is located at the same distance h_n below the mid-depth of the I-section. In both of the stress distributions for Points B and C, the depth $2h_n$ is in the middle of the section and hence the stress block having this depth contributes zero moment about the mid-depth reference axis of the cross section. In addition, it should be recognized from Figure 93 that the axial forces from the reinforcement and the shaded portions of the stress blocks from the steel shape cancel out.

If one adds the stress distributions in Figures 93b and c, the resulting axial force from the sum of these distributions is still the axial force P_C corresponding to the stress blocks in Figure 93c. This is because the total axial force in Figure 93b is zero. Furthermore, one can observe by

summing the contributions from the stress blocks in Figures 93b and c that the corresponding total axial force is equal to that given by the concrete section alone (since the contributions from the steel shape within the depth $2h_n$ also cancel out), i.e.

$$P_C = 0.85 f_c'(B_c H_c - A_s - A_{sr})$$ (6.6.4-1)

where B_c and H_c are the dimensions of the concrete section shown in Figure 93a, A_s is the area of the steel section, and A_{sr} is the area of reinforcing steel.

In a similar fashion, if the stress distribution in Figure 93b is subtracted from that of Figure 93c and the contribution of this sum to the axial force is considered, which is still equal to P_C, one obtains

$$P_C = (B_c - t_w)(2h_n)(0.85 f_c') + 2t_w(2h_n)F_y$$ (6.6.4-2)

This equation may be solved for h_n to obtain

$$h_n = \frac{P_C}{2(0.85 B_c f_c' + t_w(2F_y - 0.85 f_c'))}$$ (6.6.4-3)

Once h_n is determined, the moment capacity corresponding to points B and C is easily calculated.

- The moment corresponding to the balance point (point D), where the moment capacity is largest, is obtained when the PNA is located at the mid-depth of the cross section (since in this case, all the stress blocks contribute additively to the moment about the mid-depth reference axis). From Figure 93d, one can observe that all the contributions to the axial load from the steel shape and the reinforcement cancel out, and that the axial load P_D corresponds to $0.85 f_c'$ acting over half of the cross section, i.e.,

$$P_D = P_C / 2$$ (6.6.4-4)

The moment at the balance point is obtained as

$$M_{bal} = Z_x F_y + 0.5 B_c H_c^2 f_c' + \sum_{j=1}^{n} A_{ri} d_{ri}$$ (6.6.4-5)

where Z_x is the plastic section modulus of the steel section, A_{ri} is the area of any of the rebar, and d_{ri} is the distance from that rebar to the reference axis (equal to the plastic neutral axis in this case).

- Point E is an arbitrary point selected to improve the approximation of the "exact" cross-section strength curve between points A and C. The commentary to AISC (2016) Section I5 suggests that an appropriate calculation for this point is with the plastic neutral axis located at the flange tips of the I-section. The use of this point improves the representation of the rounded nature of the "exact" curve for weak-axis bending of encased shapes.

The above procedure defines the key points A through E, or A through D, in a very streamlined manner. Although the above example involves a relatively simple cross section, the procedure is general. For instance, the method applies for cases where the neutral axis is either in the flange of the steel shape or outside the steel shape, and it applies for any symmetrical number of and distribution of reinforcing bars. More general equations for biaxial bending and for concrete-filled shapes are provided by Roik and Bergmann (1992).

The strength envelope defined by points A through D or A through E needs to be adjusted to account for the stability effects associated with the member slenderness and the axial compression in the member. In addition, the resistance factors ϕ_c and ϕ_b need to be applied to the strengths. The commentary to AISC (2016) Section I5 recommends that these considerations may be accounted for by scaling the ordinate of all of the anchor points by $\phi_c P_n / P_{no}$, where P_{no} is the stub-column strength and $\phi_c P_n$ is the design axial compressive resistance calculated as defined in Section 6.2.7.3 of this volume using the AISC (2016) provisions, or Section 6.2.7.4 using the AASHTO (2020) provisions, and scaling the abscissa of all the anchor points by ϕ_b. This gives the anchor points A_d through E_d as shown in Figure 94.

In some cases, the above process can position point D_d outside of the nominal strength envelope between points D and B, or the design strength envelope may be quite close to the nominal strength envelope between these points. AISC (2016) suggests that this potential problem may be avoided by simplifying the method further and removing point D from the strength envelope. This results in the design strength envelope being a vertical line between points C_d and B_d as illustrated in the figure.

The first of the above approaches directly accommodates compression and biaxial bending, since Eqs. 6.6.2-1 accommodate bending about both the major and minor principal axes of the cross section. Roik and Bergmann (1992) recommend the use of linear interpolation between the strength envelopes for axial compression and bending about each of the cross-section principal axes with the second approach. The axial compressive resistance $\phi_c P_n$ is taken as the smaller resistance for column flexural buckling about either of the cross-section principal axes in determining the point A_d for each of the uniaxial strength envelopes.

The corresponding maximum second-order elastic moments along the member length are substituted into the strength interaction equation for bending about each of the principal axes (as discussed previously in the context of Eqs. 6.6.2-1, this is necessary because the interaction equations provide a simplified check of the combined influence of strength and stability for the complete unbraced length of the member, not just a check of the resistance at a given cross section).

AISC (2016) specifies $\phi_c = 0.75$ on the axial compressive strength and $\phi_b = 0.90$ for all its calculations for both encased and filled composite members.

AASHTO (2020) Article 6.9.6.3.4 recommends an alternative procedure developed by Moon et al. (2013) for determining the design strength envelope for circular concrete-filled steel tubes satisfying the requirements of Article 6.9.6.2. Figure 95 illustrates the construction of the nominal member strength curve by this procedure. Given the nominal member strengths, the ordinate of the strength envelope is scaled by ϕ_c, which is taken equal to 0.9 for composite CFSTs. The

abscissa is not scaled for CFSTs in the AASHTO LRFD Specifications since AASHTO (2020) Article 6.5.4.2 specifies $\phi_b = 1.0$.
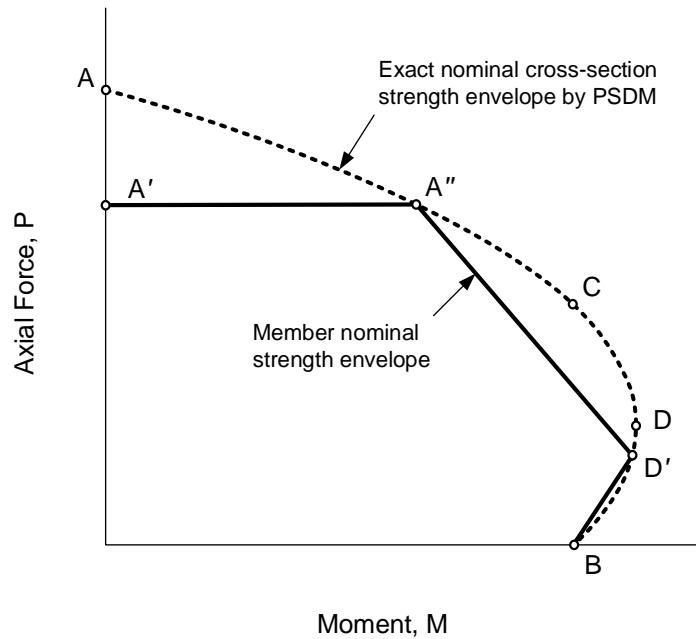
Figure 95. Construction of member strength envelope for a circular CFST using the procedure detailed in AASHTO (2020) Article 6.9.6.3.4.

The steps of the AASHTO (2020) Article 6.9.6.3.4 procedure are as follows:

- Point A′ is the member axial compressive resistance in the absence of any bending, P_n, calculated as discussed in Section 6.2.7.4 (Point A′ corresponds to the nominal, unfactored, strength associated with point A_d in the previous discussions).

- Point A″ is located at the intersection of a horizontal line through point A′ with the cross-section strength as represented by a line between points A and C.

- Point B is the member flexural resistance in the absence of any axial force, M_n, calculated as discussed in Section 6.5.9.3.

- Point C is determined as the point on the cross-section strength envelope at the same moment capacity as point B, but corresponding to a non-zero axial compression of P_C.

- Point D′ is determined as the point on the cross-section strength envelope corresponding to an axial force of

$$P_{D'} = 0.5 P_C \frac{P_n}{P_o}$$

(6.6.4-6)

One can observe that Eq. 6 defines a point that corresponds to the axial load level of point D from the previous discussions, but scaled by P_n / P_o as a consideration of the member

253

stability effects. The moment for point D′ is obtained by locating the point on the cross-section strength envelope corresponding to $P = P_{D'}$. (The notation D′ is introduced here to distinguish this point from the actual balance point, D, on the cross-section strength envelope.)

The member design strength envelope for AASHTO (2020), is obtained by connecting points A′, A″, D′, and B, then multiplying the ordinate values by $\phi_c = 0.9$ and multiplying the abscissa values by $\phi_b = 1.0$.

Moon et al. (2013) explain that the above procedure provides a more accurate estimate of the actual second-order moments at all levels of axial load compared to the AISC (2016) procedure as well as another separate procedure specified in Eurocode 4 (CEN 2004). In relationship to the discussions in Section 6.6.3.1 of this volume, illustrated by Figure 86, it is apparent that the strength envelope in Figure 95 corresponds to the maximum second-order inelastic moment labeled as $M_{2.inelastic}$ in Figure 86.

AASHTO (2020) Article C6.12.2.3.3 provides closed-form equations for the axial force, P, and the moment, M, defining the exact PSDM cross-section strength envelope for circular concrete-filled steel tubes (CFSTs) with or without internal reinforcing. The calculations using these equations start by specifying a y depth of the plastic neutral axis above a line through the center of the cross section. Given the y depth, one can directly calculate P and M. These equations can be employed to generate points on the exact strength envelope for any given CFST cross section. Points B, C and D′ can be obtained by an iterative inverse solution of these equations, or by interpolation between points determined on the exact strength curve.

6.6.7 Summary Assessment of Beam-Column Strength Calculations

It should be clear from the above discussions that the various design strength interaction equations are only coarse, albeit accurate to conservative, approximations of the true limit states response of general beam-column members. The nominal axial resistance P_n alone is governed in general by many different limit states. For axial compression of noncomposite members, these limit states include flexural buckling about the x- or y-axis of the cross section based on the effective lengths KL_x and KL_y, torsional buckling about the member centroidal axis (for doubly symmetric open-section members) or about an axis at which the transverse displacements are constrained based on the effective length KL_z, or torsional-flexural buckling based on the effective lengths KL_y and KL_z, depending on the specifics of the member geometry and boundary conditions. For most practical member lengths, the member response involves significant inelasticity and corresponding reductions in stiffness prior to achieving the strength limit states. However, for longer members, the limit states response may be dominated by the elastic stability behavior. If the member cross section contains slender elements under uniform axial compression, the column limit states response is influenced by the local buckling and post-buckling behavior of the component plates. For axial tension, the limit states include overall tension yielding, and tension fracture at a net section including shear lag effects associated with the connection geometry.

The nominal flexural resistance of noncomposite members and composite members with a composite concrete deck is governed by various idealizations of member elastic or inelastic lateral-torsional buckling, elastic or inelastic local buckling and postbuckling of the component plates,

and potential extents of yielding through the cross-section depth, depending on the cross-section type. For encased composite members, the flexural resistance is based on different extents of yielding, depending on whether shear connectors are provided and whether the concrete meets limits on its maximum compressive strength, and depending on the level of axial compression in AASHTO (2020). The AASHTO (2020) 9th Edition Specifications recognize calculations based on developing plastic strengths for compact concrete filled tube sections.

The physical interaction between the various axial and flexural resistances, and the resulting shape of the physical strength envelopes, differs in general depending on the specific combinations of the above limit states. It can be argued that explicit application of carefully validated numerical procedures, accounting for all the significant influences on the maximum strength, provides the only practical means of gaining any substantial improvement in accuracy relative to the practical design interaction equations discussed in the Section 6.6 of this volume. Appendix 1 of the AISC (2016) Specification provides guidelines for the application of this type of approach. However, in many practical situations, the simple Specification strength interaction equations are sufficient to achieve economical designs.

7.0 GENERAL NONCOMPOSITE MEMBERS USING LONGITUDINALLY STIFFENED PLATES

Longitudinal stiffening of component web and/or flange plates can be important to the overall design economy of members such as large box girders, arch ribs, arch tie girders, and steel towers in longer-span bridges. By definition in the AASHTO (2020) Section 6 provisions, longitudinally stiffened plates are always supported transversely along both longitudinal edges by attachment to other member cross-section elements. Longitudinal stiffening can be essential when added structural weight comes at a premium, and/or where the design stresses developed by a corresponding longitudinally unstiffened plate are relatively low due to local buckling effects. In addition, longitudinal stiffening can be beneficial for large plate widths where the thickness required to satisfy the strength demands is not available using a longitudinally unstiffened plate.

AASHTO (2020) Article CE6.1.3 indicates that longitudinal stiffening typically should not be considered for total plate widths less than about 60 inches. Longitudinally unstiffened plates are usually more economical in these cases. This limit is a broad guideline. Thickening the plate rather than adding longitudinal stiffeners may be more economical for plate widths larger than 60 inches in some situations.

Various articles in previous editions of the AASHTO LRFD Specifications, and their updated forms in the AASHTO (2020) Specifications, have addressed longitudinal stiffening in relatively specific contexts. These include Articles 6.10.1.9.2 and 6.10.1.10.2, which provide equations quantifying the local bend buckling resistance of longitudinally stiffened webs in flexural members, as well as the strength reduction factor, R_b, quantifying the postbuckling response of flexural members containing longitudinally stiffened webs. The background to the corresponding AASHTO (2020) equations is discussed in Sections 6.3.10.2 and 6.3.5.2.2 of this volume. These provisions are utilized by numerous other Articles of Sections 6.10, 6.11 and 6.12 of the LRFD Specifications. AASHTO Article 6.10.11.3 addresses the proportioning of web longitudinal stiffeners in flexural members (see Section 6.3.10.3 of this volume for a discussion of the background of these provisions). AASHTO Articles 6.11.8.2.2, 6.11.11.2 and C6.11.11.2 address

the design of longitudinally stiffened box flanges in composite box-girders subjected to negative bending. These design rules are discussed in Section 6.4.9.2 of this volume.

In previous editions of the AASHTO LRFD Specifications, the design of members containing longitudinally stiffened plates for general loadings (axial tension or compression, biaxial bending, flexural shear and/or torsional shear) has been addressed only in Articles 6.14.3, Orthotropic Deck Superstructures, and 6.14.4, Solid Web Arches. Furthermore, these general design considerations have been addressed in Articles 6.14.3 and 6.14.4 only in a very broad sense. AASHTO (2020) Articles E6.1.3 through E6.1.5 provide a streamlined intuitive approach for the general design of longitudinally stiffened plates for compression, based conceptually on the idealization as a series of parallel struts on an elastic foundation. Article E6.1.3 addresses the compressive resistance of plates designed using equally-spaced equal-size longitudinal stiffeners. White et al. (2019a) extend these provisions to the calculation of the compressive resistance of plates using unequally-spaced and/or unequal-size longitudinal stiffeners. AASHTO (2020) Article E6.1.1 integrates these rules into an overall procedure for calculation of the axial-compressive resistance of general members containing longitudinally stiffened plates. AASHTO (2020) Article 6.12.2.2.2d applies these rules for the calculation of the flexural resistance of noncomposite rectangular box-section members with longitudinally stiffened flanges. As noted in Section 6.4.9.2 of this volume, it is anticipated that the composite box-girder design provisions of Article 6.11 will take advantage of the advancements in Appendix E6 in a future edition of the AASHTO LRFD Specifications.

The design rules for flexural members using longitudinally stiffened webs are enhanced to some extent but are largely retained from prior editions of the Specifications in AASHTO (2020). The AASHTO (2020) procedures for general member design implement an overall strength interaction approach in which the member axial and biaxial flexural resistances are calculated separately and then evaluated in combination using the Article 6.8.2.3 and 6.9.2.2 strength interaction equations, including the consideration of torsional and flexural shear as appropriate (see Sections 6.6.2 through 6.6.4 of this volume). These provisions include the consideration of general members with longitudinally stiffened plates.

The following subsections provide a brief overview of the concepts and procedures associated with the AASHTO (2020) handling of general members using longitudinally stiffened plates. Section 7.1 presents the basic concepts employed in AASHTO Article E6.1.3 for the calculation of plate compressive resistances. Section 7.2 explains the marriage of the longitudinally stiffened plate calculations with the unified effective width approach in AASHTO Article E6.1.1. Section 7.3 discusses the concept of an equivalent flange employed for calculation of the resistance of noncomposite box-section members using a longitudinally stiffened compression flange in AASHTO Article 6.12.2.2.2d. This section also discusses the approach to handling of longitudinally stiffened webs in noncomposite box-section members, which is largely adopted from the handling of these components in I-section and composite box-section members discussed in Sections 6.3.5 and 6.4.9 of this volume. Sections 7.4 and 7.5 give an overview of the general longitudinal and transverse stiffener design requirements for longitudinally stiffened plates specified in AASHTO Articles E6.1.4 and E6.1.5.

7.1 Compressive Resistance of Longitudinally Stiffened Plates

AASHTO (2020) Article E6.1.3 provides a new approach for the design of longitudinally stiffened plates, with or without transverse stiffeners. This approach has the following salient features:

- The method considers explicitly the three elastic stiffness contributions to the plate ultimate resistance – flexural rigidity of the stiffener struts (the stiffeners plus the plate tributary to the stiffeners) in the longitudinal direction, plate transverse bending, and plate torsion – presented conceptually as a strut on an elastic foundation approach. Wide plates with a larger number of longitudinal stiffeners tend to be relatively thin and typically do not provide significant lateral bending or torsional resistance to the stiffeners. The stiffeners tend to behave largely as disconnected struts (see Figure 96a). However, for relatively narrow plates with only one or a few longitudinal stiffeners, the transverse bending and torsional stiffness contributions of the plate can be significant (see Figure 96b). The method in Article E6.1.3 captures the full range of these plate behaviors.

- The elastic buckling equations on which the calculations are based are derivable from either a strut model, considering the idealized torsional and transverse bending contributions from the plate, or from an orthotropic plate buckling idealization (King 2017; Lokhande and White 2018).

(a) Wide thin plate with a larger number of longitudinal stiffeners

(b) Relatively narrow and thick plate with a smaller number of longitudinal stiffeners
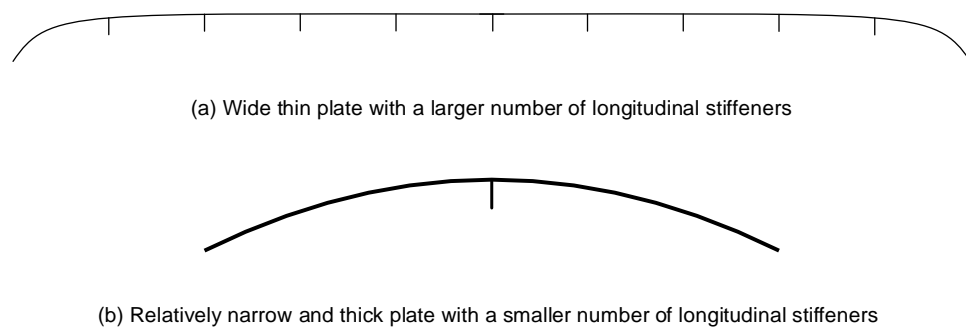
Figure 96. Cross-section views of representative buckling modes for a wide thin plate with a larger number of longitudinal stiffeners versus a relatively narrow and thick plate with a smaller number of longitudinal stiffeners.

- The recommended method combines the three stiffness contributions – flexural rigidity of the stiffener struts, plate transverse bending, and plate torsion – to give the buckling resistance of the stiffened plate, including the longer strength "plateau" arising from the plate behavior (i.e., the larger range of slenderness values, expressed as $\sqrt{F_y / F_e}$ where F_y is the yield strength and F_e is the elastic buckling stress, at which the plate is essentially able to develop its yield resistance). The explicit consideration and combination of these three contributions enables the designer to more easily optimize the design of the longitudinally stiffened plate, since the importance of each effect is clear. Since the plate effects are directly added to the compression strut effects, the designer can observe the importance of the different effects.

- The buckling wave length of the longitudinal stiffeners is provided by the method; therefore, the buckling mode is clear to the designer and the spacing of transverse stiffeners or diaphragms can be optimized. The designer can see what the effective buckling length is without transverse stiffeners, facilitating the choice of the spacing of transverse stiffeners or diaphragms.

- The method utilizes a form of the plate effective width equations, discussed in Section 6.2.4.2 of this volume, to account for plate local buckling and postbuckling effects within the longitudinally stiffened plate panels.

- The method avoids the limitations of the AASHTO LRFD method in Articles 6.11.8.2 and C6.11.11.2, discussed in Section 6.4.9.2 of this volume. For plates with more than two longitudinal stiffeners, the longitudinal stiffeners behave predominantly as compression struts spanning between the transverse stiffeners. The key property of a compression strut is its moment of inertia. When the moment of inertia is not a variable in the resistance formula, which is the case in these AASHTO Article 6.11.8.2 and C6.11.11.2 provisions, the formula cannot respond to this key property. The Article E6.1.3 method focuses directly on the design of the longitudinal stiffeners and their tributary plate width for the longitudinal compression they are subjected to.

- The direct consideration of the three stiffness contributions mentioned above captures the key behavior ranging from plate dominated actions (for relatively narrow plates with only one or two longitudinal stiffeners) to strut dominated actions (for relative wide plates with a larger number of longitudinal stiffeners) in a straightforward and design-friendly manner. The Article E6.1.3 method accounts for the structural stability effects without requiring any iteration, similar to the unified effective width method for longitudinally unstiffened plates, and it is suitable for application in a design office by spreadsheet or pencil and paper calculations. There is only one set of calculations to complete (the Eurocode 3 Part 1-5 procedures (CEN 2006) require separate "column-like" and "plate-like" strength calculations followed by interpolation between the two), and the calculations address longitudinally stiffened plates with or without transverse stiffeners.

- The method recognizes that the stresses at the supported edges of longitudinally stiffened plates tend to be larger than the stresses developed at the longitudinal stiffeners, but often less than the yield stress at the ultimate strength condition.

The primary AASHTO (2020) Article E6.1.3 calculations for the compressive resistance of a longitudinally stiffened plate are as follows:

1. Find the buckling effective length of the stiffener struts, ℓ.

   The buckling length of the longitudinal stiffener struts, ℓ, is taken as the smaller of (a) the spacing between sufficient transverse stiffeners, a, and (b) the length associated with the minimum resistance in the absence of transverse stiffeners, ℓ_c, given by

$$\ell_c = \left(\frac{EI_s \pi^4}{k_p} \right)^{1/4}$$

(7.1-1) (AASHTO E6.1.3-8)

in which I_s is the moment of inertia of the individual stiffener strut composed of the stiffener plus the tributary width of the longitudinally stiffened plate, taken about an axis parallel to the face of the plate and passing through the centroid of the combined area of the longitudinal stiffener and its gross tributary plate width, and

$$k_p = \pi^4 w \frac{EI_p}{b_{sp}^4}$$

(7.1-2)

is the transverse bending stiffness of the plate per unit length, where

w	=	plate tributary width
I_p	=	plate lateral bending moment of inertia per unit width
b_{sp}	=	total width of the plate between the other member cross section plates providing lateral support at the plate edges

Note, AASHTO Eq. E6.1.3-8 is obtained by substituting Eq. 2 into Eq. 1. Equation 1 and the equations below are written explicitly showing the stiffness k_p to emphasize the nature of the model as that of a strut on an elastic foundation.

2. Calculate the flexural buckling resistance of the stiffener struts, P_{nsF}

The flexural buckling resistance of the stiffener struts, P_{nsF}, is determined from the AASHTO column strength curve, using the elastic buckling load of the longitudinal stiffener, which is increased by the elastic transverse bending restraint (stiffness) of the plate. Put alternately, P_{nsF} is determined based on the elastic buckling load of the longitudinal stiffener and plate assembly, P_{esF}. This elastic buckling load may be written as

$$P_{esF} = \frac{\pi^2 EI_s}{\ell^2} + k_p \frac{\ell^2}{\pi^2}$$

(7.1-3) (AASHTO E6.1.3-6)

where ℓ is the buckling effective length.

3. Calculate the contribution to the buckling resistance from the torsional response of the plate, $0.15 P_{esT}$

The flexural buckling resistance, P_{nsF}, does not have the longer plateau that plates are known to exhibit since the AASHTO column strength curve has no plateau (e.g., in the Eurocodes (CEN 2005; CEN 2006), a much shorter strength plateau is defined for columns compared to that for plates). In the AASHTO (2020) Article E6.1.3 approach, the longer plateau is provided by the elastic torsional contribution of the plate, P_{esT}, multiplied by a calibration factor of 0.15. The theoretical contribution from the torsional rigidity of the plate to the elastic buckling load is obtained (from orthotropic plate theory, or

approximately, from an idealized model of the twisting of the plate between the stiffeners (King 2017; Lokhande and White 2018)) as

$$P_{esT} = \frac{\pi^2}{(1-\nu)b_{sp}^2} \frac{Gwt_{sp}^3}{3}$$

(7.1-4) (AASHTO E6.1.3-11)

It is well known that the plate torsional stiffness is a key contributor to the stability of plate elements stressed to yield (e.g., see Baker et al. (1956) and Horne (1964)). The torsional stiffness of the plate is reduced by yielding, but not as much as the lateral bending stiffness. For ideal concentric axial compression on a perfectly flat plate, incremental plasticity theory predicts that the elastic torsional stiffness of the plate is unaffected by the plasticity. For an initially imperfect plate, the torsional stiffness still is significant compared to the available transverse bending stiffness for the plate in its yielded condition. This is due to the fact that the shearing actions associated with torsion are a significant deviation from the loading normal to the yield surface of the plate material associated with plate axial compression and flexure).

4. Determine the compressive resistance of the individual stiffeners plus plate, P_{ns}

The above behavior is handled in an approximate, calibrated way in the Article E6.1.3 provisions by adding P_{esT}, multiplied by the calibration factor 0.15, to P_{nsF}. That is, in the Article E6.1.3 procedures, the compressive resistance of the individual stiffeners, including the associated effective width of the plate, P_{ns}, is calculated as the sum of (a) the flexural buckling resistance of the stiffener strut restrained by the transverse bending resistance of the plate, P_{nsF}, plus (b) a fraction of the buckling resistance offered by the elastic torsional stiffness of the plate, $0.15P_{esT}$, and it is limited by the effective yield load of the individual stiffener and its tributary plate width, P_{yes}:

$$P_{ns} = P_{nsF} + 0.15P_{esT} \le P_{yes}$$

(7.1-5) (AASHTO E6.1.3-2)

It should be noted that P_{esT} is added directly to P_{esF} to obtain the elastic buckling resistance of the stiffened plate according to orthotropic plate theory, or according to a strut on elastic foundation idealization considering the transverse bending and torsion of the stiffened plate panels (Lokhande and White 2018; King 2017).

5. Calculate the resistance from the panels adjacent to the edges of the longitudinally stiffened plate

At the edges of its total width, the longitudinally stiffened plate is restrained from out-of-plane bending. At the ultimate resistance, this plate area tends to sustain a higher stress than the area around the longitudinal stiffeners due to this restraint. Finite element test simulation studies have shown that the ultimate strength of the stiffened plate is often reached before these restrained areas reach their yield stress, but that the axial stress is larger than the average stress of in the stiffeners at this state. AASHTO (2020) Article E6.1.3 provides the following approximate expression for the contribution to the plate ultimate strength from the panels adjacent to its edges:

$$P_{nR} = \left(1 - \frac{P_{ns}}{P_{yes}}\right)\left[0.45\left(F_{ysp} + \frac{P_{ns}}{A_{es}}\right)A_{gR}\right] + \left(\frac{P_{ns}}{P_{yes}}\right)P_{yeR} \leq P_{yeR} \qquad \text{(7.1-6) (AASHTO E6.1.3-3)}$$

which is basically a linear interpolation between (a) the yield load of the plate tributary to the edge, in the limit that $P_{ns} = P_{yeR}$, and (b) the compression force given by $0.45(F_{ysp} + P_{ns}/A_{es})$ acting on A_{gR} in the limit that P_{ns} is small, where

F_{ysp} = yield stress of the plate and longitudinal stiffeners
A_{es} = effective area of an individual stiffener strut, including the plate tributary to the stiffener
A_{gR} = gross tributary area of the laterally-restrained longitudinal edge of the longitudinally stiffened plate, and
P_{yeR} = effective yield load of the tributary width of the plate at a laterally restrained longitudinal edge.

6. Sum the resistances to determine the total resistance of the longitudinally stiffened plate, P_{nsp}

The total resistance of the longitudinally stiffened plate subjected to uniform axial compression, P_{nsp}, is taken as the sum of the resistances of (a) the stiffener struts, including the associated widths of the plate, P_{ns}, multiplied by the number of longitudinal stiffeners, n, and (b) the sum of the resistances from the effective widths of the plate located at the restrained longitudinal plate edges, P_{nR}. That is,

$$P_{nsp} = nP_{ns} + 2P_{nR} \qquad\qquad \text{(7.1-7) (AASHTO E6.1.3-1)}$$

An interesting attribute from the elastic buckling theories underlying these provisions is that, for cases where the spacing of the transverse stiffening elements, a, is greater than the characteristic buckling length, ℓ_c, given by Eq. 1, and therefore $\ell = \ell_c$, the two contributions to P_{esF} in Eq. 3 are equal and the corresponding elastic buckling load may be calculated simply as

$$P_{esF} = \frac{2\pi^2 E}{b_{sp}^2}\sqrt{wI_p I_s} \qquad\qquad \text{(7.1-8) (AASHTO CE6.1.3-1)}$$

Alternatively, when $\ell = \ell_c$, P_{esF} can simply be taken as two times the elastic buckling load of the stiffener strut without consideration of the transverse bending contribution from the plate, i.e., two times the buckling load given by the first term in Eq. 3.

When the spacing between transverse stiffening elements is smaller than the characteristic buckling length, ℓ_c, the buckling length of the stiffener struts, ℓ, is taken as the corresponding spacing, a. In this case, the strength of the stiffened plate is increased due to the transverse stiffening. Otherwise, any impact of the spacing of the transverse stiffeners on the strength of the stiffened plate is neglected. The characteristic length, ℓ_c, is the theoretical length between the inflection points in the buckling mode of the stiffener struts for an infinitely long plate.

In addition, it can be observed that the contribution from the torsional stiffness of the plate, $0.15P_{esT}$, provides an increase in the plate strength as much as approximately 7 percent in the case of relatively narrow plates containing a single longitudinal stiffener, whereas this contribution becomes relatively small for wider plates with a larger number of longitudinal stiffeners.

Figure 97 illustrates the definition of a number of the variables associated with the above calculations.
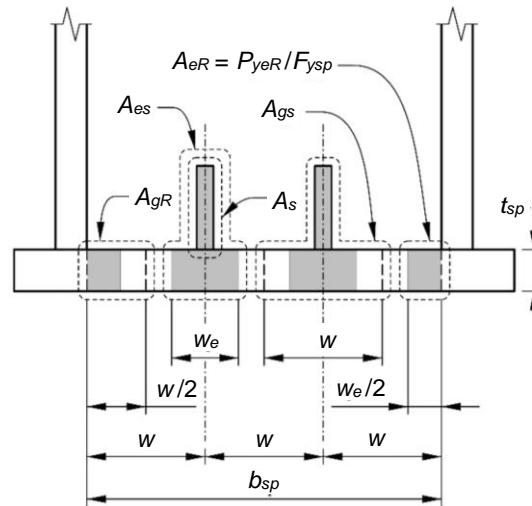
Figure 97. Illustration of variables for a longitudinally stiffened plate.

7.2 Axial Compressive Resistance of Members Using Longitudinally Stiffened Plates

The above section provides a brief outline of the procedure for calculating the compressive resistance of a longitudinally stiffened plate in AASHTO (2020) Article E6.1.3. This section summarizes the marriage of the longitudinally stiffened plate calculations with the unified effective width approach in Article E6.1.1.

The calculation of the axial compressive resistance for members composed solely of longitudinally *unstiffened* plates is discussed in Section 6.2.4.3 of this volume. This involves:

1. The calculation of a column critical stress, F_{cr}, based on the member gross cross-sectional properties and the corresponding overall slenderness pertaining to column buckling,

2. The calculation of plate effective widths as a function of F_{cr} using the appropriate form of Winter's effective width equation,

3. The multiplication of these effective widths by the corresponding plate thicknesses to obtain the plate effective areas,

4. The summation of the effective and gross areas of the cross section, as applicable, to obtain the total member effective area, A_e, and

5. The multiplication of F_{cr} with A_e to determine the overall column strength (see Eq. 6.2.4-16 of this volume).

This calculation takes advantage of (a) the ability of Winter's effective width equation to provide an estimate of the effective plate areas, A_e, and the effective contribution of the plate to the member stiffness at any level of stress less than or equal to F_y, combined with (b) the simplifications within the unified effective width method associated with the ability to use the gross cross section properties to characterize the stress level at the member axial compressive strength condition, F_{cr}, which can then be multiplied by A_e to determine the nominal axial load capacity.

Equation 7.1-7, which quantifies the compressive resistance of a longitudinally stiffened plate, does not possess the property of being able to quantify the longitudinally stiffened plate effective area, or the contribution of the plate to the member stiffness at any level of applied stress. This equation targets only the ultimate compressive resistance of an individual plate. While Winter's effective width equation is written as a function of the idealized edge stress on the effective width of a longitudinally *unstiffened* plate, and in the unified effective width method, the column ultimate stress, F_{cr}, estimated using the gross cross-section properties of the member, is substituted for this stress, Eq. 7.1-7 does not use this format. As such, a different approach is needed to account for the interaction of the ultimate strength of individual longitudinally stiffened plates with the overall member ultimate axial compressive resistance.

The routine application of the Eurocode Part 1-5 (CEN 2006) provisions is such an approach. In this method:

1. The effective area of the cross-section elements is determined at the yield stress level, F_y,

2. The effective and gross areas of the cross section are summed to obtain to member total effective cross-sectional area, A_e, and

3. The member strength is determined as $\chi\, A_e\, F_y$, where $A_e\, F_y$ is the strength for a short member length (i.e., the effective yield load of the member cross section, considering plate local buckling and postbuckling effects), and χ is a strength reduction factor that implements the column strength curve.

This calculation, in essence, focuses on the determination of an effective yield load, $A_e\, F_y$, corresponding to the ultimate strength of the component plates, and then employs this effective yield load with an appropriate column curve formula given by the χ factor. As discussed in Section 7.3 below, the applicable forms of Winter's effective width equation are employed in this manner within the AASHTO (2020) Article 6.12.2.2 provisions when quantifying the compression flange response for calculation of the flexural resistance of box-section members (i.e., the plate effective widths are determined using F_y rather than an F_{cr} in the AASHTO Article 6.12.2.2 provisions).

The above effective yield load approach is employed in AASHTO (2020) Article E6.1.1 to determine the overall axial compressive strength of a member using longitudinally stiffened plates. In Article E6.1.1, the longitudinally stiffened plate ultimate strengths from Eq. 7.1-7 are taken directly as the corresponding contribution to the effective yield load of the member.

The effective yield load approach and the unified effective width approach are indeed two different models for local-global buckling interaction when calculating member axial compressive resistances. For members composed solely of longitudinally *unstiffened* plates, the unified effective width model is employed within the AASHTO (2020) provisions. This model focusses on the calculation of plate element effective widths that are a function of the axial stress on the effective area of the member cross section at the member axial compressive ultimate strength, F_{cr}. The total resulting effective area of the member is multiplied by F_{cr} to determine the member's axial compressive capacity. Conversely, for members having cross sections composed solely of longitudinally *stiffened* plates, the effective yield load model focuses on the calculation of an effective yield load of the member. The member axial compressive resistance is then determined by employing this effective yield load with an appropriate column strength curve.

The first of these approaches has been shown to provide accurate predictions of the axial compressive resistance of members composed solely of longitudinally *unstiffened* plates. This approach also has been shown to have merit for sections composed of longitudinally stiffened plates (Schafer and Peköz, 1996; Schafer and Peköz, 1998), but not without adjustment to account for the reduced postbuckling capacity for buckling modes involving transverse movement of the longitudinal stiffeners. The second of these conceptual approaches is recommended as a more straightforward calculation for members having cross sections composed solely of longitudinally stiffened plates.

AASHTO (2020) Article E6.1.1 combines the above two approaches as follows for calculation of the axial compressive resistance of members having cross sections composed of both longitudinally unstiffened and longitudinally stiffened plates:

1. The member nominal yield resistance is determined as

$$P_{os} = F_y \left(\sum_{lusp} bt + \sum_c A_c + \sum_{lsp} \left(A_{eff} \right)_{sp} \right)$$ (7.2-1) (AASHTO E6.1.1-9)

where

$\displaystyle\sum_{lusp}$ = summation over all longitudinally unstiffened cross-section plate elements

$\displaystyle\sum_c$ = summation over all the corner areas of a noncomposite box-section member, and other similar areas not included in the plate resistance calculations for other members

$\displaystyle\sum_{lsp}$ = summation over all the longitudinally-stiffened cross-section plate elements

A_c = gross cross-sectional area of the corner pieces of a noncomposite box-section member, and other similar areas not included in the plate resistance calculations for other members

$(A_{eff})_{sp} =$ effective area of a longitudinally stiffened plate element under consideration

$$(A_{eff})_{sp} = \frac{P_{nsp}}{F_{ysp}}$$ (7.2-2) (AASHTO E6.1.3-17)

b =   gross width of the longitudinally unstiffened plate element under consideration

t =   thickness of the longitudinally unstiffened plate element under consideration

F_{ysp} =   specified minimum yield strength of the longitudinally stiffened plate.

2. The nominal yield strength, P_{os}, is employed within the AASHTO LRFD column strength equations as follows:

If $P_{os}/P_e \leq 2.25$

$$F_{cr} = \left[0.658^{(P_{os}/P_e)}\right] F_y$$ (7.2-2a) (AASHTO E6.1.1-6)

Otherwise

$$F_{cr} = 0.877 \frac{P_e}{P_{os}/F_y}$$ (7.2-2b) (AASHTO E6.1.1-7)

where P_e is the theoretical elastic buckling resistance of the member subjected to concentric axial compressive load, calculated using the member gross cross section properties using the appropriate elastic buckling equations from Sections 6.2.1 through 6.2.3-3 of this volume as appropriate.

3. The member nominal axial compressive resistance is then determined as

$$P_n = \chi F_{cr} A_e$$ (7.2-3) (AASHTO E6.1.1-1)

in which

A_e =   effective area of the member cross section

$$A_e = \sum_{lusp} b_e t + \sum_c A_c + \sum_{lsp} \left(A_{eff}\right)_{sp}$$ (7.2-4) (AASHTO E6.1.1-8)

χ = strength reduction factor accounting for local-global strength interaction

where

$$\chi = 1 - r_1 r_2$$ (7.2-5) (AASHTO E6.1.1-2)

in noncomposite rectangular box-section members containing one or more longitudinally stiffened flange plates in the direction associated with column buckling, and where $\lambda_{max} > \lambda_r$, otherwise $\chi = 1.0$

$$r_1 = 0.5\left(K\ell / r_s - 50\right)/90 \geq 0 \qquad\qquad \text{(7.2-6) (AASHTO E6.1.1-3)}$$

$$r_2 = \frac{\lambda_{max} - \lambda_r}{90 - \lambda_r} \qquad\qquad \text{(7.2-7) (AASHTO E6.1.1-4)}$$

b_e = effective width of the longitudinally unstiffened plate under consideration, determined as defined in Section 6.2.4 of this volume (Article 6.9.4.2.2b of AASHTO (2020)) for slender plate elements, and taken equal to b for nonslender plate elements

$K\ell$ = effective length in the plane of buckling

r_s = radius of gyration about the axis normal to the plane of buckling

λ_{max} = maximum w/t of the panels within the longitudinally stiffened flange plates

λ_r = $1.09\sqrt{E / F_{ysp}}$ if the flange plate has one longitudinal stiffener, or $1.49\sqrt{E / F_{ysp}}$ if the flange plate has two or more longitudinal stiffeners.

The factor χ in Equation 3 accounts for additional local-global strength interaction not captured by the AASHTO LRFD column curve strength formula for box-section members having a relatively large $K\ell/r_s$ combined with slender panels within longitudinally stiffened flanges corresponding to the direction of flexural buckling. Lokhande and White (2018) observed that the predictions using the above procedures, without adjustment, correlate well with the results from column flexural buckling parametric studies except for cases with slender panels between the longitudinal stiffeners in flange plates ($w/t > \lambda_r$) combined with $K\ell/r_s$ values larger than 50.

Lokhande and White (2018) observed that, if the less optimistic applicable Eurocode 3 (CEN 2005) column curve, or other comparable column curves such as one form of the Canadian column strength formula (CSA Group, 2014), were employed for these cases, the axial compressive resistances are predicted accurately. The χ factor adjustment was recommended to provide a similar representation of the axial compressive strengths without resorting to a separate column strength equation. The additional strength reduction is associated with the significant second-order bending stresses that occur as these types of members approach their maximum axial compressive resistance. Longitudinally stiffened flange plates with slender panels between the longitudinal stiffeners have difficulty in sustaining these additional compressive stresses.

7.3 Flexural Resistance of Noncomposite Box-Section Members Using Longitudinally Stiffened Plates

The AASHTO (2020) Article 6.12.2.2.2d provisions for calculation of the flexural resistance of noncomposite box-section members using longitudinally stiffened flange and/or web plates are a direct extension of the provisions discussed previously in Section 6.5.3 of this volume:

- For box-section members with longitudinally stiffened webs, the extensions are very straightforward. In these cases, the Article 6.12.2.2.2 provisions simply utilize the Article 6.10.1.10.2 provisions for the web bend buckling (load-shedding) factor, R_b. These provisions are discussed in Section 6.3.5.2.2 of this volume. For box sections with more than one web longitudinal stiffener loaded in compression within each web, it is recommended that only the longitudinal stiffener closest to the compression flange in each web be considered. This conservatively neglects the benefit from multiple web longitudinal stiffeners in compression; however, the predominant benefit of web longitudinal stiffening typically comes from the longitudinal stiffener closest to the compression flange.

- Longitudinal stiffeners should be included in the calculation of the elastic gross and effective cross-section properties, with the exception of cases in which the webs have different longitudinal stiffening or when calculating the cross-section plastic moment for use in the alternate interaction equation for axial tension and uniaxial or biaxial bending discussed in Section 6.6.5.3 of this volume.

- For box-section members with a longitudinally stiffened compression flange, the AASHTO Article 6.12.2.2.2d provisions work directly from the provisions outlined previously in Section 6.5.3 of this volume. However, since longitudinally stiffened compression flanges typically are unable to withstand inelastic deformations necessary to develop significant yielding throughout the depth of the box-section webs without significant reductions in their compressive resistance, the largest possible flexural resistance of these types of members is in most cases limited to the effective yield moment, M_{yce}. That is, box-section members with a longitudinally stiffened compression flange are classified as slender web sections, i.e., $R_{pc} = 1.0$. Because of the longitudinal stiffening of the compression flange, R_f is also taken equal to 1.0. (In cases where flange longitudinal stiffeners are provided but are not required for strength, the recommended provisions indicate that the longitudinal stiffeners may be neglected and the compression flange may be considered as longitudinally unstiffened for purposes of calculating the member strength; however, the requirements pertaining to longitudinal stiffeners are to be satisfied for such sections.)

For the purpose of calculating the yield moment of the effective cross section with respect to the compression flange, AASHTO Article 6.12.2.2.2d specifies that a longitudinally stiffened compression flange can be represented by an effective area "strip" of infinitesimal thickness, located at the centroid of the gross area of the entire flange plate and its longitudinal stiffener(s). This effective area is calculated as

$$A_{eff} = P_{nsp} / F_{yc} \qquad\qquad \text{(7.3-1) (AASHTO 6.12.2.2.2d-1)}$$

where P_{nsp} is the longitudinally stiffened plate capacity determined as described in Section 7.1. AISI (2016) and Eurocode 3 Part 1-5 (CEN 2006) employ a comparable approach.

All of the other calculations for longitudinally stiffened flange box-sections are essentially the same as for longitudinally unstiffened flange sections. In cases where $S_{xte} < S_{xce}$, it is recommended that D_{ce} and M_{yce}, considering the early yielding in flexural tension, should be calculated by: (1) using the value given by Eq. 1 for the effective compression flange area, including the modeling of the compression flange area as a zero thickness strip at the centroid of the compression flange and its longitudinal stiffener(s), (2) modeling the web depth between the effective compression flange elevation and the elevation of a zero-thickness strip representing the tension flange area and located at the centroid of the tension flange, and (3) neglecting any web longitudinal stiffeners. This greatly simplifies the calculation of these parameters relative to the solution based on a rigorous strain-compatibility analysis.

7.4 General Longitudinal Stiffener Design Requirements in Longitudinally Stiffened Plates

AASHTO (2020) Article E6.1.4 specifies the requirements for the design of longitudinal stiffeners intended to provide enhanced plate strengths. Key requirements specified by this article include:

- Yield strength requirements. Early yielding of lower strength longitudinal stiffeners would result in a significant reduction in their effectiveness; therefore, the specified minimum strength of the stiffeners should not be less than the specified minimum yield strength of the plate to which they are attached. Otherwise, the impact on the strength may be considered by taking F_{ysp} equal to the specified minimum yield strength of the stiffeners.

- Detailing requirements. Longitudinal stiffeners must be structurally continuous along their length to develop the resistance of the corresponding stiffened plates. AASHTO Article CE6.1.4 provides extensive detailing guidance pertaining to these requirements.

- Selection of longitudinal stiffener properties to prevent stiffener local buckling and tripping. To ensure that the resistance of longitudinal stiffeners is not impacted by local buckling of the stiffener cross-section elements, AASHTO Article E6.1.4 specifies

$$\frac{b}{t} \leq \lambda_r \qquad\qquad (7.4\text{-}1)\ (\text{AASHTO E6.1.4-1})$$

where

λ_r = nonslender plate limit for the longitudinal stiffener plate element under consideration (see Eq. 6.2.4-10a and Table 5 of this volume)

b = longitudinal stiffener plate element width as specified in AASHTO (2020) Table 6.9.4.2.1-1

t = longitudinal stiffener plate element thickness

In addition, AASHTO Article E6.1.4 specifies that tee and angle section longitudinal stiffeners should satisfy

$$\frac{J_s}{I_{ps}} \geq 5.0 \frac{F_y}{E} \qquad \text{(7.4-2) (AASHTO E6.1.4-2)}$$

to ensure against torsional buckling of these types of stiffeners about the edge of the stiffener attached to the plate. This mode of failure also is referred to as stiffener tripping. For flat plate longitudinal stiffeners, Eqs. 1 and 2 give the same requirement, and therefore only Eq. 1 needs to be checked.

Equation 2 tends to require relatively thick plates for tee and angle stiffeners to ensure that the stiffener does not fail by tripping. This equation is considered as being most appropriate for new designs. However, it neglects the warping contribution to the torsional resistance, which tends to be small in many practical cases given the length between the locations of torsional restraint at transverse stiffeners and/or diaphragms. Furthermore, it neglects the potential contribution from the stiffened plate to twisting of the stiffener about its connection to the plate. Quantification of this torsional restraint is a complex problem that has not yet been fully studied. White et al. (2019a) show the derivation of Eq. 2 and review the literature on more refined assessments of the tripping strength of open-section longitudinal stiffeners. AASHTO Article CE6.1.4 provides recommendations for practical assessment of the tripping strength of open-section longitudinal stiffeners for cases where Eq. 2 is violated in existing structures.

- Longitudinal stiffener minimum slenderness limit. AASHTO (2020) Article 6.1.4 also specifies that flange plates with b_{sp}/t_{sp} larger than 90 shall satisfy

$$a/r_s \leq 120 \qquad \text{(7.4-4) (AASHTO E6.1.4-3)}$$

where

a = longitudinal stiffener spacing between locations of transverse stiffeners or diaphragms that provide transverse lateral restraint to the longitudinally stiffened plate

b_{sp} = total width of the longitudinally stiffened plate

r_s = radius of gyration of the stiffener strut(s) about an axis parallel to the plane of the stiffened plate

$$r_s = \sqrt{I_s/A_{gs}} \qquad \text{(7.4-5) (AASHTO E6.1.4-4)}$$

t_{sp} = thickness of the longitudinally stiffened plate under consideration

A_{gs} = gross area of the individual stiffener strut(s) as illustrated in Figure 97.

I_s = moment of inertia of individual stiffener strut(s), taken as defined in Section 7.1

This limit helps ensure against excessive out-of-plane deflection of a stiffened plate under its self-weight plus a small transverse concentrated load (White et al. 2019b). This limit is applied regardless of whether or not the member is in a horizontal configuration in the final constructed geometry, to limit such deflections with the member oriented horizontally during construction operations. This limit need not be satisfied for flanges with $b_{sp}/t_{sp} \leq 90$ since the out-of-plane deformations due to the above load effects tend to be small in these cases without consideration of the longitudinal stiffening.

In addition to the above requirements, indirect requirements are placed on the longitudinal stiffeners via the dependency of the shear strength of the longitudinally stiffened plate on the longitudinal stiffener moment(s) of inertia. AASHTO (2020) Article 6.9.2.2 points to Article 6.11.8.2.3 for calculation of the shear strength of longitudinally stiffened plates. AASHTO Article 6.11.8.2.3 bases this shear strength calculation on the theoretical shear buckling load, not considering any postbuckling action. This calculation is discussed previously, in the context of longitudinally unstiffened plates, in Section 6.6.3 of this volume (see Eqs. 6.6.3-1 through 6.6.3-3 and the definition of F_{cv}, F_{cvx} and F_{cvy} in these equations). These definitions point to Eqs. 6.4.9-4 of this volume, which are adapted for the calculation of the shear strength of longitudinally stiffened plates by substituting the panel width-to-thickness ratio, w/t, for b_f/t_f. Furthermore, Eq. 6.4.9-15 of this volume is adopted for the calculation of the shear buckling coefficient for the longitudinally stiffened plate panels. This long and winding road ties the shear buckling strength of the longitudinally stiffened plate panels to the moment of inertia of the longitudinal stiffeners, I_s. Equation 6.4.9-15 is based on the idealization of an infinitely long plate having equally-spaced longitudinal stiffeners of equal stiffness. Section 3.3.2.2 of (White et al. 2019a) provides more elaborate equations for calculation of the shear buckling coefficient the account for unequally-spaced longitudinal stiffeners of unequal stiffness, as well as the influence of transverse stiffening.

7.5 General Transverse Stiffener Design Requirements in Longitudinally Stiffened Plates

The provisions in AASHTO (2020) Article E6.1.5 apply for the design of transverse stiffeners provided to enhance the resistance of a longitudinally stiffened plate. The approach to the design of the transverse stiffeners in these types of plates is parallel to other modern approaches for the design of stability bracing, such as the approaches in AISC (2016) Appendix 6. The requirements consider the out-of-plane stiffness and strength demands for the transverse stiffeners to "brace" the longitudinally stiffened plate at the stiffener locations.

In longitudinally stiffened plates containing transverse stiffeners in which:

- The characteristic length, ℓ_c, from Eq. 7.1-1 of this volume is less than the transverse stiffener spacing, a, and

- The transverse stiffeners are not subjected to any directly applied bending or axial compression,

the transverse stiffeners do not serve any purpose to enhance the axial compressive resistance of the longitudinally stiffened plate, and any potential destabilization of the transverse stiffeners from

the longitudinal compression in the plate is not a consideration. Therefore, in these cases, the stiffness and strength requirements from Article E6.1.5 are waived.

AASHTO (2020) Article E6.1.5.2 specifies the following moment of inertia requirements for routine applications of transverse stiffeners in which the stiffeners are not subjected to any directly applied axial compressive force and/or directly applied loads causing bending of the stiffener:

$$I_t \geq 0.5 \frac{P_{up}}{a_{min}} \frac{b_{sp}^3}{E}$$

(7.5-1) (AASHTO E6.1.5.2-1)

and

$$I_t \geq \left(0.0009 \frac{E}{F_y} \frac{c}{b_{sp}} + 0.02 \right) \frac{P_{up}}{a_{min}} \frac{b_{sp}^3}{E}$$

(7.5-2) (AASHTO E6.1.5.2-2)

where

a_{min} = smallest of the longitudinal spacings to the adjacent transverse stiffeners or diaphragms providing lateral restraint to the plate

c = largest distance from the neutral axis to the extreme fiber of the transverse stiffener considered in the calculation of I_t

b_{sp} = total inside width between the plate elements providing lateral restraint to the longitudinal edges of the plate under consideration

F_y = smallest specified minimum yield strength of the stiffened plate and transverse stiffener under consideration

I_t = moment of inertia of the transverse stiffener, including a width of the stiffened plate equal to $9t_{sp}$, but not more than the actual dimension available, on each side of the stiffener avoiding any overlap with contributing parts to adjacent stiffeners or diaphragms, taken about the centroidal axis of the combined section; the reduced cross section at cutouts to accommodate longitudinal stiffeners shall be considered and the smallest moment of inertia at such cutouts shall be used for I_t

P_{up} = total factored longitudinal compression force in the plate under consideration, determined from a structural analysis considering the cross section, including the longitudinal stiffeners, and including all sources of factored longitudinal normal compressive stresses from axial loading and from flexure; in cases where the plate is subjected to longitudinal normal stresses in tension over a portion of its width, the tensile stresses shall be neglected in determining this force

t_{sp} = thickness of the stiffened plate

Equation 1 is a generalized and simplified form of the moment of inertia requirement given by AASHTO (2020) Eq. C6.11.11.2-4 for transverse stiffeners in composite box-section compression flanges. This equation ensures adequate lateral stiffness to brace the longitudinal stiffeners and the stiffened plate given the factored longitudinal compression force they are transmitting.

Equation 2 is a moment of inertia requirement that indirectly ensures that the transverse stiffeners have adequate lateral strength to resist the destabilizing load effects from the factored longitudinal compression force in the plate and the longitudinal stiffeners.

White et al. (2019a) provide a detailed derivation of these equations. In addition, they provide a generalization of these equations, termed "advanced transverse stiffeners requirements," addressing the proper design of the transverse stiffeners in situations where they are also subjected to direct axial load and bending actions on top of their function to reduce the buckling length of the longitudinal stiffeners. These "advanced" applications include top and bottom struts of internal intermediate cross frames in box girders, as well as transverse stiffeners in large box sections, such as a steel bridge tower. Transverse stiffeners in steel towers can be subjected to significant direct axial loadings such as forces from wind loading, maintenance trolley loads, and varying taper of the tower at a given cross section. Furthermore, these types of transverse stiffeners are subject to direct transverse loads causing bending in the direction perpendicular to the side of the tower (White et al. 2019a).

AASHTO (2020) Article E6.1.5.1 also specifies that the moment of inertia, I_t, should be greater than or equal to the moment of inertia of the longitudinal stiffeners, I_s, defined above in Section 7.4 of this volume. This helps ensure against excessive out-of-plane deflection of a stiffened plate under its self-weight plus a small transverse concentrated load in cases where the calculated axial compression in the plate is small, and therefore the requirements from Eqs. 1 and 2 are small. One example of this situation is a case where transverse stiffeners are installed to serve only as points of termination of longitudinal stiffeners in a tension zone. In designs where b_{sp}/a_{max} is close to or greater than 1.0, where b_{sp} is the total width of the stiffened plate as defined in Article E6.1.4 and a_{max} is the largest of the longitudinal spacings to the adjacent transverse stiffeners or diaphragms providing lateral restraint to the plate, I_t may need to be larger than I_s to satisfy out-of-plane deflection criteria under service loads (White et al. 2019b)

AASHTO (2020) Article E6.1.5.1 also specifies various detailing requirements for transverse stiffeners, including the requirement that they also need to be structurally continuous and attached at their ends to the other cross-section plates providing lateral restraint to the edge of the longitudinally stiffened plate under consideration.

AASHTO (2020) Article 6.10.11.1.1 specifies that transverse stiffeners shall be spaced at less than or equal to $2D$ in webs containing longitudinal stiffeners. This requirement is intended to provide support to the web longitudinal stiffeners in flexural members designed according to the requirements of AASHTO Article 6.10.11.3. AASHTO Article C6.12.2.2.2b indicates that this requirement may be waived where a longitudinally stiffened flange plate acts as a web in one direction of bending, as long as the longitudinal stiffening is not considered in the calculation of R_b in Article 6.10.1.10.2, and provided that the transverse stiffeners are not considered in the calculation of the web flexural shear resistance in Article 6.10.9. Of course, any set of box-section plates that serve as flanges in one principal direction of bending also serve as webs in the other principal direction of bending. The implicit intent of the above waiver is to allow spacing of transverse stiffeners in box-section flanges at larger than $2D$ for longitudinally stiffened flange elements in cases where the member is subjected to just one predominant direction of bending.

8.0 CONCLUDING REMARKS

As stated in the introduction, this volume aims to aid the Engineer in reviewing and understanding the essential principles of steel system and member strength behavior and design behind various Specification provisions for the design of steel bridge structures. That is, it is intended as a relatively comprehensive resource that engineers can consult to understand the background to the various Specification provisions so that the provisions can be applied properly for "standard" designs, and so the design considerations can be extended most appropriately to the many "non-standard" situations that arise in bridge design practice. It should also be clear from the various discussions that there are always areas of potential further improvement. Nevertheless, the AASHTO (2020) and AISC (2016) Specifications represent a tremendous resource for the efficient, practical and economical design of steel bridge structures.

9.0 REFERENCES

AASHTO (2020). *AASHTO LRFD Bridge Design Specifications*, 9th Edition, American Association of State and Highway Transportation Officials, Washington, D.C.

AASHTO (2004). *AASHTO LRFD Bridge Design Specifications*, 3rd Edition with 2006 Interim Provisions, American Association of State and Highway Transportation Officials, Washington, D.C.

AASHTO (2003). *Guide Specifications for Horizontally Curved Steel Girder Highway Bridges with Design Examples for I-Girder and Box-Girder Bridges*, American Association of State Highway and Transportation Officials, Inc., Washington, D.C.

AASHTO (2002). *Standard Specifications for Highway Bridges and Interim Specifications*, 17th Edition, HB-17, American Association of State and Highway Transportation Officials, Washington, D.C.

AASHTO (1998). *AASHTO LRFD Bridge Design Specifications,* 2nd Edition with 1999, 2000, 2001, 2002 and 2003 Interim Provisions, American Association of State and Highway Transportation Officials, Washington D.C.

AASHTO/NSBA (2019). *Guidelines for Steel Girder Bridge Analysis*, G13.1-2019, American Association of State and Highway Transportation Officials and National Steel Bridge Alliance, AASHTO/NSBA Steel Bridge Collaboration.

Abu-Hawash, A., Caparelli, L., Schwartz, P. and McDonald, N. (2005). "The Use of Straddle Bent Pier with a High Performance Steel Integral Cap, Innovative Design Solutions for Complex Geometry I-235 Braided Ramps," *Time for Steel, Steel for Time*, Proceedings, 2005 World Steel Bridge Symposium, National Steel Bridge Alliance, 12 pp.

ACI (1977). *Building Code Requirements for Reinforced Concrete*, ACI 318/77, American Concrete Institute, Detroit, MI.

AISC (2021). AISC Shapes Database, V15.0, https://www.aisc.org/globalassets/aisc/manual/v15.0-shapes-database/aisc-shapes-database-v15.0.xlsx (accessed May 1, 2021).

AISC (2016). *Specification for Structural Steel Buildings*, ANSI/AISC 360-16, American Institute of Steel Construction, Chicago, IL.

AISC (2010). *Specification for Structural Steel Buildings*, ANSI/AISC 360-10, American Institute of Steel Construction, Chicago, IL.

AISC (2005). *Specification for Structural Steel Buildings*, ANSI/AISC 360-05, American Institute of Steel Construction, Chicago, IL.

AISC (1999). *Load and Resistance Factor Design Specification for Structural Steel Buildings*, American Institute of Steel Construction, Chicago, IL.

AISC (1993). *Load and Resistance Factor Design Specification for Structural Steel Buildings*, American Institute of Steel Construction, Chicago, IL.

AISC (1989). *Specification for Structural Steel Buildings: Allowable Stress Design and Plastic Design*, 9th Ed., American Institute of Steel Construction, Chicago, IL.

AISC (1978). *Specification for the Design, Fabrication and Erection of Structural Steel for Buildings*, American Institute of Steel Construction, Chicago, IL.

AISC (1986). *Load and Resistance Factor Design Specification for Structural Steel Buildings*, American Institute of Steel Construction, Chicago, IL.

AISI (2016). *North American Specification for the Design of Cold-Formed Steel Structural Members*, AISI S100-16, American Iron and Steel Institute, Washington, DC.

Allen, H.G. and Bulson, P.S. (1980) *Background to Buckling*, McGraw-Hill (UK), London.

Anderson, J.M. and Trahair, N.S. (1972). "Stability of Monosymmetric Beams and Cantilevers," *Journal of the Structural Division*, ASCE, 98(ST1), 269-286.

ASCE (2000). *Design of Latticed Steel Transmission Structures*, ASCE 10-97, American Society of Civil Engineers, Reston, VA, 71 pp.

ASCE (1997), *Effective Length and Notional Load Approaches for Assessing Frame Stability: Implications for American Steel Design*, American Society of Civil Engineers Structural Engineering Institute's Task Committee on Effective Length under the Technical Committee on Load and Resistance Factor Design, 442 pp.

ASCE (1992). *Guidelines for Design of Cable-Stayed Bridges*, Committee on Cable-Suspended Bridges, American Society of Civil Engineers, Reston, VA.

ASCE (1968). "Design of Hybrid Steel Beams," Joint ASCE-AASHO Committee on Flexural Members, *Journal of the Structural Division*, ASCE, 94(ST6), 1397-1425.

ASTM (2019). *Standard Specification for Metalic-Coated Steel Structural Wire Rope*, American Society for Testing and Materials, Designation A 603 – 19, 6 pp.

ASTM (2018). *Standard Specification for Metalic-Coated Parallel and Helical Steel Wire Structural Strand*, American Society for Testing and Materials, Designation: A 586 – 18, 6 pp.

Aslani, F. and Goel, S.C. (1991). "An Analytical Criteria for Buckling Strength of Built-Up Compression Members," *Engineering Journal*, AISC, 28(4), 159-168.

Aydemir, M., White, D.W. and Jung, S.K. (2004). "Shear Strength and Moment Shear Interaction in HPS Hybrid I-Girders," Structural Engineering, Mechanics and Materials Report No. 25, School of Civil and Environmental Engineering, Georgia Institute of Technology, Atlanta, GA.

Baker, J.F., Horne, M.R. and Heyman, J. (1956). *The Steel Skeleton*, Vol. 2, University Press, Cambridge.

Barker, M.G., Hartnagel, B.A., Schilling, C.G. and Dishongh, B.E. (1997). "Inelastic Design and Experimental Testing of Compact and Noncompact Steel Girder Bridges," Report 93-1, Missouri Cooperative Highway Research Program, 185 pp.

Barth, K.E., Hartnagel, B.A., White, D.W. and Barker, M.G. (2004). "Recommended Procedures for Simplified Inelastic Design of Steel I-Girder Bridges," *Journal of Bridge Engineering*, ASCE, 9(3), 230-242.

Barth, K.E., and White, D. W. (1997). "Finite Element Evaluation of Pier Moment-Rotation Characteristics in Continuous-Span Steel I-Girders." *Engineering Structures*, 20(8), 761-778.

Basler, K. (1963). "Discussion of K. Basler 'Strength of Plate Girders in Shear,'" *Transactions ASCE*, 128(II), 712-719.

Basler, K. (1961). "Strength of Plate Girders in Shear," *Journal of Structural Division*, ASCE, 87(ST7), 151-180.

Basler, K. and Thurlimann, B. (1961). "Strength of Plate Girders in Bending," *Journal of the Structural Division*, ASCE, 87(ST6), 153-181.

Basler, K., Yen, B.T., Mueller, J.A. and Thurlimann, B. (1960). "Web Buckling Tests on Welded Plate Girders," WRC Bulletin No. 64, Welding Research Council, New York, 1-63.

Bleich, F. (1952). *Buckling Strength of Metal Structures*, McGraw-Hill Book Company, INC., New York, NY, 508 pp.

Brockenbrough, R.L. and Johnston, B.G. (1981), *USS Steel Design Manual*, United States Steel Corporation, Pittsburgh, PA.

Brown, C.W. (1992). "Medium Span Bridges," Chapter 6.4, *Constructional Steel Design, An International Guide*, P.J. Dowling, J.E. Harding and R. Bjorhovde (ed.), Elsevier, Essex, England, 695-709.

BSI (2000). *Steel, Concrete and Composite Bridges, British Standard BS 5400: Part 3, Code of Practice for Design of Steel Bridges*, British Standards Institution, London.

BSI (1990). BS5950: Part 1: 1990, Structural Use of Steelwork in Building, Part 1, Code of Practice for Design in Simple and Continuous Construction: Hot Rolled Sections, British Standards Institution, London. Cassity, P., Serzan, K. and McDonald, N. (2003). "Fit to be Tied," Roads and Bridges, November, 28-31.

Bulson, P.S. (1970). *The Stability of Flat Plates*, Chatto and Windus, London.

Carskaddan, P.S. and Schilling, C.G. (1974). "Lateral Buckling of Highway Bridge Girders." Research Laboratory Report 22-G-001 (109-3), United States Steel Corporation, Monroeville, PA.

Cassity, P. Serzan, K. and McDonald, N. (2003). "Fit to be Tied: Designers find Good Reason for a Tied-Arch Bridge Over the Mississippi River," *Roads and Bridges*, Vol. 41, November, https://www.roadsbridges.com/fit-be-tied (accessed May 1, 2021).

CEN (2006). *Eurocode 3: Design of Steel Structures, Part 1-5: General Rules - Plated Structural Elements*, EN 1993-1-5:2006: E, Incorporating Corrigendum April 2009, European Committee for Standardization, Brussels, Belgium.

CEN (2005). *Eurocode 3: Design of Steel Structures, Part1.1 – General Rules and Rules for Buildings*, ENV 1993-1-1:2005, European Committee for Standardization, Brussels, Belgium.

CEN (2004). *Eurocode 4: Design of Composite Steel and Concrete Structures, Part 1.1 General Rules and Rules for Buildings*, EN 1994-1-1, European Committee for Standardization, Brussels, Belgium.

Chang, C.-J. and White, D.W. (2010). "Construction Simulation of Curved Steel I-Girder Bridges," Final Report to FHWA and Professional Services Industries, Inc., Curved Steel Bridge Research Project, Federal Highway Administration, November.

Chang, C.-J., White, D.W., Beshah, F. and Wright, W. (2005). "Design Analysis of Curved I-Girder Bridge Systems – An Assessment of Modeling Strategies," Annual Proceedings, Structural Stability Research Council, 349-369.

Chen, S.S., Aref, A.J., Ahn, I.-S., Chiewanichakorn, M., Carpenter, J.A., Nottis, A and Kalpakidis, I. (2005). "Effective Slab Width for Composite Steel Bridge Members," NCHRP Report 543, Transportation Research Board, 70 pp plus appendices.

Cheng, J.J.R. and Kulak, G.L. (2000). "Gusset Plate Connection to Round HSS Tension Members," *Engineering Journal*, AISC, 37(4), 133-139.

Clarke, M.J. and Bridge, R.Q. (1992). "The Inclusion of Imperfections in the Design of Beam-Columns," *Proceedings of the Annual Technical Session and Meeting*, Structural Stability Research Council, Univ. of Missouri - Rolla, Rolla, MO, 327-346.

Climenhaga, J.J. and Johnson, R.P. (1972). "Local buckling in continuous composite beams," *The Structural Engineer,"* 50(9), 367-374.

Coletti, D., Fan, Z., Holt, J. and Vogel, J. (2006). "Practical Steel Tub Girder Design," Compendium of Papers CD-ROM, TRB 85th Annual Meeting, Transportation Research Board, Washington, DC, 15 pp.

Coletti, D., Fan, Z, Gatti, W., Holt, J. and Vogel, J. (2005). "Practical Steel Tub Girder Design," National Steel Bridge Alliance, Chicago, IL, April, 51 pp.

Coletti, D. and Yadlosky, J. (2005). "Behavior and Analysis of Curved and Skewed Girder Bridges," *Time for Steel, Steel for Time*, Proceedings, 2005 World Steel Bridge Symposium, National Steel Bridge Alliance, 13 pp.

Colville, J. (1972). "Shear Connector Studies on Curved Girders," Progress Report No. 45 for Maryland State Highway Administration and FHWA, The Design of Curved Viaducts, Civil Engineering Department, University of Maryland, College Park, MD, 78 pp.

Cooper, P.B., Galambos, T.V. and Ravindra, M.K. (1978). "LRFD Criteria for Plate Girders," *Journal of the Structural Division*, ASCE, 104(ST9), 1389-1407.

Cooper, P.B. (1967). "Strength of Longitudinally Stiffened Plate Girders," *Journal of the Structural Division*, ASCE, 93(ST2), 419-451.

Cross, H. (1952). *Engineers and Ivory Towers*, R.C. Goodpasture (ed.), 1st ed., McGraw-Hill. 141 pp.

CSA Group (2014). *S16-14 - Design of Steel Structures*, Canadian Standards Association, 222 pp.

Cuk, P.E. and Trahair, N.S. (1986). "Inelastic Lateral Buckling of Steel Beam-Columns," *Journal of Constructional Steel Research*, 6(1), 21-52.

Cuk, P.E., Bradford, M.A. and Trahair, N.S. (1986). "Inelastic Lateral Buckling of Steel Beam-Columns," *Canadian Journal of Civil Engineering*, 13(6), 639-699.

Culver, C.G. (1972). "Design Recommendations for Curved Highway Bridges," Final Report for Research Project 68-32, PENDOT, Civil Engineering Department, Carnegie-Mellon University, June.

Dalal, S. T. (1969). "Some Non-Conventional Cases of Column Design." *Engineering Journal*, AISC, 6(1), January, Chicago, IL, 28-39.

Dexter, R. and Altstadt, S. (2004). "Ductile Fracture in Girders," *Steel Bridges: Emerging Technologies with Emphasis on High Performance Steel and Accelerated Bridge Construction*, Proceedings, 2004 FHWA Steel Bridge Conference, A. Azizinamini (ed.), 69-78.

Dowling, P.J. and Harding, J.E. (1992). "Box Girders," Chapter 2.7, *Constructional Steel Design, An International Guide*, P.J. Dowling, J.E. Harding and R. Bjorhovde (ed.), Elsevier, Essex, England, 175-196.

Dowswell, B. (2002). "Lateral-Torsional Buckling of Wide-Flange Cantilever Beams," *Proceedings of the Annual Technical Session and Meeting*, Structural Stability Research Council, Univ. of Missouri - Rolla, Rolla, MO, 267-290.

Duan, L., Reno, M. and Uang, C.M. (2002). "Effect of Compound Buckling on Compression Strength of Built-up Members," *Engineering Journal*, 39(1), AISC, Chicago, IL, 30-37.

Duan, L., Reno, M. and Lynch, L. (2000). "Section Properties for Latticed Members of San Francisco-Oakland Bay Bridges," *Journal of Bridge Engineering*, ASCE, 4(2), 156-164.

Dubas, C. (1948). "A Contribution to the Buckling of Stiffened Plates," IABSE 3rd Congress, Preliminary Publication, Liege, Belgium.

Dux, P.F., and Kitipornchai, S. (1983). "Inelastic Beam Buckling Experiments," *Journal of Constructional Steel Research*, 3(1), 3-9.

Dwight, J.G. and Little, G.H. (1974). "Stiffened Steel Compression Panels – A Design Approach," Technical Report CUED/C – Struct./TR 38, Cambridge University.

Earls, C.J. and Galambos, T.V. (1997). "Design Recommendations for Equal Leg Single Angle Flexural Members," *Journal of Constructional Steel Research*, 43(1-3), 65-85.

Easterling, W.S. and Gonzales, L. (1993). "Shear Lag Effects in Steel Tension Members," *Engineering Journal*, AISC, 30(3), 77-89.

Ellifritt, D.S., Wine, G., Sputo, T. and Samuel, S. (1992). "Flexural Strength of WT Sections, *Engineering Journal*, AISC, 29(2), 67-74.

El-Tayem, A. and Goel, S.C. (1986). "Effective Length Factor for the Design of X-Bracing Systems," *Engineering Journal*, AISC, 23(1), 41-45.

Fan, Z. and Helwig, T.A. (1999). "Behavior of Steel Box Girders with Top Flange Bracing," *Journal of Structural Engineering*, 125(8), 829-837.

Farris, J.F. (2018). "Lean-On Bracing for Steel I-Shaped Girders," AISC Live Webinar, April 26.

Fisher, J.W., Pense, A.W., and Hausamman, H. (1988). "Analysis of Cracking of I-79 Bridge at Neville Island, Fracture Problems in the Transportation Industry," Fall Convention, ASCE, Detroit, 1-19.

Fisher, J.W., Pense, A.W. and Roberts R. (1977). "Evaluation of Fracture of Lafayette Street Bridge," *Journal of Structural Engineering*, ASCE, 103(7), 1339-1357.

FHWA (1980). "Integral, No-Joint Structures and Required Provisions for Movement," FHWA Technical Advisory T 5140.13, Federal Highway Administration, January.

Fortney, P.J. and Thornton, W.A. (2012). "Recommendations for Shear Lag Factors for Longitudinally Welded Tension Members," *Engineering Journal*, AISC, 49(1), 11-32.

Frank, K.H. (2005). "Fabrication Tolerances for MAGLEV," presentation to HPS Design Advisory Group, AISI Bridge Task Force and AASHTO T-14, Baltimore, MD, August.

Frank, K.H. and Helwig, T.A. (1995). "Buckling of Webs in Unsymmetric Plate Girders," *Engineering Journal*, AISC, 32(2), 43-53.

Frost, R.W. and Schilling, C.G. (1964). "Behavior of Hybrid Beams Subjected to Static Loads," *Journal of the Structural Division*, ASCE, 90(ST3), 55-88.

Galambos, T.V. (2001a). "Strength of Singly Symmetric I-Shaped Beam-Columns," *Engineering Journal*, AISC, 38(2), 65-77.

Galambos, T.V. (2001b). Personal communication.

Galambos, T.V. and Chapuis, J. (1980). "LRFD Criteria for Composite Columns and Beam-Columns," Revised Draft, Dept. of Civil Engineering, Washington University, St. Louis, MO, December.

Galambos, T.V. and Ravindra, M.K. (1976). "Load and Resistance Factor Design Criteria for Steel Beams," Research Report No. 27, Structural Division, Civil and Environmental Engineering Department, Washington Univ., St. Louis, MO, 67 pp.

Galambos, T.V. (1968). *Structural Members and Frames*, Prentice-Hall, Englewood Cliffs, NJ, 373 pp.

Galambos, T.V. and Ketter, R.L. (1959). "Columns under Combined Bending and Thrust," *Journal of the Engineering Mechanics Division*, ASCE, 85(2), 1-30.

Goldberg, J.E. and Leve, H.L. (1957). "Theory of Prismatic Folded Plate Structures," *IABSE*, Vol. 16, International Association for Bridge and Structural Engineers, Zurich, Switzerland, 59-86.

Grubb, M.A., Wilson, K.E., White, C.D., and Nickas, W.N. (2015). *Load and Resistance Factor Design (LRFD) for Highway Bridge Superstructures – Reference Manual*, Report No. FHWA-NHI-15-047, Federal Highway Administration, National Highway Institute, Arlington, VA, 1698 pp.

Grubb, M. A., and Carskaddan, P. S. (1981). *Autostress Design of Highway Bridges, Phase 3: Moment Rotation Requirements*, Research Laboratory Rep., United States Steel Corporation, Monroeville, PA, 45 pp.

Grubb, M. A., and Carskaddan, P. S. (1979). *Autostress Design of Highway Bridges, Phase 3: Initial Moment Rotation Tests*, Research Laboratory Rep., United States Steel Corporation, Monroeville, PA, 36 pp.

Hall, D.H., M.A. Grubb and C.H. Yoo (1999). "Improved Design Specifications for Horizontally Curved Steel Girder Highway Bridges," Report 424, National Cooperative Highway Research Program, National Academy Press, Washington, D.C., 130 pp.

Hall, D.H. (1997). "Why Steel Box Girders?" *Bridge Crossings*, No. 6, Reprinted from *Modern Steel Construction*, National Steel Bridge Alliance, Chicago, IL, 4 pp.

Hall, D.H. (1992). "Short Span Bridges," Chapter 6.3, *Constructional Steel Design, An International Guide*, P.J. Dowling, J.E. Harding and R. Bjorhovde (ed.), Elsevier, Essex, England, 671-693.

Hanshin (1988). "Guidelines for the Design of Horizontally Curved Girder Bridges (Draft)," Hanshin Expressway Public Corporation and Steel Structure Study Subcommittee, October, 178 pp.

Hash, J.B. (2001). "Shear Capacity of Hybrid Steel Girders," M.S. Thesis, University of Nebraska, Lincoln, 407 pp.

Heins, C.P. (1978). "Box Girder Design – State of the Art," *Engineering Journal*, AISC, 15(4), 126-142.

Heins, C.P. (1975). *Bending and Torsional Design in Structural Members*, Lexington Books.

Heins, C.P., Hou, C.K., and Kato, H. (1982). "Lateral wind bracing requirements for steel composite bridges," *Engineering Journal*, AISC, 19(3), 160-169.

Heins, C.P. and Hall, D.H. (1981). "Designer's Guide to Steel Box-Girder Bridges," *Booklet No. 3500*, Bethlehem Steel Corporation, Bethlehem, PA, 20-30.

Heins, C.P. and Firmage, D.A. (1979). *Design of Modern Highway Bridges*, Wiley, New York, NY, 463 pp.

Helwig, T., Yura, J., Herman, R, Williamson, E. and Li, D. (2007). "Design Guidelines for Steel Trapezoidal Box Girder Systems," Report No. FHWA/TX-07/0-4307-1, Center for Transportation Research, University of Texas at Austin, Austin, TX, 84 pp.

Helwig, T., Herman, R. and Zhou, C. (2005). "Lean-On Bracing for Steel Bridge Girders with Skewed Supports," *Proceedings of the Annual Technical Session and Meeting*, Montreal, Quebec, Structural Stability Research Council, Univ. of Missouri - Rolla, Rolla, MO, 295-306.

Helwig, T.A., Frank, K.H. and Yura, J.A. (1997). "Lateral-Torsional Buckling of Singly Symmetric I-Beams," *Journal of Structural Engineering*, ASCE, 123(9), 1172-1179.

Herman, R., Helwig, T., Holt, J., Medlock, R., Romage, M. and Zhou, C. (2005). "Lean-On Cross-Frame Bracing for Steel Girders with Skewed Supports," *Time for Steel, Steel for Time*, Proceedings, 2005 World Steel Bridge Symposium, National Steel Bridge Alliance, 10 pp.

Horne, M.R. (1964). "Safe Loads on I-Section Columns in Structures Designed by Plastic Theory," *Proceedings of the Institution of Civil Engineers*, Sept.

Horne, M.R. and Grayson, W.R. (1983). "Parametric Finite Element Study of Transverse Stiffeners for Webs in Shear," Instability and Plastic Collapse of Steel Structures, Proceedings of the Michael R. Horne Conference, L.J. Morris (ed.), Granada Publishing, London, 329-341.

Ito, M., Hoshino, M.-A., Naga, M., Nakai, H. and Ohtsuki, S. (1992). "Long Span Bridges," Chapter 6.5, *Constructional Steel Design, An International Guide*, P.J. Dowling, J.E. Harding and R. Bjorhovde (ed.), Elsevier, Essex, England, 711-734.

Jha, A.P. (2016). "Investigation of the Shear Strength of Built-Up I-Section Members via Test Simulation," MS Thesis, School of Civil and Environmental Engineering, Georgia Institute of Technology, Atlanta, GA.

Johansson, B., and Veljkovic, M. (2009). "Review of Plate Buckling Rules in EN 1993-5," *Steel Construction*, 2(4), Ernst & Sohn Verlag für Architektur und technische Wissenschaften GmbH & Co. KG, Berlin, p 228.

Johnston, B.G. (1976). *Guide to Stability Design Criteria for Metal Structures*, 3rd ed., B.G. Johnston (ed.), Structural Stability Research Council, Wiley, New York, NY, 616 pp.

Johnston, S.B. and Mattock, A.H. (1967). "Lateral Distribution of Load in Composite Box Girder Bridges," Highway Research Record No. 167, Bridges and Structures, Washington, DC.

Johnson, D.L. (1985). "An Investigation into the Interaction of Flanges and Webs in Wide-Flange Shapes," *Proceedings of the Annual Technical Session and Meeting,* Cleveland, OH, Structural Stability Research Council, Univ. of Missouri - Rolla, Rolla, MO, 397-405.

Jung, S.-K. and White, D.W. (2010). "Inelastic Behavior of Horizontally Curved Composite I-Girder Bridge Structural Systems," Final Report to FHWA and Professional Services Industries, Inc., Curved Steel Bridge Research Project, Federal Highway Administration, April.

Jung, S.K. and White, D.W. (2006). "Shear Strength of Horizontally Curved Steel I-Girders – Finite Element Studies," *Journal of Constructional Steel Research*, 62(4), 329-342.

Jung, S.K., White, D.W., Beshah, F. and Wright, W. (2005). "Ultimate Strength of Horizontally Curved Composite I-Girder Bridge Structural Systems," Annual Proceedings, Structural Stability Research Council, 327-347.

Kalyanaraman, V., Peköz, T. and Winter, G. (1977). "Unstiffened Compression Elements," *Journal of the Structural Division*, ASCE, 103(ST9), 1833-1848.

Kase, R.A. (1997). "Twelve Commandments for Economic Steel Box Girders," *Bridge Crossings*, No. 9, reprinted from *Modern Steel Construction*, 4 pp.

Kavanagh, T.C. (1962). "Effective Length of Framed Columns," *Transactions of the American Society of Civil Engineers*, 127, 81-101.

Kemp, A.R. (1996). "Inelastic Local and Lateral Buckling in Design Codes," *Journal of Structural Engineering*, 122(4), 374-381.

Kim, Y.D., Jung, S.K. and White, D.W. (2007). "Transverse Stiffener Requirements in Straight and Horizontally Curved Steel I-Girders," *Journal of Bridge Engineering*, ASCE, 12(2), 174-183.

Kim, Y.D. and White, D.W. (2013). "Transverse Stiffener Requirements to Develop the Shear Buckling and Post-Buckling Resistance of Steel I-Girders," *Journal of Structural Engineering*, ASCE, 10.1061/(ASCE)ST.1943-541X.0000867, 04013098.

King, C.M. (2017). "A New Design Method for Longitudinally Stiffened Plates." Proceedings of the Annual Stability Conference, Structural Stability Research Council, San Antonio, TX, March.

Kitipornchai, S., Wang, C.M. and Trahair, N.S. (1986). "Buckling of Monosymmetric I-Beams under Moment Gradient," *Journal of Structural Engineering*, ASCE, 112(4), 781-799.

Kitipornchai, S. and Trahair, N.S. (1980). "Buckling Properties of Monosymmetric I-Beams," *Journal of the Structural Division*, ASCE, 109(ST5), 941-957.

Kollbrunner, C.F. and Basler, K. (1969). *Torsion in Structures*, Springer-Verlag, New York.

Kulicki, J.M. and Reiner, B. (2011). "Truss Bridges," *Structural Steel Designer's Handbook*, Chapter 13, R.L. Brockenbrough and F.S. Merritt (ed.), McGraw-Hill, New York, NY, 62 pp.

Kulicki, J.M. (2000). "Highway Truss Bridges," *Bridge Engineering Handbook*, Chapter 16, W.-F. Chen and L. Duan (ed.), CRC Press, Boca Raton, FL, 34 pp.

Latif, W. and White, D.W. (2021). "Built-Up I-Section Member Flexural Resistance: Flange Local Post-Buckling Strength and Local-Global Buckling Interaction," SEMM Research Report 21-03, School of Civil and Environmental Engineering, Georgia Institute of Technology, Atlanta, GA.

Lee, S.C., Yoo, C.H., and Yoon, D.Y. (2003). "New Design Rule for Intermediate Transverse Stiffeners Attached on Web Panels," *Journal of Structural Engineering*, ASCE, 129(12), 1607-1614.

Lee, G.C., Ketter, R.L. and Hsu, T.L. (1981). *Design of Single Story Rigid Frames*, Metal Building Manufacturers Association, Cleveland, OH, 267 pp.

Lee, G.C. and Hsu, T.L. (1981). "Tapered Columns with Unequal Flanges," *Welding Research Council Bulletin*, No. 272, November.

Lehman, D.E. and Roeder, C.W. (2012). "Rapid Construction of Bridge Piers with Improved Seismic Performance," Report CA12-1972, California Department of Transportation, Sacramento, CA.

LeMessurier, W.J. (1985). Personal communication.

Liew, J.Y.R., White, D.W., and Chen, W.F. (1992). "Beam-Columns," Chapter 2.5, *Constructional Steel Design, An International Guide*, P.J. Dowling, J.E. Harding and R. Bjorhovde (ed.), Elsevier, Essex, England, 105-132.

Lokhande, A.M. and White, D.W. (2018). "Improved Characterization of the Flexural and Axial Compressive Resistance of Welded Steel Box-Section Members," Structural Engineering Report, School of Civil and Environmental Engineering, Georgia Institute of Technology, Atlanta, GA.

Lukey, A.F., Smith, R.J., Hosain, M.U. and Adams, P.F. (1969). "Experiments on Wide-Flange Beams under Moment Gradient," *Welding Research Council Bulletin*, No. 142, July, 1-19.

Lutz, L.A. (2006). "Evaluating Single Angle Compression Struts Using an Effective Slenderness Approach," *Engineering Journal*, AISC, to appear.

Lutz, L.A. (1992). "Critical Slenderness of Compression Members with Effective Lengths about Non-principal Axes," *Proceedings of the Annual Technical Session and Meeting*, Pittsburgh, PA, Structural Stability Research Council, Univ. of Missouri - Rolla, Rolla, MO, 107-125.

Maleck, Andrea E. (2001), "Second-Order Inelastic and Modified Elastic Analysis and Design Evaluation of Planar Steel Frames," Ph.D. Dissertation, Georgia Institute of Technology, 579 pp

Maleck, A.E. and White, D.W. (2003). "Alternative Approaches for Elastic Analysis and Design of Steel Frames. I: Overview," *Journal of Structural Engineering*, ASCE, 130(8), 1186-1196.

Massonnet, C. (1960). "Stability Considerations in the Design of Steel Plate Girders," *Journal of the Structural Division*, ASCE, 86(ST1), 71-98.

McGuire, W. (1968). *Steel Structures*, Prentice-Hall, Englewood Cliffs, NJ, 1112 pp.

Moon, J., Lehman, D.E., Roeder, C.W., and Lee, H.K. (2013). "Strength of Circular Concrete-Filled Tubes With and Without Internal Reinforcement under Combined Loading," *Journal of Structural Engineering*, ASCE, 139(12), https://doi.org/10.1061/(ASCE)ST.1943-541X.0000788.

Mozer, J., R. Ohlson and C. Culver (1971). "Stability of Curved Plate Girders – P2," Prepared for the Department of Transportation, Federal Highway Administration, and Participating States under Contract Number FH-11-7389, Department of Civil Engineering, Carnegie-Mellon University, Pittsburgh, PA, 121 pp.

Munse, W.H. and Chesson, Jr., E (1963). "Riveted and Bolted Joints: Net Section Design," *Journal of the Structural Division*, ASCE, 89(ST1), 49-106.

Nakai, H. and Yoo, C.H. (1988). *Analysis and Design of Curved Steel Bridges*, McGraw-Hill, New York, NY, 673 pp.

Nethercot, D.A and Trahair, N.S. (1976). "Lateral Buckling Approximations for Elastic Beams," *The Structural Engineer*, 54(6), 197-204.

Nettleton, D.A. (1977). *Arch Bridges*, Bridge Division, Office of Engineering, Federal Highway Administration, U.S. Department of Transportation, Washington, D.C.

NSBA (2016a). *Skewed and Curved Steel I-Girder Bridge Fit*, Stand-Alone Summary, NSBA Technical Subcommittee Fit Task Force, National Steel Bridge Alliance, Chicago, IL.

NSBA (2016b). *Skewed and Curved Steel I-Girder Bridge Fit*, Guide Document, NSBA Technical Subcommittee Fit Task Force, National Steel Bridge Alliance, Chicago, IL.

NSBA (2006). "Guidelines for Design Details," AASHTO/NSBA Steel Bridge Collaboration, G1.4 – 2006, 21 pp.

NSBA (2004). "Steel Bridge Bearing Design and Detailing Guidelines," AASHTO/NSBA Steel Bridge Collaboration, G 9.1 - 2004, AASHTO Document No. SBB-1, 42 pp.

NSBA (1996). "V-Load Analysis – An Approximate Procedure, Simplified and Extended, for Determining Moments and Shears in Designing Horizontally-Curved Open-Framed Highway Bridges," Vol. I, Chap. 12, *Highway Structures Design Handbook*, Reprint, National Steel Bridge Alliance, Chicago, IL, 53 pp.

Oehlers, D.J. and Bradford, M.A. (1999). *Elementary Behavior of Composite Steel and Concrete Structural Members*, Butterworth Heinemann, Oxford, 259 pp.

Owen, D.R.J., Rockey, K.C. and Skaloud, M. (1970). "Ultimate Load Behavior of Longitudinally Reinforced Webplates Subjected to Pure Bending," IABSE Publications, Vol. 30-1, 113-148.

Peköz, T. (1987). Development of a Unified Approach to the Design of Cold-Formed Steel Members. Report CF87-1, American Iron and Steel Institute, Washington, D.C., March.

Poellot, W.N. (1997). "Curved Steel Box Girder Bridges," *Structural Engineering Handbook*, 4th ed., Section 21, E.H. Gaylord, Jr., C.N. Gaylord and J.E. Stallmeyer (eds.), McGraw-Hill.

Petzold, E. (2005). "Design, Fabrication and Erection Issues for Long Span Steel Tied Arches: A Case Study," *Time for Steel, Steel for Time*, Proceedings, 2005 World Steel Bridge Symposium, National Steel Bridge Alliance, 11 pp.

Podolny, W. and Goodyear, D. (2011). "Cable-Suspended Bridges," *Structural Steel Designer's Handbook*, Chapter 15, R.L. Brockenbrough and F.S. Merritt (ed.), McGraw-Hill, New York, NY, 92 pp.

Podolny, W. and Scalzi, J.B. (1986). *Construction and Design of Cable-Stayed Bridges*, 2nd Ed., Wiley, New York, NY, 336 pp.

Porter, D.M., Rockey, K.C. and Evans, H.R. (1975). "The Ultimate Load Behavior of Plate Girders Loaded in Shear," *The Structural Engineer*, 53(8), 313-325.

Rahal, K.N. and Harding, J.E. (1990). "Transversely Stiffened Girder Webs Subjected to Shear Loading – Part 1: Behaviour," *Proceedings of the Institution of Civil Engineers*, Part 2, 89, March, 47-65.

Richter, J.F. (1998). "Flexural Capacity of Slender Web Plate Girders," M.S. Thesis, Univ. Texas, Austin, May, 133 pp.

Robinson, B., Suarez, V., Gabr, M.A., and Kawalksy, M. (2012). "Simplified Lateral Analysis of Deep Foundation Bridge Bents: Driven Pile Case Study," *Journal of Bridge Engineering*, ASCE, 16(4), 558-569.

Roeder, C.W., Lehman, D.E. and Bishop, E. (2010). "Strength and Stiffness of Circular Concrete Filled Tubes," *Journal of Structural Engineering*, 135(12), ASCE, 1545-1553.

Roik, K. and Bergmann, R. (1992). "Composite Columns," Chapter 4.2, *Constructional Steel Design, An International Guide*, P.J. Dowling, J.E. Harding and R. Bjorhovde (ed.), Elsevier, Essex, England, 443-470.

SAA (1998). *Steel Structures*, AS4100-1998, Standards Association of Australia, Australian Institute of Steel Construction, Sydney, Australia.

Salmon, C.G. and Johnson, J.E. (1996). *Steel Structures – Design and Behavior*, 4th Ed., 1024 pp.

Sato, A. and Uang, C.-M. (2007). "Modified Slenderness Ratio for Built-up Members," *Engineering Journal*, AISC, 44, 269-280.

Schafer, B.W. and Peköz, T. (1998). "Cold-Formed Steel Members with Multiple Longitudinal Intermediate Stiffeners," *Journal of Structural Engineering*, ASCE, 124(10), 1175-1181.

Schafer, B.W. and Peköz, T. (1996). "Design of Cold-Formed Steel Stiffened Elements with Multiple Longitudinal Intermediate Stiffeners," 13th International Specialty Conference on Cold-Formed Steel Structures, St. Louis, MO, October, 47-63.

Schilling, C.G., Barker, M.G., Dishongh, B.E. and Hartnagel, B.A. (1997). "Inelastic Design Procedures and Specifications," Final report submitted to American Iron and Steel Institute, Washington, DC, 107 pp.

Schilling, C.G. (1996)."Yield-Interaction Relationships for Curved I-Girders," *Journal of Bridge Engineering*, American Society of Civil Engineers, Reston, VA, 1(1), 26-33.

Schilling, C.G. (1968). "Bending Behavior of Composite Hybrid Beams," *Journal of the Structural Division*, ASCE, 94(ST8), 1945-1964.

Schilling, C.G. (1965). "Buckling Strength of Circular Tubes," *Journal of Structural Division*, ASCE, 91(ST5), p. 325.

Sherman, D.R. (2005). Communication to AISC TC4, June.

Sherman, D.R. (1992). "Tubular Members," Chapter 2.4, *Constructional Steel Design, An International Guide*, P.J. Dowling, J.E. Harding and R. Bjorhovde (ed.), Elsevier, Essex, England, 91-104.

Sherman, D.R. (1976). "Tentative Criteria for Structural Applications of Steel Tubing and Pipe," American Iron and Steel Institute, Washington, DC.

Schillo, N., (2017). "Local and Global Buckling of Box Columns made of High Strength Steel," Doctoral dissertation, RWTH Aachen University.

Schillo, N. and Taras, A. (2018). "A Reappraisal of the Reliability of Local Buckling Rules based on the Winter Curve." Proceedings of the Annual Stability Conference, Structural Stability Research Council, Baltimore, Maryland, April.

Slein, R., Kamath, A.M., Latif, W., Phillips, M., Sherman, R.J., Scott, D.W. and White, D.W. (2021a). "Enhanced Characterization of the Flexural Resistance of Welded I-Section Members," SEMM Report 21-01, School of Civil and Environmental Engineering, Georgia Institute of Technology, Atlanta, GA.

Slein, R., Jeong, W.Y. and White, D.W. (2021b). "A Critical Evaluation of Moment Gradient (C_b) Factor Calculation Procedures for Singly Symmetric I-Section Members," SEMM Report 21-04, School of Civil and Environmental Engineering, Georgia Institute of Technology, Atlanta, GA.

SSRC (1979). "A Specification for the Design of Steel-Concrete Composite Columns," *Engineering Journal*, AISC, 16(4), 101-115.

SSSBA (2021). Short Span Steel Bridge Alliance, https://shortspansteelbridges.org (accessed May 1, 2021).

Stanway, G.S., Chapman, J.C. and Dowling, P.J. (1996). "A Design Model for Intermediate Web Stiffeners," *Proceedings of the Institution of Civil Engineers, Structures and Buildings*, 116, February, 54-68.

Subramanian, L. and White, D.W. (2017a). "Improved Noncompact Web-Slenderness Limit for Steel I-Girders," *Journal of Structural Engineering*, ASCE, 143(4), https://doi.org/10.1061/(ASCE)ST.1943-541X.0001722.

Subramanian, L.P. and White, D.W. (2017b). "Flexural Resistance of Longitudinally Stiffened Plate Girders," Updated Final Report to American Iron and Steel Institute, School of Civil and Environmental Engineering, Georgia Institute of Technology, Atlanta, GA.

Subramanian, L.P. and White, D.W. (2017c). "Improved Strength Reduction Factors for Steel Girders with Longitudinally Stiffened Webs, Structural Engineering Mechanics and Materials Report No. 17-03, School of Civil and Environmental Engineering, Georgia Institute of Technology, Atlanta, GA.

Talbot, J. (2005). "Simple Made Continuous: Simplified Continuity Details Improve Economies for Short and Medium Span Rolled Steel Girder Bridges," *Steel Bridge News*, 6(4), National Steel Bridge Alliance, 3 pp.

Tang, M.C. (2000). "Cable-Stayed Bridges," *Bridge Engineering Handbook*, W.-F. Chen and L. Duan (ed.), CRC Press, Boca Raton, FL, 18 pp.

Tang, M.C. (1976). "Buckling of Cable-Stayed Girder Bridges," *Journal of the Structural Division*, ASCE, 102(ST9), 1675-1684.

Timoshenko, S.P. and Gere, J.M. (1961). *Theory of Elastic Stability*, McGraw-Hill, New York, NY, 541 pp.

Troitsky, M.S. (1990). *Prestressed Steel Bridges: Theory and Design*, Van Nostrand Reinhold, New York, NY, 386 pp.

Troitsky, M.S. (1988). *Cable-Stayed Bridges*, Van Nostrand Reinhold, New York, NY.

Ugural, A. and Fenster, S.K. (2020). *Advanced Mechanics of Materials and Applied Elasticity*, 6th Ed., Pearson.

Viest, I.M., Fountain, R.S. and Singleton, R.C. (1958). *Composite Construction in Steel and Concrete for Bridges and Buildings*, McGraw-Hill, New York, NY, 174 pp.

Vincent, G.S. (1969). "Tentative Criteria for Load Factor Design of Steel Highway Bridges," *AISI Bulletin No. 15*, American Iron and Steel Institute, Washington, D.C., 65 pp.

von Kármán, T., Sechler, E.E., and Donnell, L.H. (1932). "The Strength of Thin Plates in Compression," *Transactions of the ASME*, 54, MP5 54-5.

Wadell, J.A.L. (1916). *Bridge Engineering*, Wiley, New York, NY.

Walther, R., Houriet, B., Isler, W., Moia, P. and Klein, J.-F. (1999). *Cable-Stayed Bridges*, Thomas Telford, London, 225 pp.

Wasserman, E.P. and Walker, J.H. (1996). "Integral Abutments for Steel Bridges," *Highway Structures Design Handbook*, Vol. II, Chapter 5, AISI, 1996.

Wasserman, E.P. (1997). "Integral Post-Tensioned Concrete Bent Caps," *Bridge Crossings*, No. 8, July, 3 pp.

Wasserman, E.P. (1987). "Jointless Bridge Decks," *Engineering Journal*, American Institute of Steel Construction, 24(3), 93-100.

Weakley, K. (2005). "VDOT Integral Bridge Design Guidelines," *Integral Abutment and Jointless Bridges*, FHWA Conference, Baltimore, MD, organized by Constructed Facilities Center, College of Engineering and Mineral Resources, W. Virginia Univ., 61-70.

White, D.W., Jeong, W.Y. and Slein, R. (2021a). *Frame Design Using Nonprismatic Members*, Steel Design Guide 25, 2nd Ed., Metal Building Manufacturers Association and American Institute of Construction.

White, D.W., Toğay, O., Slein, R. and Jeong, W.Y. (2021b), SABRE2, http://www.white.ce.gatech.edu/sabre (accessed September 12, 2021).

White, D.W., Kamath, A., Heath, J.A., Adams, B.K., and Anand, A. (2020). "Straight Steel I-Girder Bridges with Skew Index Approaching 0.3," Final Report, FDOT Contract No. BE535, School of Civil and Environmental Engineering, Georgia Institute of Technology, Atlanta, GA, 227 pp.

White, D.W., Lokhande, A., Ream, A., King, C. and Grubb, M. (2019a). "Proposed LRFD Specifications for Noncomposite Steel Box-Section Members," Report No. FHWA-HIF-19-063, Federal Highway Administration, Office of Bridges and Structures, July, 359 pp.

White, D.W., M.A. Grubb, C.M. King, and R. Slein. (2019b). "Proposed AASHTO Guidelines for Bottom Flange Limits of Steel Box Girders," Final Report for NCHRP Project 20-07, Task 415, National Cooperative Highway Research Program, Transportation Research Board, Washington, D.C.

White, D.W., Nguyen, T.V., Coletti, D.A., Chavel, B.W., Grubb, M.A. and Boring, C.G. (2015). "Guidelines for Reliable Fit-Up of Steel I-Girder Bridges," Final Report, NCHRP 20-07/355, National Cooperative Highway Research Program, 481 pp.

White, D.W., Coletti, D., Chavel, B.W., Sanchez, A., Ozgur, C., Jimenez Chong, J.M., Leon, R.T., Medlock, R.D., Cisneros, R.A., Galambos, T.V., Yadlosky, J.M., Gatti, W.J., Kowatch, G.T. (2012). "Guidelines for Analytical Methods and Construction Engineering of Curved and Skewed Steel Girder Bridges," NCHRP Report 725, National Cooperative Highway Research Program, Transportation Research Board, National Academy of Sciences, Washington, DC.

White, D.W. (2008). "Unified Flexural Resistance Equations for Stability Design of Steel I-Section Members – Overview," *Journal of Structural Engineering*, ASCE, 134(9), 1405-1424.

White, D.W., and Barker, M. (2008). "Shear Resistance of Transversely-Stiffened Steel I-Girders," *Journal of Structural Engineering*, ASCE, 134(9), 1425-1436.

White, D.W., and Jung, S.-K. (2008). "Unified Flexural Resistance Equations for Stability Design of Steel I-Section Members – Uniform Bending Tests," *Journal of Structural Engineering*, ASCE, 134(9), 1450-1470.

White, D.W., and Kim, Y.D. (2008). "Unified Flexural Resistance Equations for Stability Design of Steel I-Section Members – Moment Gradient Tests," *Journal of Structural Engineering*, ASCE, 134(9), 1471-1486.

White, D.W., Barker, M., and Azizinamini, A. (2008). "Shear Strength and Moment-Shear Interaction in Transversely-Stiffened Steel I-Girders," *Journal of Structural Engineering*, ASCE, 134(9), 1437-1449.

White, D.W., and Chang, C.-J. (2007). "Improved Flexural Stability Design of I-Section Members in AISC (2005) – A Case Study Comparison to AISC (1989) ASD," *Engineering Journal*, AISC, 44(4), 291-304.

White, D.W., and Jung, S.-K. (2007). "Effect of Web Distortion on the Buckling Strength of Noncomposite Discretely-Braced I-beams," *Engineering Structures*, 29(8), 1872-1888, doi:10.1016/j.engstruct.2006.09.020.

White, D.W. and Kim, Y.-D. (2006). "A Prototype Application of the AISC (2005) Stability Analysis and Design Provisions to Metal Building Structural Systems," Report to Metal Building Manufacturers Association, School of Civil and Environmental Engineering, Georgia Institute of Technology, Atlanta, GA, September, 157 pp.

White, D.W. and Grubb, M.A. (2005). "Unified Resistance Equations for Design of Curved and Tangent Steel Bridge I-Girders," *Proceedings of the 2005 TRB Bridge Engineering Conference*, Transportation Research Board, Washington, DC, July, 121-128.

White, D.W. and Grubb, M.A. (2003). "Lateral-Torsional Buckling Resistance of Stepped Flanges," *Three-Span Continuous Straight Composite I Girder, Load and Resistance Factor Design, Third Edition (Customary Units)*, Appendix C, National Steel Bridge Alliance, pp. C-1 to C-4.

White, D.W. and Jung, S.-K (2003a). "Simplified Lateral-Torsional Buckling Equations for I-and Channel-Section Members," Structural Engineering, Mechanics and Materials Report No. 24a, School of Civil and Environmental Engineering, Georgia Institute of Technology, Atlanta, GA, 23 pp.

White, D.W. and Jung, S.-K (2003b). "Simplified Lateral-Torsional Buckling Equations for Singly Symmetric I-Section Members," Structural Engineering, Mechanics and Materials Report No. 24b, School of Civil and Environmental Engineering, Georgia Institute of Technology, Atlanta, GA, 29 pp.

White, D.W. and Kim, S.-C. (2003). "Simplified Strength Calculations for Noncompact Web Beam-Columns," Structural Engineering, Mechanics and Materials Report No. 28, School of Civil and Environmental Engineering, Georgia Institute of Technology, Atlanta, GA, 41 pp.

White, D.W. (2002). "LRFD Article 6.10 Draft # 3, Sample Case Studies," Report to AISI-AASHTO Task Committee for Updating of AASHTO LRFD Article 6.10, October, 84 pp.

White, D.W., Zureick, A.H., Phoawanich, N. and Jung, S.-K. (2001). "Development of Unified Equations for Design of Curved and Straight Steel Bridge I-Girders," Final Report to American

Iron and Steel Institute Transportation and Infrastructure Committee, Professional Services Industries, Inc. and Federal Highway Administration, October, 551 pp.

White, D.W. and Barth, K.E. (1998). "Strength and Ductility of Compact-Flange I Girders in Negative Bending," *Journal of Constructional Steel Research*, 45(3), 241-280.

White, D. W., Ramirez, J. A., and Barth, K. E. (1997). "Moment Rotation Relationships for Unified Autostress Designs of Continuous-Span Bridge Beams and Girders." *Final Report*, Joint Transportation Research Program, West Lafayette, IN, 117 pp.

White, D.W. and Clarke, M.J. (1997a). "Design of Beam-Columns in Steel Frames. I: Philosophies and Procedures," *Journal of Structural Engineering*, ASCE, 123(12), 1556-1564.

White, D.W. and Clarke, M.J. (1997b). "Design of Beam-Columns in Steel Frames. II: Comparison of Standards," *Journal of Structural Engineering*, ASCE, 123(12), 1565-1575.

Winter, G. (1968). "Thin-Walled Structures – Theoretical Solutions and Test Results," Preliminary Publications of the Eighth Congress, IABSE, 101-112.

Wittry, D.M. (1993). "An Analytical Study of the Ductility of Steel Concrete Composite Sections," M.S. Thesis, Univ. of Texas, Austin, TX, December, 88 pp.

Wolchuk, R. (1997). "Steel-Plate-Deck Bridges and Steel Box Girder Bridges," *Structural Engineering Handbook*, 4th ed., Section 19, E.H. Gaylord, Jr., C.N. Gaylord and J.E. Stallmeyer (eds.), McGraw-Hill.

Wolchuk, R. and Mayrbaurl, R.M. (1980). "Proposed Design Specifications for Steel Box Girder Bridges," Final Report, FHWA-TS-80-205, Washington, DC, 288 pp.

Wong-Chung, A.D. and Kitipornchai, S. (1987). "Partially Braced Inelastic Beam Buckling Experiments," *Journal of Constructional Steel Research*, 7, 189-211.

Woolcock, S.T. and Kitipornchai, S. (1986). "Design of Single Angle Web Struts in Trusses," *Journal of Structural Engineering*, 112(6), 1327-1345.

Wright, R.N. and Abdel-Samad, S.R. (1968). "BEF Analogy for Analysis of Box Girders," *Journal of the Structural Division*, ASCE, 94(ST7), 1719-1739.

Wright, K.J. and Bunner, M.A. (2011). "Arch Bridges," *Structural Steel Designer's Handbook*, Chapter 14, R.L. Brockenbrough and F.S. Merritt (ed.), McGraw-Hill, New York, NY, 80 pp.

Xanthakos, P.P. (1994). *Theory and Design of Bridges*, Wiley, New York, NY, 1443 pp.

Xie, M. (2000). "Behavior and Design of Transversely Stiffened Plates Subject to Combined Shear and Direct In-Plane Loading," PhD Thesis, Department of Civil and Environmental Engineering, Imperial College, London.

Yannotti, A., Alampalli, S. and White, H. (2005). "New York State Department of Transportation's Experience with Integral Abutment Bridges," *Integral Abutment and Jointless Bridges*, FHWA Conference, Baltimore, MD, organized by Constructed Facilities Center, College of Engineering and Mineral Resources, W. Virginia Univ., 41-49.

Yoo, C.H. and Lee, S.C. (2006). "Mechanics of Web Panel Postbuckling Behavior in Shear," *Journal of Structural Engineering*, ASCE, to appear.

Yoo, C.H. and J.S. Davidson (1997). "Yield Interaction Equations for Nominal Bending Strength of Curved I-Girders," *Journal of Bridge Engineering*, ASCE, 2(2), 37-44.

Yu, D. and Sause, R. (2002). "Regression Study on the Inelastic Lateral-Torsional Buckling Strength of I-Beams," ATLSS Center, Lehigh University, Bethlehem, PA, October, 38 pp.

Yura, J.A., Helwig, T., Herman, R. and Zhou, C. (2008). "Global Lateral Buckling of I-Shaped Girder Systems," *Journal of Structural Engineering*, ASCE, 134(9), 1487-1494.

Yura, J.A. and Widianto (2005). "Lateral Buckling and Bracing of Beams – A Re-evaluation After the Marcy Bridge Collapse," *Proceedings of the Annual Technical Session and Meeting*, Montreal, Quebec, Structural Stability Research Council, Univ. of Missouri - Rolla, Rolla, MO, 277-294.

Yura, J.A. and Helwig, T.A. (1996). "Bracing for Stability," Short Course Notes, Structural Stability Research Council.

Yura, J.A. (1992). Notes on development of k_c equation for AISC LRFD Specification.

Yura, J.A., Galambos, T.V. and Ravindra, M.K. (1978). "The Bending Resistance of Steel Beams," *Journal of the Structural Division*, ASCE, 104(9), 1355-1369.

Zandonini, R. (1985). "Stability of Compact Built-Up Struts: Experimental Investigation and Numerical Simulation," *Costruzioni Metalliche*, 4.

Zhou, C. (2006). "Utilizing Lean-On Cross-Frame Bracing for Steel Bridges," Ph.D. dissertation, University of Houston, Houston, TX, 382 pp.

Ziemian, R.D. (2010). *Guide to Stability Design Criteria for Metal Structures*, 6th ed., R.D. Ziemian (ed.), Structural Stability Research Council, Wiley, New York, NY.